



HAL
open science

Newton-Euler approach for bio-robotics locomotion dynamics : from discrete to continuous systems

Shaukat Ali

► **To cite this version:**

Shaukat Ali. Newton-Euler approach for bio-robotics locomotion dynamics : from discrete to continuous systems. Automatic. Ecole des Mines de Nantes, 2011. English. NNT : 2011EMNA0001 . tel-00669588

HAL Id: tel-00669588

<https://theses.hal.science/tel-00669588>

Submitted on 13 Feb 2012

HAL is a multi-disciplinary open access archive for the deposit and dissemination of scientific research documents, whether they are published or not. The documents may come from teaching and research institutions in France or abroad, or from public or private research centers.

L'archive ouverte pluridisciplinaire **HAL**, est destinée au dépôt et à la diffusion de documents scientifiques de niveau recherche, publiés ou non, émanant des établissements d'enseignement et de recherche français ou étrangers, des laboratoires publics ou privés.

THESE

Shaukat ALI

**DOCTORAL SCHOOL: STIM
THESIS N° 2011EMNA0001**

*Thesis submitted to obtain the Doctorate degree of the Ecole des Mines
under the label of the Université Nantes, Angers, Le Mans
Discipline: Biomechanics and Bio-engineering
Defended on 20 December 2011*

**Newton-Euler Approach For
Bio-Robotics Locomotion
Dynamics: From Discrete To
Continuous Systems**

Supervisor:

BOYER Frédéric, Professor, École des
Mines de Nantes, Nantes, France

Reviewers:

LASCHI Cecilia, Associate Professor,
Scuola Superiore Sant'Anna, Pisa, Italy
CHOSET Howie, Professor, Carnegie
Mellon University, Pittsburgh, USA

Examiners:

JAULIN Luc, Professor, Université de
Bretagne Occidentale, Brest, France
ROUCHON Pierre, Professor, Mines
PariTech, Paris, France
KHALIL Wisama, Professor, Ecole
Centrale de Nantes, Nantes, France



Abstract

This thesis proposes a general and unified methodological framework suitable for studying the locomotion of a wide range of robots, especially bio-inspired. The objective of this thesis is twofold. First, it contributes to the classification of locomotion robots by adopting the mathematical tools developed by the American school of geometric mechanics. Secondly, by taking advantage of the recursive nature of the Newton-Euler formulation, it proposes numerous efficient tools in the form of computational algorithms capable of solving the external direct dynamics and the internal inverse dynamics of any locomotion robot considered as a mobile multi-body system. These generic tools can help the engineers or researchers in the design, control and motion planning of manipulators as well as locomotion robots with a large number of internal degrees of freedom. The efficient algorithms are proposed for discrete and continuous robots. These methodological tools are applied to numerous illustrative examples taken from the bio-inspired robotics such as snake-like robots, caterpillars, and others like snake-board, etc.



Contents

1	General Introduction	1
1.1	Motivations and Contents	1
1.2	Organization of the Thesis	3
2	Bio-inspired Locomotion Modeling: An Overview	5
2.1	Animal Locomotion	5
2.2	Bioinspired Locomotion Robots	9
2.3	Modeling of Bio-inspired Locomotion Systems: The Lagrangian Picture . .	16
2.4	Conclusions	34
I	Discrete Systems: Mobile Multibody Systems	37
3	Locomotion Dynamics Algorithm of Mobile Multibody Systems	39
3.1	Description of a Mobile Multibody System	41
3.2	Luh and Walker Manipulator Dynamics	47
3.3	Overview of the Proposed Algorithm	49
3.4	The Unconstrained Mobile Multibody System	54
3.5	The Constrained Mobile Multibody System	59
3.6	Kinematics of a Constrained Mobile Multibody System	59
3.7	Dynamics of the Constrained Mobile Multibody System	67
3.8	Computational Algorithm	73
3.9	Conclusions	77
4	Illustrative Examples of Mobile Multibody Systems	79
4.1	Satellite with Rotors: Unconstrained Case	79
4.2	The Snakeboard: Under-Constrained Case	83
4.3	Snake-like Robot: Fully-Constrained Case	88
4.4	Mobile Manipulator: Fully-Actuated Case	91
4.5	Conclusions	95

II	Continuum Systems: Hyper-Redundant Robots	97
5	Macro-Continuous Dynamic Modeling of Hyper-Redundant Robots	99
5.1	Modeling Approach of Hyper-Redundant Robots	100
5.2	Beam Kinematics and Hyper-Redundant Robots	105
5.3	Continuous Models of Hyper-Redundant Robots	107
5.4	Dynamic Algorithm of Hyper-Redundant Robots	112
5.5	Terrestrial Locomotion Model	114
5.6	Conclusions	122
6	Illustrative Examples of Hyper-Redundant Robots	123
6.1	Earthworm in 1D	124
6.2	Climbing Inchworm in 2D	133
6.3	2D Snake in Lateral Undulation	140
6.4	3D Snake in Lateral Undulation	149
6.5	Further Discussion: Application to Real Designs	153
6.6	Conclusions	155
7	General Discussion and Conclusions	157
7.1	Summary of the Thesis	157
7.2	First Conclusive Discussion: Projective vs Distributive Approach	158
7.3	Second Conclusive Discussion: Lagrangian vs Newton-Euler Modeling Approach	162
7.4	Perspectives	164
8	Thesis Detailed Résumé in French	167
8.1	Introduction Générale	168
8.2	La locomotion bio-inspirée	170
8.3	Problème général abordé dans cette thèse	171
8.4	Introduction aux Systèmes Multicorps Discrets	173
8.5	Dynamique inverse récursive des manipulateurs	177
8.6	Aperçu de l'algorithme	178
8.7	Les systèmes multicorps mobiles non-contraints	179
8.8	Les systèmes multicorps mobiles contraints	182
8.9	Exemples illustratifs	189
8.10	Introduction aux Robots Hyper-Redondants	193
8.11	Notations et définitions	194
8.12	Cinématique de la poutre et des robots hyper-redondants	195
8.13	Modèle continu des robots hyper-redondants	196
8.14	Algorithme dynamique des robots continus	199

8.15	Modélisation cinématique des contacts	200
8.16	Algorithme dans le cas cinématique	203
8.17	Exemples illustratifs	205
8.18	Conclusions	214
A	Appendix A	217
A.1	Extension of the Luh and Walker Algorithm to Closed Loop Kinematics . .	217
A.2	Covariants	218
A.3	3D Snake: Compatibility Condition	219
B	Fundamentals of Lie Group Theory	221
B.1	Lie Group	221
B.2	Adjoint Operators	223
B.3	Lie Group in 2D Space ($G=SE(2)$)	224
	References	227


List of Figures

2.1	Action-reaction principal of a locomotion system	6
2.2	(a) Sandfish (<i>Scincus scincus</i>): a lizard that can swim in granular media such as sand; (b) microscopic view of shark skin	7
2.3	Gecko: a lizard with adhesive setae on its feet	7
2.4	How snakes move	8
2.5	The swimming robots of RoboTuna by MIT: (a) The "Charlie-I"; (b) The "RoboTuna-II"	10
2.6	The pioneering snake-like robot ACM-III with passive castor wheels	11
2.7	ACM-R5 snake-like robot with passive wheels	12
2.8	Snake-like robots designed by NTNU: (a) Wheeko with passive wheels; (b) Kulko with tactile sensors	12
2.9	Uncle Sam: snake-like robot at CMU	13
2.10	(a) Sandfish robot; (b) Stickybot-III	14
2.11	Robotic arms: (a) CardioArm; (b) Elephant trunk-like manipulator	15
2.12	Octopus Arm robot bio-inspired from octopus	15
2.13	Soft robot inspired from caterpillar	16
2.14	Configuration space of a double pendulum: example manifold	17
2.15	Configuration space of a rigid body	18
2.16	Configuration space as the principal fiber bundle	19
2.17	Configuration space of a locomotion system: the principal fiber bundle	20
2.18	Flow chart of the recursive locomotion dynamics algorithm	21
2.19	Problem of locomotion	22
2.20	Connection between motions (\dot{r}) on \mathcal{S} and motions (η) on G (from [32])	23
2.21	Fiber bundle: (a) principal fiber bundle $G \times \mathcal{S}$; (b) Tangent bundle TM of a manifold M	23
2.22	(a) Gauss-Bonnet theorem illustrated on \mathcal{S}^2 ; (b) A cyclic change of shape produces a net displacement in G	24
2.23	Mechanical connection: falling cat and satellite with rotors	25
2.24	Kinematic connection: snake in lateral undulation and unicycle-platform	27

2.25	Example of fluid contact dynamics	30
2.26	Under-constrained systems (a) Snakeboard (b) Trikke	33
3.1	Tree-like structure of a mobile multibody system: (a) Manipulator; (b) Wheeled system	42
3.2	Concept of isolated and composite body	42
3.3	Axes of a wheel	43
3.4	Types of unidirectional wheel	44
3.5	Newton-Euler parametrization of a mobile multibody system	46
3.6	Luh and Walker computational torque algorithm	48
3.7	Wheeled mobile multibody system with passive wheels: (a) Two-axles mobile multibody system; (b) Three-axles mobile multibody system	49
3.8	Scope of locomotion dynamics algorithm	51
3.9	Flow chart of the recursive locomotion dynamics algorithm	53
3.10	Execution of proposed algorithm in case of an unconstrained mobile multibody system	57
3.11	Execution of the general algorithm in mixed kinematic and dynamic case	77
4.1	Satellite with rotors: (a) Outline sketch; (b) Tree-like structure	80
4.2	Inertia rotors for re-orientation of satellite in space	81
4.3	(a) Commercial snakeboard; (b) Robotic prototype of the commercial snakeboard	83
4.4	Snakeboard: (a) Outline sketch; (b) Tree-like structure	83
4.5	Tree-like structure of snake-like robot	88
4.6	Outline sketch of snake-like robot	89
4.7	Motion of the head body S_o in the xy plane	91
4.8	Joint torque τ_{10}	92
4.9	All joint torques at $t = 10 \text{ sec}$	92
4.10	(a) Staubli manipulator mounted on a car like platform; (b) Top view of the platform, $R2 = 0.42, D3 = R4 = 0.45$	93
4.11	Top view of the car-like platform, $l = 1.0, L = 0.5$	94
4.12	(a) Torque τ_1 for two different values of ξ ; (b) Wheel torque for $\xi = 1$	95
5.1	Frames and parametrization of a hyper-redundant robot	102
5.2	Representation of vector fields $\eta(X)$ and $\xi(X)$	104
5.3	General algorithm of hyper-redundant robots	112
5.4	Execution of the general algorithm of a hyper-redundant robot	114
5.5	(a) Locked anchorage; (b) sweeping anchorage	116
5.6	Cross sectional follower Annular contact	117

5.7	(a) Reaction wrench on an anchored cross section; (b) Reaction wrench on a cross section in annular contact	119
5.8	Algorithm of a hyper-redundant robot with kinematic constraint model	120
5.9	Execution of kinematic algorithm of a hyper-redundant robot	121
6.1	A natural earthworm	124
6.2	(a) Initial reference configuration; (b) Deformed configuration with sweeping anchorage point $C(t)$	125
6.3	A cylindrical cross section in three different forms. A_o is the area of relaxed cross section	126
6.4	Earthworm locomotion along x -axis	131
6.5	(a) Time vs head position; (b) Time vs head velocity	132
6.6	Internal control forces $N(X)$ over the length with constant c	133
6.7	With variable $c(t)$: (a) Axial contact force N_c at $X = C$; (b) Internal control forces $N(X)$ over the length of earthworm	134
6.8	(a) Ω -shaped bending configuration of an inchworm; (b) Inchworm in unstructured environment	135
6.9	Ω -shaped bending configuration of an inchworm	136
6.10	Bilateral reaction forces at the anchorage point	137
6.11	Climbing inchworm locomotion along vertical y -axis	139
6.12	(a) Time vs head position; (b) Time vs head velocity	139
6.13	(a) Vertical reaction force N_{cY} at head; (b) Reaction torque C_{cZ} at head	140
6.14	Internal control torque over the length	140
6.15	(a) Discrete Kirchhoff-snake; (b) Discrete Reissner-snake	141
6.16	Bilateral nonholonomic constraint imposed on cross section X by cross sectional follower annular contact	142
6.17	2D snake with cross sectional follower type annular contacts which imposes the lateral contact forces	145
6.18	Curvature profile along the snake's backbone	147
6.19	2D snake straight line locomotion in xy plane	148
6.20	2D snake turning locomotion in xy plane	149
6.21	At $t = 2.0s$ (a) Contact force (N_{cY}) over the length; (b) Internal torque (C_Z) over the length	149
6.22	(a) Head turning locomotion; (b) Snapshots of snake 3D turning locomotion	153
6.23	At $t = 2.0s$ (a) Contact forces (N_{cY}, N_{cZ}) over the length; (b) Internal torques (C_Y, C_Z) over the length	154
6.24	Proposed design of a 3D snake: (left) cross-sectional view, (right) longitudinal view	155

8.1	Structures arborescentes d'un système multicorps mobile: (a) un manipulateur; (b) un système à roues	175
8.2	Systèmes multicorps à roues: (a) Système multicorps avec deux essieux; (b) Système multicorps avec three essieux	179
8.3	Le Snakeboard	189
8.4	Les trois premiers modules du robot serpent	191
8.5	(a) le mouvement de S_o dans le plan xy ; (b) couple articulaire τ_{10}	192
8.6	(a) Ancrage verrouillé; (b) Ancrage glissant	201
8.7	Contact annulaire	202
8.8	La locomotion du ver dans le plan xy	207
8.9	Avec c variable: (a) les forces externes de reaction N_c ; (b) les forces internes N	207
8.10	La locomotion de la chenille dans le plan xy plane	208
8.11	(a) Couple de reaction externe à la tête; (b) les couples internes	209
8.12	(a) Serpent-Kirchhoff discret; (b) Serpent-Reissner discret	209
8.13	Profile de courbure du serpent	212
8.14	Serpent 2D avec p contacts annulaires	213
8.15	Le mouvement du serpent 2D avec le virage dans un plan xy	214
8.16	(a) Forces de contact (N_y); (b) les couples internes	214



List of Tables

3.1	Classification of mobile multibody system dynamics	75
5.1	Actuated degrees of freedom vs Beam theory	106
5.2	Internal degrees of freedom vs natural applications	106
5.3	Contacts in terrestrial locomotion	115
6.1	Reduction of 3D parameters to 1D parameters	127
7.1	Overview of the modeling approaches discussed in the thesis	162

1

General Introduction

1.1 Motivations and Contents	1
1.2 Organization of the Thesis	3

1.1 Motivations and Contents

More or less deliberately, from its beginning, robotics took inspiration from nature to design its robots. Robots resembling to human arm were designed using discrete mechanisms devoted to the manipulation tasks of industrial manufacturing processes. These discrete mechanisms consist of serial chains of rigid bodies connected by lumped degrees of freedom and are today included into the wider class of systems known as multibody systems. After manipulators, robots designers started to build mobile robots as wheeled platforms. When the environments become unstructured, legs are more adapted than wheels and mobile robotics oriented its investigations towards legged robots inspired from walking animals so opening consciously the way of bio-inspiration. With the passage of time, taking inspiration from the wide diversity of the animal kingdom, the researchers in this field started developing mechanisms with more and more internal degrees of freedom, hence introducing a new generation of robots called as hyper-redundant systems since they may be considered as having an infinite degree of redundancy with respect to the six dimensional task consisting of moving a rigid body in space. Even, nowadays, the robotics have entered into the era of soft robotics where the robots have no rigid bodies in their structure. In this case, the source of bio-inspiration is provided by soft animals, named as hydrostats, such as worms, caterpillars, octopus, etc. From the mechanist's point of view these systems can be considered as continuous systems having an infinite number of degrees of freedom.

These increasing complexities of the design is in particular due to the diversification of locomotion modes involving more and more complex leaning media such as versatile grounds,

air, water, etc. Today, active researches in bionics allow us to progressively discover the subtle mechanisms that animals have discovered along evolution of species to improve their dynamic performances in terms of energetic consumption or manoeuvrability. As such locomotion systems become more and more complex, so do their mathematical models. Consequently, we need today efficient methodological tools that can help the roboticists in modeling, design, control, motion planning (gait generation, transit maneuvers), etc. In this regard, the dynamic models along with their associated algorithms are of great interest to researchers due to their active role in simulation, design and control. Keeping in view this growing interest, in this thesis we propose a unified methodological framework that is capable to address the problem of bio-inspired locomotion to a greater extent. More precisely, the aim of this thesis is two folds. Firstly, it contributes to the classification of locomotion robots. Secondly, it proposes new efficient tools for their dynamic computation. As regards the first objective, we will use mathematical tools introduced by the American school of geometric mechanics after Marsden [60, 49, 59]. Remarkably, these abstract tools will allow us to exhibit the common geometric structures shared by apparently very different locomotion ways as for instance snakes creeping and swimming at high Reynolds.

As regards the second objective, starting from manipulators there are two major algorithmic approaches to solve the problems of robots dynamics. The first approach is based on Lagrangian mechanics and leads to explicit formulations parameterized through a minimal set of generalized independent coordinates [92]. The second approach is based on the application of Newton's laws and Euler's theorem to each of the isolated bodies, and is consequently named Newton-Euler formulation [4]. Whether applied to the inverse dynamics through the algorithm of Luh and Walker [115] or to the forward dynamics through the algorithm of Featherstone [40], Newton-Euler formulation leads to $O(n)$ algorithms (where n is the number of bodies of the system). On the other hand, Lagrangian formulation leads to $O(n)$ or $O(n^4)$ algorithms depending upon whether they are recursive (like the Newton-Euler based algorithms) [54] or not [114, 58]. The Newton-Euler approach, once coupled with a symbolic customized code, gives the most optimized algorithms [64]. This advantage is crucial when we investigate some systems with large number of links and degrees of freedoms such as in case of hyper-redundant manipulators [52, 100, 25, 72]. Moreover, Newton-Euler algorithms are particularly interesting when considering modular or reconfigurable robots [24] since, in this case, changing the topology of the system only changes the indexation of the bodies without compromising the structure of the algorithm.

Despite these advantages, a general Newton-Euler based framework exists only for manipulators, i.e. for multibody systems with a fixed base [40], while the most unified theory of dynamics of locomotion systems is based on the Lagrangian geometric mechanics on principal fiber bundles [87, 60, 76, 101]. As an asymptotic case, we will see that hyper-

redundant robot dynamics can be modeled by a continuous version of the Newton-Euler formulation with no Lagrangian counterpart in this case [13, 16]. In fact, the existing approaches used to model hyper-redundant robots can be categorized into two main sets depending on whether the robot is considered as a discrete multibody system with a large number of degrees of freedom [63, 78], or directly as a continuous deformable medium. In the first case, the modeling is facilitated by the fact that mathematical tools from usual discrete robotics are already available. On the other hand, adopting a continuous model from the beginning can greatly facilitate the formulation, analysis and resolution of the robotics problems related to manipulation [26, 83] and locomotion [52, 18, 50]. This thesis deals with both the modeling approaches and develops a unified classification and algorithmic framework for discrete multibody systems as well as continuous systems.

1.2 Organization of the Thesis

This thesis is organized as follows.

Chapter 2 provides a brief overview of the bio-inspired locomotion systems and their modeling approach. First, the animal locomotion and state of the art work in bio-inspired robots are presented in order to prepare ground for further discussion. The basic dynamic problem of locomotion that will be addressed all along the thesis, is then stated. Then, this basic problem is (quickly) addressed in the perspective of Lagrangian dynamics. This allows one to fix the framework in which all the following chapters will progress, as well as to point out the directions and contributions of the thesis.

Then the thesis is divided in two parts. Part I is related to the discrete mobile multibody systems, while part II is devoted to the continuous locomotion systems. The first part consists of the following two chapters.

In chapter 3 a general computational algorithm for mobile multibody systems is developed by extending the Luh and Walker computational algorithm, originally developed for standard manipulators, to a general class of mobile tree-like systems. This includes the modeling process based upon the Newton-Euler formulation. In parallel to these investigations, the systems are classified in several classes and subclasses depending on their geometric structures. The reduced dynamic model is presented as a counterpart for the reduced Lagrangian dynamics discussed in chapter 2. Then, in chapter 4 the proposed computational algorithm is applied to some existing systems, each one playing an archetypical role in each of the subclasses defined in chapter 3.

In chapter 5 the above computational algorithm for mobile multibody systems is extended to the continuous locomotion systems where the system is modeled as a strain-actuated Cosserat beam, i.e. a continuous version of a rigid mobile multibody system. This algorithm is named as macro-continuous dynamics algorithm since it is adapted to the study of hyper-redundant and soft robots at a macroscopic scale. In a second step, this general

continuous algorithm is applied to the case of terrestrial locomotion systems with the help of kinematic models of ideal contacts between the system and the surrounding. In chapter 6 the proposed algorithm is applied to some elongated body animals such as earthworm, inchworm and snakes.

A general discussion and conclusion is given in chapter 7, which concludes the whole work and gives some future perspectives based upon the work in this thesis. Finally, in chapter 8, a detailed summary of the thesis is presented in French language.



Bio-inspired Locomotion Modeling: An Overview

2.1	Animal Locomotion	5
2.2	Bioinspired Locomotion Robots	9
2.2.1	Bio-Inspired Snake-like Robots	10
2.3	Modeling of Bio-inspired Locomotion Systems: The Lagrangian Picture	16
2.3.1	Definition of a Mobile Multibody System	16
2.3.2	Configuration Space of a Mobile Multibody System	17
2.3.3	General Problem Addressed in this Thesis	20
2.3.4	Forward Locomotion Dynamics: The Kinematic Case	22
2.3.5	Forward Locomotion Dynamics: The General Case	28
2.3.6	Forward Locomotion Dynamics: The Mixed Case	32
2.3.7	Inverse Torque Dynamics	33
2.4	Conclusions	34

This chapter presents a comprehensive overview of the bio-inspired locomotion in Robotics. Starting from animals, some archetypical examples in the field of bio-inspired locomotion robots are presented in order to prepare the ground for further discussion. Then, the general problem of locomotion that will be addressed in the rest of this thesis will be stated. In the perspective of solving this problem, we will remind the Lagrangian picture of locomotion dynamics as it has been produced in the last ten years by geometric mechanics. In this regard, our choice in this introductory chapter is to privilege intuition over rigorous formalism. We hope that this choice will allow the reader unfamiliar with geometric mechanics to gain insight this beautiful theory.

2.1 Animal Locomotion

Animal locomotion is the study of how animals move in the world. Locomotion is the ability to move from place to place in 3D space. For a system, either natural or artificial, the locomotion can be defined more precisely as follows:

”The process of producing net (overall) displacement (motion) of a system through internal shape changes (deformations) and interaction with the external world.”

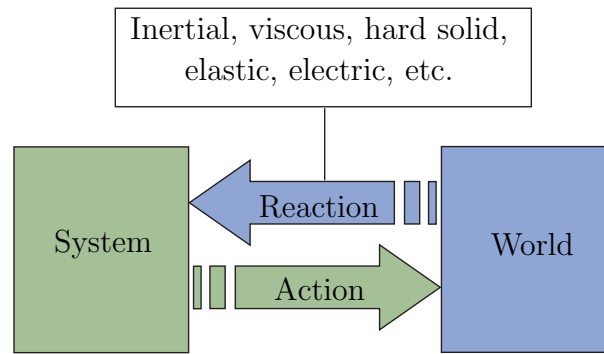


Figure 2.1 – *Action-reaction principal of a locomotion system*

In nature, the internal shape changes varies from organism to organism, depending upon their morphology, their structural characteristics and medium of interaction. When these internal shape changes are found to be cyclic maneuvers, they are known as gaits of locomotion. Animals also perform some transient maneuvers such as turning, jumping, etc. A vast variety of locomotion is observed in animals. For example, flying of a bird, walking of a cat, running of a horse, creeping of a snake, swimming of a fish, burrowing of a worm, etc. In all these cases the locomotion is possible due to the contact with the surrounding medium e.g. air, water, earth, etc. In its essence, locomotion is based on the following principle. Any animal when moving in space first changes its shape in order to exert some forces on its surroundings. Then, by virtue of the action-reaction principal, i.e. the Newton's third law of motion, the surroundings exerts some reaction forces onto the animal body which propel it in space (see Fig. 2.1). The reaction forces exerted by the world onto the animal body depends upon the size of the animal's body, and the physical properties of the surrounding medium on which the animal leans to move. For instance, swimming and flying at high Reynolds numbers involves inertial (pressure) forces (produced by the acceleration of the fluid surrounding the animal), while at low Reynolds, small animals such as flagella or cilia protists use viscous (friction) forces to move. In case of walking, hard discontinuous contact forces are involved, while snakes control their body surface in contact with the ground to maximize the propelling reaction forces. Among the most mysterious modes of locomotion, we find the sandfish *Scincus scincus*, a lizard of the Sahara desert, which is capable of swimming in the sand (see Fig. 2.2)(a). This animal seems to be a natural case of super-lubricity, and current researches on its locomotion, attempt to show that the secret of its performances is probably hidden in the properties of its skin at low scale. It is in fact a remarkable thing that animals have developed a wide diversity of mechanisms allowing them to intensively exploit the physical possibilities of their leaning medium. Among these mechanisms, let us mention the multi-scale physical phenomena involved at the contact interfaces where very low scale forces can be collected by sophisticated organs to produce strong forces at a macroscopic scale. This is for in-



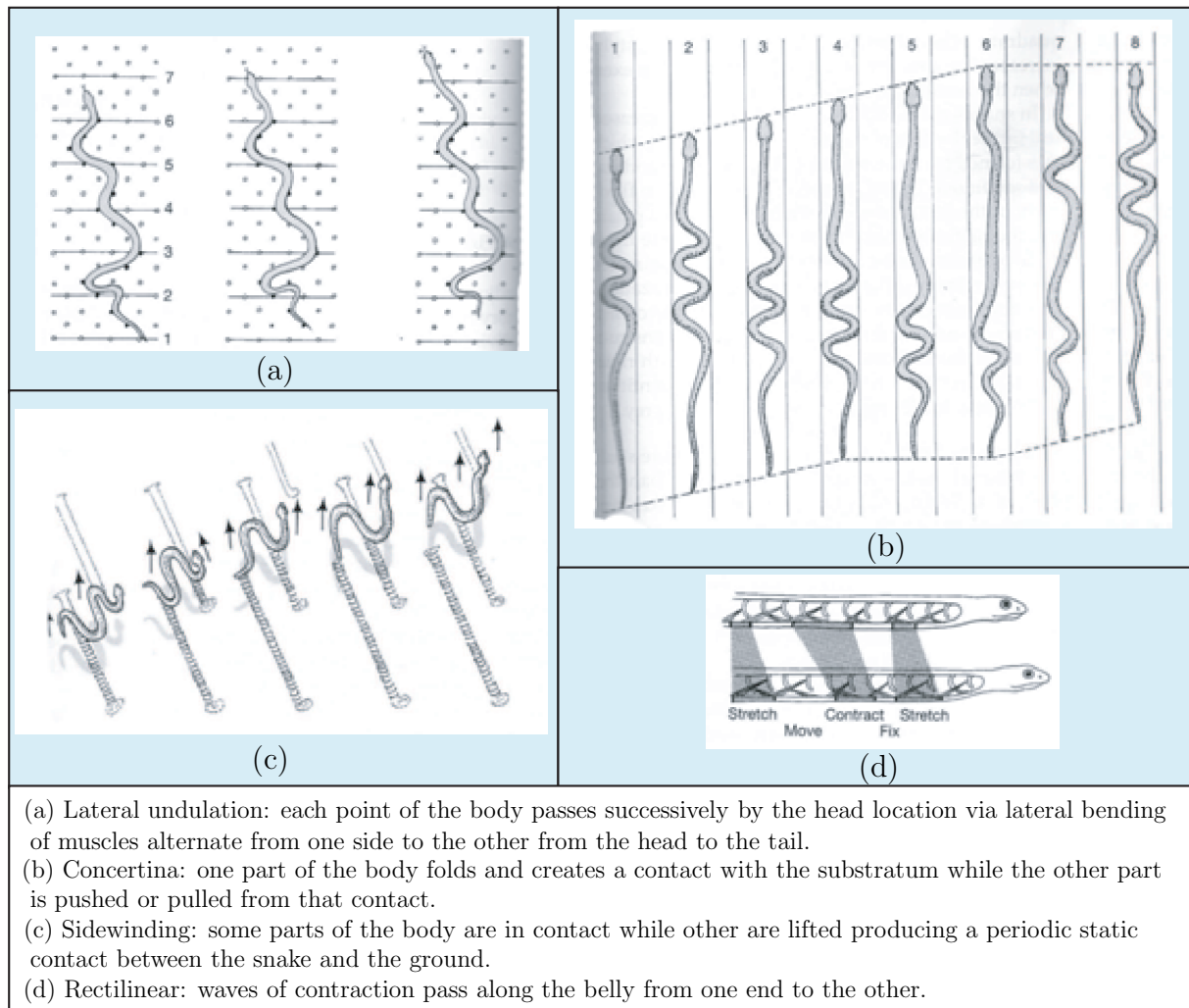
Figure 2.2 – (a) *Sandfish* (*Scincus scincus*): a lizard that can swim in granular media such as sand; (b) microscopic view of shark skin



Figure 2.3 – *Gecko*: a lizard with adhesive setae on its feet

stance the case of the geckoes which can produce adherence forces of high magnitude on any smooth surface (as glass) by using microscopic van-der-Waals forces. Another example of such a subtle multi-scale interaction is that of sharks skin whose microscopic structure allows the fish to control its boundary layer in order to reduce drag forces (see Fig. 2.2)(b). At a more macroscopic scale, animals move their surrounding medium in order to take advantage of their surrounding and facilitate their motion. For instance, animals moving in the sand fluidify the granular medium by agitating it in a suited way [73], while fish order the fluid around them into big vortical structures to control their net motions. In fact, most of fish have developed subtle mechanisms of interactions with the surrounding flow in order to extract kinetic momentum and energy from it. For instance, trouts can swim in turbulent rivers without efforts [6], while most of fish extract energy from their wake, which would be definitely lost otherwise. These observations on living animals are today the topic of intense researches in hydrodynamics and naval engineering related to the well known problem of drag reduction. In a similar perspective, the study of hovering flight has lead researchers to restate the basic laws of a new unsteady aerodynamics [36]. In particular, they discovered that when it reverses its stroke, the flapping wing of a hawk moth captures its own wake to reuse a part of the energy of the flow for lift generation [98].

From the point of view of the roboticist, animals morphology can be grossly classified

Figure 2.4 – *How snakes move*

in three classes depending if they have an endoskeleton, an exoskeleton or no skeleton at all. In the first case we meet all the vertebrates such as snakes, fishes, mammals, etc., while in the second major set (i.e. exoskeleton), we find the branch of arthropods which contains the class of insects or that of arachnids. Finally, other animals have no skeleton and recover the rigidity required by the contact efficiency by contracting isovolume tissues. Among these animals, named hydrostats, we find the worms or the octopus which is probably the most achieved living creature based on this principle. Another major classification of morphologies relevant to robotics is their body's topology, each animal's body being possibly symbolized by a topological chain as those handled by multibody systems mechanics. In this case, simple open chain systems like the elongated body animals with no lateral appendices, are in fact very interesting for the roboticists since for a same simple morphology, they show a wide set of possibilities ranging from swimming like eels, to burrowing like worms, creeping like snakes and so on. One of the reasons of the success of this morphology in the animal kingdom, is probably due to the fact that these animals have a high number of internal degrees of freedom (some big snakes have more than 500

vertebrae) which make them what the roboticist names a hyper-redundant system. In this case, the degree of redundancy is the difference between the number of joint degrees of freedom of the skeleton with the six dimensions of their net displacements.

Beyond these bio-physics considerations, roboticists also get inspiration from the outstanding capabilities of animal locomotion to adapt to different environments. For example a same specie of snake has the ability to creep through undulation, sidewinding, rectilinear or concertina motion. In Fig. 2.4, these locomotion modes are shown and defined briefly[1]. All this is possible with the same morphology while shifting from one set of internal deformations to another which responds well to the environmental changes. More generally, the animal's body is in fact capable of adapting to unstructured environments and their nervous control system has the ability to switch quickly and smoothly from one locomotion pattern to another according to the physical changes in the surrounding.

2.2 Bioinspired Locomotion Robots

For all the above mentioned reasons, a great deal of interest has been shown over the last few decades toward the design of locomotion robots inspired by animals. In the beginning, locomotion robots were designed on the basis of prior knowledge of the conventional industrial manipulators, i.e. as discrete multibody systems. Moreover, with the passage of time and the increase of targeted robots performances and understanding of animal locomotion, the designing aspects of the artificial locomotion systems were getting more and more inspiration from the nature. In this regard, the robot designs were shifted from the conventional discrete mechanisms toward novel hyper-redundant continuous structures with a dramatic increase in internal degrees of freedom as well as the number of bodies. Such hyper-redundant systems get inspiration mostly from elongated body animals such as snakes, eel-fish, etc. Here we present some successful prototypes of such highly articulated multibody systems. In underwater robotics when targeting manoeuvrability with high efficiency in open waters, the most achieved animals for bio-inspiration are probably the tuna fish whose cruising speed can reach 50km/h, while the red tuna can accelerate up to 75km/h and turns on it self in a fraction of second. Thus, seeking new solutions for drag reduction in naval hydrodynamics, Triantafyllou and co-workers of MIT were among the pioneers to investigate bio-inspired paradigm in this context. Under the RoboTuna project that was started at MIT in 1993, the fish-like robot called as "Charlie-I" (Fig. 2.5(a)) inspired from the locomotion capabilities of the biological fish "tuna" was designed and built in 1995. The major structural component of the robot fish is a segmented backbone made up from eight discrete rigid vertebra connected with ball bearing joints. These eight vertebra are driven through an elaborate system of pulleys and cable tendons by six servo motors mounted outside the robot body. These tendon drives are the mechanical analog of the biological fish's muscles. As in the biological fish "tuna", the principal of propulsion

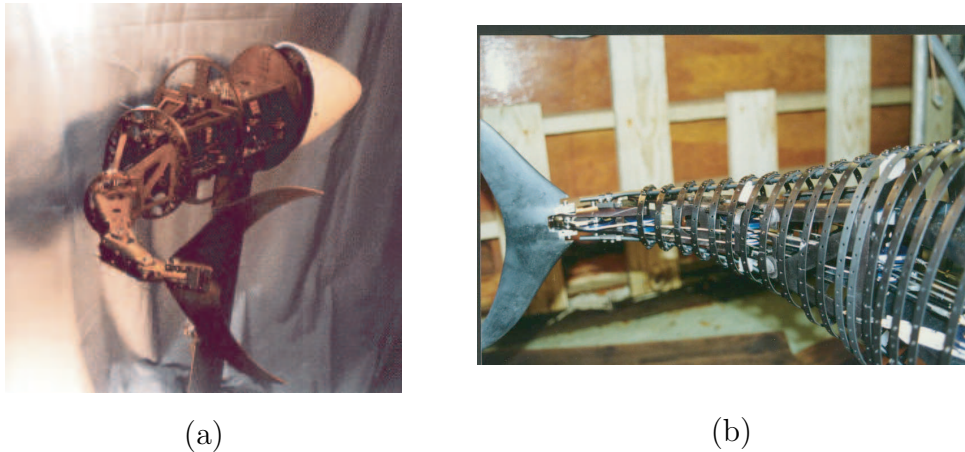


Figure 2.5 – The swimming robots of RoboTuna by MIT: (a) The "Charlie-I"; (b) The "RoboTuna-II"

was based upon the change in the internal orientation of the vertebra to each other that produced oscillation over the rear part of the body of robot. The main objective of this project being to study efficient systems of propulsion for the autonomous underwater vehicles with reduced drag and enhanced propulsion, the robot is towed and the resultant of hydrodynamic forces is measured for given cruising speeds and oscillations. The last robot of the RoboTuna project is the advanced version of the robotic fish Charlie-I, called as "Robotuna-II" with several significant modifications as shown in Fig. 2.5(b). After RoboTuna, another robotic fish was designed at MIT called as "RoboPike". The aim of this new project is to reproduce the high accelerations of the pike (*Esox lucius*) which can reach 15g ($g=9,81 \text{ ms}^{-2}$) when catching a prey. Contrary to the Robotuna, this robot has its actuation mechanism inside its body. After these works, many swimming robots were then developed. Inspired from elongated anguilliform fishes such as eel and lamprey, some of them were using the undulation of the high number of internal degrees of freedom over the whole body instead of making use of oscillations of the rear part of their body like RoboTuna to propel in water. Examples of such robots are the eel-like robot of the French project RAAMO [2] or the amphibious snake-like robots called as Amphibot [35] and ACM-R5 [119], etc.

2.2.1 Bio-Inspired Snake-like Robots

As an emblematic example of the discrete mobile multibody mechanism, the snake-like robot ACM-III [52] is a pioneering prototype and a first milestone in bio-inspired terrestrial locomotion (Fig. 2.6). In 1972, this first bio-inspired serpentine robot called as "Active Cord Mechanism" was made by Shigeo Hirose [52]. This robot was a two meter wheeled multibody system with twenty-one segments serially connected through (twenty) actuated single degree of freedom revolute joints. The purpose was to design and build a snake-like robot that is capable of producing an artificial serpentine movement same

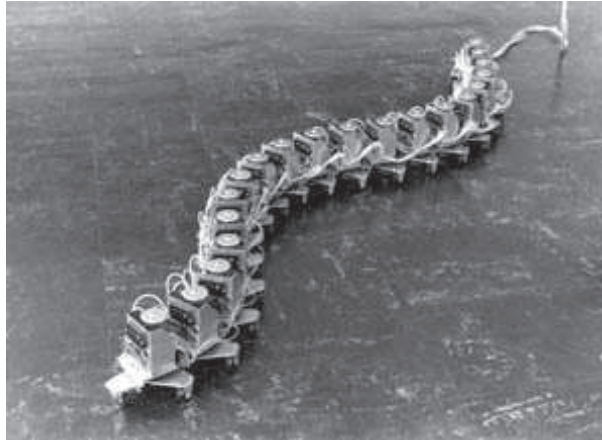


Figure 2.6 – *The pioneering snake-like robot ACM-III with passive castor wheels*

as that of actual snakes. This was the first successful attempt to mimic the serpentine movement, i.e. the forward movement produced with the help of internal actuated degrees of freedom. The passive castor wheels were used to form contact with the flat surfaces. These passive wheels ensure the frictional anisotropy of the ground friction forces, i.e. that the friction coefficient characterizing the ground friction forces in the normal (lateral) direction of each segment is larger than the friction coefficient characterizing the ground friction forces in the tangential (axial) direction of the segment. In natural snakes, the frictional anisotropy is provided by the ventral scales present on the snake belly [44, 55]. Taking advantage of the fact that, the propulsion mechanism of snakes is almost the same in both water and on ground, an amphibious version of the "Active Cord Mechanism" series, called the ACM-R5 was presented in 2005 [119]. The snake-like robot ACM-R5, shown in Fig. 2.7(a), has the ability to move on the ground through "crawling" as well as in the water through "anguilliform" swimming. This water proof robot consists of nine segments serially connected through eight universal joints (i.e. through two degrees of freedom revolute joints between the consecutive segments). The universal joint allows the pitch and yaw degrees of freedom between segments as shown on Fig. 2.7(b). This robot has paddles with passive wheels (Fig. 2.7(c)) that provide the necessary anisotropic ground friction properties required by lateral undulation i.e. allowing motion in the tangential direction, while preventing it in the normal direction.

Developed by NTNU university of Norway with the research organization SINTEF, the wheeled robot "Wheeko" is an experimental platform for studying wheeled snake-like robot locomotion across flat surfaces. As shown in Fig. 2.8(a) Wheeko consists of ten identical modules serially connected through universal joints. Each module of Wheeko is enclosed by a plastic ring mounted with twelve plastic passive wheels. The purpose of this prototype was to carry out motion control experiments in order to investigate the straight line path following controller.

In short, the above wheeled designs were successfully tested on flat surfaces. The loco-

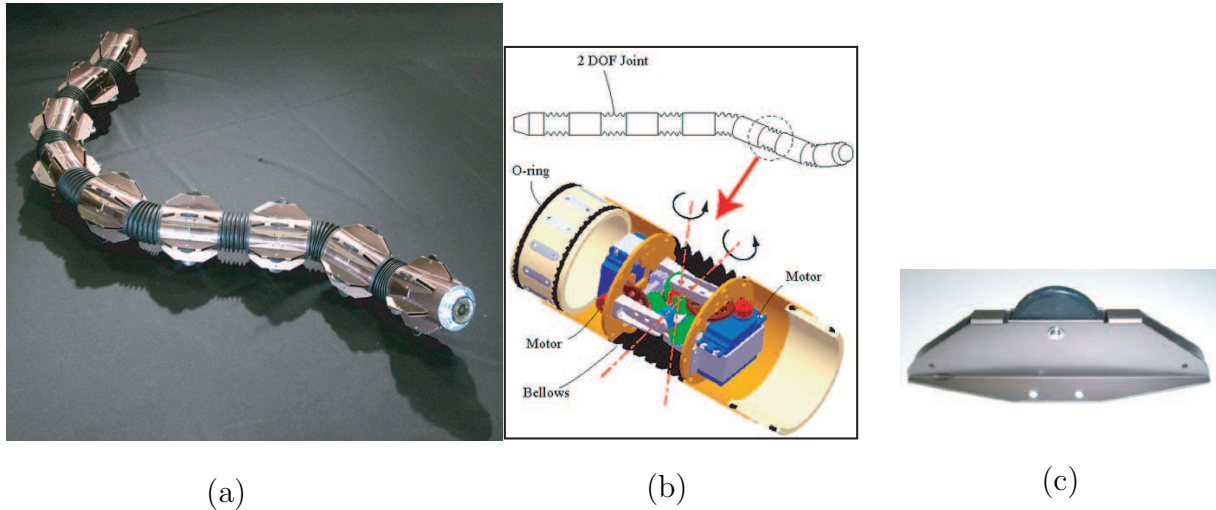


Figure 2.7 – ACM-R5 snake-like robot with passive wheels

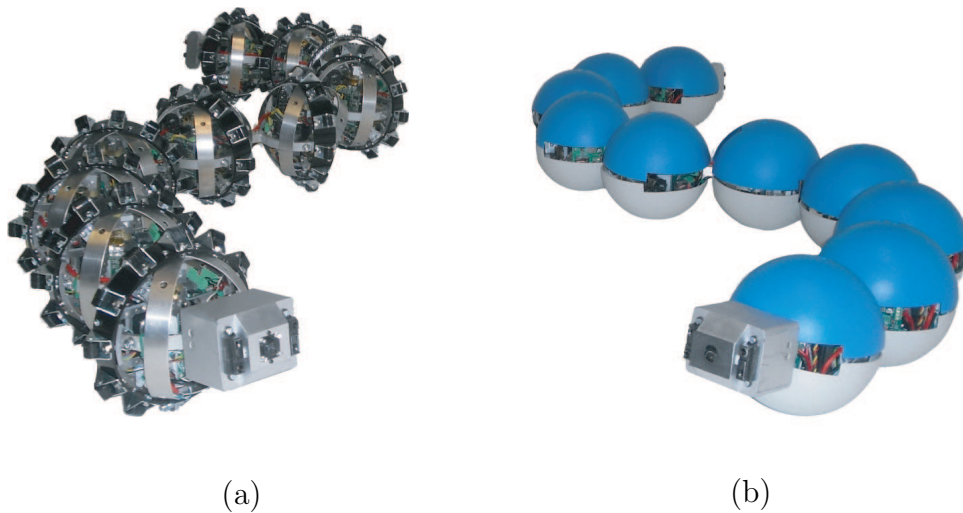


Figure 2.8 – Snake-like robots designed by NTNU: (a) Wheeko with passive wheels; (b) Kulko with tactile sensors

motion through undulation was investigated and controlled both on ground and in water. From these successful developments, the researchers pushed the goal one step further to design the snake-like robots for performing tasks in highly unstructured environments in which case the above wheeled robots will definitely face difficulties to perform locomotion tasks, since they are good on flat surfaces. Thus, the wheel-less snake-like robots were designed for this purpose.

Kulko is a snake-like robot equipped with tactile sensors (Fig. 2.8(b)). The purpose of this model is to experimentally investigate the snake robot locomotion and control in environments with obstacles where this robot makes use of the obstacles as push points, like real snakes, to propel forward [70]. A set of force sensing resistors (FSRs), used as the tactile sensors, are placed on the modules to measure the environmental contact forces due to contact with obstacles.

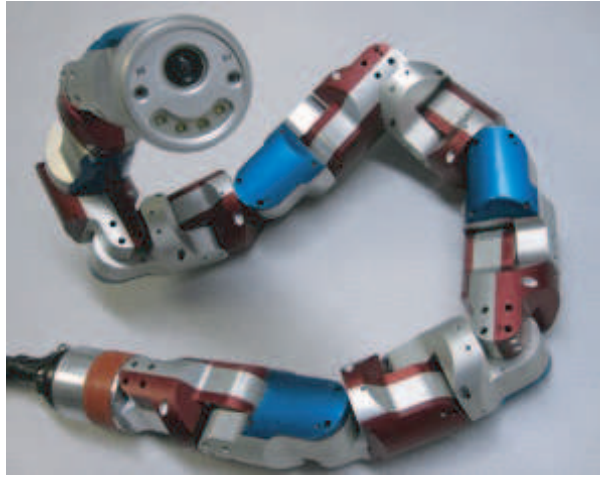


Figure 2.9 – *Uncle Sam: snake-like robot at CMU*

Among the most advanced results on snake-like robots, several modular robots were designed and built by researchers of the Biorobotics Laboratory at Carnegie Mellon University (CMU) under the direction of Howie Choset [118, 50, 109]. One of such robots, called as "Uncle Sam" is shown in Fig. 2.9. These wheel-less snake robots go beyond the capabilities of above mentioned conventional wheeled robots being limited to crawling and swimming. The modules are inter-connected in series via a single degree of freedom rotational joint in such a way that each module's axis of rotation is rotated ninety degrees ($\pi/2$ rad) from the previous module in order to produce motions in all three dimensions [118]. Thus, capable of bending in the two lateral directions, these highly articulated snake-like robots can perform more difficult tasks such as stair climbing, gap crossing, channel climbing and many more. In short, one of the key problems posed by this kind of systems is to develop novel gaits capable of producing net displacement on difficult terrain [50].

With the success of snake-like robots in unstructured environments, an interest was developed in the research that involves interaction of animals with complex world such as granular media. Inspired from the locomotion of the sandfish in complex granular media, the sandfish robot (Fig. 2.10(a)) has recently been designed by the Complex Rheology And Biomechanics (CRAB) Laboratory in the School of Physics at the Georgia Institute of Technology. The basic mechanical design of this robot get inspiration from the existing snake-like robots to perform undulatory locomotion in sand. This robot has seven identical modules serially connected through single degree of freedom joints. The purpose is to investigate the locomotion on the surface as well as inside a granular media [74]. As regards climbing robots, the Van der Valls adherence forces of high magnitude produced by the setae present on the toes of gecko lizard was the inspiration for the design of the vertical locomotion robot called as "Stickybot" as shown in Fig. 2.10(b). This robot has four sticky legs with a rubber-like material with tiny polymer hairs made from a micro-scale

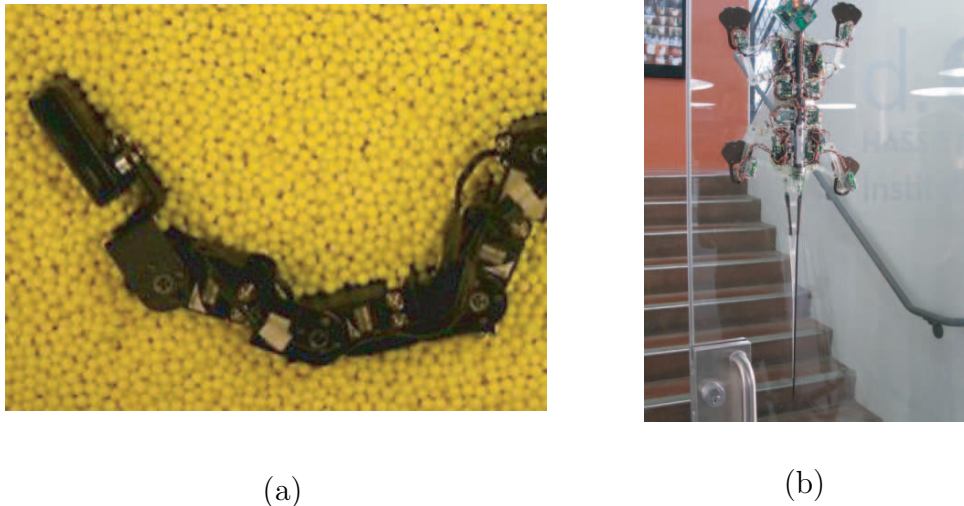


Figure 2.10 – (a) *Sandfish robot*; (b) *Stickybot-III*

mold, that allows the robot to climb smooth surfaces such as glass and metal.

Recent advances have shown the power of the bio-inspired approach in the field of control command. In fact, starting from works in neurobiology [45] on one of the most primitive fish, the anguilliform fish *Lampetra fluviatilis*, Auke Ijspeert and co-workers have implemented in [56] a distributed control on a real robotic artifact, mimicking the central pattern generators of the animal with a string of coupled nonlinear oscillators. Remarkably, the approach inherits from the virtues of its natural model. In particular, when applied to an amphibious robot inspired from the salamander, it allows to shift smoothly from walking to swimming and vice versa.

Considering robots with more and more internal joints, the elephant trunk-like manipulator developed by Hannan and Walker [47] is an example of highly articulated elongated system (see Fig. 2.11(b)). Another example of a hyper-redundant manipulator is the highly articulated robotic probe called as "CardioArm" developed by the Biorobotics Laboratory at Carnegie Mellon University [90]. The first prototype of this robotic probe has already been developed and tested (see Fig. 2.11(a)). The purpose of this robot is to perform the minimally invasive cardiac surgery.

In all the above designs, the rigidity required by the propulsion is ensured by the presence of rigid bodies in their structures. However, inspired from hydrostats capable of continuous deformations along their body, researchers are nowadays designing soft body robots with no rigid bodies in their structure. They are inspired from tentacles, octopus arm, elephant trunk, inchworm, earthworm, etc. A soft robotic arm inspired from octopus is being developed by Cecilia Laschi's crew under the European project "OCTOPUS" [3]. This soft arm robot, with no rigid bodies in its structure, is composed of silicone and is driven by cables and shape memory alloy technologies [31]. As a fundamental unit of the octopus-like soft robotic arm, an "artificial muscular-hydrostat" unit, as shown in Fig.

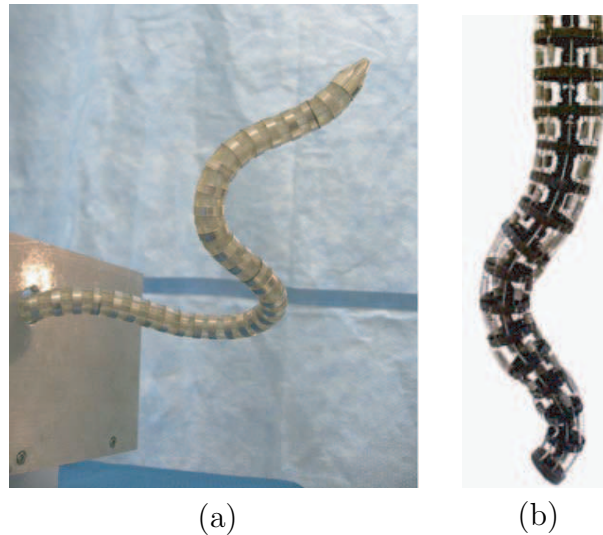


Figure 2.11 – *Robotic arms: (a) CardioArm; (b) Elephant trunk-like manipulator*

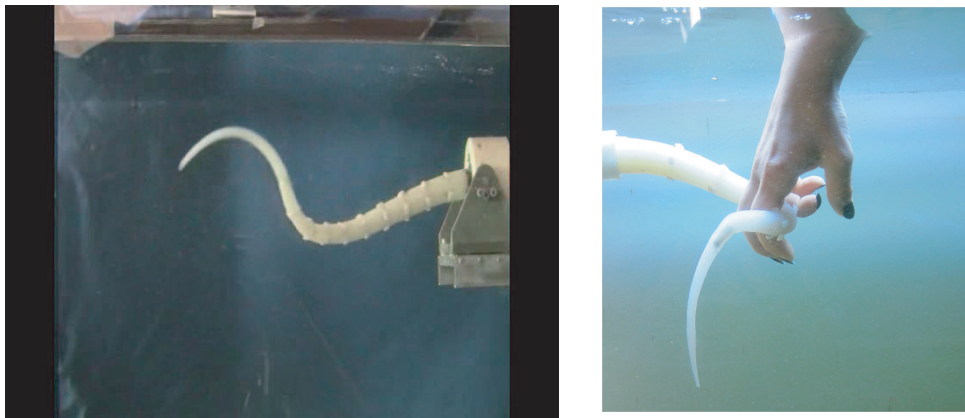


Figure 2.12 – *Octopus Arm robot bio-inspired from octopus*

2.12 has been developed to mimic the natural movements of a living octopus. The basic application of this waterproof soft robot is to perform underwater tasks such as movement and manipulation. The arm is used in water and it is able to elongate, shorten, and pull, as well as to bend in all the directions. As another example, a soft robot inspired from the caterpillar (a fluid-filled hydrostat) as shown in Fig. 2.13 is currently designed by the Tufts Neuromechanics and Biomimetic Devices Laboratory. The goal of these researches is to develop "Biomimetic Technologies for Soft Bodied Robots", i.e. to carry out investigations into innovative biologically-based technologies that use soft materials and to incorporate them into a new generation of highly flexible robot.

In short, all these researches indicate a high level of interest in the design, modeling, control, gait generation, etc., of highly articulated robots as well as soft robots that perform difficult tasks in highly unstructured and complex world.

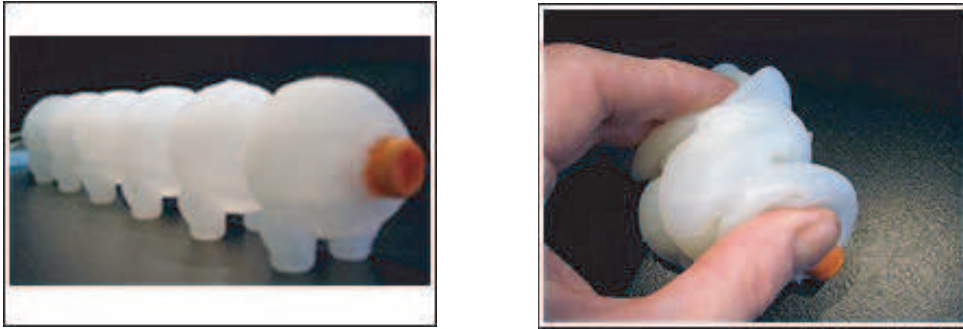


Figure 2.13 – *Soft robot inspired from caterpillar*

2.3 Modeling of Bio-inspired Locomotion Systems: The Lagrangian Picture

2.3.1 Definition of a Mobile Multibody System

In the following we adopt the model of multibody systems to derive a general unified framework devoted to the modeling of locomotion - in particular bio-inspired - in robotics. A multibody system is a set of bodies interconnected through internal joints, and with the rest of the world through external joints or contacts. In all the thesis, we will consider the constitutive bodies as well as the joints as being rigid. This assumption is in fact justified by many of the technological artifacts as those introduced before and can be partially released as we will see in chapter 6 when we will consider the case of soft robots. Based on this basic model, we will first consider the case of discrete multibody systems consisted of a finite set of countable bodies, and in chapter 5 we will see how it is possible to extend this model to the case of continuous robots. The usual model of rigid multibody systems is in fact very well developed in the context of manipulation, but much less when dealing with locomotion. In fact, contrary to classical multibody systems any body included in a locomotion system generally endure not only relative motion with respect to the other bodies, but also rigid overall motions due to the net displacements of the structure in the ambient space. Furthermore, these net motions are in general not imposed through explicit time laws, as on a manipulator mounted on a wheeled platform (or mobile manipulator for instance), but are produced at each time by the contact forces applied onto the whole system, i.e. by what we will name the locomotion dynamics of the system. By extension of the current terminology, in all the thesis we will name such a system a Mobile Multibody System or MMS and will distinguish it from classical Multibody System or MS. In spite of this semantic distinction, a MS is a particular case of MMS with rigid overall motions fixed through time laws, and in fact the methodological framework that we will develop about MMS will also be applicable to any MS. Finally referring to the usual designs of robotics, the "mobile multibody systems" will include a lot of robotic systems ranging

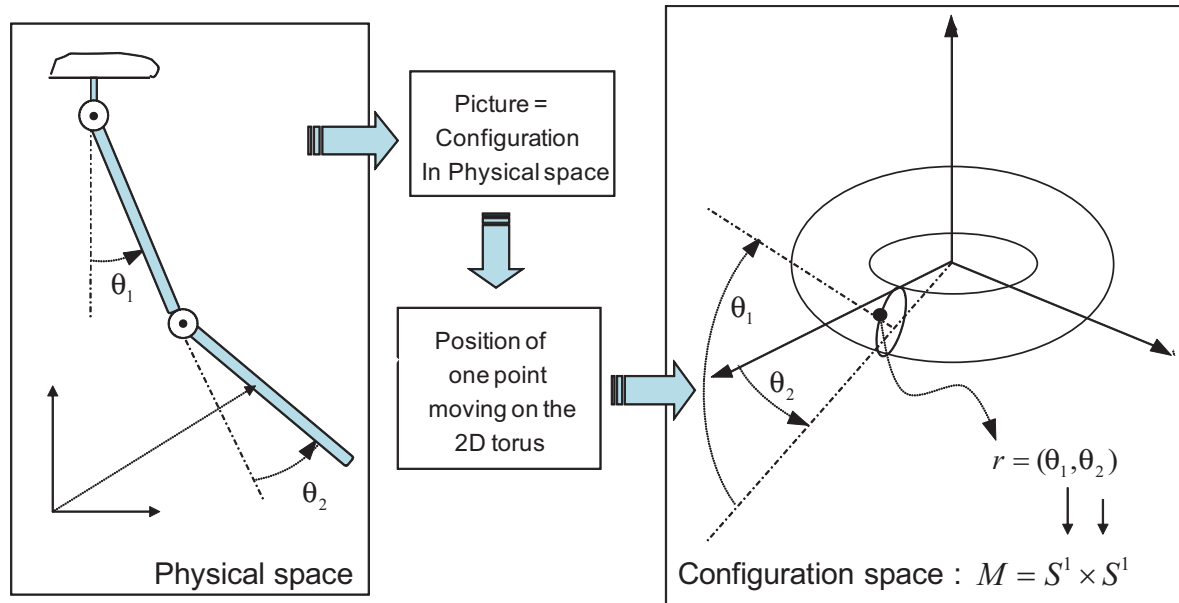


Figure 2.14 – Configuration space of a double pendulum: example manifold

from a fully constrained system (such as a wheeled platform) to free floating system (such as space shuttles, satellites, etc.) via the conventional industrial manipulators, the under-constrained nonholonomic systems (e.g. the snakeboard, the trikke), etc. Before introducing our own contributions to the modeling of these systems (purpose of chapters 3, 4, 5 and 6), in the rest of this chapter we focus onto the most general existing theory today available in this context: the Lagrangian theory.

2.3.2 Configuration Space of a Mobile Multibody System

By "Lagrangian" we here mean a theory which seeks to entirely derive the dynamics of a mechanical system from the knowledge of a unique function of its state, named Lagrangian of the system. Mathematically, such a theory enjoys a nice geometric basis which takes its roots in the theory of Riemannian geometry on manifolds. In mechanics, the key definition of this model is the concept of configuration manifold, or more simply of configuration space. Intuitively, the configuration space is the set of points whose coordinates are the parameters of the system. Thus, such a space is naturally endowed with a system of local coordinates or charts which gives the structure of a manifold to it. To any point of this abstract space, noted \mathcal{C} , corresponds one and only one configuration of the whole system in the physical space \mathbb{R}^3 . For a usual MS, as a manipulator with n revolute joints parameterized by the vector of joint angles $r = (r_1, r_2, \dots, r_n)^T$, each r_i being related to a circle S^1 , the configuration space is a hyper torus of dimension n defined by $\mathcal{C} = S^1 \times S^1 \times \dots \times S^1 = (S^1)^n$ (see Fig.2.14). Then, to a point of \mathcal{C} corresponds one configuration or "shape" of the MS in 3D space. In the case of MMS, the parametrization

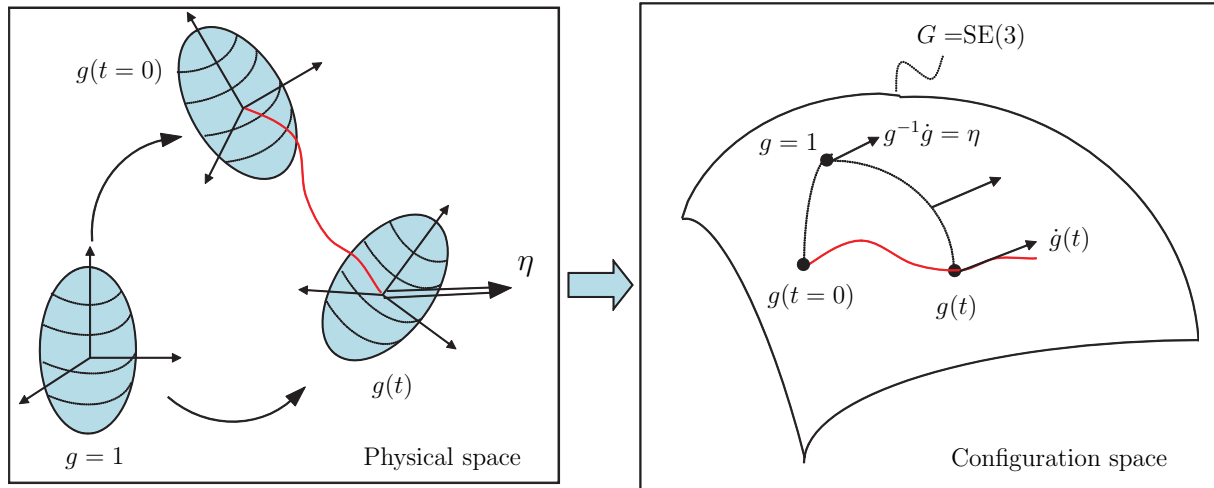


Figure 2.15 – Configuration space of a rigid body

of the system requires not only to manage its shapes with the previous space that we name in this context "shape space" and denote as \mathcal{S} , but also its absolute position and orientation in the ambient space. Hence, we will say that a MMS has internal degrees of freedom defining its shape, and external degrees of freedom related to an external frame fixed to space. In the Lagrangian picture of geometric mechanics, the external degrees of freedom are parameterized by the transformations g applying a frame fixed to ambient space on a frame moving with the MMS. This mobile frame is called "reference frame" and is generally attached to an arbitrarily distinguished body, named reference body, of the whole MMS. Of course the choice of this reference frame is not unique. In particular, among all the possibilities, we can define such a frame as a basis of three independent vectors attached to one of the body (which is the reference body) but originating in a non material point as for instance the gravity center of the whole MMS. In this case, the reference frame floats in space and is called "floating frame".

Geometrically, the transformations g , called "net transformations", are the elements of a Lie group G , i.e. a manifold endowed with an internal composition law satisfying the algebraic structure of a group¹. There are several possibilities of such a group according to the case under consideration. For example, when the reference frame endures one dimensional translations, $G = \mathbb{R}$. In case of translations in a plane, $G = \mathbb{R}^2$. In case of motions in plane, G is named the group of Euclidean displacements in \mathbb{R}^2 and denoted $G = \text{SE}(2)$. For translations in three dimensional space, $G = \mathbb{R}^3$ and for rotations in three dimensional space, G is the special orthogonal group $G = \text{SO}(3)$. All these, and others, are included into the most general group $G = \text{SE}(3)$ which defines the configuration space of a 3D rigid body and whose transformation elements g , can be represented by the 4×4

¹For more details on the Lie groups see Appendix B.

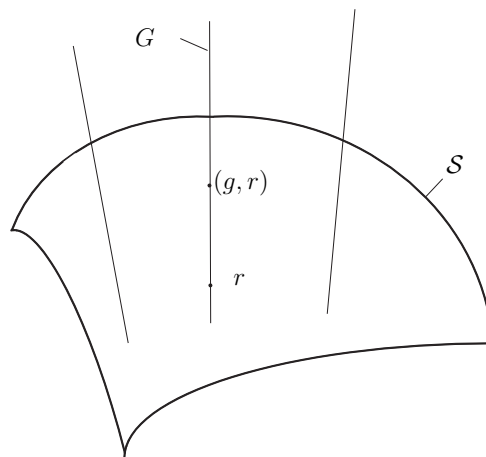


Figure 2.16 – Configuration space as the principal fiber bundle

homogeneous matrices:

$$g = \begin{pmatrix} R & p \\ 0 & 1 \end{pmatrix},$$

where R and P respectively denote the rotation and the translation parts of the transformation. On its group of configurations, a motion of the rigid body defines a time parameterized curve and any of its tangent vector \dot{g} is named a velocity of transformation (see Fig. 2.15). Now the composition of two transformation in \mathbb{R}^3 corresponds on the group to a translation of one by the other. Such a translation defining a map from points to points on G , we can take its tangent to translate \dot{g} in any point of G . In particular its translation on the left by g^{-1} moves the base point of \dot{g} from g to the unit element 1 and defines the twist of the body in its mobile frame or "material twist" η , which we detail as:

$$g^{-1}\dot{g} = \begin{pmatrix} \Omega & V \\ 0 & 0 \end{pmatrix} = \eta,$$

where Ω and V respectively denote the angular and the linear velocities of the body in its mobile frame². The set of the twists spans the tangent space to G at $g = 1$ noted T_1G . Once endowed with the commutator such that for any $\eta_1, \eta_2 \in T_1G$, $[\eta_1, \eta_2] = \eta_1\eta_2 - \eta_2\eta_1$, this space also defines the Lie algebra \mathfrak{g} of the group G , denoted $\mathfrak{se}(3)$ in the case of $\text{SE}(3)$. In the case of a MMS as shown in Fig. 2.17, to each configuration of the system corresponds a pair (g, r) , i.e. a point of the configuration space (see Fig. 2.16):

$$\mathcal{C} = G \times \mathcal{S}. \tag{2.1}$$

²In this chapter, we do not distinguish a skew symmetric angular velocity matrix from its 3×1 vector, this is the same in the case of $\text{SE}(3)$, where the 4×4 matrix η is not distinguished from its 6×1 vector.

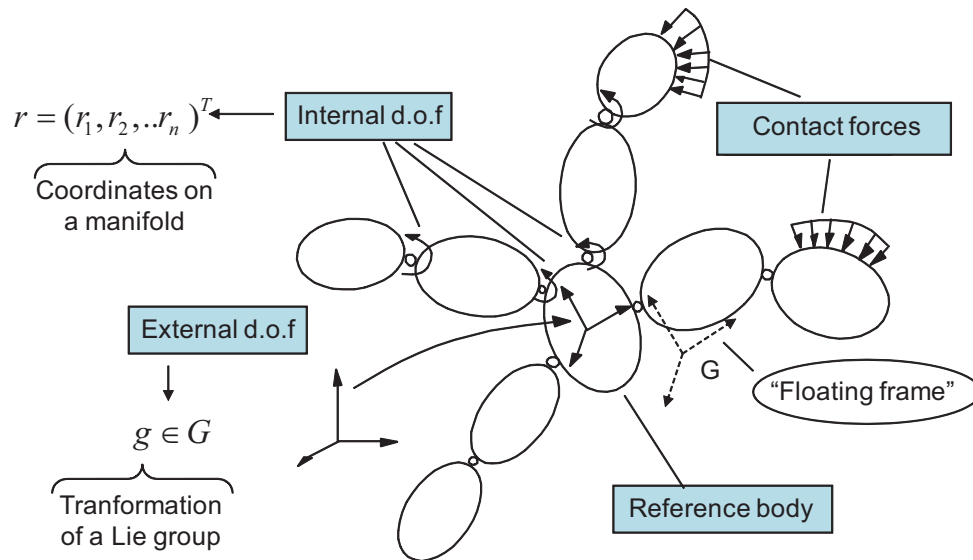


Figure 2.17 – Configuration space of a locomotion system: the principal fiber bundle

Such a space is indeed well known from differential geometry under the name of "principal fiber bundle". In differential geometry, a bundle is a manifold defined (at least locally) as the product of a manifold, named "base manifold" with another space, named "fiber" which is endowed with an algebraic structure. For example, if the fiber is a vector space, then the fiber bundle is a "vector bundle" (more generally a "tensor bundle"). If, as it is the case here, the fiber is a Lie group, then the fiber bundle is called a "principal fiber bundle". Finally, there exists a very rich corpus of results in geometric physics related to the structure of fiber bundle where it plays a crucial important role, for instance in gauge theory or general relativity. Hence, one of the strengths of the Lagrangian approach, whose we are going to remind a few key results, consists in having exploited this richness to use it to the benefit of a locomotion theory in robotics. In particular, in all the model of physics, a geometrical object is intimately associated to the concept of fiber bundle and even plays a more crucial role for the physicist; this is the concept of a "connection". However, before to introduce this concept and its use in locomotion, we are going to state the general problem that we will deal in the sequel of this thesis.

2.3.3 General Problem Addressed in this Thesis

The general problem of locomotion can be envisaged in multiple ways. In this thesis, we will solve the following problem. Knowing the time evolution on the internal joints r , we seek to compute:

1. The external net motions, which corresponds to solve the forward external dynamics called "forward locomotion dynamics" (see Block2, Fig. 2.18).
2. The internal torques which corresponds to solve the inverse internal dynamics or

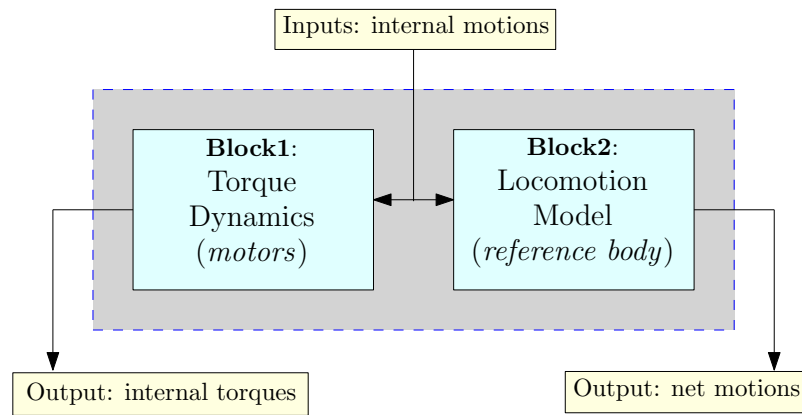


Figure 2.18 – Flow chart of the recursive locomotion dynamics algorithm

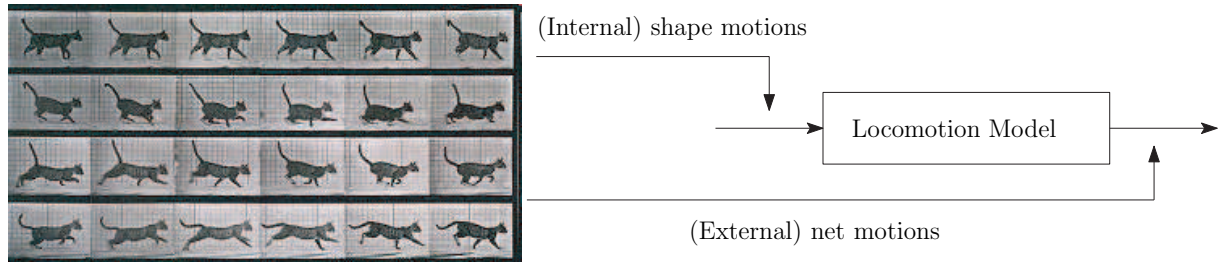
more simply the "inverse torque dynamics" (see Block1, Fig. 2.18).

This computation will be achieved by an algorithm whose general structure is illustrated in Fig. 2.18. Before to pursue our developments, let us do a few remarks.

First remark: The first dynamics are named "locomotion dynamics" since by relating the internal to the external degrees of freedom (d.o.f), they involve the model of the contact forces which is at the base of the locomotion. On the other hand, the second dynamics are those usually met on standard MS as in the case of manipulators where they find their instantiation in the well known computed torque algorithms.

Second remark: A natural question arises from this statement: Why we opt for the choice of internal motions as inputs, why not to take torques as input? There are two main reasons. Firstly, it is an easy task to specify the motion of a locomotion robot in terms of its internal motion, while on the other hand it is not easy at all to infer its net motions from the torques exerted by its actuators on its internal joints. Secondly, and in relation to the first argument, this problem (and its solution) can be coupled to biological experiments based upon locomotion films of the animals (see Fig. 2.19). In fact, once internal motions are extracted from such films, they can be imposed as inputs of the algorithm which feeds back the corresponding (modeled) external motions. Then, these external motions can be compared to the real ones extracted from the same films, and the matching of the measured and computed external motions, is a precious tool for the study of the model of the contact. In parallel, the inverse torque dynamics allows one to qualify the feasibility of the imposed internal motions with respect to the resources of actuators.

Third remark: Another relevant problem related to locomotion is the inverse of the above locomotion model, i.e. to find the internal shape motions in order to ensure given

Figure 2.19 – *Problem of locomotion*

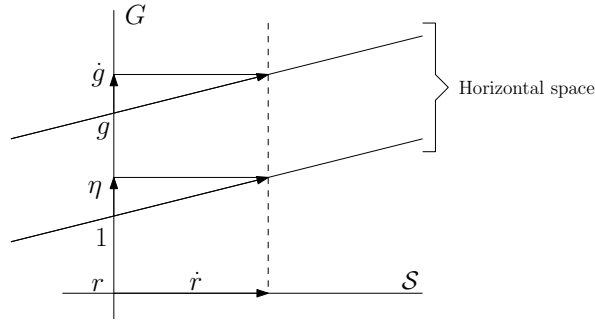
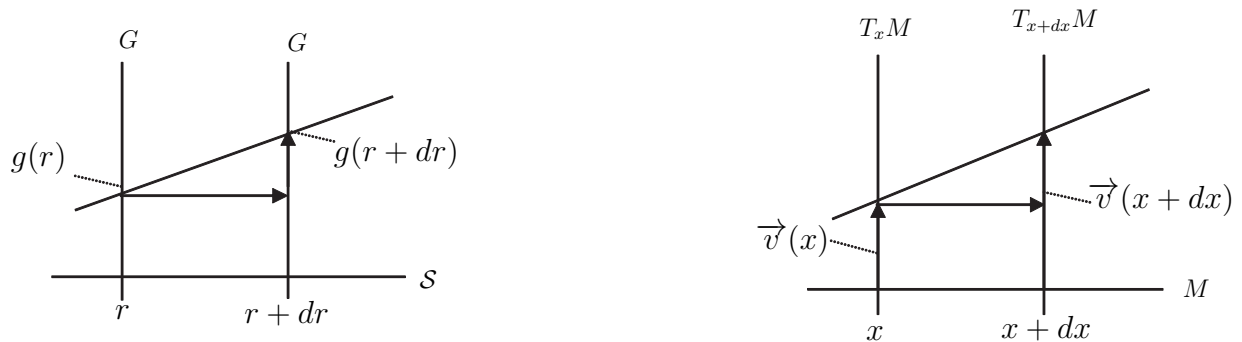
external net motions. This is a control problem (for instance solved by optimal control theory). This problem will be not dealt in this work. However, let us remark that instead of inverting the locomotion model, one can seek to minimize the error between actual and desired values of external motions with respect to the unknown shape motions. This alternative way to solve the inverse problem (as an optimization problem) indeed uses the forward locomotion model that we study in this thesis. Finally, the algorithmic solution to the problem stated above is a useful tool for the design of gaits and transient maneuvers. On the other hand, solving the forward internal dynamics (i.e. torques as input, internal and external motions as output) has its own interests when seeking to model passive internal deformations as those exploited by animals through compliant locomotion organs allowing them to reduce their energetic consumption.

2.3.4 Forward Locomotion Dynamics: The Kinematic Case

Now based upon these concepts, motions on the manifold \mathcal{S} are described by the internal shape motions while motions along Lie group G are the net motions of the reference body. Therefore, in order to solve the forward locomotion dynamics (see Fig. 2.19), we need to develop a relation between these two types of motions on the principal fiber bundle. In general to develop such relation, a dynamic model is required, i.e. the contact dynamics between the system and the surrounding medium has to be solved that we will discuss later in this chapter. However, there is a particular elegant case where locomotion is entirely defined by kinematics. This is when the model of the contact is encoded into what we name a connection on the principal fiber bundle of configurations [37]. In locomotion theory, such a connection exists when:

- there is a linear relation between small displacements on \mathcal{S} and small displacements on G ,
- this relation is such that (left) infinitesimal displacements in G are independent of g (left invariance).

This context is illustrated in Fig. 2.20. Replacing displacements by velocities, note that such a connection is free from dynamics and hence relates the net motions and the (in-


 Figure 2.20 – Connection between motions (\dot{r}) on \mathcal{S} and motions (η) on G (from [32])

 Figure 2.21 – Fiber bundle: (a) principal fiber bundle $G \times \mathcal{S}$; (b) Tangent bundle TM of a manifold M

ternal) shape motions through simple kinematics as follows:

$$\eta + \mathcal{A}(r)\dot{r} = 0. \quad (2.2)$$

On the principal fiber bundle this relation operates in any point (g, r) through $Ad_g(\eta + \mathcal{A}(r)\dot{r}) = 0$ which defines the space of admissible velocities of the system, or in the language of differential geometry, a particular distribution on \mathcal{C} named "horizontal space" as illustrated on Fig. 2.20. In the literature on geometric mechanics, $\mathcal{A}(r)$ is known as the local connection 1-form or more simply the local form of the connection. It is a function of the shape variables r only in virtue of the second condition mentioned above. In a more general way, a connection associates univocally a fiber element above a point over the base manifold to an element of the fiber above another infinitesimally close to the first one. This pairing is illustrated in Fig. 2.21(a) for a principal fiber bundle and for the tangent bundle of a manifold \mathcal{M} in Fig. 2.21(b). In fact, this last context is very well known from Riemannian geometry where to any metric is naturally associated a connection named Levi-Civita connection and noted ω consisting in parallel transporting any tangent vector on the manifold along the geodesics of the metric [21]. In order to illustrate such a Riemannian connection, let us consider the case of the two dimensional sphere S^2 endowed with the Euclidian metric induced from \mathbb{R}^3 . Along any piece of great

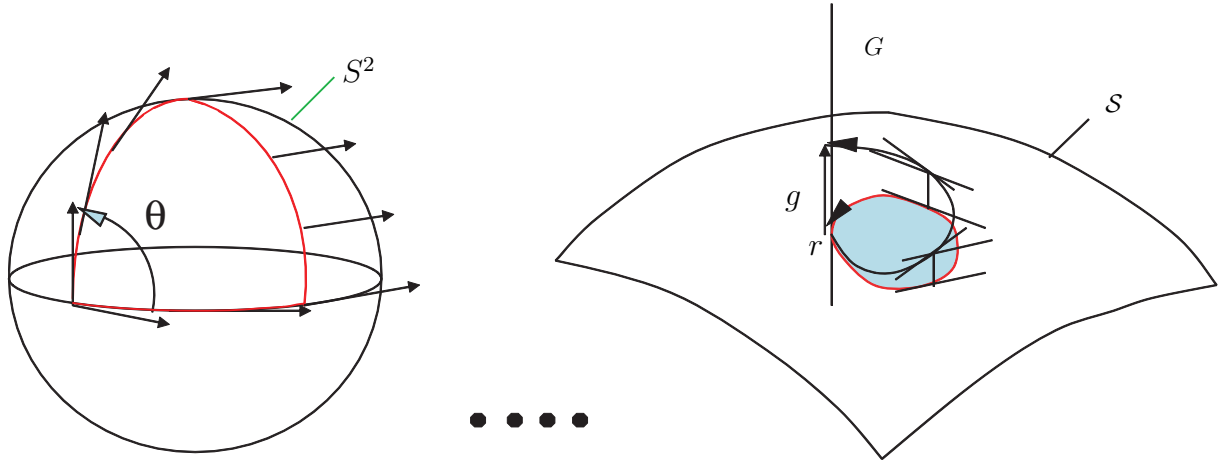


Figure 2.22 – (a) Gauss-Bonnet theorem illustrated on S^2 ; (b) A cyclic change of shape produces a net displacement in G

circle (which are the geodesics of S^2), a vector tangent to the sphere can be parallel transported from one point to another. Finally, by considering any curve on S^2 as an infinite set of infinitesimally short pieces of geodesics, parallel transport can be defined along any curve on S^2 . In particular, considering the particular case of closed curves starting and finishing in a same point of \mathcal{S} . When any vector is parallel transport along such a closed path, the vector after the whole transport appears as shifted of a given angle θ with respect to its antecedent. Furthermore, in virtue of the well known Gauss-Bonnet theorem this shift is in fact proportional to the area of the surface enclosed by the path and the curvature of the sphere (Fig. 2.22(a)). In other terms, this shift is a manifestation of the curvature of the manifold, and we have more generally:

$$\theta = \int_{Path} \omega = \int_{Enclosed\ area} d\omega, \quad (2.3)$$

which is nothing but a particular case of the Stokes theorem where $d\omega$ is named the curvature 2-form of the Riemannian manifold. Remarkably, this context can be recovered in the case of the principal fiber bundle of a MMS when the fiber group is commutative (Fig. 2.22(b)). In this case, we can associate to (2.2) a curvature 2-form $d\mathcal{A}$ relating the infinitesimally small closed paths of a given gait on the shape space to the corresponding net displacements it produces in the fiber. As a results, this geometric picture is a precious tool of gait generation in robotics [8, 51]. Now, we are going to remind the two cases in robotics where forward locomotion dynamics can be modeled through kinematics using a connection.

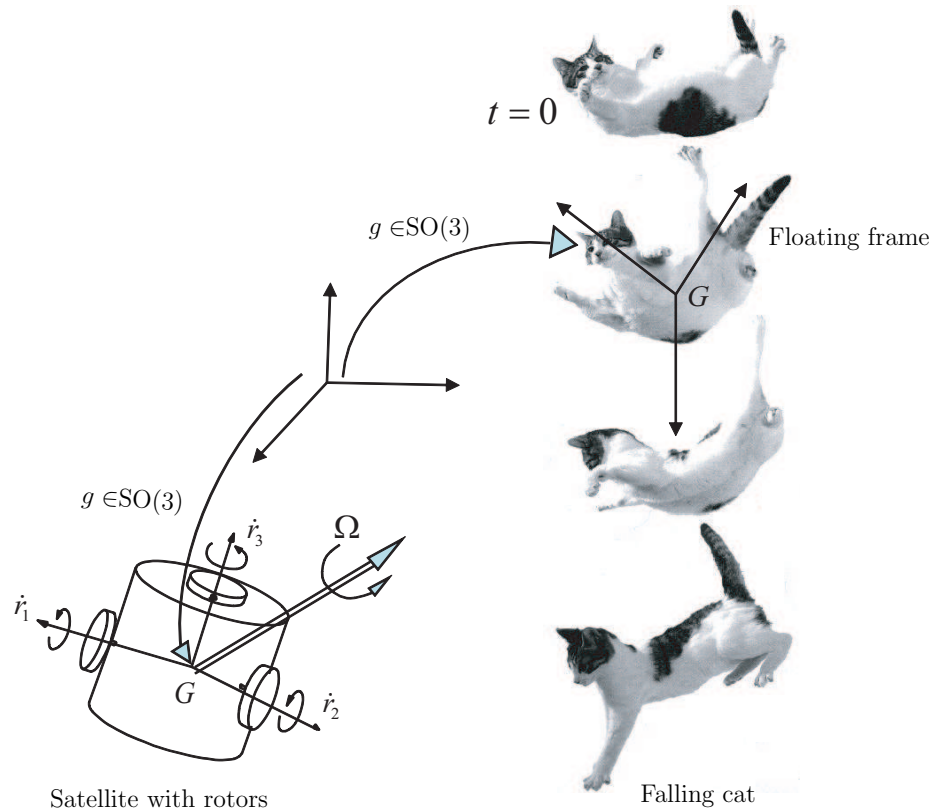


Figure 2.23 – Mechanical connection: falling cat and satellite with rotors

Case1: Mechanical Connection

Let us take the example of a free-falling cat or a satellite reorientation system³ as shown in Fig. 2.23. It is well known that a cat, initially maintained in a steady position with its four legs up and then dropped, reorients its head by twisting its body through a complex shape motion. Finally at the end of its fall, the cat touch down with the shape it had at the initial time but with the four legs on the ground. By doing so, the falling cat solves a problem of locomotion without any contact, since air has no influence at all on its motion. In fact, as an orbiting satellite equipped with inertia wheels, the cat use transfers of inertia momentum between its internal and external d.o.f in order to reorient itself. Referring to our geometric point of view, the configuration space of these systems (the cat and the satellite) is a principal fiber bundle $G \times \mathcal{S}$ with \mathcal{S} the shape space of the cat skeleton in one case and the three dimensional torus in the case of the full actuated satellite⁴, and $G = \text{SO}(3)$ in both cases. More precisely, we take the floating frame as the reference frame centered onto the gravity center of the system whose orientation with respect to a frame fixed to space is $R \in \text{SO}(3)$. Then, according to the law of conservation of angular momentum, since no external forces are applied onto the system, its total angular momentum remains null all along the motion, i.e. $\sigma = 0$. Therefore, in this case the

³This system is treated in detail as an illustrative example in chapter 4.

⁴Note that in the case of a failure of inertia wheels, nice problem of control accessibility arise.

locomotion is ruled by the following relation:

$$\sigma = \sigma_{\text{floating frame}} + \sigma_{\text{shape}} = 0, \quad (2.4)$$

where, $\sigma_{\text{floating frame}}$ is the angular momentum due the floating frame motions (i.e. the net motions of the reference body), while σ_{shape} is the angular momentum due to the internal shape motions. Thus, further analysis gives the angular momentum as follows:

$$R^T \sigma = I_o(r)\Omega_o + I_r(r)\dot{r} = 0, \quad (2.5)$$

where, I_o is the angular inertia matrix of the system when it is rigidified in its current shape r , or locked inertia matrix; and I_r is the inertia coupling matrix between internal and external accelerations. As the above relation is left invariant (I_o and I_r are R -independent) and linear, it defines the following connection:

$$\mathcal{A}(r) = I_o^{-1}(r)I_r(r) = 0. \quad (2.6)$$

In literature on geometric mechanics, such a connection is known as the "mechanical connection" [84]. It encodes all the information about the kinetic exchanges between the internal and external degrees of freedom. In spite of appearances, note that referring to our introductory considerations about animal locomotion, the locomotion mechanism used by the cat is again a kind of action-reaction principle, but where the inertia (Coriolis and centrifugal) forces replace the external forces of the general context. Finally, before to close this example, let us remark that applying the same considerations to the translations of the floating frame gives in virtue of the mass center theorem:

$$\mathcal{A}(r) = 0. \quad (2.7)$$

since no external forces is applied to the system. Thus, in this second case, the internal shape motions cannot act onto the linear motions of the floating frame. In simple words there is no "connection" between these motions.

Case2: Kinematic Connection

Now we consider the examples of an undulatory snake and a nonholonomic wheeled (unicycle) platform as shown in Fig. 2.24. The reference frame is attached to the head of the snake and to the platform. Since both systems evolves in the plane, the principle fiber bundle of their configurations is $SE(2) \times \mathcal{S}$ where \mathcal{S} stands for the space of the snake skeleton in one case, and for the two dimensional torus of the unicycle wheels, in the other. Once again, there exists a connection [60, 99, 89] between internal shape motions and external net motions of these two systems. This connection is deduced by assuming

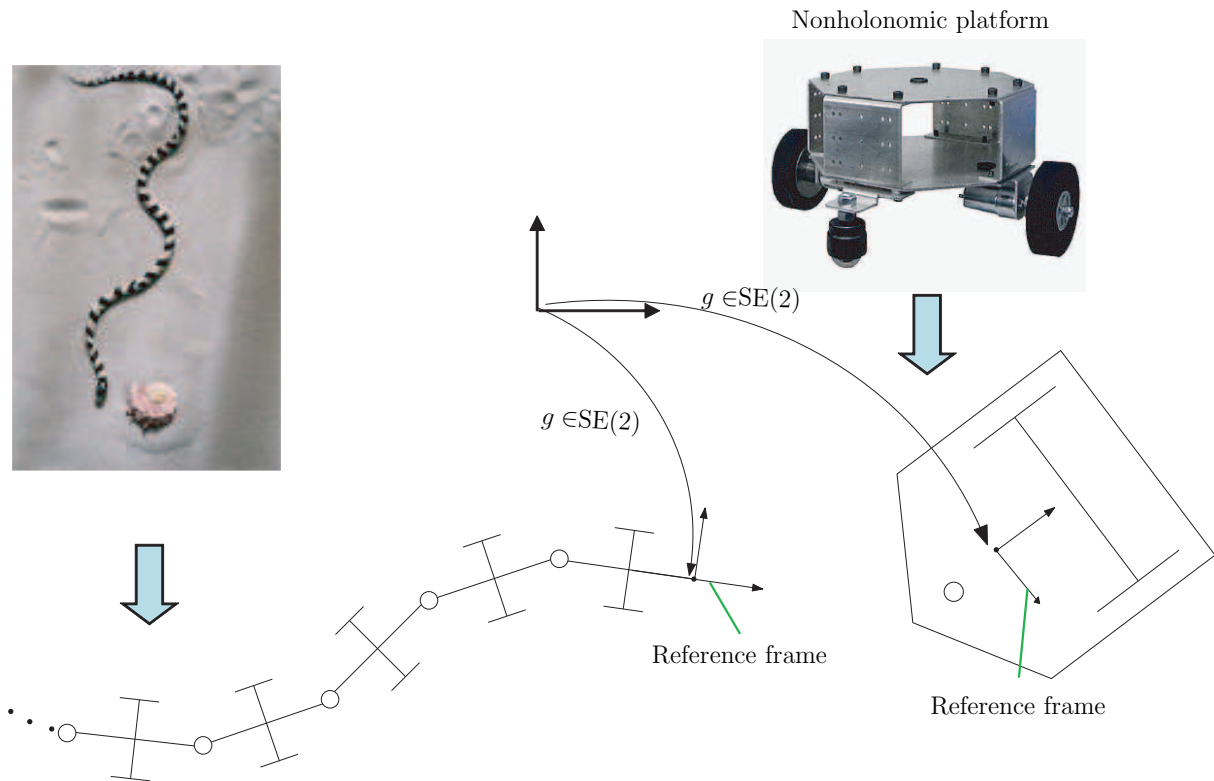


Figure 2.24 – *Kinematic connection: snake in lateral undulation and unicycle-platform*

that the contacts between the ground and the scales in one case, and the wheels in the other are modeled by ideal non-sliding (NS) and rolling without slipping (RWS) conditions⁵. To derive the expression of this connection, it suffices to insert the motion of the reference frame in the NS and RWS conditions and to gather in both cases a set of 3 ($=\dim(SE(2))$) independent nonholonomic constraints on the principal fiber bundle. In this way, we obtain the well known kinematic model of wheeled mobile platforms:

$$\eta + \mathcal{A}(r)\dot{r} = 0. \quad (2.8)$$

Where once again the $\mathcal{A}(r)$ matrix, being g independent, defines the local form of a connection known as the principal kinematic connection [8]. Note, that in case of snake-like robot, this connection is built up from the lateral non-sliding constraints (the wheels being passive), while the unicycle platform requires to use the rolling without slipping constraints of the two actuated wheels in addition. These nonholonomic constraints are discussed in detail in chapter 3 while dealing with wheeled systems.

⁵In the case of the snake, the strong frictional anisotropy of its skin along axial and lateral directions justifies such assumptions.

2.3.5 Forward Locomotion Dynamics: The General Case

As mentioned above, in the general case, dynamics are required to solve the forward locomotion model. Due to the structure of principal fiber bundle, the derivation of dynamics required a special attention. In particular, thanks to the structure of Lie group, the standard variational calculus applied on the charts of any manifold, can be replaced by an intrinsic calculus directly achieved on the group. Such a calculus has the advantage of providing formulation of the dynamics with the minimum of nonlinearities. Indeed, in such an approach, all the nonlinearities are due to the curvature of the group (which can be intuitively considered as a geometric manifestation of the non-commutativity on the algebraic side) and not to any of its parameterizations. This general idea has been in fact explored before the emergence of Lie groups in history of sciences, by Euler starting from the case of the rigid top. However, the geometric insight of the "Eulerian" approach of dynamics has waited a long time after Euler to find its complete elucidation in the works of Poincaré [93] followed by Cetajev [22], Rumyantsev [96] and Arnold [5] on the Russian side and by the American school of geometric mechanics after Marsden [77]. The idea of Poincaré consists in applying the Hamilton variational principle to the action of a system directly defined in terms of the transformations and not as a function of its parameters as in the approach due to Lagrange [17]. In our case, the action of the MMS will be defined as:

$$\int_{t_1}^{t_2} L(g, r, \dot{g}, \dot{r}) dt = \int_{t_1}^{t_2} (T(g, r, \dot{g}, \dot{r}) - U(g, r)) dt, \quad (2.9)$$

where L , T and U respectively denote the Lagrangian, the kinetic energy and the potential energy of the system on the principal fiber bundle of its configurations. Then, from Hamilton principle, the trajectory of the system between two fixed times t_1 and t_2 satisfies the stationarity condition:

$$\forall \delta g \text{ s.t. } \delta g(t_1) = \delta g(t_2) = 0, \quad \delta \int_{t_1}^{t_2} L(g, r, \dot{g}, \dot{r}) dt = - \int_{t_1}^{t_2} \delta W_{\text{ext}} dt, \quad (2.10)$$

where $\delta W_{\text{ext}} = \delta \zeta^T F_c$ stands for the virtual work of the eventual external non-conservative forces exerted by the contacts. Now replacing the (real and virtual) velocities of transformation by the material (or body related) twist of virtual displacements $\delta \zeta = g^{-1} \delta g$ and real velocities $\eta = g^{-1} \dot{g}$, and posing $L(g, r, g\eta, \dot{r}) = l(g, r, \eta, \dot{r})$ we can restate the above condition as:

$$\forall \delta \zeta \text{ s.t. } \delta \zeta(t_1) = \delta \zeta(t_2) = 0, \quad \delta \int_{t_1}^{t_2} l(g, r, \eta, \dot{r}) dt = - \int_{t_1}^{t_2} \delta W_{\text{ext}} dt. \quad (2.11)$$

where $l(g, r, \eta, \dot{r})$ is named the reduced left Lagrangian of the system, which takes the general form:

$$l(g, r, \eta, \dot{r}) = \frac{1}{2} (\eta^T, \dot{r}^T) \begin{pmatrix} \mathcal{M} & M \\ M^T & m \end{pmatrix} \begin{pmatrix} \eta \\ \dot{r} \end{pmatrix} - U(g, r). \quad (2.12)$$

Finally, when the potential energy U is independent of g , the Lagrangian is said to be left invariant since in this case we have:

$$L(g, r, \dot{g}, \dot{r}) = L(hg, r, h\dot{g}, \dot{r}), \quad \forall h \in G, \quad (2.13)$$

with in particular for $h = g^{-1}$, $L(1, r, g^{-1}\dot{g}, \dot{r}) = l(r, \eta, \dot{r})$. This properties is in fact a symmetry property very frequently checked by the external forces exerted onto a MMS. Now, to achieve the calculation of (2.11), we have to exploit two remarks, both resulting from the fact that the variation δ is applied while the time is maintained fixed. First r and \dot{r} being considered as inputs known by their time evolution, we have $\delta r = \delta \dot{r} = 0$. Secondly, we necessary have $\delta(dg/dt) = d(\delta g)/dt$ which leads:

$$\delta \eta = \frac{d\delta \zeta}{dt} + [\eta, \delta \zeta]. \quad (2.14)$$

This relation which rules the commutation between variation and derivation, plays a key role in variational calculus on Lie groups [93]. Finally, based on these remarks, it is possible to show that any solution to the previous variational principle is also solution of the Poincaré equations [93]:

$$\frac{d}{dt} \left(\frac{\partial l}{\partial \eta} \right) - \text{ad}_\eta^* \left(\frac{\partial l}{\partial \eta} \right) = X_g(U) + F_c, \quad (2.15)$$

where, $\text{ad}_{(\cdot)}^*(\cdot) : \mathfrak{se}(3) \times \mathfrak{se}(3)^* \rightarrow \mathfrak{se}(3)^*$ is the co-adjoint map of $\text{SE}(3)$, i.e. the dual map to the adjoint map of $\mathfrak{se}(3)$ on $\mathfrak{se}(3)$ denoted $\text{ad}_{(\cdot)}(\cdot)$ and defined by: $\text{ad}_{\eta_1}(\eta_2) = [\eta_1, \eta_2]$; F_c is the resultant of the contact forces and moments, while the $X_g(U)$ are the conservative external forces and $F_{\text{ext}} = F_c + X_g(U)$. Note here that $X_g(U)$ models the symmetry defect of the Lagrangian system whose expression is detailed in [17] in an intrinsic form. In the first part of this thesis, we will propose a Newton-Euler recursive algorithm [10] able to compute the locomotion dynamics that we finally reformulate as:

$$\begin{pmatrix} \dot{\eta} \\ \dot{g} \end{pmatrix} = \begin{pmatrix} \mathcal{M}^{-1} F \\ g\eta \end{pmatrix}, \quad (2.16)$$

where, $F = F_{\text{ext}} + F_{\text{inertial}}$. This algorithm will be then extended to the case of a class of continuous locomotion systems [11]. The second line of the above equation forms the reconstruction equation from η to g . Going Further into the Lagrangian dynamics, the ma-

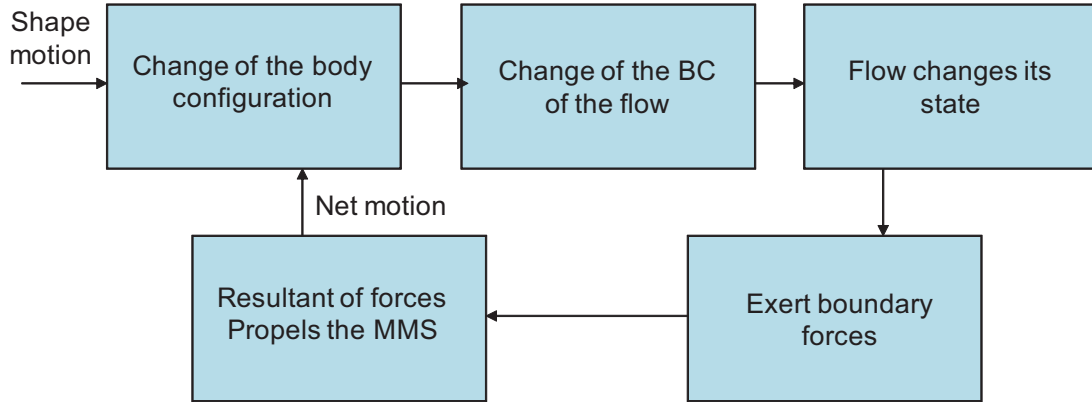


Figure 2.25 – Example of fluid contact dynamics

For difficulty in way of the dynamic locomotion model is the external forces which requires to solve the dynamics of the physical contact between the system and the surrounding which can be extremely difficult, as they are normally ruled by those of:

- the ground (non regular dynamics, tribology, etc.),
- a fluid (involving Navier-Stokes equations),
- more exotic surrounding as granular media (rheology).

For instance in case of swimming, the computation of F_{ext} requires to solve the fluid dynamics through the sequence of causes and effects shown in Fig. 2.25. Obviously, such computations are incompatible with the real time constraint imposed by robotics applications. Fortunately, in such a dynamic case, there exists subcases which require no physics but only geometry to solve the locomotion model. This geometric case occurs when F_{ext} is left invariant and Lagrangian [7]. That means that there exists a Lagrangian function $l_{\text{ext}}(r, \eta, \dot{r})$ such that:

$$F_{\text{ext}} = -\frac{d}{dt} \left(\frac{\partial l_{\text{ext}}}{\partial \dot{\eta}} \right) + \text{ad}_{\eta}^* \left(\frac{\partial l_{\text{ext}}}{\partial \dot{\eta}} \right), \quad (2.17)$$

then the dynamic locomotion model can be rewritten as follows:

$$\frac{d}{dt} \left(\frac{\partial (l + l_{\text{ext}})}{\partial \dot{\eta}} \right) - \text{ad}_{\eta}^* \left(\frac{\partial (l + l_{\text{ext}})}{\partial \dot{\eta}} \right) = 0.$$

Furthermore, if the system starts at rest, i.e. if we have the following situation at $t = 0$:

$$\frac{\partial (l + l_{\text{ext}})}{\partial \dot{\eta}} = 0,$$

Then:

$$\frac{\partial (l + l_{\text{ext}})}{\partial \dot{\eta}} = 0, \quad \forall t. \quad (2.18)$$

For example, in case of swimming at high Reynolds number, if a MMS is immersed in an ideal fluid initially at rest, the hydrodynamic forces exerted onto the system derive from a Lagrangian function which is equal to the added kinetic energy⁶ of the corresponding potential flow [67]:

$$l_{\text{ext}}(g, r, \eta, \dot{r}) = \frac{1}{2} (\eta^T, \dot{r}^T) \begin{pmatrix} \mathcal{M}_{\text{add}} & M_{\text{add}} \\ M_{\text{add}}^T & m_{\text{add}} \end{pmatrix} \begin{pmatrix} \eta \\ \dot{r} \end{pmatrix},$$

which implies, from (2.18) with l having the form of (2.12) with $U = 0$, the conservation law of kinetic wrench:

$$\tilde{\mathcal{M}}\eta + \tilde{M}\dot{r} = 0,$$

where $\tilde{\mathcal{M}} = \mathcal{M} + \mathcal{M}_{\text{add}}$, $\tilde{M} = M + M_{\text{add}}$. But then, with $\mathcal{A} = \tilde{\mathcal{M}}^{-1}\tilde{M}$:

$$\eta + \mathcal{A}\dot{r} = 0. \tag{2.19}$$

In this case we recover the same structure as that of the falling cat with \mathcal{A} sometimes named "hydrodynamic connection", this connection encoding the kinetic momentum exchanges between the body and the surrounding fluid [75, 59, 61, 81].

Remarks:

- Remark 1: Since in (2.19) $\eta \in \mathfrak{se}(3)$, the hydrodynamic connection, in contrast to the mechanical connection of the free-falling cat or the orbiting satellite, can change the position along with the orientation of the system. As a result, this simple model can explain how at high Reynolds, a MMS can swim in a quiescent fluid in all directions of translation and rotation.
- Remark 2: It is stated by the well known "scallop theorem" that any animal with one internal degree of freedom cannot move in a quiescent ideal fluid [94]. In fact, by opening its shell, such a "mathematical scallop" would loose the net displacement it would gain by closing it, so producing a zero net motion after one cycle. Modeling this locomotion mode by the "hydrodynamic connection" gives a straightforward geometric interpretation to this result. In fact from the context of 2.3.4, a closed one d.o.f path on \mathcal{S} encloses a surface of null area so forcing a zero net displacement after one cycle.
- Remark 2: Remarkably, swimming at low Reynolds can also be modeled through a connection named "Stokes' connection" [49]. In fact, this context has been the first

⁶The term "added" means here that this kinetic energy corresponds to the fluid mass accelerated with the body, in such a manner that it can be simply added to the body mass.

application of gauge theory on principal bundle to a case of animal locomotion by Shaper et Wilczek [102, 103]. Intuitively, in this case the inertial forces exerted onto the body by the fluid are negligible compared to the viscous ones. Thus the resultant of viscous forces which are essentially proportional to the body velocity field is zero. Once expressed on the principle bundle of configurations, these velocities are linear with respect to \dot{r} and η so leading to the Stokes connection.

In the above discussion, we discovered that behind an apparent wide diversity of locomotion modes, is hidden common geometric structures which draw a general subjacent picture. In order to complete this picture, we introduce in the next section a subclass of systems situated between the falling cat and the undulating snakes.

2.3.6 Forward Locomotion Dynamics: The Mixed Case

Let us now reconsider the case of constrained MMS where some of their constitutive bodies are wheeled. This subclass of MMS plays an important role in locomotion robotics. From this view point, the kinematic case of section 2.3.4 and the dynamic case of section 2.3.5 are two extreme cases where the number of constraints induced by the wheels on the fiber bundle is respectively maximum and minimum. Indeed, in the first case the number of independent constraints is equal to the dimension of the fiber while in the second, it is zero, since the contacts introduce no constraint⁷. Now, it is easy to imagine MMS which belong to the intermediate case where, the system is constrained but with a set of constraints whose number does not exceed the dimension of the fiber. As a particular case of such MMS, relevant with robotics but also with sport mechanics, we consider in the following of this section those submitted to no other contact forces, except those transmitted by the constraints. Indeed, in this case the MMS locomotion dynamics obeys partly to kinetic exchanges between internal and external d.o.f and partly to kinematic contacts. Slightly anticipating the results of the next chapter, let us remark that in such a case, the reference twist of net motions takes the general form:

$$\eta = H(r)\eta_r + J(r)\dot{r} \quad (2.20)$$

where J and H are two matrices, the columns of H spanning in each r , the kernel of the constraints. As a consequence η_r defines the (admissible) reduced twist. Before pursuing, let us remark here that when $J = 0$ and $H = 1$, we recover the unconstrained case of section 2.3.5, while when $H = 0$, the general kinematic model (2.20) degenerates into the kinematic case of section 2.3.4 with the kinematic connection $J = \mathcal{A}$. Now, since r is

⁷This does not mean that the MMS does not contain any wheels. In fact, if there are some, they are modeled by forces themselves ruled by a physical contact law, e.g. of Coulomb.



(a)



(b)

Figure 2.26 – Under-constrained systems (a) Snakeboard (b) Trikke

known in (2.20), the forward locomotion dynamics (2.16) reduces to:

$$\begin{pmatrix} \dot{\eta}_r \\ \dot{g} \end{pmatrix} = \begin{pmatrix} \mathcal{M}_r^{-1} F_r \\ g(H\eta_r + J\dot{r}) \end{pmatrix}, \quad (2.21)$$

which rules the time evolution of η_r , and is named reduced dynamics. Such a reduced dynamics will be found by projecting the unconstrained dynamics onto the kernel of constraints, what will give the expressions of the reduced inertia operators and forces \mathcal{M}_r and F_r . As examples of MMS ruled by such equations, we find all the systems whose locomotion principle consists in transferring kinetic momentum from internal degrees of freedom to external ones via non-holonomic constraints as the snakeboard, the trikke (see Fig. 2.26) but also a skier sliding down a steep slope, or an ice-skater performing a given choreography. In this last case the ice-skater will use the mechanical connection when jumping over the ice and a constrained version of it when touching it. Finally, these last examples explain why in the original theory of Lagrangian locomotion due to Marsden and co-workers the above reduced twist η_r is replaced by a reduced momentum $p = \frac{\partial l}{\partial \eta_r}$, with l as the reduced Lagrangian (2.12) and the reconstruction equation by a connection equation [87].

2.3.7 Inverse Torque Dynamics

Now, we discuss the second model, i.e. torque dynamics (see Block1, Fig. 2.18), which computes the internal torques of the locomotion system. Reconsidering the Lagrangian (2.12), and forcing the kinematic model (2.20) in it, the reduced Lagrangian on the ad-

missible subspace of the principal fiber bundle can be written as:

$$\tilde{l}(\eta_r, r, \dot{r}) = \frac{1}{2} \eta_r^T \mathcal{M}_r \eta_r + \eta_r^T (H^T M) \dot{r} + \frac{1}{2} \dot{r}^T (m + J^T \mathcal{M} J + J^T M + M^T J) \dot{r}, \quad (2.22)$$

which from Lagrange equations give the torque dynamics as follows:

$$\tau = \frac{d}{dt} \left(\frac{\partial \tilde{l}}{\partial \dot{r}} \right) - \left(\frac{\partial \tilde{l}}{\partial r} \right). \quad (2.23)$$

In the resulting equations, the reduced net accelerations and velocities $\dot{\eta}_r$ and η_r are assumed to be known from the forward locomotion dynamics (2.21), and (2.23) finally gives the torques that actuators have to provide in order to ensure the desired internal and computed external motions. As a particular case, in the fully constrained case where (2.20) changes into the connection equation (2.8), the two first terms of (2.22) can be removed. Moreover, when the number of actuators increases, the torques generally depend upon the choice of \mathcal{A} which is not unique as in the case of systems with redundant actuated wheels.

2.4 Conclusions

In this chapter, we have done a brief overview of several aspects related to locomotion in robotics. Starting from animals and pursuing with real robots, we have showed that there is a need of developing methodological tools for designing, modeling, control, motion planning and others, of a new generation of robots with a lot of degrees of freedom. As regards, the modeling aspects, this chapter presented the basic Lagrangian picture using reduced velocities instead of momentum. A particular attention has been paid to the problem of the classification of systems. We have discovered that behind an apparent diversity, many locomotion modes share common geometric structures. In spite of its purely qualitative value, this knowledge is useful for solving locomotion problem since it allows one to produce general solutions and is in itself a precious tool for guiding intuition. This classification effort has been achieved in the perspective of solving a general basic problem that will be investigated further in the sequel of this thesis. This problem consists in computing the net motions (solution of the forward external dynamics) of a MMS as well as the internal torques (solution of the inverse internal dynamics) from the knowledge of the internal joints evolution. Although the Lagrangian approach offers a general synthetic point of view of a wide class of multibody systems, it suffers from lack of something. In particular, when the number of internal degrees of freedom increases, Lagrangian models and their associated algorithms are more and more heavy to handle even numerically. Furthermore, in the asymptotic case of continuous robots, the Lagrangian models of the external and internal dynamics are even impossible to reach.

For all these reasons, and also to complete the knowledge on robotics locomotion, we will work in the rest of this thesis on the production of an alternative solution to the Lagrangian formulation well known under the name of Newton-Euler formulation. This formulation will lead to easily programmable and fast algorithms, capable of solving both forward external and inverse internal dynamics. In spite of these pragmatic goals, we will pursue our effort of classification, by tuning the Newton-Euler formulation to the geometric mechanics point of view. Finally, we can now state more precisely the major contributions of the thesis. They are twofold.

1. Firstly, a general algorithm is proposed to solve the forward external and inverse internal dynamics of discrete mobile multibody systems.
2. Secondly, this algorithm is extended to the novel bio-inspired continuous systems such as hyper-redundant systems and soft body robots.

With these tools one can study the problems posed by locomotion of a wide range of systems as it is illustrated in this thesis by applying them to certain systems ranging from the discrete MMS to a class of continuous systems bio-inspired from terrestrial elongated body animals.

Part I

Discrete Systems: Mobile Multibody Systems

3

Locomotion Dynamics Algorithm of Mobile Multibody Systems

3.1	Description of a Mobile Multibody System	41
3.1.1	Basic Assumptions	44
3.1.2	Configuration Spaces of a Mobile Multibody System	45
3.1.3	Basic Mathematical Expressions	46
3.2	Luh and Walker Manipulator Dynamics	47
3.3	Overview of the Proposed Algorithm	49
3.3.1	Scope of the Algorithm	50
3.4	The Unconstrained Mobile Multibody System	54
3.4.1	Dynamic Locomotion Model	54
3.4.2	Torque Dynamics	56
3.4.3	Unconstrained Cases with Symmetries	58
3.5	The Constrained Mobile Multibody System	59
3.6	Kinematics of a Constrained Mobile Multibody System	59
3.6.1	Kinematics of an Isolated Nonholonomic Body	59
3.6.2	Kinematics of the Composite Body S_o^+	61
3.6.3	Admissible Spaces of the Reference Body	66
3.7	Dynamics of the Constrained Mobile Multibody System	67
3.7.1	Reduced Dynamic Locomotion Model	67
3.7.2	Reduced Torque Dynamics	70
3.8	Computational Algorithm	73
3.8.1	Summary of Discussion	73
3.8.2	Generalized Algorithm Execution	76
3.9	Conclusions	77

In this chapter the Newton-Euler based locomotion dynamics are presented for discrete mobile multibody systems with tree-like topology. Before entering into the details of these developments, let us first remind its principle in the simple case of a usual manipulator. In this case, the general problem of section 2.3.3 reduces to the inverse torque dynamics, which is trivially solved by removing the fiber kinematic variables in (2.22, 2.23):

$$\tau = m(r)\ddot{r} + Q_{in}(r, \dot{r}) + Q(r) \quad (3.1)$$

where C and Q represent the generalized forces due to centrifugal and Coriolis accelera-

tions, and those due to gravity, respectively.

Now, it is well known that to compute the torques (3.1), the most efficient approaches exploit the chained topology of the system to replace the heavy Lagrangian-based $O(n^4)$ computations of (3.1), by $O(n)$ recursive computations. Among the recursive solutions, Newton-Euler based algorithms are undoubtedly the most efficient. They are based on the dynamic balance of bodies (using Newton's laws and Euler's kinematic momentum theorem) isolated one after the other, that are reconnected through the kinematic constraints imposed by the joints. Then, due to the chained topology, these two sets of equations define recursions on the body kinematics as well as on the interbody forces. Exploiting this implicit formulation, Featherstone [40] and Luh and Walker [115] have respectively proposed fast computational algorithms to solve the forward and inverse torque dynamics of a manipulator, respectively. In its principle, the Luh and Walker algorithm is based on two recursions on the body indices, both included into a global time loop. Based on the joints motion (inputs), the first recursion computes the body kinematics (position, velocities and accelerations). Then, the second (backward) recursion uses these body kinematics to compute the interbody torques (outputs). Beyond these computational complexity aspects, Newton-Euler models lead to a set of few very compact formulations (can be expressed even manually) independent of the number of joints.

In spite of these advantages, till to date the Newton-Euler formulation has been only applied to a very few particular cases of bio-inspired locomotion systems. In [72], the Newton-Euler formulation has been used with a friction contact model of ground forces in order to address the inverse dynamics problem of a creeping snake. In [110], the Newton-Euler formulation has been used to solve the forward dynamics of a planar snake submitted to non-smooth contact forces. Nevertheless, although these works extend the Newton-Euler formulation to multibody system dynamics, the resulting algorithms do not exploit the recursive formulation and they do not generalize (to the locomotion) either the inverse Luh and Walker algorithm or the Featherstone forward algorithm. Looking further for such generalized algorithms, in [62] the Luh and Walker inverse algorithm and the Featherstone forward Newton-Euler based dynamic algorithm have been proposed for studying the locomotion of an eel-like robot, while in [82] a Luh and Walker computed torque algorithm has been proposed to solve the inverse dynamics of a mobile manipulator. In spite of these recent works, to our knowledge no general Newton-Euler framework for the inverse recursive dynamics of multibody systems with joints and wheels has been proposed till today.

Although the Newton-Euler formulation has been discussed by various authors, the unified computation for the Newton-Euler based locomotion dynamics in the context of geometric

mechanics is new to our knowledge. This chapter presents such a unified computational method based on the Newton-Euler formulation for the discrete mobile multibody systems with tree-like topology [10]. For this purpose, the existing computational torque algorithm of Luh and Walker [115], which is limited to manipulators, is extended to a wide range of mobile multibody systems. Furthermore, using some of the concepts of geometric mechanics, the approach also proposes a general classification of a wide range of systems going from fully-constrained systems (e.g. snake-like robots) to free-floating systems (e.g. shuttle arms, satellites, etc.) via the standard or mobile manipulators and including any of the under-actuated nonholonomic systems such as the snakeboard, the trikke, etc.

In the sequel of this chapter, first of all a general description of the mobile multibody system is given followed by a set of basic assumptions to fix the idea. Then, in section 3.2, the Luh and Walker computational torque algorithm is presented for a manipulator to explain the fundamental recursions based upon the Newton-Euler formulation. In section 3.3, the extension of the Luh and Walker algorithm to a wide class of mobile multibody systems is briefly discussed in order to streamline the basic modeling approach. Then, in a first step, in section 3.4 the extension process is applied on a subclass of mobile multibody systems called as "unconstrained systems". In a second step, in section 3.5 the algorithm is extended to another subclass of mobile multibody systems called as "constrained systems" through a projection process based upon the nonholonomic kinematic constraints of the wheels. At the end, these extensions allow us to propose a general unified algorithmic framework to solve the problem of locomotion of a vast variety of the mobile multibody systems.

3.1 Description of a Mobile Multibody System

A mobile multibody system considered here is an open chain¹ tree-like structure of rigid bodies interconnected through joints as shown in Fig. 3.1. The structure is composed of $p + 1$ rigid bodies, denoted as $S_o, S_1, S_2, \dots, S_p$, as shown in Fig. 3.1. These tree-like structures are labeled by following the usual Newton-Euler conventions [64]. The indices of bodies increase from the reference body S_o toward the terminal bodies² as illustrated in Fig. 3.1. In all subsequent computations the index i is strictly reserved to denote the antecedent of the current index j . Moreover, the bodies numbering fulfills the following convention: $i < j$. With this numbering convention, let us note that in the case of simple chain systems $i = j - 1$ whereas for a tree-like structures i is not necessarily equal to $j - 1$,

¹Closed kinematic chains can be modeled as open chains with certain preliminary steps [63]. A brief description is available in Appendix A.1.

²A tree-like mobile multibody system may have more than one terminal body.

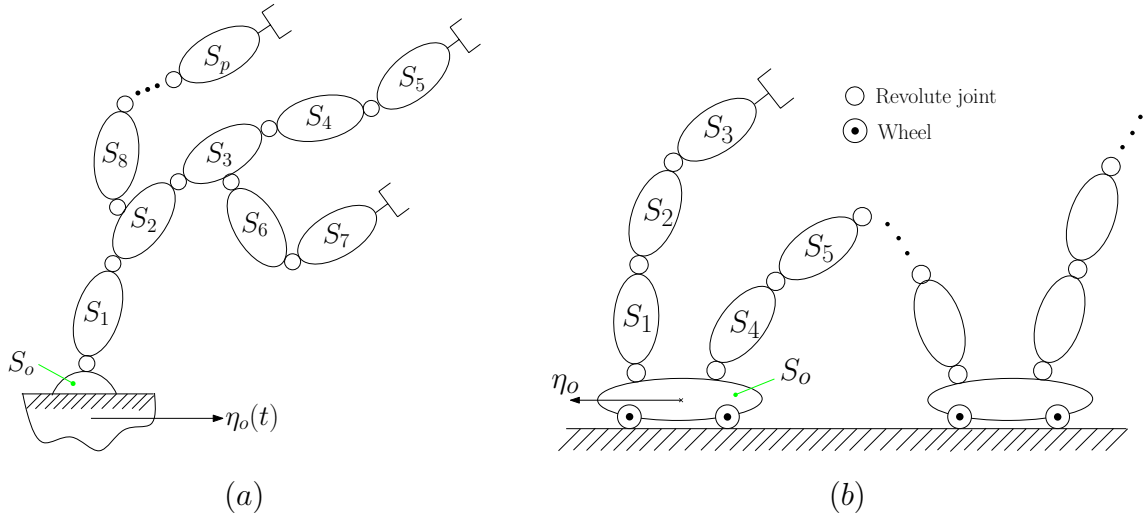


Figure 3.1 – Tree-like structure of a mobile multibody system: (a) Manipulator; (b) Wheeled system

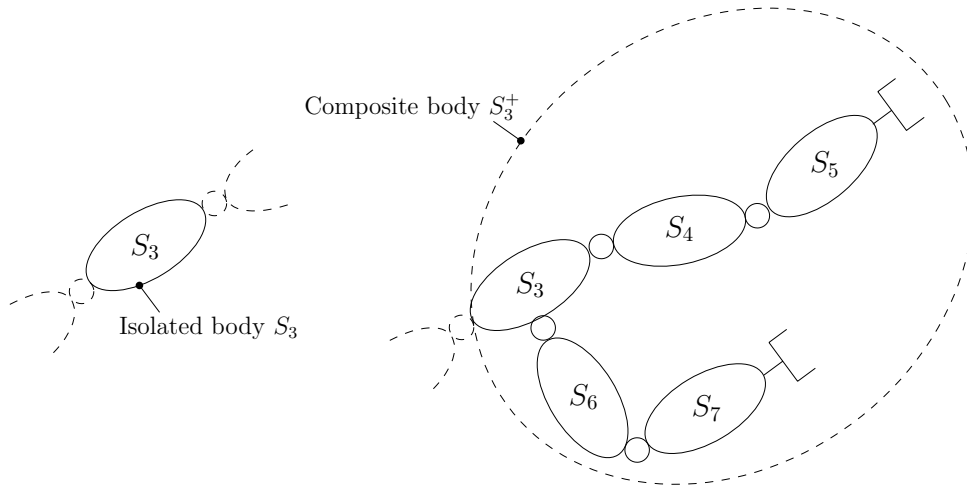


Figure 3.2 – Concept of isolated and composite body

e.g. in Fig. 3.1(a) for body S_8 we have S_2 as its antecedent body then $j = 8$ and $i = 2$.

In the following, we also need the concept of composite body [117]. Any composite body S_j^+ is a rigid body that consists of body S_j and all its successors up to the terminal bodies frozen in the current shape and animated by the motion of body S_j . While S_j alone is considered as an isolated body S_j as explained in Fig. 3.2 (for a body S_3 of the manipulator in Fig. 3.1(a)). In particular, for any mobile multibody system, the composite reference body S_o^+ consists of the whole structure enduring an overall rigid motion as that of S_o . Finally, in the following, S_o^+ means the reference body S_o rigidly connected to the rest of the structure, while S_o alone means the reference body S_o considered as a single isolated body.

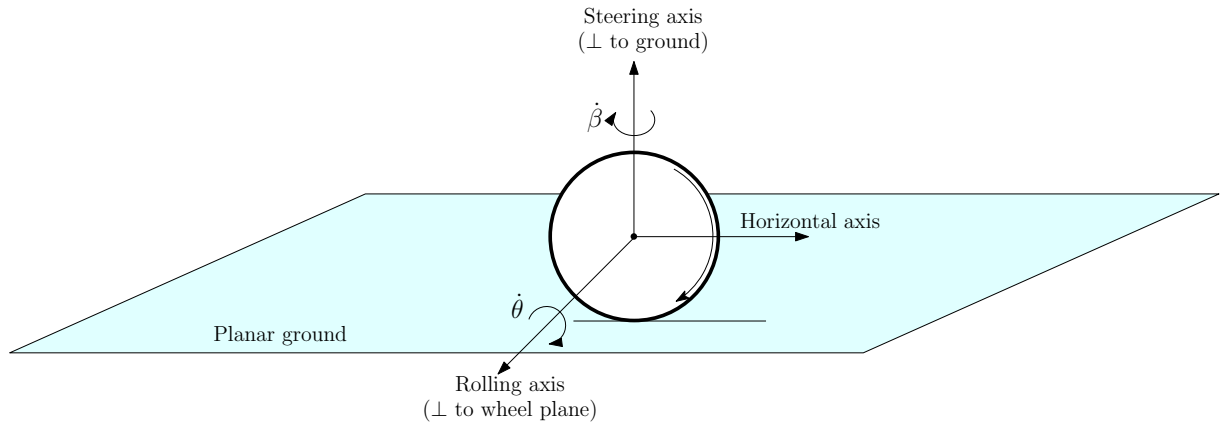


Figure 3.3 – Axes of a wheel

Joints: Types and Parametrization

For the sake of simplicity the bodies are supposed to be interconnected through single degree of freedom revolute joints only. Such restriction on types of joint is not basic since what follows can be easily extended to a mobile multibody system with any type of joint. The joints are assumed to be ideal, i.e. no backlash and no friction. Each interbody joint is parameterized by a joint angle r_j and is actuated by a motor producing the torque τ_j around the joint unit axis a_j with $j \in \{1, 2, \dots, p\}$, where:

$$r = \begin{pmatrix} r_1 & r_2 & \cdots & r_p \end{pmatrix}^T, \quad \tau = \begin{pmatrix} \tau_1 & \tau_2 & \cdots & \tau_p \end{pmatrix}^T.$$

Wheels: Types and Parametrization

Any body may be connected to the ground through wheels (see Fig. 3.1(b)). The bodies are classified into "wheeled bodies" (whose set of indices is noted as \mathbb{N}_w) and "unwheeled bodies" (with indices in \mathbb{N}_{uw}). Wheels are mainly classified into omnidirectional and unidirectional wheels. The unidirectional wheels are further classified as "steering", "castor" or "fixed wheels" depending upon whether their steering axes (axes normal to the ground as shown in Fig. 3.3) are actuated, free or clamped in the bodies as shown in Fig. 3.4.

The modeling requires two sets of kinematic parameters for the wheels. Since we do not take wheels' inertia into account, thus these parameters are not considered as actual configuration parameters. For any body S_j , the first set is that of steering wheel angles gathered in the vector β_j , while the second set is that of the rolling angles gathered in the vector θ_j as follows:

$$\theta_j = \begin{pmatrix} \theta_{j,1} & \theta_{j,2} & \cdots & \theta_{j,N_j} \end{pmatrix}^T,$$

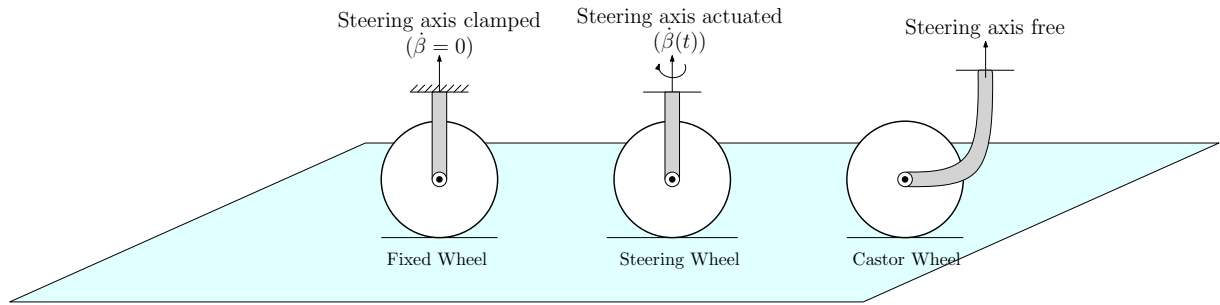


Figure 3.4 – Types of unidirectional wheel

where N_j is the total number of wheels (excluding castor wheels) of any body S_j , $j \in \mathbb{N}_w$. It is assumed that the actuated wheels (if any) are contained only by the reference body S_o . Thus, if N_a wheels are actuated around their rolling axes (cf. Fig. 3.3), then θ_o can be block-partitioned into vectors of actuated and free (passive) wheels as follows:

$$\theta_o = \begin{pmatrix} \theta_{oa} \\ \theta_{of} \end{pmatrix}, \quad (3.2)$$

with $\dim(\theta_{oa}) = N_a$. Finally, for all the actuated wheels, the $(N_a \times 1)$ vector of their motor torques is denoted as Γ .

3.1.1 Basic Assumptions

As the assumptions made during the above discussion will be referred during the course of this work. Therefore, we sum up the basic assumptions of the proposed algorithm as follows.

1. The ground is considered as a horizontal planar surface. This imposes three planar ground holonomic constraints on the general 3D motion of the wheeled bodies. One constraint prevents the body from vertical translation whereas the other two prevent it from rolling and pitching rotations.
2. If the system has actuated wheels, then the only body equipped with actuated wheels will be the reference body S_o .
3. The inertia of the wheels are negligible compared to those of the bodies. Consequently, they will only intervene in the modeling through their kinematics.
4. Castor wheels (if any) just maintain the horizontal static balance with respect to the ground. Consequently, they will be removed from the modeling process.
5. All the bodies of the system are connected with each other through (holonomic) joints that are assumed to be ideal (no friction or backlash) and actuated.

6. In case of ideal³ wheels, the wheels are modeled through nonholonomic constraints which verify the non-sliding and rolling without slipping conditions.
7. As this article deals only with the dynamics, we assume that the compatibility conditions required to ensure the mobility of the mechanism under the constraints induced by the ideal wheels are verified through design and motion planning.

Note that the last two assumptions are only valid in case of ideal wheels.

3.1.2 Configuration Spaces of a Mobile Multibody System

Let us first remind that the expected solution (in the form of algorithm) to the general problem stated in section 2.3.3 is structured into two blocks according to the flow chart of Fig. 2.18. When dealing with the inverse torque dynamics (Block1 of Fig. 2.18), the configuration space of the mobile multibody system will be defined as the following Cartesian power of Lie group:

$$\mathcal{C}_1 = \underbrace{G \times G \times \dots \times G}_{p+1 \text{ copies}} = G^{p+1}, \quad (3.3)$$

where each copy of G stands for the configuration Lie group of each of the $p+1$ bodies considered as isolated from one another. Also, in this first definition S_o is not distinguished from the other bodies. On the other hand, when dealing with the locomotion model (Block2 of Fig. 2.18), S_o becomes the reference body, i.e. a body whose motions fix the overall rigid motions of the whole structure with respect to which the shape variations are measured. As such, the motion of S_o may be imposed through arbitrary known time-laws (as in the particular case of a manipulator where S_o is the base), or more generally it is computed through the time-integration of the locomotion model whose configuration space is defined as the principal fiber bundle:

$$\mathcal{C}_2 = G \times (S^1)^p. \quad (3.4)$$

In this second definition of the mobile multibody system configuration space, $(S^1)^p$ stands for the configuration shape-space \mathcal{S} of the p revolute joints parameterized by the vector r of joint angles, while G is the configuration Lie group of the composite reference body S_o^+ (i.e. of S_o connected to the whole mobile multibody system structure locked in its current shape). Finally, since in any case $G \subseteq \text{SE}(3)$, we will generally consider that $G = \text{SE}(3)$ and will remove this assumption in next chapter while dealing with illustrative examples.

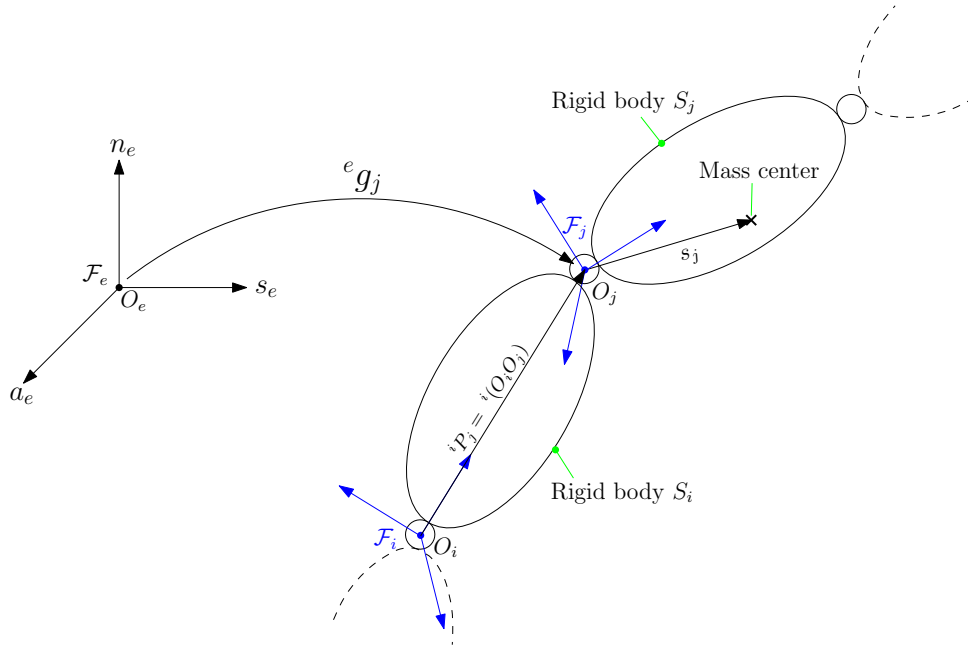


Figure 3.5 – Newton-Euler parametrization of a mobile multibody system

3.1.3 Basic Mathematical Expressions

Before starting the mathematical modeling of mobile multibody systems, let us first present some basic mathematical terms and expressions that will be helpful for better understanding of the subsequent equations. For any vector $V \in \mathbb{R}^3$, V^\wedge (or \widehat{V}) denotes the cross-product matrix of V while if $V = (v^T, \omega^T)^T \in \mathbb{R}^6$, then $V^\wedge = \begin{pmatrix} \widehat{\omega} & v \\ 0 & 0 \end{pmatrix}$, where $\omega \in \mathbb{R}^3$ and $(\widehat{V})^\vee = V$. Each body S_j is given a body frame $\mathcal{F}_j = (O_j, s_j, n_j, a_j)$ at the joint center O_j as shown in Fig. 3.5, where a_j is the axis of rotation of the single degree of freedom revolute joint. Like all the other frames used in the following, \mathcal{F}_j is orthonormal. The ambient geometric space is provided with a fixed spatial frame denoted as $\mathcal{F}_e = (O_e, s_e, n_e, a_e)$. The rigid body transformation (elements of $\text{SE}(3)$), which maps any frame \mathcal{F}_l onto any other frame \mathcal{F}_k is represented by a 4×4 homogeneous matrix denoted by ${}^l g_k \in \text{SE}(3)$, e.g. the transformation matrix ${}^i g_j$ which maps the frame \mathcal{F}_i of body S_i onto the frame \mathcal{F}_j of body S_j , is given as follows:

$${}^i g_j = \begin{pmatrix} {}^i R_j & {}^i P_j \\ 0 & 1 \end{pmatrix},$$

where, ${}^i P_j = {}^i(O_i O_j)$ and ${}^i R_j$ is a (3×3) orientation matrix of \mathcal{F}_j with respect to \mathcal{F}_i . Moreover, \mathcal{M}_j denotes the (6×6) inertia matrix, containing the inertia components of

³When the contact between the wheel and the ground is perfect.

body S_j on $\text{se}(3)^* \otimes \text{se}(3)$, expressed in \mathcal{F}_j . Where:

$$\mathcal{M}_j = \begin{pmatrix} m_j \mathbf{1}_3 & -m_j \widehat{s}_j \\ m_j \widehat{s}_j & I_j \end{pmatrix}, \quad (3.5)$$

where, m_j is the mass of body S_j , whereas $m_j s_j$ and I_j are the vector of first inertia moments and the matrix of second inertia moments, respectively, both expressed in \mathcal{F}_j . Note that if a parameter is expressed in a frame other than its own body frame, then a superscript is used before a vector or matrix to denote the frame e.g. ${}^o\mathcal{M}_j$ denotes the inertia matrix of body S_j expressed in \mathcal{F}_o , while \mathcal{M}_j denotes the inertia matrix of body S_j expressed in \mathcal{F}_j . Furthermore, adopting the \mathbb{R}^6 space of twists as definition of $\text{se}(3)$, the twist of S_j is defined by a (6×1) vector of body velocity components expressed in \mathcal{F}_j denoted by η_j , while its time derivative $\dot{\eta}_j$ denotes the (6×1) vector of body accelerations, where:

$$\eta_j = \begin{pmatrix} V_j \\ \Omega_j \end{pmatrix}, \quad \dot{\eta}_j = \begin{pmatrix} \dot{V}_j \\ \dot{\Omega}_j \end{pmatrix}.$$

Passing to the dual, F_j denotes the (6×1) wrench of the forces applied onto body S_j by its antecedent body S_i , expressed in its own body frame \mathcal{F}_j . Where:

$$F_j = \begin{pmatrix} N_j \\ C_j \end{pmatrix}.$$

Moreover, any twist can be pushed forward from \mathcal{F}_i onto \mathcal{F}_j through the relation: ${}^j\eta_i = \text{Ad}_{jg_i}\eta_i$, where Ad_{jg_i} is known as the (6×6) adjoint map operator and is given by:

$$\text{Ad}_{jg_i} = \begin{pmatrix} {}^jR_i & {}^jR_i {}^i\widehat{P}_j^T \\ 0 & {}^jR_i \end{pmatrix}. \quad (3.6)$$

On the dual side, any wrench can be pulled back from \mathcal{F}_j to \mathcal{F}_i through: ${}^iF_j = \text{Ad}_{jg_i}^T F_j$, while $F_{\text{gyr},j}$ and $F_{\text{ext},j}$ denote the wrenches of gyroscopic and external forces applied onto S_j , respectively.

3.2 Luh and Walker Manipulator Dynamics

Since the proposed algorithm is an extended version of the Newton-Euler based Luh and Walker computational torque algorithm [115] for industrial manipulators. Thus we recall it in detail here for a tree-like manipulator with single degree of freedom revolute joints where the net motions of the base S_o are predefined as shown in Fig. 3.1(a). As explained in Fig. 3.6, the purpose of the algorithm is to compute at each current time t of a global

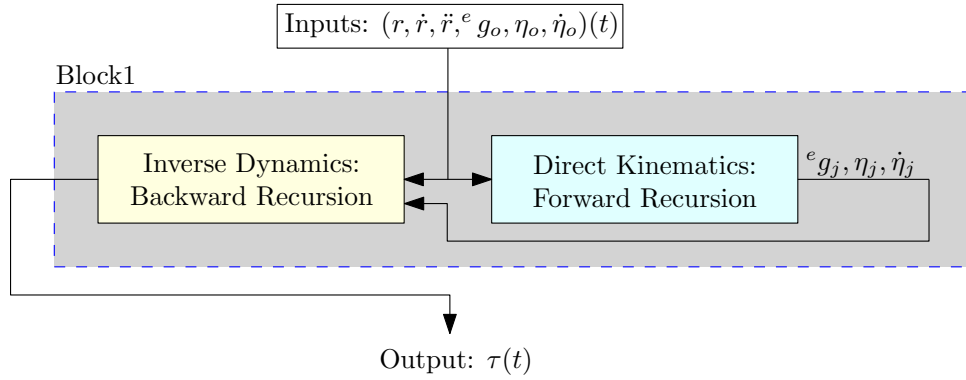


Figure 3.6 – Luh and Walker computational torque algorithm

time loop, the vector of joint torques $\tau(t)$ as output, from the knowledge of the current values of inputs: $({}^e g_o, \eta_o, \dot{\eta}_o, r, \dot{r}, \ddot{r})(t)$. Consequently, it is the inverse dynamics, called as internal torque dynamics in this work, whose computations are done with the following two sets of recursive equations.

Forward recursion: this first set solves the following recursive direct kinematic model to compute each body kinematics:

for $j = 1, 2, \dots, p$, and with boundary conditions: $({}^e g_o, \eta_o, \dot{\eta}_o) = ({}^e g_o, \eta_o, \dot{\eta}_o)(t)$:
Computation of the body transformations:

$${}^e g_j = {}^e g_i {}^i g_j(r_j). \quad (3.7)$$

Computation of the body velocities:

$$\eta_j = \text{Ad}_{j g_i} \eta_i + \dot{r}_j A_j. \quad (3.8)$$

Computation of the body accelerations:

$$\dot{\eta}_j = \text{Ad}_{j g_i} \dot{\eta}_i + \zeta_j(\dot{r}_j, \ddot{r}_j). \quad (3.9)$$

Where, A_j is a (6×1) vector given by:

$$A_j = \begin{pmatrix} 0 \\ a_j \end{pmatrix}, \text{ with } a_j = \begin{pmatrix} 0 \\ 0 \\ 1 \end{pmatrix}.$$

We also denote by $\zeta_j(\dot{r}_j, \ddot{r}_j)$, a (6×1) vector as follows:

$$\zeta_j = \begin{pmatrix} {}^j R_i(\Omega_i \times (\Omega_i \times {}^i P_j)) \\ {}^j \Omega_i \times \dot{r}_j a_j \end{pmatrix} + \ddot{r}_j A_j. \quad (3.10)$$

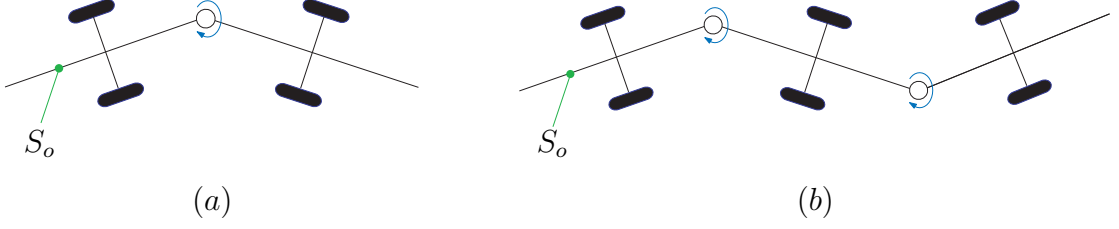


Figure 3.7 – Wheeled mobile multibody system with passive wheels: (a) Two-axes mobile multibody system; (b) Three-axes mobile multibody system

Backward recursion: this second set solves the following recursive dynamic model to compute the interbody wrenches:

for $j = p + 1, p, \dots, 1$, and with the boundary conditions: $F_j = 0$, if S_i is a terminal body free of any contact forces:

$$\begin{cases} \text{if } i = j - 1 : & F_i = \mathcal{M}_i \dot{\eta}_i - F_{\text{ext},i} - F_{\text{gyr},i} + \text{Ad}_{j_{g_i}}^T F_j; \\ \text{else:} & F_{\text{gyr},i} = F_{\text{gyr},i} - \text{Ad}_{j_{g_i}}^T F_j. \end{cases} \quad (3.11)$$

Finally, the applied wrenches are projected onto the joint axes to obtain the joint torques as follows:

$$\text{for } j = 1, 2, \dots, p : \quad \tau_j = A_j^T F_j. \quad (3.12)$$

Where, $F_{\text{gyr},i}$ is a (6×1) vector of gyroscopic wrenches given by the following relation:

$$F_{\text{gyr},i} = - \begin{pmatrix} \Omega_i \times (\Omega_i \times m_i s_i) + \Omega_i \times m_i V_i \\ \Omega_i \times (I_i \Omega_i) + m_i s_i \times (\Omega_i \times V_i) \end{pmatrix}. \quad (3.13)$$

Finally, let us note that the recursive Newton-Euler based model (3.7-3.11) gives the dynamics of the system in its configuration space defined by (3.3)⁴, while on the other hand the Lagrangian model (3.1) of the same robot expresses its dynamics in the configuration space defined as the manifold of its joint coordinates $\mathcal{S} = (S^1)^p$.

3.3 Overview of the Proposed Algorithm

The Luh and Walker algorithm is limited to the case where the net motions of the reference body S_o are imposed à priori as depicted in Fig. 3.1(a). Now to discuss the generalization of the Luh and Walker algorithm let us consider a planar wheeled mobile multibody system as shown in Fig. 3.7 where the wheeled bodies are connected through actuated single degree of freedom revolute joints. By imposing motions on the actuated joints, the bodies of this system are subjected not only to internal "shape motions", like those found in a

⁴With one copy of G removed since the motion of the base is now imposed.

manipulator, but also to net rigid motions defined as those of an arbitrary reference body S_o . Consequently, the desired generalization of the Luh and Walker algorithm requires a knowledge of the net motions of S_o which are generally no longer imposed but must be computed from a new model, here called as *locomotion model*. This model is a direct (or forward) model since it relates the motions of joints to those of the reference body S_o . This relation can be modeled either through a simple kinematic model (i.e. not involving forces) or through a dynamic model. Therefore, we can quickly conclude that there exists two types of locomotion models.

Dynamic locomotion model: where the net motions of the mobile multibody system are related to the joint motions via a dynamic model.

Kinematic locomotion model: where the net motions of the mobile multibody system are related to the joint motions via a kinematic model.

Before going into detailed discussion of such locomotion models, let us remind that external forces of any nature of contact other than that of ideal wheels, such as those of fluid contact or ground contact via non-ideal wheels, are supposed to be known through state dependant physical laws. While in case of ideal wheels, the contact is modeled through nonholonomic constraints (see assumption 6 in section 3.1.1). With this consideration that is based upon the modeling approach of external contacts, the mobile multibody systems can be classified into the following two main categories (see also Fig. 3.8).

Unconstrained mobile multibody system: any mobile multibody system (wheeled or unwheeled) whose external contacts are modeled through external forces model by applying some physical laws, e.g. the use of a friction model for a ground contact via non-ideal wheels.

Constrained mobile multibody system: any wheeled mobile multibody system connected to the ground through wheels where the wheeled contact is modeled as the nonholonomic (non-sliding and/or rolling without slipping) constraints.

3.3.1 Scope of the Algorithm

The aim of this section is to illustrate the scope and principle of the proposed algorithm based upon the locomotion model. Because this new locomotion model plays a key role in the general algorithm, we will now consider it case by case starting with the wheeled mobile multibody systems.

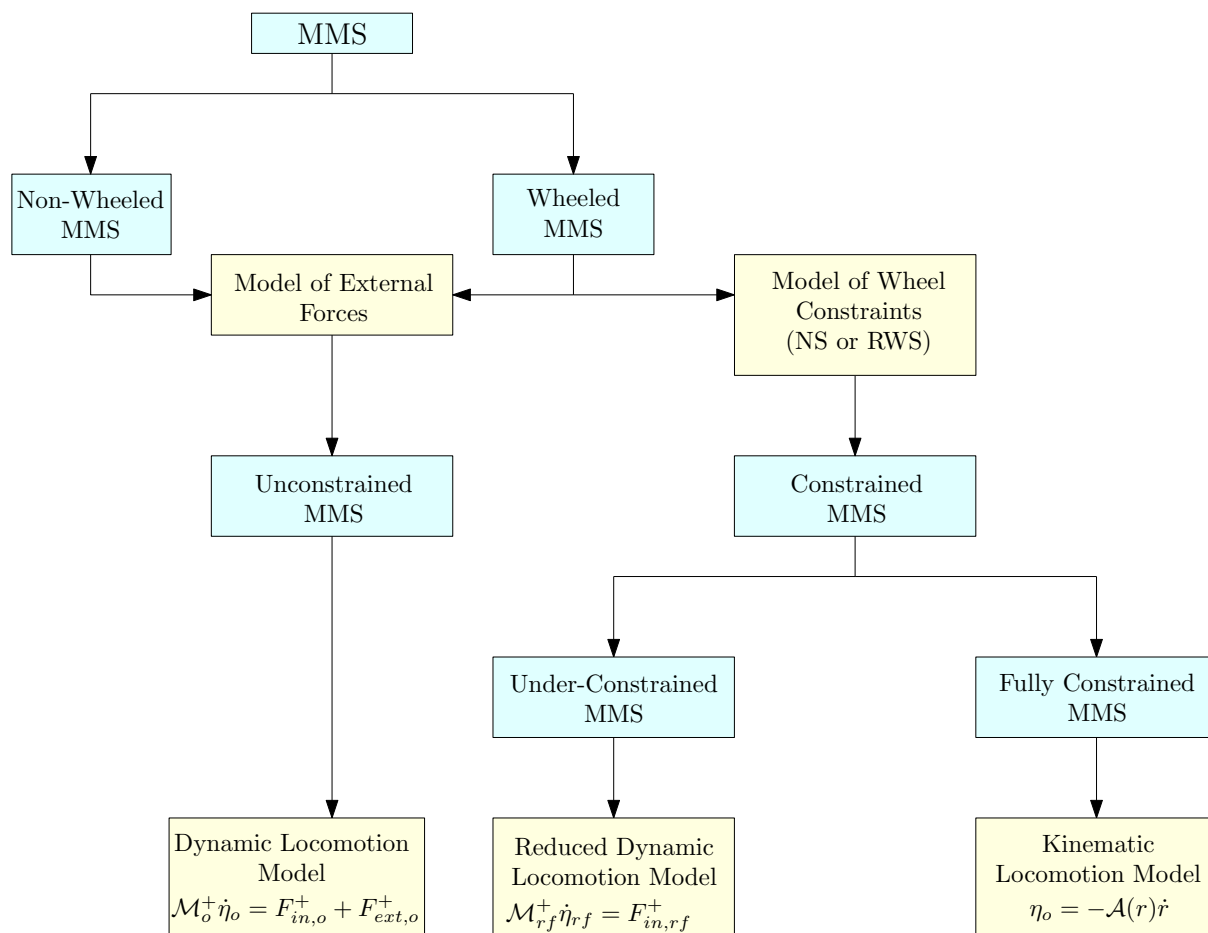


Figure 3.8 – Scope of locomotion dynamics algorithm

3.3.1.1 Wheeled Mobile Multibody Systems

Example 1: Two-Axles Mobile Multibody System

First, let us consider the wheeled system given in Fig. 3.7(a). In this case the wheels, being passive, introduce only two independent kinematic (nonholonomic) non-sliding constraints. These two constraints are insufficient, compared to the 3 degrees of freedom of S_o in the planar ground, to calculate its net motions through pure kinematics, i.e. through a *kinematic locomotion model*. Consequently, in this case the locomotion model is achieved by the dynamic balance of S_o controlled by the joint motions, i.e. through a *dynamic locomotion model*. As such, this balance includes a model of the contact forces which can be defined in the following two ways:

1. As external frictional forces, in case of unconstrained mobile multibody systems.
2. By the Lagrange multipliers which force the non-sliding constraints, in case of constrained mobile multibody systems.

In the first unconstrained case, the dynamic locomotion model takes the following form:

$$\mathcal{M}_o^+ \dot{\eta}_o = F_{\text{in},o}^+ + F_{\text{ext},o}^+, \quad (3.14)$$

where \mathcal{M}_o^+ , $F_{\text{in},o}^+$ and $F_{\text{ext},o}^+$ are, respectively, the composite inertia matrix, inertia wrench and external wrench of the whole structure, expressed in reference frame \mathcal{F}_o . The $\dot{\eta}_o$ is the acceleration of the composite reference body S_o^+ . In the second constrained case, the contact forces can be eliminated by projecting the above dynamic locomotion model (3.14) into the kernel of the wheels constraints. The locomotion model then takes the following alternative "reduced" form:

$$\mathcal{M}_{rf}^+ \dot{\eta}_{rf} = F_{\text{in},rf}^+, \quad (3.15)$$

where, we find the same quantities as in (3.14) but projected into the kinematically admissible space of S_o^+ restricted by the two non-sliding constraints. Consequently, in the sequel of this work, such locomotion model will be called as the *reduced dynamic locomotion model*. Let us note that in this case the system will be called as under-constrained mobile multibody system as shown in Fig. 3.8.

Moreover, when developing such locomotion models, we will see that the computation of all the matrices appearing in (3.14,3.15) can be carried out recursively by exploiting the Newton-Euler formulation.

Example 2: Three-Axles Mobile Multibody System

Continuing the generalization, if we now add another wheeled body identical to the first two (see Fig. 3.7(b)), the number of non-sliding kinematic constraints becomes three which is sufficient to entirely specify the net motions of S_o^+ through pure kinematics i.e. with a kinematic locomotion model. Consequently, the locomotion model turns into a kinematic locomotion model of the following general form:

$$\eta_o = -\mathcal{A}(r)\dot{r}(t), \quad (3.16)$$

where \mathcal{A} is a matrix that depends upon the vector of the joint variables r . Let us note that the reference acceleration is no longer deduced from the dynamic locomotion model (3.14 or 3.15) but from the time-differentiation of the kinematic locomotion model (3.16). Therefore, in this case the system will be called as fully-constrained mobile multibody system as mentioned in Fig. 3.8, since the net motions of the composite reference body S_o^+ are fully defined by the kinematic constraints (here the three non-sliding constraints). As another example, the under-constrained mobile multibody system in Fig. 3.7(a) becomes a fully-constrained mobile multibody system if one of its wheels is actuated since in this case the rolling without slipping constraint imposed by the actuated wheel acts as the

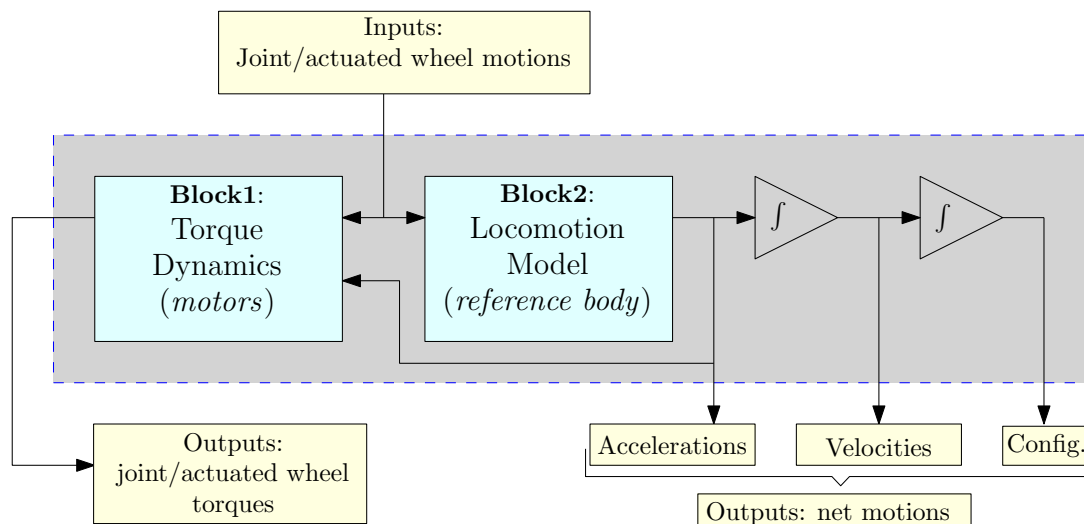


Figure 3.9 – Flow chart of the recursive locomotion dynamics algorithm

third kinematic constraint along with the two non-sliding constraints. Furthermore, in this case since $\dot{\eta}_o$ is known from kinematic locomotion model, the dynamics (3.14) can be exploited for the computation of external contact forces and in particular to compute the torque applied onto the actuated wheels.

Finally, if the number of actuated wheels or axles increases, the kinematics become over-constrained and the constraints must be compatible for mobility to be possible. In the following, this compatibility is presumed to be verified as it depends on the design and/or the gait generation [101], two problems not dealt with in this research work.

3.3.1.2 Unwheeled Mobile Multibody Systems

The Luh and walker algorithm can also be extended to a locomotion system without wheels. To do this, the same algorithm structure is considered but the external contact forces of the wheels in dynamic locomotion model (3.14) are replaced by those induced by the environment (e.g. a fluid) on which the robot pushes to propel its reference body. Finally, the extreme case in this context is an articulated system without any external contact such as the arm of a space shuttle or a satellite. Here, the external forces in the dynamic locomotion model (3.14) disappear and the dynamic locomotion model turns again into a kinematic locomotion model of the form (3.16) but this time it is no longer the kinematic constraints that are encoded in \mathcal{A} , but the laws of conservation of initially null kinetic momentums.

The Fig. 3.9 represents the flow chart of the general algorithm applicable to any of the aforementioned mobile multibody systems. Where, Block1 contains an extension of the two recursions of the standard Luh algorithm to the case of wheeled systems, while Block2 contains a recursive computation of the (constrained or unconstrained) locomotion model.

3.4 The Unconstrained Mobile Multibody System

In this section, we extend the standard Luh algorithm of section 3.2 to the case of an unconstrained mobile multibody system. In this case, the tree-like structure is either completely disconnected from the earth (i.e. $\mathbb{N}_w = \emptyset$) or connected with it through non-ideal wheels. Examples of completely disconnected mobile multibody systems contain the aerial, aquatic and spatial systems. For example a satellite whose attitude is controlled with kinematic momentum exchange devices such as simple inertia wheels or more sophisticated systems such as control momentum gyroscopes, a swimming eel-like robot or a walking robot in its flying phase, etc. In short, it includes any mobile multibody system for which the interaction with the rest of the world can be modeled through external contact forces explicitly computable (e.g. with simple laws of the body motions) or numerically by a solver (e.g. of Fig. 2.25). To fix the ideas, in the following, the external contact forces applied on any body S_j will be modeled by state-dependent physical laws of the following form:

$$F_{\text{ext},j} = F_{\text{ext},j}(t, r(t), \dot{r}(t), {}^e g_o, \eta_o). \quad (3.17)$$

In this scenario, the Luh and Walker recursive algorithm of section 3.2 can be easily extended to the case of an unconstrained mobile multibody system by computing the accelerations $\dot{\eta}_o$ of the reference body S_o^+ . Therefore, first we develop the dynamic locomotion model (Block2 of Fig. 3.9) in order to compute the current accelerations $\dot{\eta}_o$ of S_o^+ from the current inputs $((r, \dot{r}, \ddot{r})(t))$ and the current reference state $(({}^e g_o, \eta_o)(t))$. Then this reference acceleration is used as boundary conditions for the Luh and Walker recursive torque dynamics (Block1 of Fig. 3.9) in order to compute motor torques $\tau(t)$.

3.4.1 Dynamic Locomotion Model

This model is based on the reference body dynamics controlled by the imposed joint motions based upon Newton-Euler formulation, such a dynamic balance applied onto S_o^+ is stated in the following form:

$$\mathcal{M}_o^+(r(t))\dot{\eta}_o = F_o^+(r(t), \dot{r}(t), \ddot{r}(t), {}^e g_o, \eta_o). \quad (3.18)$$

These dynamics can be derived either from a Lagrangian approach through variational calculus on a principal fiber bundle or more simply by applying the principle of virtual work as follows. For the sake of simplicity, a simple chain mobile multibody system is considered, for which the virtual work balance applied to the entire system can be stated

as follows: for $\forall j = 0, 1, \dots, p$ and $\forall \delta\eta_j \in \mathbb{R}^6$:

$$\begin{aligned} & \delta W_{\text{acc}} - \delta W_{\text{ext}} - \delta W_{\text{int}} = \\ & \sum_{j=0}^{j=p} \delta\eta_j^T (\mathcal{M}_j \dot{\eta}_j - F_{\text{gyr},j} - F_{\text{ext},j} + \text{Ad}_{(j+1)g_j}^T F_{j+1} - F_j) = 0. \end{aligned} \quad (3.19)$$

Where the first two terms of the summation symbol stand for the virtual work produced by the acceleration amounts of the bodies, denoted δW_{acc} , the next term stands for the virtual work of external forces δW_{ext} , while the last two terms is the total virtual work produced by the interbody forces (here modeled by inter-bodies wrenches): δW_{int} . Now two more operations have to be done in order to derive (3.18). Firstly, the virtual twists are taken compatible with internal joint kinematics, i.e. they verify (3.8) with δ replacing the time differentiation. Secondly, because we are looking for the reference body dynamics controlled by the internal motions ruled by explicit time laws, the frozen time condition imposes to have $\delta r(t) = 0$ and finally we just have to force the virtual twists $\delta\eta_j$ in (3.19) to verify for any $\delta\eta_o \in \mathbb{R}^6$:

$$j = 0, 1, \dots, p-1 : \delta\eta_j = \text{Ad}_{jg_{j-1}} \delta\eta_{j-1}, \quad (3.20)$$

and with simple transformations, we have for:

$$j = 0, 1, \dots, p : \delta\eta_j = \text{Ad}_{jg_o} \delta\eta_o, \quad (3.21)$$

while with the same transformations, the equation (3.9) allows one to state:

$$\dot{\eta}_j = \text{Ad}_{jg_o} \dot{\eta}_o + \sum_{l=1}^{l=j} \text{Ad}_{jg_l} \zeta_l. \quad (3.22)$$

Now taking into account (3.21) and (3.22) in the virtual work (3.19), we get the dynamic balance (3.18) for a simple chain mobile multibody system submitted to external forces (3.17). Where, $\mathcal{M}_o^+(r(t))$ is the composite inertia matrix of the composite reference body S_o^+ and is given by:

$$\mathcal{M}_o^+(r(t)) = \sum_{j=0}^{j=p} \text{Ad}_{jg_o}^T \mathcal{M}_j \text{Ad}_{jg_o}, \quad (3.23)$$

and $F_o^+(r(t), \dot{r}(t), \ddot{r}(t), {}^e g_o, \eta_o)$ is the resultant wrench of all inertial and external forces exerted onto S_o^+ and is given by:

$$F_o^+ = F_{\text{gyr},o} + F_{\text{ext},o} + \sum_{j=1}^{j=p} \text{Ad}_{jg_o}^T \left(F_{\text{gyr},j} + F_{\text{ext},j} - \mathcal{M}_j \left(\sum_{l=1}^{l=j} \text{Ad}_{jg_l} \zeta_l \right) \right). \quad (3.24)$$

Here let us remark that the joints being ideal, we simply have $\delta W_{\text{int}} = 0$, since the internal reaction forces do not work in any virtual field compatible with the joint kinematics. Furthermore, with reference to (3.14):

$$F_o^+ = F_{\text{in},o}^+ + F_{\text{ext},o}^+, \quad (3.25)$$

with:

$$\begin{cases} F_{\text{in},o}^+ = F_{\text{gyr},o} + \sum_{j=1}^{j=p} \text{Ad}_{j_{g_o}}^T \left(F_{\text{gyr},j} - \mathcal{M}_j \left(\sum_{l=1}^{l=j} \text{Ad}_{j_{g_l}} \zeta_l \right) \right), \\ F_{\text{ext},o}^+ = F_{\text{ext},o} + \sum_{j=1}^{j=p} \text{Ad}_{j_{g_o}}^T (F_{\text{ext},j}). \end{cases} \quad (3.26)$$

Now keeping in view the tree like topology, the matrices \mathcal{M}_o^+ and F_o^+ of equations (3.23, 3.24) can be numerically computed through the following backward recursive computations initialized by the boundary conditions: $\mathcal{M}_j^+ = 0$, $F_j^+ = 0$ if S_i is a terminal body: for $j = p + 1, p, \dots, 1$:

Compute \mathcal{M}_o^+ through:

$$\begin{cases} \text{if } i = j - 1 : & \mathcal{M}_i^+ = \mathcal{M}_i + \text{Ad}_{j_{g_i}}^T \mathcal{M}_j^+ \text{Ad}_{j_{g_i}}; \\ \text{else:} & \mathcal{M}_i = \mathcal{M}_i + \text{Ad}_{j_{g_i}}^T \mathcal{M}_j^+ \text{Ad}_{j_{g_i}}. \end{cases} \quad (3.27)$$

Compute F_o^+ through:

$$\begin{cases} \text{if } i = j - 1 : & F_i^+ = F_{\text{gyr},i} + F_{\text{ext},i} - \text{Ad}_{j_{g_i}}^T \mathcal{M}_j^+ \zeta_j - \text{Ad}_{j_{g_i}}^T F_j^+; \\ \text{else:} & F_{\text{gyr},i} = F_{\text{gyr},i} - \text{Ad}_{j_{g_i}}^T F_j^+ - \text{Ad}_{j_{g_i}}^T \mathcal{M}_j^+ \zeta_j. \end{cases} \quad (3.28)$$

Finally, the dynamic locomotion model can be written in state-space form on $\text{SE}(3) \times \text{se}(3)$ as:

$$\begin{pmatrix} \dot{\eta}_o \\ {}^e \dot{g}_o \end{pmatrix} = \begin{pmatrix} (\mathcal{M}_o^+)^{-1} F_o^+ \\ {}^e g_o \widehat{\eta}_o \end{pmatrix}, \quad (3.29)$$

where the second row is the reconstruction kinematic equation from η_o to ${}^e g_o$. In order to update the reference state for the next step of the time loop, (3.29) is numerically integrated, for instance, with a geometric time integrator on Lie groups [91] or more simply with a quaternion-based integrator. These two integrators exploit the advantages of the intrinsic modeling approach here pursued. In particular, they are free of singularities and artificial nonlinearities like those introduced by any three-angle parametrization of orientations of S_o .

3.4.2 Torque Dynamics

Once the reference acceleration $\dot{\eta}_o$ of the reference body S_o^+ is known at the current time, the acceleration $\dot{\eta}_j$ and interbody wrenches F_j are computed through forward recursive

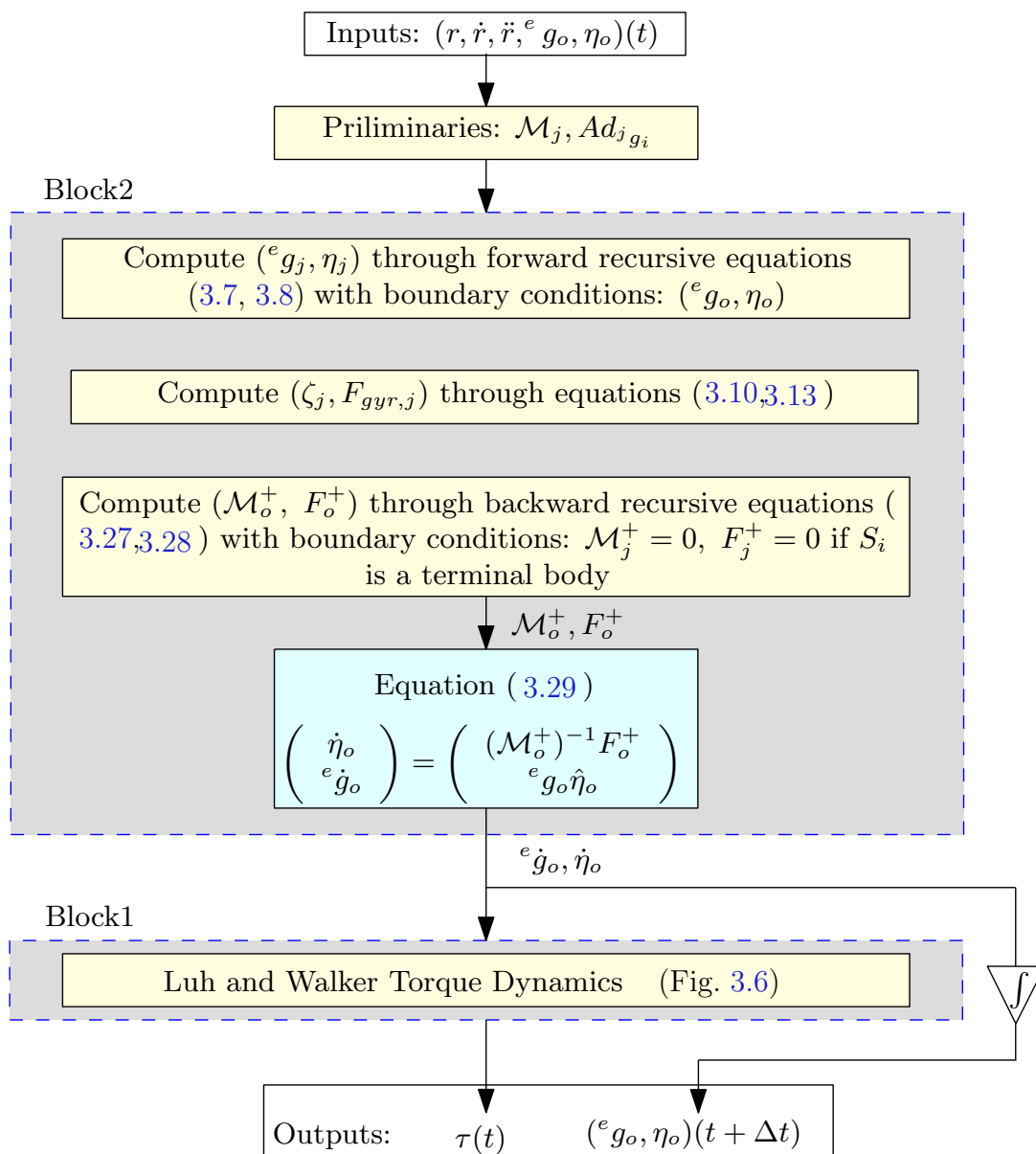


Figure 3.10 – Execution of proposed algorithm in case of an unconstrained mobile multibody system

equation (3.9) and backward recursive equation (3.11) of the standard Luh and Walker algorithm (Fig. 3.6), respectively. Then, these interbody wrenches are projected onto the joint axes in order to compute the joint torques $\tau(t)$ by using equation (3.12).

In short, the extension of standard Luh and Walker algorithm to the case of an unconstrained mobile multibody system only requires the dynamic locomotion model (3.29) along with the recursions (3.27, 3.28) in addition to the torque dynamics (3.7-3.12).

Finally, the execution of the proposed algorithm for an unconstrained mobile multibody system is stated in Fig. 3.10.

3.4.3 Unconstrained Cases with Symmetries

In certain conditions related to the external forces (3.17), the previous general context can be simplified. In particular, this occurs when:

1. A robot is floating in space, e.g. a shuttle arm or any satellite equipped with a reorientation system based on inertial exchange devices.
2. A robot is immersed in an ideal fluid initially at rest.

In the context of section 2.3.5, for both of the above cases the external forces F_{ext} are ${}^e g_o$ -independent and Lagrangian [7]. Mathematically, it means that there exists a Lagrangian function $l_{\text{ext}} = l_{\text{ext}}(r, \dot{r}, \eta_o)$ such that equation (2.17) is satisfied. We now recall it with the new notations ($F_{\text{ext}} = F_{\text{ext},o}^+$ and $\eta = \eta_o$):

$$F_{\text{ext},o}^+ = \frac{d}{dt} \left(\frac{\partial l_{\text{ext}}}{\partial \eta_o} \right) - \text{ad}_{\eta_o}^* \left(\frac{\partial l_{\text{ext}}}{\partial \eta_o} \right), \quad (3.30)$$

where, $\text{ad}_{(\cdot)}^*(\cdot) : \mathfrak{g} \times \mathfrak{g}^* \rightarrow \mathfrak{g}^*$ is the co-adjoint map of G . Let us remind that in the first case mentioned above $G = \text{SO}(3)$ and $l_{\text{ext}} = 0$, while in the second case l_{ext} is equal to the added kinetic energy of the fluid [67]. Further analysis of such cases shows that, with $l_{\text{ext}} + l = \frac{1}{2} \eta_o^T (\widetilde{\mathcal{M}}_o^+ \eta_o + {}^o \widetilde{M}_r \dot{r})$, l being the Lagrangian of the system free of external forces, the acceleration part of (3.29) can be explicitly time-integrated to state the following set of nonholonomic constraints:

$$\widetilde{\mathcal{M}}_o^+ \eta_o + {}^o \widetilde{M}_r \dot{r} = 0, \quad (3.31)$$

where, $\widetilde{\mathcal{M}}_o^+ = I_o^+$ and ${}^o \widetilde{M}_r = {}^o I_r$ in the first case, while $\widetilde{\mathcal{M}}_o^+ = \mathcal{M}_o^+ + \mathcal{M}_{\text{add},o}^+$ and ${}^o \widetilde{M}_r = {}^o M_r + {}^o M_{\text{add},r}$ in the second case⁵. Finally, equation (3.31) stands for the conservation of the kinetic momentum of a system initially at rest. Furthermore, in (3.31), ${}^o \widetilde{M}_r$ is a $(6 \times p)$ matrix which can be computed column by column from a tilde version of (3.28) by imposing successively $\ddot{r} = (-1, 0, 0, \dots, 0)$, $\ddot{r} = (0, -1, 0, \dots, 0)$, \dots , $\ddot{r} = (0, 0, 0, \dots, -1)$ while $\dot{r}(t) = 0$, $\eta_o = 0$ and r is "frozen" in its current value $r(t)$. Finally, (3.31) allows the dynamic locomotion model (3.29) to be replaced by the following kinematic locomotion model:

$$\widehat{\eta}_o = {}^e g_o^{-1} {}^e \dot{g}_o = (-\mathcal{A}\dot{r})^\wedge, \quad \dot{\eta}_o = -\mathcal{A}\ddot{r} - \dot{\mathcal{A}}\dot{r}, \quad (3.32)$$

where $\mathcal{A} = (\widetilde{\mathcal{M}}_o^+)^{-1} {}^o \widetilde{M}_r$ is the local form of a connection on the principal fiber bundle \mathcal{C}_2 known as a "mechanical connection" [76, 89, 59]. In this case, the dynamic locomotion model reduces into kinematic locomotion model due to the symmetry properties of the system dynamics [76].

⁵The subscript "add" refers to the added mass of the fluid accelerated by the body

3.5 The Constrained Mobile Multibody System

Now we extend the algorithm of the unconstrained mobile multibody system further to the case of a constrained mobile multibody system. As mentioned earlier that a constrained mobile multibody system is a structure always in contact with the ground through ideal wheels. Thus, this extension is basically a reduction process based upon the nonholonomic constraints of the wheels. Before carrying out this reduction process, we first recall the nonholonomic kinematics of a constrained mobile multibody system. Note that, in case of constrained mobile multibody system, any wheeled body is alternatively called as a nonholonomic body since it is always constrained through nonholonomic kinematic constraints. Consequently, any unwheeled body of a constrained mobile multibody system is called as a holonomic body.

3.6 Kinematics of a Constrained Mobile Multibody System

3.6.1 Kinematics of an Isolated Nonholonomic Body

We here investigate the kinematic model of a nonholonomic body S_j , $j \in \mathbb{N}_w$ endowed with N_j wheels. The body is considered isolated from the rest of the structure. Mathematically, this is equivalent to consider the nonholonomic constraints on the definition (3.3) of the configuration space, i.e. on each copy of $SE(3)$. Being ideal, each unidirectional wheel experiences two constraints, one due to the axial rolling without slipping condition and the other due to the lateral non-sliding condition. On the other hand, each omnidirectional wheel experiences only one rolling without slipping constraint. Note that only the non-sliding constraints of all the N_j wheels are involved in the reduction process.

3.6.1.1 Non-sliding Constraints of an Isolated Nonholonomic Body

In this section, we consider the tree-like system of the general type shown in Fig. 3.1(b) for which $\mathbb{N}_w \neq \emptyset$. Then, we isolate each nonholonomic body S_j , $j \in \mathbb{N}_w$ endowed with N_j wheels. Consequently, this is equivalent to consider the non-sliding constraints on the definition (3.3) of the configuration space, i.e. on each copy of $SE(3)$. Moreover, since the non-sliding constraints prevent the wheels from sliding along the directions perpendicular to their planes hence they are modeled by left-invariant 1-forms on the configuration group $SE(3)$ of their body. In fact, once written in the dual of the Lie algebra of the material infinitesimal transformations of $SE(3)$ (i.e. the space of the twist of S_j expressed in \mathcal{F}_j), they do not depend any more on the platform configuration of $SE(3)$. Thus, they can be written as:

for $k = 1, 2, \dots, m_j$, $\forall t \in \mathbb{R}^+$, $\forall j \in \mathbb{N}_w : \omega_{j,k}(\beta_j(t), \cdot) = 0$, with:

$$\omega_{j,k} : (t, \eta_j) \in \mathbb{R}^+ \times se(3) \mapsto \omega_{j,k}(\beta_j(t), \eta_j) \in \mathbb{R}, \quad (3.33)$$

where for each S_j , the $\omega_{j,k}$'s are $m_j (\leq N_j)$ independent co-vectors of $se(3)^*$ which can be time-dependent through the vertical steering angles $\beta_{j,k=1,\dots,N_{S_j}}$ of S_j . Now, let us define \mathcal{V}_j the subspace of $se(3)$, said "admissible" since it contains any twist of S_j compatible with the constraints (3.33). Once the three holonomic constraints imposed by the contact with the horizontal planar ground added to (3.33), the \mathcal{V}_j space is spanned by any set of $6 - m_j - 3 \triangleq n_j$ time-varying independent vectors of $se(3)$: $(h_{j,l}(\beta_j(\cdot)), l = 1, 2, \dots, n_j)$ which verifies at any time the planar ground constraints and the non sliding ones (3.33), i.e.:

for $k = 1, 2, \dots, m_j + 3$, $l = 1, 2, \dots, n_j, \forall t \in \mathbb{R}^+$:

$$\omega_{j,k}(\beta_j(t), h_{j,l}(\beta_j(t))) = 0. \quad (3.34)$$

In the following, we will identify $se(3)^*$ to $se(3)$ thanks to the natural isomorphism between the row and the column vectors of \mathbb{R}^6 . This allows one to rewrite the non-sliding constraints (3.33) along with the three planar ground holonomic constraints imposed by the ground as:

for $k = 1, 2, \dots, m_j + 3$, $\forall t \in \mathbb{R}^+$:

$$\omega_{j,k}(\beta_j(t), \eta_j) = (h_{j,k}^\perp(\beta_j(t)))^T \eta_j = 0, \quad \forall \eta_j \in se(3),$$

where, the space $\text{span}(h_{j,k}^\perp(\beta_j(t)))_{k=1,2,\dots,m_j+3}$ is the orthogonal complement of the admissible space $\mathcal{V}_j = \text{span}(h_{j,l}(\beta_j(t)))_{l=1,2,\dots,n_j}$ in $se(3)$ and will be denoted by \mathcal{V}_j^\perp . Finally, in order to identify the admissible space \mathcal{V}_j along with its dual \mathcal{V}_j^* (a condition required for the dynamic reduction process of the isolated non-holonomic bodies of section 3.7) we shall impose to the base $(h_{j,l})_{l=1,\dots,n_j}$ of \mathcal{V}_j to be orthonormal for the Euclidean metric of \mathbb{R}^6 , i.e. to verify: $h_{j,l}^T h_{j,q} = \delta_{lq}, \forall l, q = 1, 2, \dots, n_j$, or more concisely, in matrix form:

$$\forall j \in \mathbb{N}_w : H_j^T H_j = 1_{n_j}, \quad (3.35)$$

where:

$$H_j(t) = (h_{j,1}(\beta_j(t)), h_{j,2}(\beta_j(t)), \dots, h_{j,n_j}(\beta_j(t))). \quad (3.36)$$

For instance, this can be achieved thanks to the Gram-Schmidt ortho-normalization algorithm. Moreover, as assumed earlier that the motion of any mobile platform S_j is confined to the planar ground $SE(2)$, then the dimensions of \mathcal{V}_j (i.e. n_j) do not exceed 3, and this algorithm can be applied symbolically. Further, we assume that such an orthonormal base $(h_{j,l})_{l=1,2,\dots,n_j}$ of \mathcal{V}_j is known. With these definitions and notations, any admissible twist

of the platform can be expressed as:

$$\forall j \in \mathbb{N}_w : \eta_j = H_j(t)\eta_{rj}. \quad (3.37)$$

This relation defines the reduced kinematics of an isolated non-holonomic body S_j , where η_{rj} defines the $(n_j \times 1)$ vector of the components of η_j in the base of \mathcal{V}_j . This vector will be named "reduced twist" of S_j and H_j will be named the $(6 \times n_j)$ "reduction matrix" of the j^{th} isolated body.

Moreover, the orthogonal complement of H_j is defined by:

$$H_j^\perp(t) = (h_{j,1}^\perp(\beta_j(t)), h_{j,2}^\perp(\beta_j(t)), \dots, h_{j,m_j+3}^\perp(\beta_j(t))), \quad (3.38)$$

such that $H_j^T H_j^\perp = 0_{n_j \times (m_j+3)}$. Finally, in virtual terms, equation (3.37) defines the virtual twist of body S_j compatible with its non-sliding and planar ground constraints as follows:

$$\delta\eta_j = H_j(t)\delta\eta_{rj}, \quad (3.39)$$

where $\delta\eta_{rj}$ is the reduced virtual twist of the isolated body S_j .

3.6.1.2 Rolling Without Slipping Constraints of an Isolated Nonholonomic Body

The rolling kinematics of the wheels of any body S_j , $j \in \mathbb{N}_w$ are considered as a reconstruction problem from the time (integrated) evolution of its reduced twist η_{rj} . Let us note that η_{rj} will be deduced later from our final recursive algorithm. This reconstruction recovers the evolution of each of the wheels of any wheeled S_j by carrying the twist (3.37) from the body frame \mathcal{F}_j to the center of each of the wheel. Then, by invoking the rolling without slipping constraints for any wheeled body S_j , we obtain a relation of the following form:

$$\dot{\theta}_j = B_j(t)\eta_{rj}, \quad (3.40)$$

with B_j as a $(N_j \times n_j)$ matrix depending upon the geometry of the body S_j and its wheels, as well as the current time via the steering angles $\beta_j(t)$.

3.6.2 Kinematics of the Composite Body S_o^+

3.6.2.1 Non-sliding Constraints of the Reference Composite Body S_o^+

We now examine the consequences of the non-sliding constraints of the whole system upon the motions of S_o^+ . This is equivalent to consider the non-sliding constraints of the whole system on the principal fiber bundle of its configuration space \mathcal{C}_2 defined by

equation (3.4). Note that, due to the possible existence of other nonholonomic bodies in the structure, the admissible space \mathcal{V} of composite body S_o^+ is generally more constrained than that of isolated body S_o (i.e. $\mathcal{V} \subseteq \mathcal{V}_o = \text{span}(H_o)$). Consequently, for the m independent non-sliding constraints of S_o^+ we have $m \geq m_o$. Going further, we can always exhibit a maximal set of m independent constraint 1-forms on $T(\text{SE}(3) \times \mathcal{S})$ which are time-dependent because of steering wheel angles $\beta(t)$ and revolute joint angles $r(t)$. Furthermore, due to the non-sliding conditions, these constraints are G -invariant with respect to the left action of $\text{SE}(3)$ on the principal fiber bundle of configurations. Consequently, they will take the following general form:

$$\omega_k(\beta(t), r(t), \dot{r}(t), \eta_o) = 0. \quad (3.41)$$

Once these constraints are gathered together with the three planar-ground constraints imposed by the planar ground, then reapplying the same procedure as in the previous section 3.6.1.1, the resulting $m + 3$ constraints can be written in a matrix form as follows:

$$A(\beta(t), r(t))\eta_o + B(\beta(t), r(t))\dot{r}(t) = 0, \quad (3.42)$$

where A is a $((m + 3) \times 6)$ matrix and B is a $((m + 3) \times p)$ matrix. The rank of matrix A plays a key role in the mobility analysis of such nonholonomic systems. In fact, from expression (3.42), we identify the following two cases depending upon the relative values of $\dim(\text{SE}(3))=6$ and $\text{rank}(A)$:

$$\begin{cases} \text{Case(a),} & \text{fully-constrained: } \text{rank}(A) = 6 \text{ i.e. } m + 3 \geq 6; \\ \text{Case(b),} & \text{under-constrained: } \text{rank}(A) < 6 \text{ i.e. } m + 3 < 6. \end{cases}$$

Case(a): Fully-Constrained Mobile Multibody System

In this case, (3.42) can be block-partitioned as:

$$\begin{pmatrix} \bar{A} \\ \tilde{A} \end{pmatrix} \eta_o + \begin{pmatrix} \bar{B} \\ \tilde{B} \end{pmatrix} \dot{r} = \begin{pmatrix} 0 \\ 0 \end{pmatrix}, \quad (3.43)$$

with \bar{A} as a (6×6) square invertible matrix. In this case, the matrix \bar{A} being invertible, η_o is completely defined by the time evolution of $r(t)$ and $\beta(t)$. Thus, the net motions of the mechanism are completely computable through kinematics. Geometrically, including $\beta(t)$ into the vector of shape coordinates $r(t)$, allows one to define $\mathcal{A}_k \triangleq \bar{A}^{-1}\bar{B}$ as the local form of a connection on the principal fiber bundle of configurations [66]. Furthermore, if $m + 3 = 6$, then the mobile multibody system can move in any case whereas if $m + 3 > 6$, then the residual $(m + 3) - 6 = m - 3$ equations of (3.43) can be used to find the joint velocities \dot{r} preserving the mobility of the whole system, i.e. verifying the following

compatibility condition:

$$(\tilde{B} - \tilde{A}\mathcal{A}_k)(r)\dot{r} = 0, \quad (3.44)$$

which admits nontrivial solution ($(\dot{r} \neq 0)$) in virtue of assumption 7 of section 3.1.1. Finally, in case (a), there are enough independent non-sliding constraints to replace entirely the dynamic locomotion model (3.29) of section 3.4 by the following kinematic locomotion model:

$$\eta_o = -\mathcal{A}_k(r)\dot{r}(t), \quad (3.45)$$

along with its differential and integral consequences given as follows:

$$\begin{cases} \dot{\eta}_o = -\mathcal{A}_k(r)\ddot{r}(t) - \dot{\mathcal{A}}_k(r)\dot{r}(t), \\ {}^e\dot{g}_o = {}^e g_o(-\mathcal{A}_k\dot{r})^\wedge. \end{cases} \quad (3.46)$$

The equation (3.45) along with (3.46) gives the net motions of the reference body S_o^+ through pure kinematics i.e. without involving dynamics. Thus in a fully-constrained case the net motions are completely solved through the locomotion kinematic model (3.45). In the literature on Lagrangian dynamics (see chapter 2), \mathcal{A}_k is often mentioned as the local form of the principal kinematic connection [87, 60].

Case(b): Under-Constrained Mobile Multibody System

In this case, the under-constrained mechanism ($\text{rank}(A) < 6$) has not enough non-sliding constraints to define the net motions uniquely through kinematics and thus, further analysis is required. In this regard, applying generalized inversion to (3.42) allows one to state that any twist of S_o^+ should verify:

$$\eta_o = H(t)\eta_r + J(t)\dot{r}(t), \quad (3.47)$$

where, if A^\dagger denotes the pseudo-inverse of matrix A , $J = -A^\dagger B$, and denoting $n \triangleq (6 - \text{rank}(A))$, H is a $(6 \times n)$ matrix whose columns span the kernel of A . Furthermore, the \mathcal{V} space is spanned by the n column vectors of H i.e. $\mathcal{V} = \text{span}(H)$. Thus, η_r stands for an undetermined $(n \times 1)$ vector named as "reduced twist". Geometrically, this vector naturally takes the sense of the reduced twist of S_o^+ . Thus, in under-constrained case the reference twist η_o cannot be determined uniquely from non-sliding constraints, but requires rolling without slipping constraints and/or dynamics to be invoked. Furthermore, S_o may be equipped with actuated as well as free (around their rolling axis) wheels. To distinguish them, we introduce an "actuated-free" block partition of η_o and rewrite (3.47)

in more detailed form as follows:

$$\eta_o = \begin{pmatrix} H_a(t) & H_f(t) \end{pmatrix} \begin{pmatrix} \eta_{ra}(t) \\ \eta_{rf} \end{pmatrix} + J(t)\dot{r}(t), \quad (3.48)$$

where, with $n = n_a + n_f$, $t \in \mathbb{R}^+ \mapsto \eta_{ra}(t)$ is an $n_a \times 1$ vector of imposed (actuated) velocities (known through motion planning and control laws), while η_{rf} is a $(n_f \times 1)$ vector of unknown (free) velocities that our recursive algorithm will have to compute. Finally, (3.48) defines the most general form of the reduced kinematics of S_o^+ under our basic assumptions (section 3.1.1). In literature on geometric mechanics, this under-constrained case is referred to as a mixed kinematic and dynamic case [87] (see section 2.3.6 of chapter 2).

Before closing this section, let us consider the case where the velocities of the equation (3.48) are replaced by virtual displacements. In this case, the internal shape motions, being defined by some known time laws, induce no variation and we have:

$$\delta\eta_o = H(t)\delta\eta_r.$$

In the language of the principal fiber bundle, such a virtual displacement is defined in the vertical space of $SE(3) \times \mathcal{S}$. Going further, the actuated component η_{ra} induced by actuated wheels being explicitly time-dependent too, we finally have the following virtual displacement compatible with all the non-sliding, rolling without slipping and planar-ground constraints of the composite body S_o^+ :

$$\delta\eta_o = H_f(t)\delta\eta_{rf}, \quad (3.49)$$

which is the virtual form of (3.48).

3.6.2.2 Rolling Without Slipping Constraints of the Reference Composite Body S_o^+

A relation similar to (3.40) can be derived but this time for the reference composite body S_o^+ rather than the isolated body S_o . With equation (3.2) and based upon the rolling without slipping condition, we can write the following general expression for S_o^+ supposed to be equipped with both actuated and free wheels:

$$\begin{pmatrix} \dot{\theta}_{oa}(t) \\ \dot{\theta}_{of} \end{pmatrix} = \begin{pmatrix} B_{aa} & 0 \\ B_{fa} & B_{ff} \end{pmatrix} \begin{pmatrix} \eta_{ra} \\ \eta_{rf} \end{pmatrix}. \quad (3.50)$$

Which encodes the fact that $\dot{\theta}_{of}$ may depend upon η_{ra} (as in the case when the free wheels follow the leading actuated ones), while $\dot{\theta}_{oa}$ obviously never depends upon η_{rf} . The first

row of (3.50) gives the following kinematic model:

$$\dot{\theta}_{oa}(t) = B_{aa}\eta_{ra}, \quad (3.51)$$

where, B_{aa} is a $(N_a \times n_a)$ matrix (n_a is the number of actuated admissible degrees of freedom of S_o^+ while N_a is its number of actuated wheels). Furthermore, we have $n_a \leq N_a$. Consequently, it is always possible to split the above equation in the following form:

$$\begin{pmatrix} \dot{\bar{\theta}}_{oa}(t) \\ \dot{\tilde{\theta}}_{oa}(t) \end{pmatrix} = \begin{pmatrix} \bar{B}_{aa} \\ \tilde{B}_{aa} \end{pmatrix} \eta_{ra}, \quad (3.52)$$

where \bar{B}_{aa} is a $(n_a \times n_a)$ full rank invertible square matrix. Thus the first row of the above equation states the following kinematic model used by the algorithm in order to compute η_{ra} from $\dot{\bar{\theta}}_{oa}$:

$$\eta_{ra} = \bar{B}_{aa}^{-1} \dot{\bar{\theta}}_{oa}(t). \quad (3.53)$$

Note that the second row of (3.52) exists only if $n_a < N_a$ and implies the following subsidiary relation:

$$\dot{\tilde{\theta}}_{oa} = \tilde{B}_{aa} \bar{B}_{aa}^{-1} \dot{\bar{\theta}}_{oa}, \quad (3.54)$$

which can be interpreted as a set of compatibility relations for the rolling without slipping constraints of actuated wheels, i.e. if (3.54) is violated then some of the actuated wheels slip on the ground.

Finally, the second row of (3.50) is used to deduce $\dot{\theta}_{of}$ as output from η_{rf} , where η_{rf} is itself computed by the algorithm through the integration of a locomotion model as detailed later.

Remarks

It is worth noting that when $n = n_a$, i.e. $H = H_a$, (3.48) can be then rewritten simply as:

$$\eta_o = H_a(t)\eta_{ra}(t) + J(t)\dot{r}(t).$$

Now taking into account (3.53), the above equation can be rewritten in the following form:

$$\eta_o = -\mathcal{A}_k(\bar{r})\dot{\bar{r}}, \quad (3.55)$$

with:

$$\mathcal{A}_k = - \begin{pmatrix} J & H_a(\bar{B}_{aa})^{-1} \end{pmatrix}, \quad \dot{\bar{r}} = \begin{pmatrix} \dot{r} \\ \dot{\bar{\theta}}_{oa} \end{pmatrix}. \quad (3.56)$$

Thus in this scenario, the system becomes fully-constrained as well as fully-actuated, and needs only the kinematic locomotion model (3.55) in order to get the net motions. Note that in case of a fully actuated single wheeled body (e.g. car-like platform, unicycle, etc.) we have the following simplified form of the kinematic locomotion model:

$$\eta_o = H_a(t) \overline{B}_{aa}^{-1} \dot{\theta}_{oa}. \quad (3.57)$$

Where we recognize the general form of the kinematic model of a nonholonomic mobile platform.

3.6.3 Admissible Spaces of the Reference Body

Here we sum up the different spaces related to S_o and S_o^+ .

1. $\mathcal{V}_o = \text{span}(H_o)$: the space of admissible twists of the isolated reference body S_o compatible with the non-sliding and planar-ground constraints, with η_{ro} as the vector of the corresponding reduced twist components.
2. $\mathcal{V} = \text{span}(H)$: the space of the admissible twists of S_o^+ compatible with the joints and, the non-sliding and planar-ground constraints, with η_r as the vector of the corresponding reduced twist components.
3. $\mathcal{V}_f = \text{span}(H_f)$: the space of the free admissible twists of S_o^+ compatible with the joints and, non-sliding and planar-ground constraints, with η_{rf} as the vector of the corresponding reduced (free) twist components.
4. $\mathcal{V}_a = \text{span}(H_a)$: the space of actuated admissible twists of S_o^+ compatible with the joints and, non-sliding, rolling without slipping and planar-ground constraints, with η_{ra} as the vector of the corresponding reduced (actuated) twist components.

Moreover, these spaces verify: $\mathcal{V}_f \oplus \mathcal{V}_a = \mathcal{V} \subset \mathcal{V}_o$. Finally, note that \mathcal{V} can be derived in a constructive manner through the alternative definitions:

$$\mathcal{V} = \bigcap_{j \in \mathbb{N}_w} \text{span}(\text{Ad}_{g_j} H_j) = \left(\bigcup_{j \in \mathbb{N}_w} \text{span}(\text{Ad}_{g_o}^T H_j^\perp) \right)^\perp. \quad (3.58)$$

In other terms \mathcal{V} is the kernel of all the non-sliding constraints carried from the axles to the reference frame in the current locked configuration. Alternatively, this is the intersection of all the admissible spaces of the isolated bodies, once carried from their own frame to the reference one.

3.7 Dynamics of the Constrained Mobile Multibody System

In this section, we reconsider the dynamic locomotion model (3.29) and the recursive torque dynamics (which is simply the standard Luh and Walker computational torque dynamics) of an unconstrained mobile multibody system where, in case of wheeled mobile multibody systems, the non-ideal wheels were modeled by ground reaction forces (section 3.4). Then, since the wheels are ideal in case of constrained mobile multibody system, we apply the following two step reduction process on the locomotion dynamics algorithm of the unconstrained mobile multibody system in order to obtain the reduced locomotion dynamics algorithm for a constrained mobile multibody system.

1. To project the dynamic locomotion model (3.29) onto the admissible space \mathcal{V} of the composite reference body S_o^+ . This will give a reduced dynamic locomotion model.
2. To project the torque dynamics onto the admissible spaces \mathcal{V}_j 's of the individual (isolated) bodies S_j 's. This will give the reduced torque dynamics.

Let us note that, the purpose of these projections onto the admissible spaces is to simply eliminate all the lateral (external) contact forces that are always perpendicular to the admissible space and are imposed by the ground due to the non-sliding constraints. On the other hand, there is another type of external contact forces, denoted as $F_{\text{ext},ra}$ that are acting in the admissible space \mathcal{V} and are imposed by the ground due to the rolling without slipping constraints of actuated wheels. As such, the algorithm should compute these forces $F_{\text{ext},ra}$ to solve the dynamics. At the end, the resulting model gives a generalized form of that of section 3.4 which can be applied to any type of system of Fig. 3.1(b).

3.7.1 Reduced Dynamic Locomotion Model

This first step of the reduction process concerns the projection of the dynamic locomotion model (3.29) of S_o^+ onto its admissible space \mathcal{V} . Also, since $\mathcal{V} = \mathcal{V}_a \oplus \mathcal{V}_f$. Therefore, the algorithm has to compute the following two unknowns at each step of time.

1. The reduced acceleration $\dot{\eta}_{r,f}$ of the composite reference body S_o^+ in its free admissible subspace \mathcal{V}_f .
2. The reduced external wrench $F_{\text{ext},ra}^+$ of the composite reference body S_o^+ imposed by the ground due to rolling without slipping constraints of actuated wheels.

These computations are done in the following sections.

3.7.1.1 Computation of $\dot{\eta}_{rf}(t)$

Let us first reconsider the balance of virtual work (3.19) applied to the whole mobile multibody system with variations still verifying (3.21):

$$\delta W_{\text{acc}} - \delta W_{\text{ext}} = \delta \eta_o^T \left(\sum_{j=0}^{j=p} \text{Ad}_{j_{g_o}}^T (\mathcal{M}_j \dot{\eta}_j - F_{\text{gyr},j} - F_{\text{ext},j}) \right) = 0. \quad (3.59)$$

Then, the $\dot{\eta}_j$ verifying the recursive kinematics (3.9), (3.59) can be rewritten as follows:

$$\delta \eta_o^T \left(\mathcal{M}_o^+ \dot{\eta}_o - F_{\text{in},o}^+ - \sum_{j=0}^{j=p} \text{Ad}_{j_{g_o}}^T F_{\text{ext},j} \right) = 0. \quad (3.60)$$

Now let us reduce these dynamics by imposing the condition that the general virtual twist of S_o^+ must be compatible with (3.48), i.e. to verify (3.49) for any $\delta \eta_{rf} \in \mathbb{R}^{n_f}$. At this level, let us temporarily assume that the external forces are due to the ideal contact of wheels with the ground only. Hence, the external wrenches of lateral contact forces takes the following form:

$$F_{\text{ext},j} = H_j^\perp(t) \lambda_j, \quad (3.61)$$

where λ_j is a $(m_j + 3) \times 1$ vector of Lagrange multipliers which here stand for the reaction forces forcing the non-sliding and planar-ground constraints induced by the N_j wheels contained by body S_j . Then taking into account (3.49) and (3.61), we can rewrite the balance of virtual work (3.60) as follows:

$$\delta \eta_{rf}^T H_f^T \left(\mathcal{M}_o^+ \dot{\eta}_o - F_{\text{in},o}^+ - \sum_{j=0}^{j=p} \text{Ad}_{j_{g_o}}^T H_j^\perp \lambda_j \right) = 0, \quad (3.62)$$

then, let us remark that for any $j \in \mathbb{N}_w$, we have:

$$(\text{Ad}_{o_{g_j}} H_j)^T (\text{Ad}_{j_{g_o}}^T H_j^\perp) = H_j^T \text{Ad}_{o_{g_j}}^T \text{Ad}_{j_{g_o}}^T H_j^\perp = H_j^T \text{Ad}_{j_{g_o}}^{-T} \text{Ad}_{j_{g_o}}^T H_j^\perp = H_j^T H_j^\perp = 0.$$

Hence, from (3.58) and since $\text{span}(H_f) \subset \text{span}(H)$, we necessarily have: $H_f^T \text{Ad}_{j_{g_o}}^T H_j^\perp = 0$, for any $j = 0, 1, \dots, p$. Therefore, the virtual work due to the external contact forces becomes zero i.e.:

$$\delta W_{\text{ext}} = \delta \eta_{rf}^T H_f^T \left(\sum_{j=0}^{j=p} \text{Ad}_{j_{g_o}}^T H_j^\perp \lambda_j \right) = 0, \quad (3.63)$$

and the virtual work balance (3.62) reduces to the following form:

$$\delta \eta_{rf}^T H_f^T (\mathcal{M}_o^+ \dot{\eta}_o - F_{\text{in},o}^+) = 0. \quad (3.64)$$

At last, taking into account the reduced velocities (3.48) and accelerations (time-derivative of (3.48)) of the composite reference body S_o^+ given as follows:

$$\begin{cases} \eta_o = H_f \eta_{rf} + H_a \eta_{ra}(t) + J\dot{r}, \\ \dot{\eta}_o = H_f \dot{\eta}_{rf} + H_a \dot{\eta}_{ra}(t) + \dot{H} \eta_r + \dot{J}\dot{r} + J\ddot{r}, \end{cases} \quad (3.65)$$

into the virtual work balance (3.62), we get the following reduced dynamics of the composite reference body S_o^+ :

$$\mathcal{M}_{rf}^+ \dot{\eta}_{rf} = F_{rf}^+, \quad (3.66)$$

where we introduced the following reduced matrices:

$$\begin{cases} \mathcal{M}_{rf}^+ = H_f^T \mathcal{M}_o^+ H_f, \\ F_{rf}^+ = H_f^T (F_{in,o}^+ - \mathcal{M}_o^+ (H_a \dot{\eta}_{ra} + \dot{H} \eta_r + \dot{J}\dot{r} + J\ddot{r})), \end{cases} \quad (3.67)$$

with \mathcal{M}_o^+ still given by (3.23) and recursively computed through (3.27) whereas $F_{in,o}^+$ is given by (3.26) and recursively computed through the following backward recursive computation initialized by the boundary condition $F_{in,j}^+ = 0$ if S_i is the terminal body: for $j = p + 1, p, \dots, 1$:

$$\begin{cases} \text{if } i = j - 1 : & F_{in,i}^+ = F_{gyr,i} - \text{Ad}_{jg_i}^T \mathcal{M}_j^+ \zeta_j - \text{Ad}_{jg_i}^T F_{in,j}^+; \\ \text{else:} & F_{gyr,i} = F_{gyr,i} - \text{Ad}_{jg_i}^T \mathcal{M}_j^+ \zeta_j - \text{Ad}_{jg_i}^T F_{in,j}^+. \end{cases} \quad (3.68)$$

Finally, the following set of equations gives the reduced dynamic locomotion model for a constrained mobile multibody system on the reduced state-space $\text{SE}(3) \times \mathcal{V}$:

$$\begin{pmatrix} \dot{\eta}_{rf} \\ {}^e \dot{g}_o \end{pmatrix} = \begin{pmatrix} (\mathcal{M}_{rf}^+)^{-1} (F_{rf}^+) \\ {}^e g_o (H_f \eta_{rf} + (H_a \eta_{ra} + J\dot{r})(t))^\wedge \end{pmatrix}, \quad (3.69)$$

where the first row corresponds to the velocity dynamics whereas the second row is deduced from (3.48) and stands for the kinematic reconstruction equation from the time-evolution of η_{rf} to the motion of ${}^e g_o$. Finally, at each step of the global time loop, the computation of (3.69) gives the current $\dot{\eta}_{rf}(t)$, while as like in the unconstrained case, the time-integration of the second row of (3.69) allows updating of the reference state. As a last note, any external forces other than wheels contact forces can be included in the model through (3.68) by replacing the $F_{gyr,i}$ by $F_{gyr,i} + F_{ext,i}$ with $F_{ext,i}$ given by equation (3.17).

3.7.1.2 Computation of $F_{\text{ext},ra}^+(t)$

Now if we project (3.29) onto $\mathcal{V} = \mathcal{V}_a \oplus \mathcal{V}_f$ (instead of \mathcal{V}_f as in previous section), we obtain the dynamic locomotion model in the actuated-free block partition as follows:

$$\begin{pmatrix} \mathcal{M}_{ra}^+ & {}^{ra}\mathcal{M}_{rf}^+ \\ {}^{rf}\mathcal{M}_{ra}^+ & \mathcal{M}_{rf}^+ \end{pmatrix} \begin{pmatrix} \dot{\eta}_{ra}(t) \\ \dot{\eta}_{rf} \end{pmatrix} = \begin{pmatrix} F_{\text{in},ra}^+ + F_{\text{ext},ra}^+ \\ {}^{rf}F_f^+ \end{pmatrix}. \quad (3.70)$$

From the first row we can write the reduced external wrench $F_{\text{ext},ra}^+$ of S_o^+ as follows:

$$F_{\text{ext},ra}^+ = {}^{ra}\mathcal{M}_{rf}^+ \dot{\eta}_{rf} + \mathcal{M}_{ra}^+ \dot{\eta}_{ra}(t) - F_{\text{in},ra}^+, \quad (3.71)$$

where the terms on the right side of the expression are given by:

$$\begin{cases} {}^{ra}\mathcal{M}_{rf}^+ = H_a^T \mathcal{M}_o^+ H_f, \\ \mathcal{M}_{ra}^+ = H_a^T \mathcal{M}_o^+ H_a, \\ F_{\text{in},ra}^+ = H_a^T F_{\text{in},o}^+, \end{cases} \quad (3.72)$$

and the accelerations $\dot{\eta}_{rf}$ and $\dot{\eta}_{ra}(t)$ are given by (3.69) and the time-derivative of (3.53), respectively.

3.7.2 Reduced Torque Dynamics

This is the second step of reduction process. It consists in projecting each of the recursion of the Luh and Walker algorithm onto the isolated bodies admissible spaces \mathcal{V}_j . This process allows one to remove all the unknown reaction forces exerted by the ground through the wheels. As a result, we obtain a reduced version of the Luh and Walker recursions that we simply name "reduced recursions".

3.7.2.1 Reduced Recursive Kinematics

As this is a body by body projection, then let us first insert (3.37) and its time-derivative into (3.8) and (3.9), then we left-apply the projection operator H_j^T (onto \mathcal{V}_j), and finally we invoke the orthonormality property (3.35), which results in the following reduced recursive kinematics: for $j = 1, 2, \dots, p$:

Compute the reduced velocities:

$$\eta_{rj} = \text{Ad}_{rj}{}_{g_{ri}} \eta_{ri} + \dot{r}_j A_{rj}. \quad (3.73)$$

Compute the reduced accelerations:

$$\dot{\eta}_{rj} = \text{Ad}_{rj}{}_{g_{ri}} \dot{\eta}_{ri} + \zeta_{rj}(\dot{r}_j, \ddot{r}_j), \quad (3.74)$$

where, we introduced the notations:

$$\begin{cases} \text{Ad}_{r_j g_{ri}} = H_j^T \text{Ad}_{j g_i} H_i, \\ A_{rj} = H_j^T A_j, \\ \zeta_{rj} = H_j^T (\text{Ad}_{j g_i} \dot{H}_i \eta_{ri} - \dot{H}_j \eta_{rj} + \zeta_j). \end{cases} \quad (3.75)$$

In the above, $\text{Ad}_{r_j g_{ri}}$ is the transformation which allows a reduced twist to be carried from \mathcal{V}_i to \mathcal{V}_j , with $H_i = 1_6$ (respect. $H_j = 1_6$) if S_i (respect. S_j) is a holonomic body. Note that the reduced recursive kinematic equations (3.73,3.74) are initialized by the following boundary conditions:

$$\begin{cases} \eta_{ro} = H_o^T \eta_o \\ \dot{\eta}_{ro} = H_o^T \dot{\eta}_o + \dot{H}_o^T \eta_o, \end{cases} \quad (3.76)$$

with η_o and $\dot{\eta}_o$ given by (3.65) which further requires, at the current time of the global time loop, the knowledge of $\dot{\eta}_{rf}(t)$ deduced from the reduced locomotion model (3.69).

3.7.2.2 Reduced Recursion on InterBody Wrenches

Let us first consider the dynamics of any of the isolated wheeled body S_j , $j \in \mathbb{N}_w - \{0\}$. In order to remove the external reaction wrenches which force the non-sliding and planar-ground constraints imposed by the wheels, the dynamics of S_j have to be projected onto the admissible space \mathcal{V}_j . This is practically achieved by reapplying the virtual work principle, but a set of independent virtual twists of the form (3.39). As a result we can state the balance of virtual work for a simple chain system as follows: for $j = 1, 2, \dots, p$, and $\forall \delta \eta_{rj} \in \mathbb{R}^{n_j}$:

$$\delta \eta_{rj}^T H_j^T (\mathcal{M}_j \dot{\eta}_j - F_{\text{gyr},j} - F_{\text{ext},j} + \text{Ad}_{j+1 g_j}^T F_{j+1} - F_j) = 0. \quad (3.77)$$

Then, taking into account the external wrench relation (3.61) along with the definition of the orthogonal complement matrices (3.38) in the virtual work (3.77), we can eliminate the virtual work done by the external wrenches and get more simply for $j = 1, 2, \dots, p$, and $\forall \delta \eta_{rj} \in \mathbb{R}^{n_j}$:

$$\delta \eta_{rj}^T H_j^T (\mathcal{M}_j \dot{\eta}_j - F_{\text{gyr},j} + \text{Ad}_{j+1 g_j}^T F_{j+1} - F_j) = 0. \quad (3.78)$$

Furthermore, as far as the velocities and accelerations are concerned, they must be compatible with the non-sliding and planar-ground constraints too, i.e. they should verify the following relations:

$$\begin{cases} \eta_j = H_j(t) \eta_{rj}, \\ \dot{\eta}_j = H_j(t) \dot{\eta}_{rj} + \dot{H}_j(t) \eta_{rj}. \end{cases} \quad (3.79)$$

Moreover, the dual counterpart of (3.37) relates the total and reduced interbody wrenches as follows:

$$F_{rj} = H_j^T(t)F_j, \quad (3.80)$$

and since the reduced base of \mathcal{V}_j is orthonormed for the Euclidean metric of \mathbb{R}^6 , the covariant reduced components of F_j given by (3.80) and their associative contravariant reduced components of η_j transform identically (see appendix A.2 for proof), i.e. we also have:

$$F_j = H_j(t)F_{rj}, \quad (3.81)$$

which is the same relation as that of (contravariant) velocity vectors of (3.79). Finally, inserting (3.79) and (3.81) into the virtual work balance (3.78), gives the following reduced dynamic balance of any wheeled body S_j , $j \in \mathbb{N} - \{0\}$ ruling their velocities in $\mathcal{V}_j \in \text{se}(3)$:

$$\mathcal{M}_{rj}\dot{\eta}_{rj} - F_{\text{gyr},rj} + \text{Ad}_{r^{(j+1)}g_{rj}}^T F_{r^{(j+1)}} - F_{rj} = 0. \quad (3.82)$$

Consequently, for a tree-like structure, the backward recursions on interbody wrenches initialized by $F_{rj} = 0$ if S_i is a terminal body with free ends, are given below: for any $j = p + 1, p, \dots, 1$:

$$\begin{cases} \text{if } i = j - 1 : & F_{ri} = \mathcal{M}_{ri}\dot{\eta}_{ri} - F_{\text{gyr},ri} + \text{Ad}_{rjg_{ri}}^T F_{rj}; \\ \text{else:} & F_{\text{gyr},ri} = F_{\text{gyr},ri} - \text{Ad}_{rjg_{ri}}^T F_{rj}, \end{cases} \quad (3.83)$$

along with the following notations:

$$\begin{cases} \mathcal{M}_{ri} = H_i^T \mathcal{M}_i H_i, \\ F_{\text{gyr},ri} = -H_i^T (\mathcal{M}_i \dot{H}_i \eta_{ri} - F_{\text{gyr},i}). \end{cases} \quad (3.84)$$

Note that any external forces other than the wheels contact forces can be included into the model through the gyroscopic wrench in equation (3.84). The model also works for any holonomic body S_k , $k \in \{i, j\}$, but with $H_k = 1_6$. In short, to extend the torque dynamics from an unconstrained mobile multibody system to a constrained mobile multibody system, we just have to replace the recursive kinematics (3.8, 3.9) by reduced recursive kinematics (3.73, 3.74) and the recursion on wrenches (3.11) by (3.83), while (3.7) works in any case.

3.7.2.3 Torque Computation

The joint torques are deduced from the following reduced projection:

$$j = 1, 2, \dots, p : \tau_j = A_{rj}^T F_{rj}. \quad (3.85)$$

As for the actuated wheel torques Γ , we can define the block partition $\Gamma = (\bar{\Gamma}^T, \tilde{\Gamma}^T)^T$ which is the dual of (3.52). Then, let us remind that the reduced wrench $F_{\text{ext},ra}^+$ in (3.71) actually belongs to the dual space of the η_{ra} and models the forces exerted by the ground onto S_o^+ through the actuated wheels. Then, the wheels being ideal, we have by virtue of the action-reaction principle:

$$\bar{B}_{aa}^T \bar{\Gamma} + \tilde{B}_{aa}^T \tilde{\Gamma} = -F_{\text{ext},ra}^+, \quad (3.86)$$

where, due to the possible over-actuated character of the actuated admissible space (i.e. $N_a > n_a$), in the general case an infinity of wheel torque vectors Γ are capable of supplying the desired $F_{\text{ext},ra}^+$. Moreover, the distribution of the total torque over several actuated wheels in case of $N_a > n_a$ is useful to control traction e.g. in vehicles. Finally, in a particular case of $N_a = n_a$, the solution is unique:

$$\bar{\Gamma} = -\bar{B}_{aa}^{-T} F_{\text{ext},ra}^+. \quad (3.87)$$

3.8 Computational Algorithm

3.8.1 Summary of Discussion

Table 3.1 displays an overall view of all the cases treated by the proposed modeling approach. It is worth noting that in all cases the torque computation is always performed with (3.73-3.74), (3.83,3.85) and (3.71,3.86) whereas the locomotion model for a particular case can always be deduced from the general locomotion model (3.69) as follows:

Unconstrained Case: In this case, we have $H = 1_6$, $J = 0$. This simplifies the general locomotion model (3.69) to the dynamic locomotion model given by (3.29). Furthermore, in the absence of external forces, if the system starts at rest, then we have $H = 0$, $J = -\mathcal{A}(r)$ and as a result (3.29) further reduces to the pure locomotion kinematic model (3.32).

Constrained case: There are the two following cases based upon (3.69):

Fully-Constrained Case: In this case, when the system is completely constrained only by the non-sliding constraints (i.e. $\dim(\text{SE}(3)) = \text{rank}(A)$), then we have $H = 0$, $J = -\mathcal{A}_k(r) = -A^{-1}B$ and as a result (3.69) reduces to the pure locomotion kinematic model given by (3.46). Whereas, if the system is completely constrained by both the non-sliding and rolling without slipping constraints (i.e. $\dim(\text{SE}(3)) > \text{rank}(A)$ but $\mathcal{V} = \mathcal{V}_a$), then the system is said to be fully actuated and we have $H = H_a$. Consequently, (3.69) reduces to the pure locomotion kinematic model given by (3.55).

Under-Constrained case: In this case the system may be either 1) partially actuated (i.e. $\mathcal{V} = \mathcal{V}_a \oplus \mathcal{V}_f$ with $H = \begin{pmatrix} H_a & H_f \end{pmatrix}$) or 2) completely free (i.e. $\mathcal{V} = \mathcal{V}_f$ with $H = H_f$). These two cases are considered as mixed kinematics and dynamics, and hence require (3.69) to be entirely solved.

	Unconstrained case		Constrained case			
	Free of external forces	External forces	Fully-constrained case		Under-constrained case	
Admissible space of S_o^+	$\mathcal{V} = \mathfrak{g}$ (Lie algebra of G in (3.4))	$\mathcal{V} = \mathfrak{g}$	$\mathcal{V} = \mathcal{V}_f$	$\mathcal{V} = \mathcal{V}_a$	$\mathcal{V} = \mathcal{V}_a \oplus \mathcal{V}_f$	$\mathcal{V} = \mathcal{V}_f$
Locomotion model (Block2 of Fig. 3.9)	Pure kinematics (Mechanical connection) (3.32)	Dynamics (3.29)	Pure kinematics (Kinematic connection) (3.46)	Pure kinematics (Kinematic connection) (3.55)	Reduced dynamics (3.69)	Reduced dynamics (3.69)
Torque dynamics (Block1 of Fig. 3.9)	Joints (3.73-3.74) + (3.83-3.85)	Joints (3.73-3.74) + (3.83,3.85)	Joints (3.73-3.74) + (3.83,3.85)	Joints (3.73-3.74) + (3.83,3.85) + Wheels (3.71,3.86)	Joints (3.73-3.74) + (3.83,3.85) + Wheels (3.71,3.86)	Joints (3.73-3.74) + (3.83,3.85)
Illustrative examples	Satellite with rotors	Fish-like robot	Snake-like robot (ACM)	Car, Mobile manipulator	Uni-cycle mobile robot*	Snakeboard

(*with one actuated and one passive wheel on the same axle)

Table 3.1 – Classification of mobile multibody system dynamics

3.8.2 Generalized Algorithm Execution

For the sake of generality, we consider the mixed kinematics and dynamics case. Assume that at the current time t of a global time loop the inputs and the reference state $({}^e g_o, \eta_o)(t)$ are known. The inputs of the algorithm are the following time evolutions:

Inputs: $t \mapsto (\beta, \theta_{oa}, \dot{\theta}_{oa}, \ddot{\theta}_{oa}, r, \dot{r}, \ddot{r})(t)$.

We are going to show how the algorithm computes all the following outputs at time t as well as updates the current reference state at $(t + \Delta t)$ before resuming ($s = 0, 1, 2$ is the order of time differentiation: for $j \in \mathbb{N}_w - \{0\}$):

Outputs: $t \mapsto (\theta_j^{(s)}, \theta_{of}^{(s)}, g_{eo}^{(s)}, \tau, \Gamma)(t)$

The execution of the algorithm, shown in Fig. 3.11, is explained as follows:

Preliminaries: First of all, the algorithm performs the preliminary computations of all the \mathcal{M}_j 's, as well as all the matrices dependent on the steering wheel angles: H_j ($j = 1, 2, \dots, p$), H_f , H_a , B_j ($j \in \mathbb{N}_w$), B_{ff} , B_{aa} , B_{fa} , J and their time derivatives if necessary. Then $(\eta_{ra}, \dot{\eta}_{ra})(t)$ are computed from (3.53) and its time derivative.

Locomotion Model: Then the algorithm computes the ${}^e g_j(t)$'s and the $\eta_j(t)$'s from the forward recurrences (3.7) and (3.8) initialized by $({}^e g_o, \eta_o)(t)$. Then it computes $F_{\text{gyr},j}(t)$'s and $\zeta_j(t)$'s from (3.13) and (3.10), respectively. Then $\mathcal{M}_o^+(t)$ and $F_o^+(t)$ are computed by using the backward recursions (3.27) and (3.28), respectively. After that, the algorithm computes $\dot{\eta}_{rf}(t)$ from (3.69) and from (3.65), we get $({}^e g_o, \eta_o, \dot{\eta}_o)(t)$.

Torque Dynamics: Then the algorithm computes the forward reduced kinematics (3.73, 3.74) initialized by (3.76). Then, injecting the results of this computation into the reduced backward recurrences on the reduced wrenches (3.83) allows $F_{rj}(t)$'s to be computed.

Outputs: Then, using (3.85), the joint torques $\tau(t)$ are calculated as the desired output of the algorithm. As for wheel torques $\Gamma(t)$, the algorithm computes $F_{\text{ext},ra}(t)$ from (3.71), and then $\Gamma(t)$ from (3.86). Finally, $\theta_j(t)$'s and $\theta_{of}(t)$ are deduced from (3.40) and (3.50), respectively.

Update: Finally, the algorithm time integrates (3.69), so updating the reference state through (3.48) for the next time step.

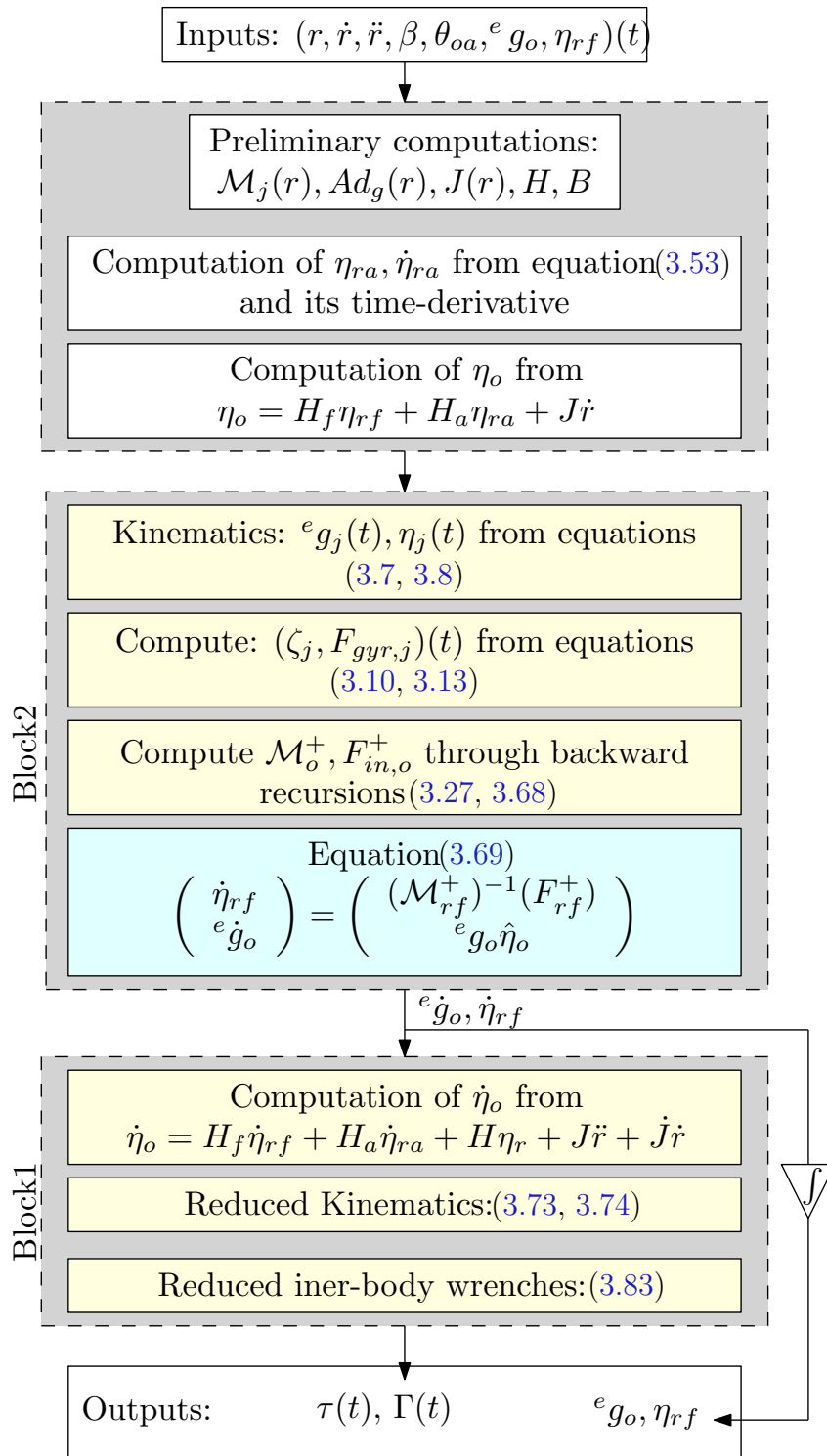


Figure 3.11 – Execution of the general algorithm in mixed kinematic and dynamic case

3.9 Conclusions

The purpose of this chapter was to generalize the computed torque algorithm of Luh and Walker to a wider class of systems contrary to the conventional manipulators with the base either fixed or submitted to known motions. In fact, the systems considered here

were composed of a "tree-like connection" of any conventional bodies which may or may not be wheeled. A general unified algorithm was proposed that solved the following two problems of locomotion.

1. It enables the net motions of a reference body to be computed from the known data of internal motions applied to the joints and/or actuated wheels.
2. It gives the joint and/or actuated wheel torques required to impose these motions.

Moreover, this algorithm fulfils the second stage of the control problem since the desired internal motions are given by the first stage through motion planning. The given framework provides the Newton-Euler-based efficient dynamic modeling counterpart of the Lagrangian dynamic model proposed by geometric mechanics in [87, 60, 76]. From an algorithmic point of view, it is noteworthy that, despite its application to a wide range of systems, the proposed algorithm conserves its basic structure. We will see this in the next chapter where the proposed algorithm is applied to different mobile multibody systems in order to solve the problem of locomotion.

4

Illustrative Examples of Mobile Multibody Systems

4.1	Satellite with Rotors: Unconstrained Case	79
4.1.1	Reduced Dynamic Locomotion Model of S_o^+	81
4.1.2	Torque Dynamics	82
4.2	The Snakeboard: Under-Constrained Case	83
4.2.1	Reduced Dynamic Locomotion Model of S_o^+	86
4.2.2	Torque Dynamics	87
4.3	Snake-like Robot: Fully-Constrained Case	88
4.3.1	Kinematic Locomotion Model of S_o^+	89
4.3.2	Torque Dynamics	90
4.3.3	Numerical Results	90
4.4	Mobile Manipulator: Fully-Actuated Case	91
4.4.1	Reduced Dynamic Locomotion Model	94
4.4.2	Torque Dynamics	94
4.4.3	Numerical Results	95
4.5	Conclusions	95

After developing the dynamics and associate algorithms of mobile multibody systems in a generalized way, in this chapter we now work out a few examples to further explain the practical applications of the proposed algorithm. The first two examples studied here are simple enough to be treated by hand while the last two are solved through computer programming using Matlab. In the following examples, the sine and cosine functions are abbreviated by s and c respectively.

4.1 Satellite with Rotors: Unconstrained Case

The first example is the well known case of a spinning satellite equipped with inertia wheels called rotors which are used to control the orientation of the satellite. The outline sketch of such a setup is shown in Fig. 4.1(a). In our terminology, this is a tree-like structure consists of four bodies, where the satellite is connected to the three inertia rotors through single degree of freedom revolute joints. The Fig. 4.2 shows a set of three inertia rotors. The system is not in contact with the ground and hence will be treated as an unconstrained mobile multibody system.

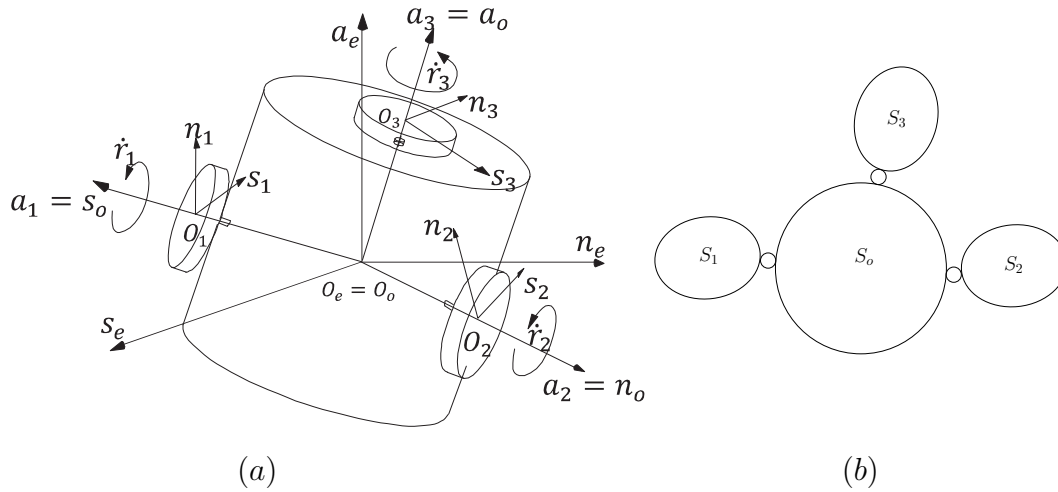


Figure 4.1 – *Satellite with rotors: (a) Outline sketch; (b) Tree-like structure*

Assumptions and Considerations

The system consists of a main body S_o (satellite) to which three rotors S_1, S_2, S_3 are connected through revolute joints. We consider that the joints are at the mass center of each rotor, hence the frames $\mathcal{F}_j = (O_j, s_j, n_j, a_j)$, $j = 1, 2, 3$ attached to the rotors are at the mass center. The mass center of each rotor intersects one of the principle inertia axis of the frame \mathcal{F}_o attached to the mass center of the satellite.

Modeling Approach

As said earlier, the satellite is an unconstrained system with no ground contact. Furthermore, there are no external contact forces applied on it. Therefore, the working principle of the attitude control is based upon the law of conservation of the kinetic momentum which appears as a set of non-integrable constraints discussed as a particular reduced case of an unconstrained mobile multibody system (see section 3.4.3). Due to the conservation of the kinetic resultant, the mass center of the satellite does not observe translational motions due to the internal motions imposed by the revolute joints. Hence, the principle fiber bundle reduces to $\mathcal{C}_2 = \text{SO}(3) \times (S^1)^3$. Where $\text{SO}(3)$ describes the configuration of the satellite S_o^+ , denoted as ${}^e R_o \in G$, with respect to the inertial frame \mathcal{F}_e whereas $(S^1)^3$ denotes the configuration shape-space of the three revolute joints parameterized by the vector $r = \begin{pmatrix} r_1 & r_2 & r_3 \end{pmatrix}^T \in \mathcal{S}$. Such a reduced¹ setup corresponds to applying the general algorithm with $H_f = H_j = \begin{pmatrix} 0_{3 \times 3} & 1_3 \end{pmatrix}^T$, $j = 0, 1, 2, 3$. Moreover, as the net motions of the composite body S_o^+ are also reduced to rotations only, we take $\eta_{r,f} = \Omega_o$.

¹This is due to the reduced configuration group, i.e. $G = \text{SO}(3)$

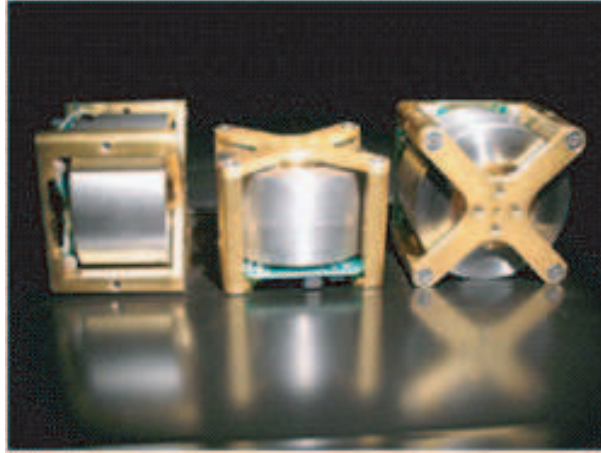


Figure 4.2 – Inertia rotors for re-orientation of satellite in space

Preliminaries

To start computation, we enter the geometric and inertial data of the system in order to calculate the following matrices for $j = 1, 2, 3$:

$$\text{Ad}_{jg_o} = \begin{pmatrix} {}^jR_o & {}^jR_o {}^o\hat{P}_j^T \\ 0 & {}^jR_o \end{pmatrix}, \quad \mathcal{M}_j = \begin{pmatrix} m_j 1_3 & 0 \\ 0 & I_j \end{pmatrix}, \quad (4.1)$$

where $I_j = \text{diag}(I_{jx}, I_{jy}, I_{jz})$ with $I_{jz} = I_w$, whereas the reference body inertia matrix is given by $I_o = \text{diag}(I_{ox}, I_{oy}, I_{oz})$.

4.1.1 Reduced Dynamic Locomotion Model of S_o^+

The reduced composite inertia matrix is computed through the relation (3.67) along with the composite inertia relation (3.27) as follows:

$$\mathcal{M}_{rf}^+ = I_o + \sum_{j=1}^3 ({}^oI_j + m_j {}^o\hat{P}_j^T {}^o\hat{P}_j) \triangleq I_o^+.$$

This reduced composite inertia matrix is known as the locked inertia matrix in [87]. The reduced composite wrench is given by (3.67) and (3.24) as:

$$F_{rf}^+ = H_f^T (F_{\text{gyr},o} + \sum_{j=1}^3 \text{Ad}_{jg_o}^T (F_{\text{gyr},j} - \mathcal{M}_j \zeta_j)), \quad (4.2)$$

where the gyro wrenches generally given by equation (3.13) are simplified here to the following form due to the fact that all the frames are at the mass centers:

$$F_{\text{gyr},k} = - \begin{pmatrix} 0_{3 \times 1} \\ \Omega_k \times (I_k \Omega_k) \end{pmatrix}, \quad k = 0, 1, 2, 3;$$

while the term ζ_j is given by (3.10) with $i = 0$ and $j = 1, 2, 3$, whereas the angular velocities are given by the recursive equation (3.73) initialized by Ω_o . After simplifying (4.2), we get the reduced wrench of the reference body as follows:

$$F_{rf}^+ = -I_r \ddot{r} - \Omega_o \times (I_o^+ \Omega_o + I_r \dot{r}), \quad (4.3)$$

where $I_r = I_w 1_3$. Hence, the dynamics of the reference body (satellite) reduce to:

$$I_o^+ \dot{\Omega}_o = -I_r \ddot{r} - \Omega_o \times (I_o^+ \Omega_o + I_r \dot{r}) \quad (4.4)$$

Finally, (4.4) has to be completed with the reconstruction equation (3.29) which here reduces to ${}^e \dot{R}_o = {}^e R_o \hat{\Omega}_o$ initialized by ${}^e R_o(t=0) = {}^e R_{oo}$. Thus in case of the satellite, equation (3.29) becomes:

$$\begin{pmatrix} \dot{\Omega}_o \\ {}^e \dot{R}_o \end{pmatrix} = \begin{pmatrix} -(I_o^+)^{-1} (I_r \ddot{r} + \Omega_o \times (I_o^+ \Omega_o + I_r \dot{r})) \\ {}^e R_o \hat{\Omega}_o \end{pmatrix}. \quad (4.5)$$

4.1.2 Torque Dynamics

Now, let us compute the joint torques from the backward reduced recursion (3.83), which gives after their projection:

$$\tau_j = A_{rj}^T (\mathcal{M}_{rj} \dot{\eta}_{rj} - F_{\text{gyr},rj}) = a_j^T (I_j \dot{\Omega}_j + \Omega_j \times (I_j \Omega_j)),$$

where the angular accelerations are given by the recursive equation (3.74) initialized with $\dot{\Omega}_o$. After computations, we thus find:

$$\tau = I_r (\dot{\Omega}_o + \ddot{r}). \quad (4.6)$$

Finally, equations (4.5) and (4.6) give the closed form of the satellite dynamics as given by the Lagrangian framework, using Poincaré equations applied to the following Lagrangian:

$$l(r, \dot{r}, \Omega_o) = \frac{1}{2} (\Omega_o^T I_o^+ \Omega_o + \dot{r}^T I_r \dot{r} + 2\Omega_o^T I_r \dot{r}).$$

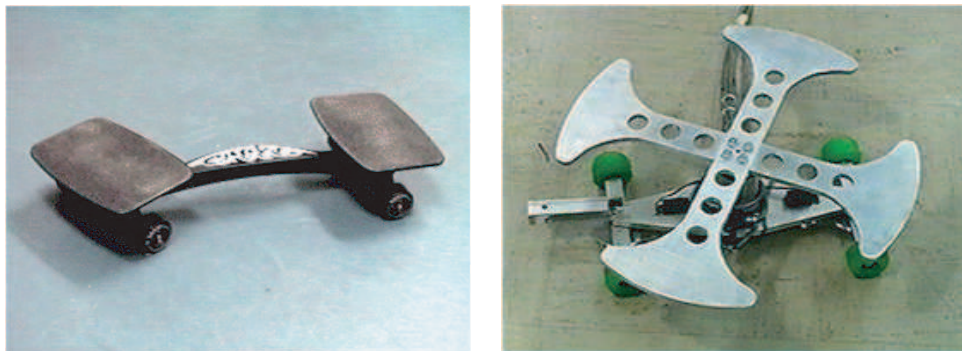


Figure 4.3 – (a) Commercial snakeboard; (b) Robotic prototype of the commercial snakeboard

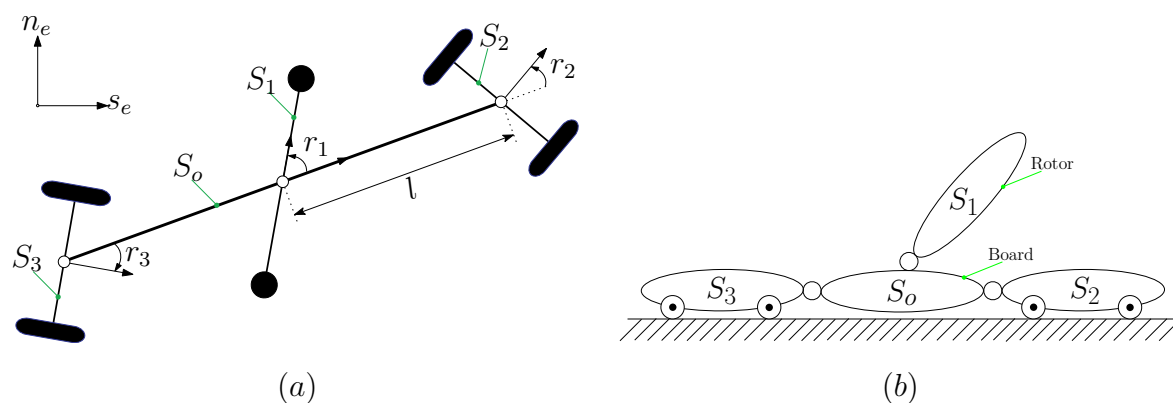


Figure 4.4 – Snakeboard: (a) Outline sketch; (b) Tree-like structure

4.2 The Snakeboard: Under-Constrained Case

In this section, we take the example of the snakeboard. To manually apply the proposed locomotion dynamics algorithm, we consider the existing robotic prototype (see Fig. 4.3(b)) of a commercial snakeboard (Fig. 4.3(a)). An outline model of the snakeboard mechanism is shown in Fig. 4.4(a). The snakeboard has a tree-like topology consists of four bodies interconnected through single degree of freedom revolute joints (see Fig. 4.4(b)).

Assumptions and Considerations

Since this robot has no actuated wheels, when numbering the system the choice of the reference body is free. Therefore, the board is taken as the reference body S_o , the mechanical rotor representing the human torso is denoted as body S_1 and the two identical wheeled bodies are called as S_2 and S_3 . Due to geometrical symmetry, the mass centers of S_o , S_2 and S_3 are aligned along the platform axis. A frame \mathcal{F}_j is assigned to body S_j at the mass center. Following the description and notations given in [87], here we make two assumptions. First we assume that the wheeled bodies are rotating out of phase to each other. Hence we adopt the following notations:

$r_1 = \psi$: the joint angle of S_1 with respect to S_o ,

$r_2 = -\phi$: the joint angle of S_2 with respect to S_o ,

$r_3 = \phi$: the joint angle of S_3 with respect to S_o .

Secondly, in order to simplify the manual computation of the algorithm, we make the following assumption related to mass and inertia of the snakeboard:

$$m = m_o + m_r + 2m_w, \quad I = I_o + I_r + 2I_w = ml^2,$$

where l is the length between the center of mass and the wheel base (see Fig. 4.4(a)), while the subscripts r and w stand for rotor and wheeled body, respectively.

In this planar case, the configuration space of the snakeboard is defined as $\mathcal{C}_2 = \text{SE}(2) \times (S^1)^3$. Where $\text{SE}(2)$ describes the planar configuration of the board S_o^+ , denoted as $({}^e g_o)^\vee = \begin{pmatrix} x_o & y_o & \theta_o \end{pmatrix}^T \in G$, with respect to the inertial frame \mathcal{F}_e whereas $(S^1)^3$ denotes the configuration shape-space of the three revolute joints parameterized by the vector $r = \begin{pmatrix} r_1 & r_2 & r_3 \end{pmatrix}^T \in \mathcal{S}$.

Modeling Approach

Being free (passive), the ideal wheels impose only the non-sliding constraints. As the two wheeled bodies apply only two independent constraints which are one less than the dimensions ($\dim(\text{SE}(2))=3$) on the principal fiber bundle. Thus, it is not possible to determine the net motions of the reference body S_o^+ through pure kinematics. Consequently, the system falls into the category of under-constrained mobile multibody systems for which the reference body motions are solved through a mixed kinematic and dynamic model. This is done with the help of reduced dynamics given in (3.69) along with the generalized kinematics (3.48). In this case, the two independent non-sliding constraints reduces the net motions of the reference body S_o^+ to a 1D free admissible subspace \mathcal{V}_f . Therefore, from the generalized kinematics (3.48), the board velocity is given by:

$$\eta_o = H_f \xi + J \dot{r}, \tag{4.7}$$

where ξ is the reduced velocity of the board in the free admissible subspace.

Construction of H_f

In the present case, the non-sliding condition determines two independent constraints that can be expressed in the reference body frame \mathcal{F}_o as linear functions of the velocities:

$$\begin{aligned} -s(-\phi)V_{x,o} + c(-\phi)V_{y,o} + lc(-\phi)\Omega_{z,o} - 0\dot{\phi} &= 0, \\ -s\phi V_{x,o} + c\phi V_{y,o} - lc\phi\Omega_{z,o} + 0\dot{\phi} &= 0, \end{aligned} \tag{4.8}$$

now writing in matrix form we have:

$$\begin{pmatrix} s\phi & c\phi & lc\phi \\ -s\phi & c\phi & -lc\phi \end{pmatrix} \eta_0 + 0\dot{\phi} = 0. \quad (4.9)$$

Comparing with equation (3.42), we have:

$$A = \begin{pmatrix} s\phi & c\phi & lc\phi \\ -s\phi & c\phi & -lc\phi \end{pmatrix}, \quad B = 0. \quad (4.10)$$

As $\dim(\text{SE}(2))=3$ and $\text{rank}(A) = 2$, then $\ker(A) = 1$ and hence a H_f whose columns span the kernel of the matrix A is given along with its time derivative as follows:

$$H_f = \begin{pmatrix} -2lc^2\phi \\ 0 \\ s2\phi \end{pmatrix}, \quad \dot{H}_f = \begin{pmatrix} 2ls2\phi\dot{\phi} \\ 0 \\ 2c2\phi\dot{\phi} \end{pmatrix}. \quad (4.11)$$

Furthermore, as $B = 0$, then $J = A^{-1}B = 0$, and finally from equation (4.7) we get the board velocity as follows:

$$\eta_o = \begin{pmatrix} -2lc^2\phi \\ 0 \\ s2\phi \end{pmatrix} \xi. \quad (4.12)$$

Here it is noteworthy that $B = 0$ physically means that the internal motions of the wheeled bodies alone (i.e. if $\dot{\psi} = 0$) do not produce net motions of the board, imposed by the design.

Preliminaries

We start our computation by defining the reduction matrices as follows:

$$H_o = H_1 = 1_3, \quad H_2 = H_3 = \begin{pmatrix} 1 & 0 \\ 0 & 0 \\ 0 & 1 \end{pmatrix},$$

while the transformation matrices are given as follows:

$$\text{Ad}_{1g_o} = \begin{pmatrix} c\psi & s\psi & 0 \\ -s\psi & c\psi & 0 \\ 0 & 0 & 1 \end{pmatrix}, \quad \text{Ad}_{2g_o} = \begin{pmatrix} c\phi & -s\phi & -ls\phi \\ s\phi & c\phi & lc\phi \\ 0 & 0 & 1 \end{pmatrix},$$

$$\text{Ad}_{3g_o} = \begin{pmatrix} c\phi & s\phi & -ls\phi \\ -s\phi & c\phi & -lc\phi \\ 0 & 0 & 1 \end{pmatrix}.$$

The inertia matrices are given as follows:

$$\begin{aligned}\mathcal{M}_o &= \text{diag}(m_o, m_o, I_o), \mathcal{M}_1 = \text{diag}(m_r, m_r, I_r), \\ \mathcal{M}_2 &= \mathcal{M}_3 = \text{diag}(m_w, m_w, I_w).\end{aligned}$$

Furthermore, as the body is in planar motion and the joints are at the mass center (i.e. $ms_j = 0$), thus equation (3.13) gives for $j = 0, 1, 2, 3$:

$$F_{\text{gyr},j} = 0, \quad (4.13)$$

while using equation (3.10), ζ_j , $j = 1, 2, 3$ is given as:

$$\zeta_1 = \begin{pmatrix} 0 \\ 0 \\ \ddot{\psi} \end{pmatrix}, \zeta_2 = \begin{pmatrix} -lc\phi s^2 2\phi\xi^2 \\ -ls\phi s^2 2\phi\xi^2 \\ -\ddot{\phi} \end{pmatrix}, \zeta_3 = \begin{pmatrix} lc\phi s^2 2\phi\xi^2 \\ -ls\phi s^2 2\phi\xi^2 \\ \ddot{\phi} \end{pmatrix}.$$

4.2.1 Reduced Dynamic Locomotion Model of S_o^+

As snakeboard requires the reduced dynamic equation (3.67) to be solved along with the kinematic equation (4.12). Therefore, we first solve its dynamics as follows. We start by computing the composite inertia of the snakeboard through (3.27) as follows:

$$\mathcal{M}_o^+ = \sum_{j=0}^3 \text{Ad}_{j_{g_o}}^T \mathcal{M}_j \text{Ad}_{j_{g_o}} = \begin{pmatrix} m & 0 & 0 \\ 0 & m & 0 \\ 0 & 0 & ml^2 \end{pmatrix}. \quad (4.14)$$

and projecting this composite inertia onto the 1D free admissible subspace \mathcal{V}_f through the relation (3.67) gives the reduced composite inertia as follows:

$$\mathcal{M}_{r_f}^+ = H_f^T \mathcal{M}_o H_f = 4ml^2 c^2 \phi. \quad (4.15)$$

This reduced composite inertia matrix is called as the locked inertia matrix in [87]. Then we compute the composite inertial wrench by using equation (3.26) along with zero gyroscopic wrench from (4.13):

$$F_{\text{in},o}^+ = - \sum_{j=1}^3 \text{Ad}_{j_{g_o}}^T \mathcal{M}_j \zeta_j = \begin{pmatrix} 0 \\ 0 \\ I_r \ddot{\psi} \end{pmatrix}.$$

As $J = 0$ and $H_a = 0$, then the reduced composite wrench in the free admissible subspace is given by the relation (3.67) as follows:

$$F_{r_f}^+ = H_f^T F_{\text{in},o}^+ - H_f^T (\mathcal{M}_o^+ \dot{H}_f \xi) = -I_r s 2\phi \ddot{\psi} + 2ml^2 s 2\phi \dot{\phi} \xi. \quad (4.16)$$

Now by injecting equations (4.15) and (4.16) in the reduced locomotion dynamic model (3.69), we compute the reduced acceleration $\dot{\xi}$ of the board as follows:

$$\dot{\xi} = tg\phi\left(-\frac{I_r}{2ml^2}\ddot{\psi} + \dot{\phi}\xi\right), \quad (4.17)$$

which has to be completed with the kinematic model (4.12). Finally, the simplified form of the reduced dynamic model (3.69) for the snakeboard is given as follows:

$$\begin{pmatrix} \dot{\xi} \\ {}^e\dot{g}_o \end{pmatrix} = \begin{pmatrix} tg\phi\left(-\frac{I_r}{2ml^2}\ddot{\psi} + \dot{\phi}\xi\right) \\ {}^e g_o \left(\begin{pmatrix} -2lc^2\phi & 0 & s2\phi \end{pmatrix}^T \xi \right)^\vee \end{pmatrix}. \quad (4.18)$$

4.2.2 Torque Dynamics

Now we solve the reduced torque dynamic model in order to get the joint torques. For this, we first calculate the reduced acceleration $\dot{\eta}_{rj}$ of each body S_j through recursive equation (3.74) initialized by $\dot{\eta}_o$ which is deduced from the time derivative of (4.18):

$$\dot{\eta}_o = H_f\dot{\xi} + \dot{H}_f\xi = \frac{I_r}{2ml^2} \begin{pmatrix} ls2\phi \\ 0 \\ -2s^2\phi \end{pmatrix} \ddot{\psi} + \begin{pmatrix} ls2\phi \\ 0 \\ 2c^2\phi \end{pmatrix} \dot{\phi}\xi \quad (4.19)$$

Then, the inter-body wrenches are calculated with the help of equation (3.83). Finally, the algorithm uses the torque relationship (3.85) to project the applied wrenches upon the joint axes as follows²:

$$\begin{aligned} \tau_1 &= A_1^T(\mathcal{M}_1\dot{\eta}_1), \\ \tau_j &= A_{rj}^T(\mathcal{M}_{rj}\dot{\eta}_{rj}), \quad j = 2, 3; \end{aligned}$$

where for the snakeboard $A_1^T = (0, 0, 1)$ and $A_{rj}^T = (0, 1)$. The snakeboard planar motion and also the wrench projection over the rotation axis verify the involvement of only the third component of equation (4.19) in the torque computation. That is:

$$\begin{aligned} \tau_1 &= \left(I_r - \left(\frac{I_r}{ml^2}\right)s^2\phi\right)\ddot{\psi} + 2c^2\phi I_r \dot{\phi}\xi, \\ \tau_2 &= -\left(\frac{I_w I_r}{ml^2}\right)s^2\phi\ddot{\psi} + 2c^2\phi I_w \dot{\phi}\xi - I_w \ddot{\phi}, \\ \tau_3 &= -\left(\frac{I_w I_r}{ml^2}\right)s^2\phi\ddot{\psi} + 2c^2\phi I_w \dot{\phi}\xi + I_w \ddot{\phi} \end{aligned}$$

²Note that, from (3.84), $F_{\text{gyr},rj}$ is also zero because of (4.13) and $\dot{H}_j = 0$ for all bodies.

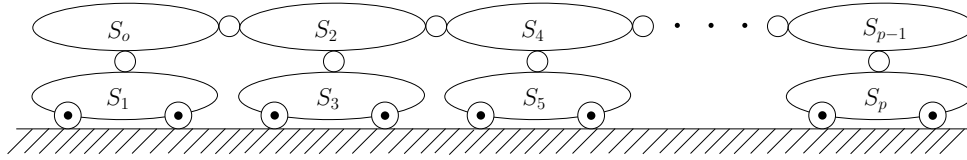


Figure 4.5 – Tree-like structure of snake-like robot

Alternatively, in terms of generalized forces applied to the two independent internal coordinates, we get:

$$\begin{aligned}\tau_\psi &= I_r \left(\left(1 - \left(\frac{I_r}{ml^2} \right) s^2 \phi \right) \ddot{\psi} + 2c^2 \phi \dot{\phi} \dot{\xi} \right), \\ \tau_\phi &= \tau_3 - \tau_2 = 2I_w \ddot{\phi}\end{aligned}\tag{4.20}$$

The above torques are the desired output of the algorithm. Consequently, equations (4.17) and (4.20) agree with the momentum and reduced dynamics of [87] deduced from the geometric Lagrangian framework of the principal fiber bundle.

4.3 Snake-like Robot: Fully-Constrained Case

The snake-like robot system presented here is based on a planar robot of Hirose [53]. The configuration space is defined as $\mathcal{C}_2 = \text{SE}(2) \times (S^1)^p$. The snake-like robot represents a modular tree-like mobile multibody system with wheeled bodies (see Fig. 4.5). It consists of $p + 1$ rigid bodies interconnected through single degree of freedom revolute joints. Each wheeled body is an assembly of free (i.e. passive) wheels (see Fig. 4.6). A frame $\mathcal{F}_j = (O_j, s_j, n_j, a_j)$ is attached at the joint center of each body S_j . Here we consider that each unwheeled body and its corresponding wheeled body (collectively called here as a module) are connected to each other at their mass centers. The modules are then connected serially to form the snake-like robot. After numbering the bodies, we have $\mathbb{N}_{uw} = \{0, 2, 4, \dots, p - 1\}$ and $\mathbb{N}_w = \{1, 3, 5, \dots, p\}$, as the sets of indices of unwheeled and wheeled bodies respectively. Being free, the ideal wheels of the snake-like robot only impose the non-sliding constraints. In this planar case with $\dim(\text{SE}(2)) = 3$, if at least 3 independent non-sliding constraints are available, then the snake-like robot becomes a fully-constrained system. As a result, it can be modeled through pure kinematics by using the kinematic locomotion model given in (3.45). If the number of independent non-sliding constraints is more than 3, then the system must verify the compatibility condition given by (3.44) in order to preserve mobility of the whole system.

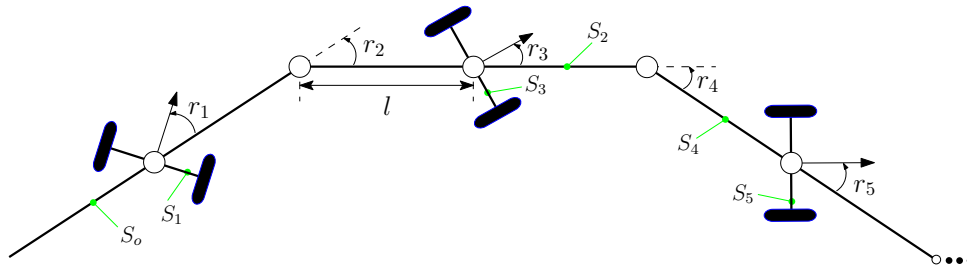


Figure 4.6 – Outline sketch of snake-like robot

Preliminaries

First we define the reduction matrices as follows:

$$H_j = 1_3 \text{ for } j \in \mathbb{N}_{uw}, \text{ and } H_j = \begin{pmatrix} 1 & 0 \\ 0 & 0 \\ 0 & 1 \end{pmatrix} \text{ for } j \in \mathbb{N}_w,$$

and the transformation matrices in $SE(2)$ are given by:

$$\text{Ad}_{j_{g_i}} = \begin{pmatrix} cr_j & sr_j & lsr_j \\ -sr_j & cr_j & lcr_j \\ 0 & 0 & 1 \end{pmatrix} \text{ for } j \in \mathbb{N}_w,$$

$$\text{Ad}_{j_{g_i}} = \begin{pmatrix} cr_j & sr_j & 2lsr_j \\ -sr_j & cr_j & 2lcr_j \\ 0 & 0 & 1 \end{pmatrix} \text{ for } j \in \mathbb{N}_{uw},$$

where l is half the length of any unwheeled body. According to equation (3.84), the reduced inertia matrices are given by:

$$\mathcal{M}_{r_j} = \text{diag}\{m_w, I_w\} \text{ for } j \in \mathbb{N}_w,$$

$$\mathcal{M}_{r_j} = \begin{pmatrix} m & 0 & 0 \\ 0 & m & ml \\ 0 & ml & I \end{pmatrix} \text{ for } j \in \mathbb{N}_{uw},$$

where the subscript w stands for wheeled bodies.

4.3.1 Kinematic Locomotion Model of S_o^+

This robot has enough nonholonomic (non-sliding) constraints to model the kinematics of the reference body S_o^+ without entering into dynamics [88]. In fact, once gathered the non-sliding conditions imposed by the first three modules (see Fig. 4.6) take the form of

the first line of the (3.43) where \bar{A} is a (3×3) invertible full rank matrix and \bar{B} is a (3×2) matrix given as:

$$\bar{A} = \begin{pmatrix} -sr_1 & cr_1 & 0 \\ -s\bar{r}_3 & c\bar{r}_3 & a_{23} \\ -s\bar{r}_5 & c\bar{r}_5 & a_{33} \end{pmatrix}, \bar{B} = \begin{pmatrix} 0 & 0 \\ lcr_3 & 0 \\ b_{31} & lcr_5 \end{pmatrix},$$

with:

$$\begin{cases} \bar{r}_3 = r_2 + r_3, \\ \bar{r}_5 = r_2 + r_4 + r_5, \\ a_{23} = l(cr_3 + c\bar{r}_3), \\ b_{31} = l(cr_5 + 2c(r_4 + r_5)), \\ a_{33} = b_{31} + lc\bar{r}_5. \end{cases}$$

Thus, matrix \bar{A} being invertible, we can compute the head velocity η_o in the form of (3.45) where $\mathcal{A}_k(r) = \bar{A}^{-1}\bar{B}$ stands for the local form of the principal kinematic connection of the snake-like robot.

Finally, in this degenerate case, (3.46) will be used to find the head acceleration $\dot{\eta}_o$ and the updated configuration for the next time step through integration of ${}^e\dot{g}_o$.

4.3.2 Torque Dynamics

To calculate the joint torque applied onto each body, we first calculate the reduced velocities and accelerations $(\eta_{rj}, \dot{\eta}_{rj})$ of each body through forward recursive equations (3.73) and (3.74) initialized by (3.45) and (3.46), respectively. Then, we calculate the reduced wrenches F_{rj} for $j = p, \dots, 1$ through the backward recursive equation (3.83). Finally, the joint torques τ_j are given by (3.85).

4.3.3 Numerical Results

For the numerical results, let us suppose a snake-like robot shown in Fig. 4.5 with 10 identical modules. Thus the robot has total of twenty bodies (i.e. $p = 19$) of which 10 are wheeled while 10 are unwheeled. The simulation parameters are given as follows:

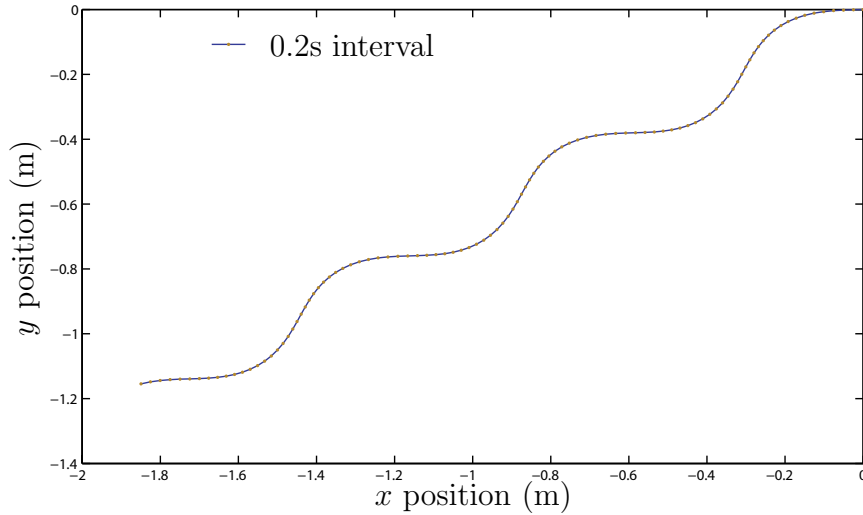
Length of each module: $l = 0.1\text{m}$.

Mass of each module: $m = 0.3\text{kg}$.

A *serpentine* gait is imposed with the joint motions given by:

$$r_j = a_j \sin(w_j t + \phi_j),$$

where a_j , w_j and ϕ_j are the amplitudes, frequencies and phases of the joints $j = 1, 2, \dots, 5$ of the first three leading modules, respectively. We take, $a_j = (0.2, 0.6, -0.2, 0.6, 0.2)$, $w_j =$

Figure 4.7 – Motion of the head body S_o in the xy plane

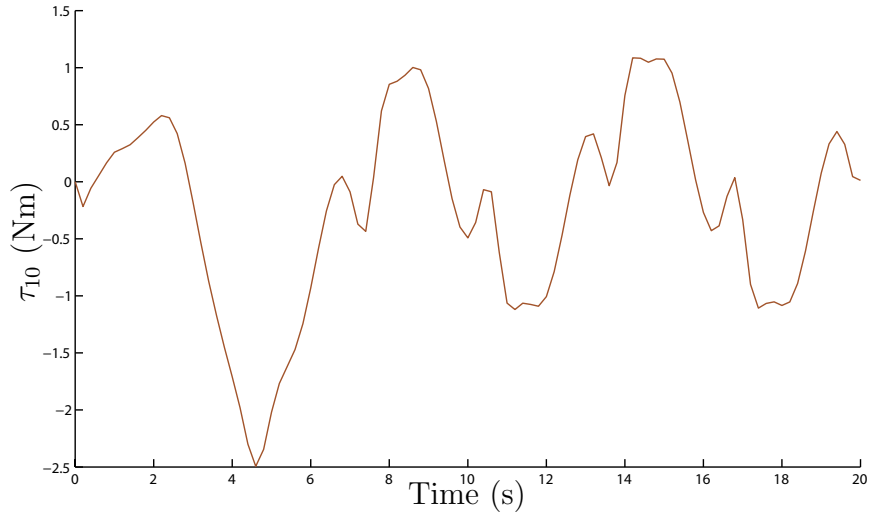
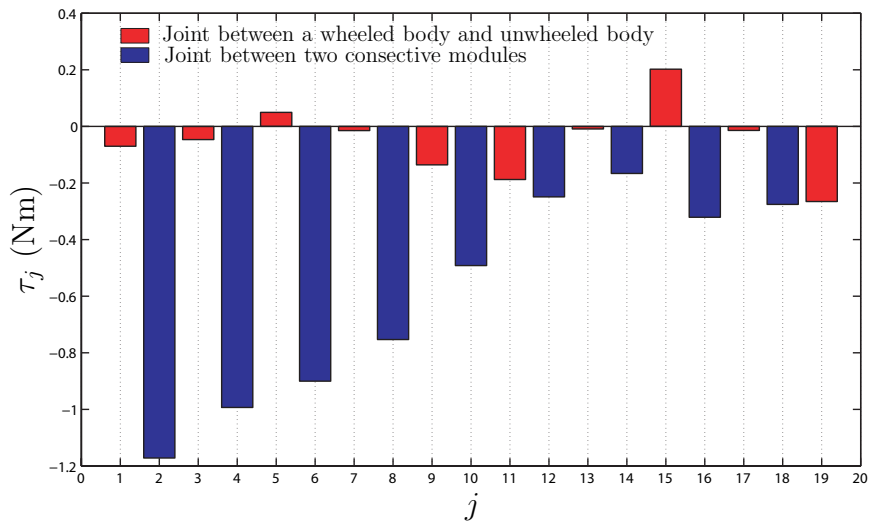
1, and $\phi_j = (\frac{\pi}{16}, \frac{9\pi}{16}, 0, \frac{7\pi}{16}, -\frac{\pi}{16})$ for the first three leading modules. In order to maintain mobility, the additional modules must obey the compatibility condition (3.44) imposed by the non-sliding constraints of the wheels. By controlling the degree of freedom of the wheeled body through known time laws, the algorithm integrates at each time step the following recursive governing equation in order to compute the desired joint angle $r_j, j = 6, 8, \dots, p - 1$ between two consecutive modules r_j and r_{j-2} :

$$\dot{r}_j = -\frac{1}{l \cos(r_{j+1})} (A_k \eta_o + B_k \dot{r}),$$

where the subscript $k (= \frac{j}{2} + 1)$ labels the k^{th} row of the system of constraint equations (3.43) with A_k and B_k being the k^{th} row of the matrices A and B , respectively. Due to the open chain topology of the system, the matrix B is a lower triangular matrix and the above relation is explicitly solvable with respect to \dot{r}_j . Now simulating for 20s, we get the net motions of the reference body S_o^+ in the xy plane as shown in Fig. 4.7. The Fig. 4.8 shows the time evolution of the joint torque applied between S_8 and S_{10} while in Fig. 4.9 the torques of all the joints ($j = 1, \dots, 19$) are plotted at $t = 10s$.

4.4 Mobile Manipulator: Fully-Actuated Case

The mobile manipulator considered in this section is of a Staubli manipulator mounted on (coupled with) a car-like platform as shown in Fig. 4.10(a). The configuration space is defined as $\mathcal{C}_2 = \text{SE}(3) \times (S^1)^p$. The system consists of seven rigid bodies S_o, S_1, \dots, S_6 (as shown in Fig. 4.10) interconnected through six single degree of freedom revolute joints (i.e. $p = 6$). According to the Denavit-Hartenberg convention, a frame $\mathcal{F}_j = (O_j, s_j, n_j, a_j)$ is attached to the joint center of each body $S_j, j = 1, 2, \dots, 6$. The car-like platform carries

Figure 4.8 – Joint torque τ_{10} Figure 4.9 – All joint torques at $t = 10$ sec

out only planar motion and is taken as the reference body S_o to which the frame \mathcal{F}_o is attached. The remaining six bodies (S_1, S_2, \dots, S_6) form the Staubli arm.

Modeling Approach

In this case, a wheeled platform is coupled with a manipulator arm. Our purpose is to study the dynamic coupling effects of the platform on the arm and vice-versa. We want the platform to move on a desired trajectory, and at the same time the arm should manipulate. Thus the platform should compensate the dynamic effects of the arm and vice-versa in terms of the internal control torques as well as the actuated wheel torques. These torques will be computed through the proposed algorithm.

The platform is fully actuated through the rolling without slipping and non-sliding con-

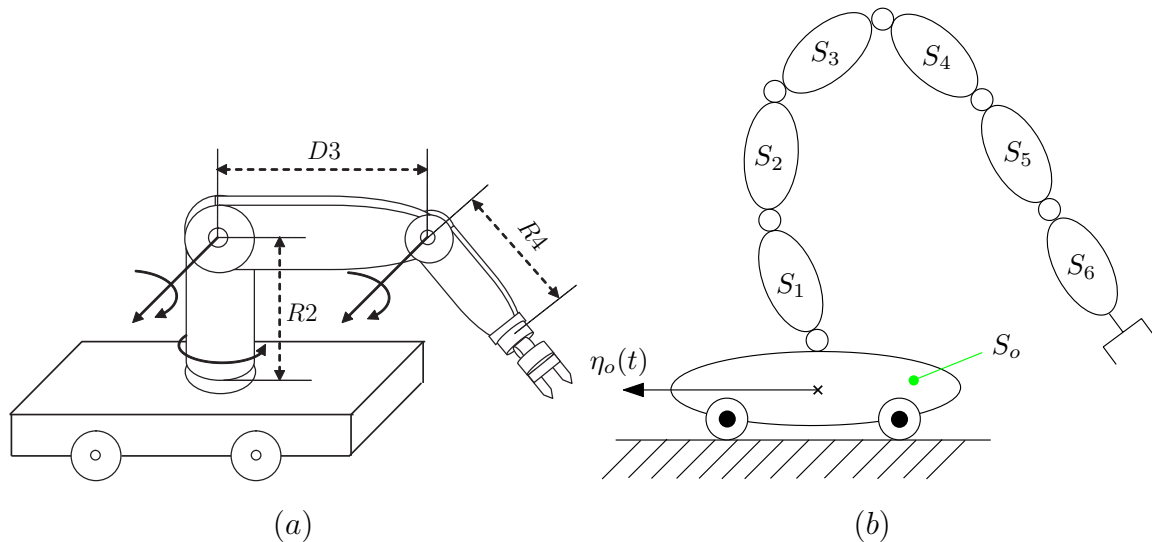


Figure 4.10 – (a) Staubli manipulator mounted on a car like platform; (b) Top view of the platform, $R2 = 0.42$, $D3 = R4 = 0.45$

straints imposed by the wheels of the platform. Therefore, the net motions of the platform are computed through pure kinematic locomotion model (3.57) whereas the manipulator arm takes these motions to solve its dynamics (i.e. computes the desired internal control torques τ_j) through simple Luh and Walker algorithm. On the other hand, the reduced dynamic locomotion model is utilized to compute the desired wheel torques Γ which compensates the dynamic coupling effects.

Preliminaries

As the platform is fully actuated then we have $\mathcal{V} = \mathcal{V}_a$, $H = H_a$. The preliminary kinematics required by the algorithm are:

$$H_a = \begin{pmatrix} 1 \\ b \\ a \end{pmatrix}, \text{ with: } b = 2^{-1}tg\beta \text{ and } a = l^{-1}tg\beta. \quad (4.21)$$

Since the car-like platform is a wheeled body, (3.50) gives $\dot{\theta}_{oa} = B_{aa}\eta_{ra}$ with:

$$B_{aa} = \begin{pmatrix} \bar{B}_{aa} \\ \tilde{B}_{aa} \end{pmatrix} = \frac{1}{R} \begin{pmatrix} (1 + (L/l)b)c\beta_1 + s\beta_1tg\beta \\ (1 - (L/l)b)c\beta_2 + s\beta_2tg\beta \end{pmatrix}. \quad (4.22)$$

In the above relation, $\beta \in]-\pi/2, \pi/2[$ is the time-varying steering angle of a virtual wheel placed at the center of the steering wheel axle (see Fig. 4.11), and is compatible with the two real actuated front wheels (i.e. verifying: $tg\beta = (1 + L/2l)tg\beta_1 = (1 - L/2l)tg\beta_2$). In the following, we use the new notation: $\xi = \eta_{ra}$, which is, for instance, imposed through: $\xi(t) = \bar{B}_{aa}^{-1}(t)\dot{\theta}_{oa}(t)$ and allows the platform posture to be computed thanks to

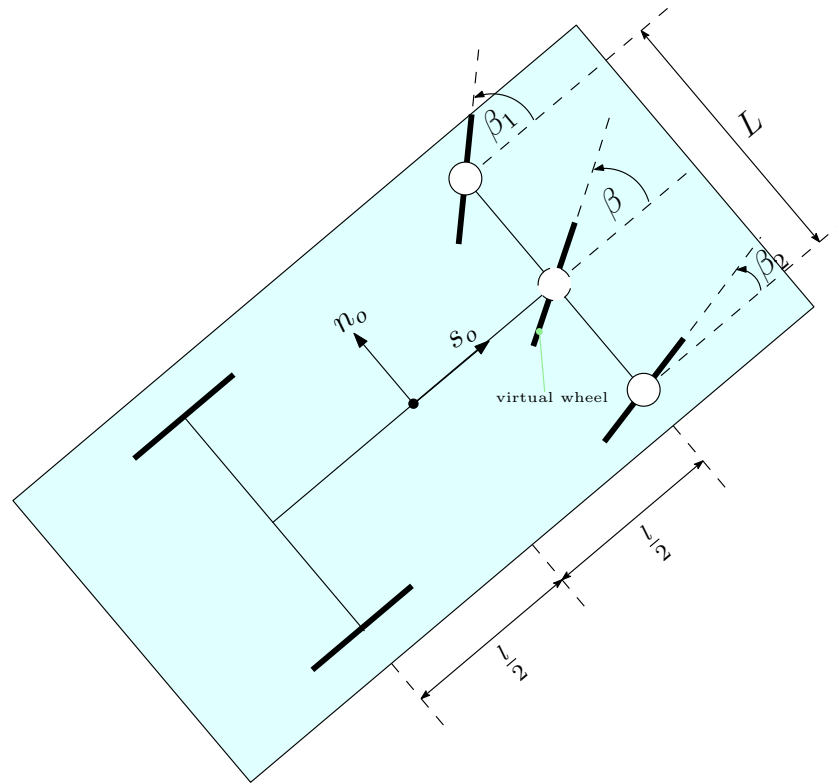


Figure 4.11 – Top view of the car-like platform, $l = 1.0$, $L = 0.5$

the reconstruction equation (3.69), with $J = 0$, $H_f = 0$.

4.4.1 Reduced Dynamic Locomotion Model

The reduced dynamics are computed step by step by starting with the computation of the composite inertia matrix \mathcal{M}_o^+ from (3.27) which is then projected onto the fully actuated admissible space \mathcal{V}_a , so giving \mathcal{M}_{ra}^+ from (3.72). Next, the algorithm computes $F_{in,o}^+$ from (3.68), which is reduced to $F_{in,ra}^+$ thanks to the projection (3.72).

4.4.2 Torque Dynamics

To compute the joint torque, the algorithm computes the reduced forward kinematics (3.73) and (3.74) with $\eta_o = H_a \xi$ and $\dot{\eta}_o = H_a \dot{\xi} + \dot{H}_a \xi$ as initial conditions. Then the backward recursion (3.83) is computed and the reduced wrenches are projected according to (3.85), so giving the joint torques as outputs. Regarding the wheel torques, since the admissible space is fully actuated (i.e. $\mathcal{V} = \mathcal{V}_a$), we first calculate the external wrench $F_{ext,ra}^+$ from (3.71) with $\dot{\eta}_{rf} = 0$ and $\dot{\eta}_{ra} = \dot{\xi}$. Then, from relations (3.86) along with (4.22), and by supposing that both actuated wheels produce the same torque, one finds $\tilde{\Gamma} = \bar{\Gamma} = \Gamma = -(\bar{B}_{aa}^T + \tilde{B}_{aa}^T)^{-1} F_{ext,ra}^+$.

4.4.3 Numerical Results

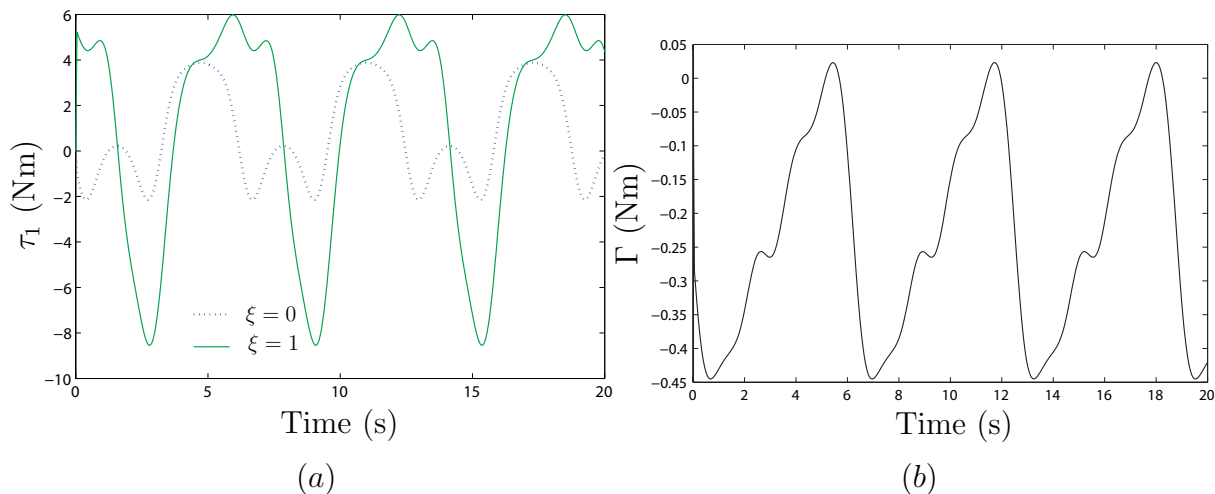


Figure 4.12 – (a) Torque τ_1 for two different values of ξ ; (b) Wheel torque for $\xi = 1$

The numerical results are obtained through the algorithm for the above mentioned mobile manipulator. The dynamic effects of the first three bodies of the manipulator are taken into account by actuating the first three joints while the rest of joints are stationary. Each body of the manipulator is assumed to be cylindrical. The inertia of the platform is 10 times that of the maximum inertia of the system about the z-axis.

In simulation, the wheel and joint torques are computed for: $r_j(t) = \sin(w_j t)$, and $\beta(t) = \sin(w_b t)$. Then, with the same joint motions, the torques are computed for $\xi = 1$ and $\xi = 0$. The plot in Fig. 4.12(a) shows the effect of the reference body (platform) dynamics on the manipulator joint torques due to the dynamic coupling between the arm and the platform. On the other hand, Fig. 4.12(b) shows the required wheel torques ($\tilde{\Gamma} = \bar{\Gamma} = \Gamma$) for $\xi = 1$.

4.5 Conclusions

In this chapter, the general algorithm proposed in chapter 3 was applied to a wide range of multibody systems including unconstrained and constrained systems. The constrained systems further included the under-constrained (snakeboard) and fully constrained (snake-like robot) systems as well as the case of a manipulator with a mobile base subject to some imposed motions. All these inclusions lead to the fact that the more general algorithm works for all these cases like some particular ones. Moreover, the final algorithm is very easy to implement and the complexity of the initial mechanism has no effect on its implementation since, thanks to its recursive character, the addition of more and more bodies just increases the final indices of the recurrences. As a final note, the proposed Newton-Euler based dynamic model is homologous to the Lagrangian-based dynamics as

it is shown in the case of snakeboard and satellite. In the next chapter, we are going to extend the algorithm proposed in this first part of the thesis to the case of continuous systems. We will see that such an extension actually results in an algorithm which is a continuous version of the Newton-Euler based algorithm of discrete systems.

Part II

Continuum Systems: Hyper-Redundant Robots



Macro-Continuous Dynamic Modeling of Hyper-Redundant Robots

5.1	Modeling Approach of Hyper-Redundant Robots	100
5.1.1	Assumptions and Considerations	102
5.2	Beam Kinematics and Hyper-Redundant Robots	105
5.3	Continuous Models of Hyper-Redundant Robots	107
5.3.1	Continuous Model of Transformations	107
5.3.2	Continuous Model of Velocities	107
5.3.3	Continuous Model of Accelerations	108
5.3.4	Dynamics on C_1 : Continuous Model of Internal Wrenches	108
5.3.5	Dynamics on C_2 : Dynamics of the Reference Body	111
5.4	Dynamic Algorithm of Hyper-Redundant Robots	112
5.5	Terrestrial Locomotion Model	114
5.5.1	Kinematic Modeling of Contacts	115
5.5.2	Model of Contact Forces	118
5.5.3	Algorithm in Kinematic Case	119
5.6	Conclusions	122

This chapter develops an algorithmic tool to solve the problem of locomotion of the new generation of robots called as hyper-redundant robots. In case of bio-inspired locomotion these hyper-redundant robots are usually inspired from vertebrate elongated body animals with large number of internal degrees of freedom such as snakes [52] and anguilliform fish [13], where the vertebrae correspond to the rigid bodies of the associated multibody system. From this point of view, these animals can be effectively considered as continuous deformable medium such as the European eel having more than 130 vertebrae, while some species of big snakes have more than 500. Nowadays, thanks to the research on biomimetic robots, the concepts of soft body robots are extending robotics even further. In fact, unlike traditional robots, these robots, inspired by the invertebrate organisms known as hydrostats, do not contain any rigid organs. Also, their shape changes are continuous along their body length similar to that of an elephant trunk [48], the mammalian tongue [107], caterpillars [9], earthworms [65], octopus arms [68] etc. Finally, all these systems today form the general class of continuous-like systems.

Regarding their potential impact, let us first note that using the same single chain mor-

phology, elongated continuous robots may offer a wide spectrum of applications ranging from manipulation to locomotion on earth as well as in water. Moreover, once connected to a discrete mechanism, they could be used as versatile manipulators as well as grippers [79]. Finally, due to their slender morphology, they could play a crucial role to achieve rescue missions in unstructured, highly cluttered and confined environments, e.g. collapsed buildings, narrow spaces etc.

Several researchers have done extensive work related to hyper-redundant as well as soft robots in order to investigate the usual problems of robotics such as motion planning, gait generation, kinematic and dynamic modeling, design and control, etc. We refer the reader to [113] which surveys the state of the art on soft robotics. Historically, the initiative was undoubtedly taken by Hirose through his pioneering work related to the design and control of snake-like devices [52]. Based on these seminal works, many contributions to kinematic modeling have been proposed [28, 18, 85, 57, 48]. Concerning dynamics of continuous robots, a few works on this topic have been proposed [26, 41, 83, 108]. Applying the continuous modeling approach necessitates to give a material reality to the continuous kinematics. For instance, the backbone curves of references [28, 18] have to be completed with a material lateral extension enabling the inertia of the robot to be defined as achieved in [26, 83] for planar robots. Alternatively, the geometrically exact beam theory of J.C. Simo [105, 104] has been used for the modeling of passive steerable needles in the context of medical robotics [116],[95], while in [113] and [112], it has been applied to the real soft robot OctArm [46]. With the progress of these researches, the extension of the classical robot models (i.e. geometric, kinematic and dynamic models) to these new systems became a crucial step towards their future success. Thus, the second major goal of this thesis is to propose a modeling and simulation tool in a unified framework suited to the study of locomotion of such continuum systems [11]. Furthermore, this tool is applied to the terrestrial locomotion systems as a first illustration.

In the sequel of this chapter, first of all an overview of the proposed modeling approach is given to point out the basic assumptions and considerations of the modeling process. In a first step, proceeding with the mathematical modeling, the kinematic and dynamic models are developed in section 5.3. These models are then used to form a general algorithm applicable to hyper redundant systems. In a second step, this algorithm is modified for the terrestrial locomotion systems inspired from elongated body animals.

5.1 Modeling Approach of Hyper-Redundant Robots

In the geometrically exact beam theory, a beam is modeled as a one dimensional Cosserat medium [33], i.e. a multibody system made of an infinite number of rigid bodies, or cross sections, of infinitesimal length assembled along the line of their centroids, where each cross section is able to move with respect to the other due to some controlled strain time-

variations. Starting from this point of view, in [13] a continuous eel-like robot is modeled as a strain (curvature) - actuated geometrically exact beam. Pursuing a macroscopic modeling approach, each Cosserat cross section of the actuated beam mimics a vertebra of the animal (here the eel), while the imposed strain law models the actuated infinitesimal joints of the corresponding continuous rigid robot. Once related to the general theory of locomotion on principal fiber bundles [76], such a model can be used to solve the general problem stated in section 2.3.3 that we now recall by using the curvature time law as control input.

1. Computes the net motions of a reference cross section (for instance attached to the head) propelled by the external forces exerted by the surroundings (i.e., solves the forward locomotion dynamics).
2. Computes the internal control torques (and/or forces), i.e. solves the inverse torque dynamics.

This modeling approach was termed macro-continuous in [13] since, like the Variable Geometry Truss evoked in [26], it is suitable for modeling hyper-redundant robots at a macroscopic scale where they can be approximated as a beam. It is naturally adapted to the highest levels of the mechanical design as well as the generation of complex gaits involving a lot of degrees of freedom as this is usually the case of hyper-redundant robots [50].

In this chapter, we reconsider this macro-continuous approach for locomotion and extend it to the following cases.

1. The configuration space of the cross sections is an arbitrary Lie group.
2. The control strain law is arbitrary (curvature, twist, stretching, etc.).
3. The external forces responsible for the propulsion are not necessarily to be those produced by a fluid but can be imposed by the contact with the ground and modeled through kinematic constraints.

In this case, similar to discrete multibody systems discussed in the first part of this thesis [10], when the number of independent constraints is larger than the number of net motions degrees of freedom, the locomotion dynamics can be replaced by a kinematic model entirely governed by the constraints. Geometrically, these forward locomotion kinematics are nothing but a continuous version of the finite-dimensional kinematic connections of nonholonomic mechanics [76, 8]. As a consequence and contrary to the case of eel swimming, the locomotion dynamics are not required to deduce the net motions but are used in their inverse form to compute the resultant and moment of external forces produced by the external contacts. Once these elements are computed, they are distributed on the

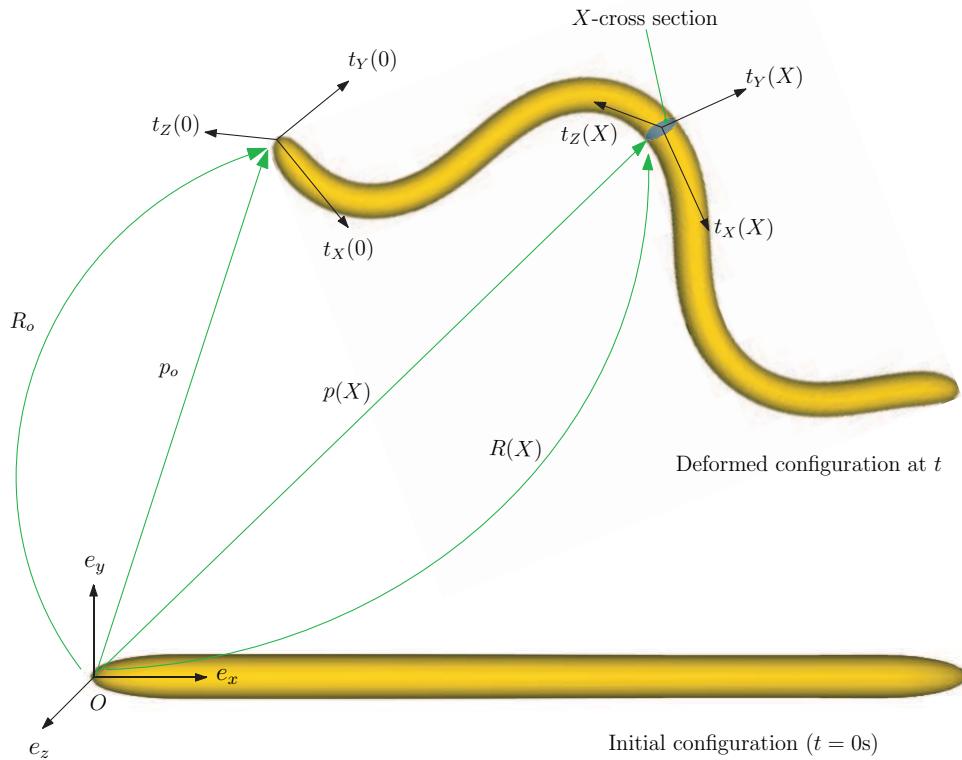


Figure 5.1 – *Frames and parametrization of a hyper-redundant robot*

contacts in order to fix a possible set of external reaction forces and couples which are used in a second step by the algorithm to compute the desired internal actuation torques and/or forces to impose the desired strain law. Finally, the kinematic constraints are deduced from the model of a few types of contacts. This will allow us, in the next chapter, to apply the macro-continuous approach to terrestrial locomotion of several elongated body animals as earthworms, inchworms, snakes in planar and three-dimensional lateral undulations, etc.

5.1.1 Assumptions and Considerations

The hyper-redundant robot is considered as a 1D Cosserat beam along with the geometrically exact beam theory developed by J. C. Simo [106] in 1980's. The basic idea of Cosserat theory [33] is to consider the beam as a serial assembly of rigid cross sections assembled along a centroidal line passing through the geometric center of each cross section. With such considerations, a hyper-redundant robot may be modeled as a Cosserat beam in finite 3D transformations and small strains with the backbone curve of the robot assimilated to the beam centroidal line. In this approach, each rigid cross section of the beam (of length l) is labeled by its abscissa X in the initial straight configuration in which the

beam is aligned along the axis (O, e_x) of the fixed orthonormal frame $\mathcal{F}_s = (O, e_x, e_y, e_z)$ as shown in Fig. 5.1. A mobile orthonormal frame $t \mapsto \mathcal{F}_m(X, t) = (P, t_X, t_Y, t_Z)(X, t)$ is attached to any rigid cross section X . The origin $P(X)$ and the first vector $t_X(X)$ coincide with the mass center of the cross section and its unit normal vector, respectively.

Configuration Spaces of a Hyper-Redundant Robot

For any function $f(X, t)$, the partial derivative operators $\frac{\partial}{\partial X}f(X, t)$ and $\frac{\partial}{\partial t}f(X, t)$ will be simply indicated as $f'(X, t)$ and $\dot{f}(X, t)$, respectively. With the above considerations, the configuration of any mobile frame $\mathcal{F}_m(X, t)$ attached to a cross section X is defined by the action of an element of $g \in \text{SE}(3)$ applied to the fixed frame \mathcal{F}_s . It thus becomes possible to introduce the first definition of the robot configuration space as a functional space of curves in $\text{SE}(3)$, parameterized by the material abscissa, i.e.:

$$\mathcal{C}_1 = \{g : \forall X \in [0, l] \mapsto g(X) \in \text{SE}(3)\}, \quad (5.1)$$

with:

$$g(X) = \begin{pmatrix} R(X) & p(X) \\ 0 & 1 \end{pmatrix}.$$

On the robot, two vector fields are defined in $\text{se}(3)$. The first is the time-twist field defined as follows:

$$\widehat{\eta} : X \in [0, l] \mapsto \widehat{\eta}(X, t) = g^{-1}\dot{g} \in \text{se}(3), \quad (5.2)$$

where $\eta(X, t)$ defines the infinitesimal transformation undergone by the cross section X between two infinitely close instants t and $t + dt$ as depicted in Fig. 5.2. The second is the space-twist field such that:

$$\widehat{\xi} : X \in [0, l] \mapsto \widehat{\xi}(X, t) = g^{-1}g' \in \text{se}(3), \quad (5.3)$$

where $\xi(X, t)$ defines the infinitesimal transformation undergone by the cross section X at fixed time t when the material axis slides from X to $X + dX$ as depicted in Fig. 5.2. Now depending on the considered robot, certain degrees of freedom between any two contiguous cross sections are actuated while others are constrained to constant values through the design of internal joints (that are assumed ideal). Mathematically, this corresponds to identify $\widehat{\xi}(X, t)$ to a desired control field explicitly dependent on the time and noted $\widehat{\xi}_d(t)$, i.e.:

$$\xi(X) = \xi_d(X, t), \forall (X, t) \in [0, l] \times \mathbb{R}^+. \quad (5.4)$$

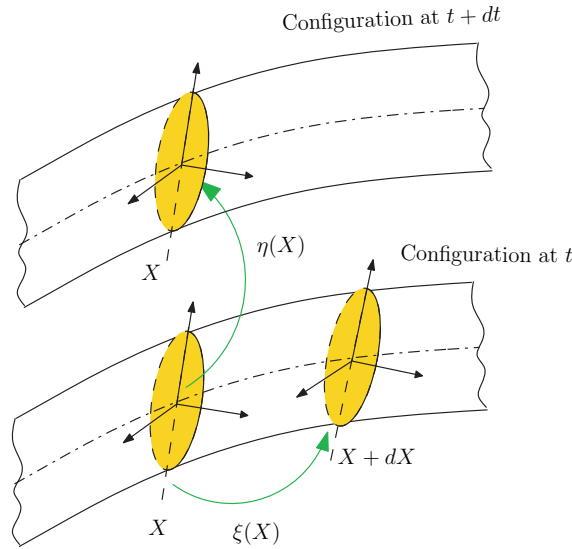


Figure 5.2 – Representation of vector fields $\eta(X)$ and $\xi(X)$

It is also possible to reconstruct the configuration of the beam from the knowledge of the reference configuration g_o and that of the strain field $\xi_d(t)$. Thus, a second definition of the configuration space of a robot can be given as the principal fiber bundle:

$$\mathcal{C}_2 = G \times \mathcal{S}, \quad (5.5)$$

where G stands for the configuration of the head frame $\mathcal{F}_m(0, t)$, while \mathcal{S} is the shape space here defined as the following functional space of curves in the Lie algebra of the configuration group $\text{SE}(3)$:

$$\mathcal{S} = \{\xi : \forall X \in [0, l] \mapsto \xi(X) \in \text{se}(3)\}. \quad (5.6)$$

In this second definition of the robot configuration space, the cross section $X = 0$ plays the role of reference body, i.e. a body whose motion defines the reference of net motions with respect to which the shape deformations are measured. In bio-mimetics, the head of the bio-inspired robot is usually considered as the reference body.

Finally, $\xi_d(X, t)$ parameterizes the internal kinematics of the robot, i.e. the continuous infinitesimal homologous of the usual internal joints $r_j(t)$ of discrete multibody systems, with X playing the role of the continuous body index. Note that in the theory of continuum mechanics, X is a Lagrangian (material) label.

5.2 Beam Kinematics and Hyper-Redundant Robots

We now list the different possible actuations of the strain field $\xi_d(t)$ and comment their relations to continuum robotics and beam theory. For this, we start from definition (5.4) which we detail as follows:

$$g^{-1}g' = \begin{pmatrix} R^T R' & R^T p' \\ 0 & 0 \end{pmatrix} = \begin{pmatrix} \widehat{K}_d(X, t) & \Gamma_d(X, t) \\ 0 & 0 \end{pmatrix} = \widehat{\xi}_d(X, t), \quad (5.7)$$

where:

$$K_d(X, t) = \begin{pmatrix} K_{dX} \\ K_{dY} \\ K_{dZ} \end{pmatrix} (X, t), \quad \Gamma_d(X, t) = \begin{pmatrix} \Gamma_{dX} \\ \Gamma_{dY} \\ \Gamma_{dZ} \end{pmatrix} (X, t). \quad (5.8)$$

The components of these two vectors represent the following strain fields of a beam:

Torsion: $K_{dX}(X, t)$ is the rate of torsion per unit of material beam length.

Curvature: $K_{dY}(X, t)$ and $K_{dZ}(X, t)$ represent the curvatures of the beam centroidal line in the planes (P, t_X, t_Z) and (P, t_X, t_Y) , respectively.

Stretch: $(\Gamma_{dX} - 1)$ is the rate of stretching of the centroidal line.

Shear: $\Gamma_{dY}(X, t)$ and $\Gamma_{dZ}(X, t)$ are the local transverse shearing rotations around the axes (P, t_Z) and (P, t_Y) , respectively.

Since in robotics, such strain fields represent the inter-bodies joint kinematics which are either actuated, passive¹ or constrained through design. Therefore, different cases relevant to bio-inspired robotics are possible ranging from the most actuated to the least actuated internal kinematics. Such cases are summarized in table 5.1 along with their corresponding beam theory. In nature, each of these internal degrees of freedom finds an application in case of elongated body animals' locomotion. In fact, one of the two curvatures $K_{dY}(X, t)$ and $K_{dZ}(X, t)$ actuates the yaw in the plane of propulsion, while the other actuates the pitch for complex 3D maneuvers involving the body. The torsion $K_{dX}(X, t)$ has a direct action on the roll whose control is crucial to stabilize the orientation of the head of a bio-inspired robot e.g. eel-fish, snake, etc. As for linear degrees of freedom, $\Gamma_{dX}(X, t)$ actuates the traction-compression as used by large snakes while $\Gamma_{dY}(X, t)$ and $\Gamma_{dZ}(X, t)$ can be actuated through the movements of the skin and scales with respect to the backbone. Different scenarios found in nature are interpreted in table 5.2. Furthermore, the time-

¹ We do not consider passive joints in this work.

Table 5.1 – Actuated degrees of freedom vs Beam theory

Case	Constraints	degrees of freedom	Beam Theory	Remarks
1	No constraints	06	Timoshenko-Reissner	Fully actuated beam
2	$\Gamma_{dY} = \Gamma_{dZ} = 0$	04	Extensible Kirchoff	Cross sections stay perpendicular to vertebral axis
3	Case 2 with $\Gamma_{dX} = 1$	03	Inextensible Kirchoff	infinitesimal version of a spherical joint
4	Case 3 with $K_{dX} = 0$	02	No corresponding beam	In passive beams, 3D bending always produce torsion
5	Case 4 with $K_{dY} = 0$	01	Inextensible planar Kirchoff	Planar case with Yaw degree of freedom actuation

Table 5.2 – Internal degrees of freedom vs natural applications

Case	Controlled degrees of freedom	Nature	Example
1	01	Stretching	Earthworm
2	01	Bending (pitch)	Inchworm
3	01	Bending (yaw)	2D snakes
4	02	Bending (pitch+yaw)	3D snakes
5	05	Bending (pitch+yaw) + 2 transverse shearing	3D snakes + model of scales

twist field $\hat{\eta}(X, t)$, given in (5.2) can be detailed as follows:

$$g^{-1}\dot{g} = \begin{pmatrix} R^T \dot{R} & R^T \dot{p} \\ 0 & 0 \end{pmatrix} = \begin{pmatrix} \hat{\Omega}(X, t) & V(X, t) \\ 0 & 0 \end{pmatrix} = \hat{\eta}(X, t), \quad (5.9)$$

with:

$$V(X, t) = \begin{pmatrix} V_X \\ V_Y \\ V_Z \end{pmatrix} (X, t), \quad \Omega(X, t) = \begin{pmatrix} \Omega_X \\ \Omega_Y \\ \Omega_Z \end{pmatrix} (X, t), \quad (5.10)$$

where, $V(X, t)$ and $\Omega(X, t)$ are, respectively, the vectors of linear and angular velocities of the cross section X in the cross sectional (material) frame $\mathcal{F}_m(X, t)$.

Remark

A similar relation to the vector fields (5.7) and (5.9) exist in the case of any subgroup of $SE(3)$. Also, in the following, we will consider g belonging to one of these subgroups G of Lie algebra \mathfrak{g} .

5.3 Continuous Models of Hyper-Redundant Robots

From now on, g_o , \dot{g}_o and \ddot{g}_o denote the position, velocity and acceleration of the cross section $X = 0$ on G , respectively. The continuous dynamic model of a hyper-redundant robot splits into 5 sub-models detailed in the following subsections.

5.3.1 Continuous Model of Transformations

This is immediately deduced from the definition (5.7) of internal degrees of freedom (i.e. strain field $\xi_d(t)$):

$$g' = g\widehat{\xi}_d(t), \quad (5.11)$$

with boundary conditions: $g(X = 0) = g_o$.

5.3.2 Continuous Model of Velocities

By taking partial derivative of the model of transformations (5.11) with respect to time we get:

$$\frac{\partial}{\partial t} g' = \frac{\partial}{\partial t} (g\widehat{\xi}_d),$$

this implies that:

$$\dot{g}' = \dot{g}\widehat{\xi}_d + g\dot{\widehat{\xi}}_d.$$

With $\dot{g} = g\widehat{\eta}$ we get:

$$(g\widehat{\eta})' = g\widehat{\eta}\widehat{\xi}_d + g\dot{\widehat{\xi}}_d,$$

then multiplying both sides by g^{-1} and rearranging we get:

$$\widehat{\eta}' = -(\widehat{\xi}_d\widehat{\eta} - \widehat{\eta}\widehat{\xi}_d) + \dot{\widehat{\xi}}_d,$$

where we recognize, in the parenthesis, the Lie bracket of ξ_d and η , and we have in terms of twist in \mathbb{R}^6 .

$$\eta' = -\text{ad}_{\xi_d(t)}(\eta) + \dot{\xi}_d(t), \quad (5.12)$$

with boundary conditions: $\eta(X=0) = \eta_o = (g_o^{-1}\dot{g}_o)^\vee$.

5.3.3 Continuous Model of Accelerations

This is inferred by taking derivative of the previous model (5.12) with respect to time:

$$\dot{\eta}' = -\text{ad}_{\xi_d(t)}(\dot{\eta}) - \text{ad}_{\dot{\xi}_d(t)}(\eta) + \ddot{\xi}_d(t), \quad (5.13)$$

whose solutions are fixed by the boundary conditions: $\dot{\eta}(X=0) = \dot{\eta}_o = (g_o^{-1}\ddot{g}_o - g_o^{-1}\dot{g}_o g_o^{-1}\dot{g}_o)^\vee$.

5.3.4 Dynamics on \mathcal{C}_1 : Continuous Model of Internal Wrenches

Following [15], we can extend the Poincaré approach (2.15) presented in chapter 2 to the case of a Cosserat beam. This consists in deriving the dynamics of the beam from a Lagrangian approach directly on the intrinsic definition (5.1) of the beam configuration space. Technically, this is achieved by applying the extended Hamilton principle [80]:

$$\delta \int_{t_a}^{t_b} L dt = \delta \int_{t_a}^{t_b} \int_0^l \mathcal{L} dX dt = \int_{t_a}^{t_b} -\delta W_{\text{ext}} dt, \quad (5.14)$$

where δ denotes any variation applied along the trajectory of the system while the configuration at the two ends of $[t_a, t_b]$ is maintained fixed, and δW_{ext} is the virtual work produced by the nonconservative external forces. Furthermore, L and \mathcal{L} respectively denote the Lagrangian and the Lagrangian density of the beam free of external load. According to the intrinsic setting of the Poincaré-Cosserat approach, \mathcal{L} is directly defined as a function of the cross-section transformations and their space and time derivatives $\mathcal{L}(g, g', \dot{g})$; and not, like in the case due to Lagrange, as a function of any parameterization of the g 's in \mathbb{R}^6 . Then, let us recall that the variation is applied onto any motion in \mathcal{C}_1 while the

space and time variables are maintained fixed. In fact, $\delta t = 0$ in accordance with the D'Alembert principle of virtual work, while $\delta X = 0$ since the variable X is a material (configuration-independent) label (note here that this imposes δ to follow the cross section X along any virtual displacement). Then, introducing the definitions (5.2,5.3) into the Lagrangian density of the beam allows one to rewrite the Lagrangian L of the (5.14) as follows:

$$L = \int_0^l \mathcal{L}(g, g', \dot{g}) dX = \int_0^l \mathfrak{L}(g, \xi, \eta) dX, \quad (5.15)$$

where \mathfrak{L} is a new function named the reduced Lagrangian density (in the Lie algebra of $SE(3)$) when it does not depend explicitly on the transformation g . In fact, this property is named left-invariance and traduces the symmetry of the dynamics as seen by an observer attached to the beam material. In the rest of this section, we shall assume that the Lagrangian of the beam free of external load is left-invariant. Now, let us derive the beam dynamics by applying the variational principle (5.14) with L defined by (5.15). For this, we have to invoke the constraints of variation at a fixed time and material label:

$$\delta \frac{\partial g}{\partial t} = \frac{\partial \delta g}{\partial t}, \quad \delta \frac{\partial g}{\partial X} = \frac{\partial \delta g}{\partial X}, \quad (5.16)$$

where $\delta \varsigma = g^{-1} \delta g \in \mathfrak{se}(3)$ is a field of material variation of g , with $\delta \varsigma(t_a) = \delta \varsigma(t_b) = 0$. Then inserting " $\delta g = g \delta \varsigma$ " into (5.16) gives the following relations, that play a key role in the variational calculus on Lie groups:

$$\delta \eta = \frac{\partial \delta \varsigma}{\partial t} + \text{ad}_\eta^*(\delta \varsigma), \quad \delta \xi = \frac{\partial \delta \varsigma}{\partial X} + \text{ad}_\xi^*(\delta \varsigma). \quad (5.17)$$

Finally, applying the standard uses of the variational calculus to (5.14), with (5.17) applied before the usual integration by parts (here in time and space), gives the Poincaré equations of a Cosserat beam in the material setting as follows:

$$\frac{\partial}{\partial t} \left(\frac{\partial \mathfrak{L}}{\partial \eta} \right) - \text{ad}_\eta^* \left(\frac{\partial \mathfrak{L}}{\partial \eta} \right) + \frac{\partial}{\partial X} \left(\frac{\partial \mathfrak{L}}{\partial \xi} \right) - \text{ad}_\xi^* \left(\frac{\partial \mathfrak{L}}{\partial \xi} \right) = \overline{F}, \quad (5.18)$$

whose solutions are fixed at each instant by the following boundary conditions:

$$\frac{\partial \mathfrak{L}}{\partial \xi}(0) = -F_-, \text{ and: } \frac{\partial \mathfrak{L}}{\partial \xi}(l) = F_+, \quad (5.19)$$

where we assume that the external load is defined by the density field of wrench $X \in]0, l[\mapsto \overline{F} \in \mathfrak{se}(3)^*$, and the two boundary wrenches $F_- \in \mathfrak{se}(3)^*$ and $F_+ \in \mathfrak{se}(3)^*$ applied onto the first and last cross-sections of the beam, respectively, i.e., we assume that $\delta W_{\text{ext}} = \int_0^l \overline{F} \delta \varsigma dX + F_- \delta \varsigma(0) + F_+ \delta \varsigma(l)$ in (5.14). Finally, these external wrenches generally depend on the beam configuration. Nevertheless, when this is not the case, the external load is

said to be left-invariant. This is particularly true for most of the contact forces involved in animal locomotion. In our case, we fix the reduced Lagrangian density of (5.15) as follows:

$$\mathfrak{L}(\eta, \xi, t) = \mathfrak{T}(\eta) - \mathfrak{U}(\xi, t),$$

where, the left-invariant density of the kinetic energy \mathfrak{T} of the beam is defined by:

$$\mathfrak{T}(\eta) = \frac{1}{2} \eta^T (\mathcal{M} \eta),$$

with $\mathcal{M}(X) \in \mathfrak{g}^* \otimes \mathfrak{g}$ as a (6×6) matrix of inertia tensor density in the case of $G = \text{SE}(3)$:

$$\mathcal{M} = \begin{pmatrix} m & 0 \\ 0 & I \end{pmatrix}.$$

Moreover, the left-invariant density of the internal energy \mathfrak{U} , imposed by the constraints (5.4), is defined as:

$$\mathfrak{U}(\xi, t) = \Lambda^T(\xi - \xi_d(t)),$$

with $\partial \mathfrak{U} / \partial \xi = \Lambda(X, t) \in \mathfrak{g}^*$ as a (6×1) vector (in case of $\text{SE}(3)$) of the density of internal wrenches whose components are given as:

$$\Lambda(X, t) = \begin{pmatrix} N \\ C \end{pmatrix} (X, t), \text{ with } N(X, t) = \begin{pmatrix} N_X \\ N_Y \\ N_Z \end{pmatrix} (X, t), \text{ and } C(X, t) = \begin{pmatrix} C_X \\ C_Y \\ C_Z \end{pmatrix} (X, t),$$

where $\Lambda(X, t)$ ensures the forcing of the Lagrangian internal kinematic constraints: $\xi = \xi_d(t)$. Let us note here that $\Lambda(X, t)$ is a field of Lagrange multipliers such that for the actuated internal degrees of freedom, the associated multipliers are the forces or/and the torques exerted by the actuators, while for the non-actuated internal degrees of freedom, the multipliers are the internal reaction torques or forces. Note also that with such a choice, the internal kinematics are assumed to be inelastic and the robot turns out to be a continuous rigid robot². Furthermore, we note $\partial \mathfrak{T} / \partial \eta = \mathcal{M} \eta$ as the density of kinetic wrenches along the robot. Finally, with above notations, the Poincaré equations (5.18) of a Cosserat beam can be rewritten as follows:

$$\mathcal{M} \dot{\eta} - \text{ad}_\eta^* (\mathcal{M} \eta) - \Lambda' + \text{ad}_{\xi_d(t)}^* (\Lambda) = \overline{F}, \quad (5.20)$$

²Alternatively, the model of internal dynamics can be enriched by adding elastic and viscous terms in \mathfrak{U} .

with the following boundary conditions:

$$\text{at } X = 0: \Lambda(0) = -F_- \text{ and at } X = l: \Lambda(l) = F_+. \quad (5.21)$$

The partial differential equation (5.20) along with (5.21) are considered in the following as the dynamics of the internal wrenches or more simply as the "internal dynamics". Obviously, this is the continuous counterpart of the internal torque dynamics (3.11) in the discrete case.

5.3.5 Dynamics on \mathcal{C}_2 : Dynamics of the Reference Body

The dynamics on \mathcal{C}_2 are derived from those on \mathcal{C}_1 by forcing the virtual and real velocity fields in the Hamilton principle to verify the following constraint:

$$\eta = \text{Ad}_k(\eta_o), \quad (5.22)$$

where, $k = g^{-1}g_o$. Note that, the defined field (5.22) is simply the time-twist field on the beam induced by the movement of the head alone, while the body is frozen in its current shape. In these conditions, the internal wrenches do not work in such a field and the balance of virtual work reduces to:

$$\int_0^l \text{Ad}_k^*(\mathcal{M}\dot{\eta} - \text{ad}_\eta^*(\mathcal{M}\eta) - \bar{F})dX = \text{Ad}_{k_+}^*F_+ - F_-, \quad (5.23)$$

where $\dot{\eta}$ is replaced by the acceleration field compatible with (5.22), i.e.:

$$\begin{aligned} \dot{\eta} &= \text{Ad}_k(\dot{\eta}_o) + \text{ad}_\eta(\text{Ad}_k(\eta_o)) + \text{Ad}_k(\eta_o^2) - (\text{Ad}_k(\eta_o))^2 \\ &= \text{Ad}_k(\dot{\eta}_o) + \zeta, \end{aligned} \quad (5.24)$$

which defines $\zeta(X)$ as the material (or body) acceleration of cross section X induced by the body shape motion and the movement of the head except for its pure acceleration (i.e. $\dot{\eta}_o$).

Finally, when the calculations are done and the kinematic reconstruction equation $\dot{g}_o = g_o\hat{\eta}_o$ is taken into account, the dynamic equations on \mathcal{C}_2 can be written as:

$$\begin{pmatrix} \dot{\eta}_o \\ \dot{g}_o \end{pmatrix} = \begin{pmatrix} \mathcal{M}_o^{-1}(\xi_d)F_o(\xi_d, \dot{\xi}_d, \ddot{\xi}_d, g_o, \eta_o) \\ g_o\hat{\eta}_o \end{pmatrix}, \quad (5.25)$$

with: $F_o = F_{\text{in}} + F_{\text{ext}}$, and where we introduced the inertia tensor of the whole robot reduced to the reference cross section i.e. in $X = 0$:

$$\mathcal{M}_o = \int_0^l \text{Ad}_k^*\mathcal{M}\text{Ad}_kdX, \quad (5.26)$$

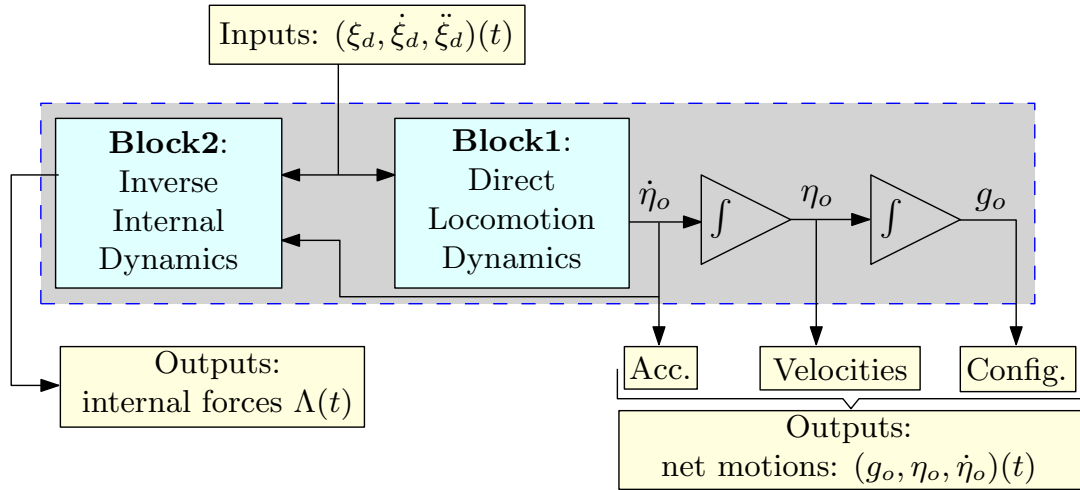


Figure 5.3 – General algorithm of hyper-redundant robots

as well as the external wrenches, reduced to the reference cross section:

$$F_{\text{ext}} = -F_- + \text{Ad}_{k_+}^* F_+ + \int_0^l \text{Ad}_k^*(\bar{F}) dX, \quad (5.27)$$

and the inertial wrenches reduced to the reference cross section:

$$F_{\text{in}} = - \int_0^l \text{Ad}_k^*(\mathcal{M}\zeta - \text{ad}_\eta^*(\mathcal{M}\eta)) dX. \quad (5.28)$$

In the following, (5.25) will be considered as the dynamics of the reference body net motions controlled by the shape time variations, i.e. the "locomotion dynamics". Note that, this is obviously the continuous counterpart of the locomotion dynamics (3.29) in the discrete case.

5.4 Dynamic Algorithm of Hyper-Redundant Robots

Now, with the above mentioned continuous kinematic and dynamic models, a macro-continuous dynamic algorithm is proposed to solve the general problem of section 2.3.3 of chapter 2. First, by defining the kinematic state vector $\mathcal{X}_1 = (g, \eta, \dot{\eta})$, the kinematic models (5.11, 5.12, 5.13) can be easily grouped together into a set of first order spatial ordinary differential equations as follows:

$$\mathcal{X}'_1 = f_1(\mathcal{X}_1, \xi_d(t), \dot{\xi}_d(t), \ddot{\xi}_d(t)), \quad (5.29)$$

with:

$$f_1 = \begin{pmatrix} g\widehat{\xi}_d(t) \\ -\text{ad}_{\xi_d(t)}(\eta) + \dot{\xi}_d(t) \\ -\text{ad}_{\xi_d(t)}(\dot{\eta}) - \text{ad}_{\dot{\xi}_d(t)}(\eta) + \ddot{\xi}_d(t) \end{pmatrix}. \quad (5.30)$$

Similarly, the terms appearing in the locomotion dynamics (5.25) can be computed by spatial integration of a set of ordinary differential equations of the state vector $\mathcal{X}_2 = (\mathcal{X}_1, \mathcal{M}_o, F_o)$:

$$\mathcal{X}'_2 = f_2(\mathcal{X}_2, \xi_d(t), \dot{\xi}_d(t), \ddot{\xi}_d(t)), \quad (5.31)$$

with:

$$f_2 = \begin{pmatrix} f_1 \\ \text{Ad}_k^* \mathcal{M} \text{Ad}_k \\ \text{Ad}_k^* (\text{ad}_\eta^* (\mathcal{M}\eta) + \overline{F} - \mathcal{M}\dot{\eta}) \end{pmatrix}, \quad (5.32)$$

where the ζ of (5.28) can be replaced by $\dot{\eta}$ in (5.32) if the initial spatial conditions of (5.31) verify $\dot{\eta}(X=0) = \dot{\eta}_o = 0$. In fact, in this case (5.24) shows that $\zeta = \dot{\eta}$ all along the beam. Finally, as we will now see, in every case the algorithm integrates (5.31) in these conditions, so that (5.32) makes sense.

Finally, the internal dynamics (5.20) can be stated in the form of the following set of spatial ordinary differential equations, of the state vector $\mathcal{X}_3 = (\mathcal{X}_1, \Lambda)$:

$$\mathcal{X}'_3 = f_3(\mathcal{X}_3, \xi_d(t), \dot{\xi}_d(t), \ddot{\xi}_d(t)), \quad (5.33)$$

with:

$$f_3 = \begin{pmatrix} f_1 \\ \text{ad}_{\xi_d(t)}^* (\Lambda) + \mathcal{M}\dot{\eta} - \text{ad}_\eta^* (\mathcal{M}\eta) - \overline{F} \end{pmatrix}. \quad (5.34)$$

All the above ordinary differential equations form a general algorithm as shown in Fig. 5.3 to solve the dynamics of a hyper-redundant robot. The execution of the algorithm is summarized in Fig. 5.4.

Remarks

1. Let us remark that the above algorithm is nothing else but a continuous version of the Newton-Euler discrete algorithm of mobile multibody systems presented in chapter 3, where (5.29) stands for the forward recursive kinematics, (5.31) stands for the recursive computation of the dynamic locomotion model, and (5.33) for the backward recursive computation of inter-body wrenches.

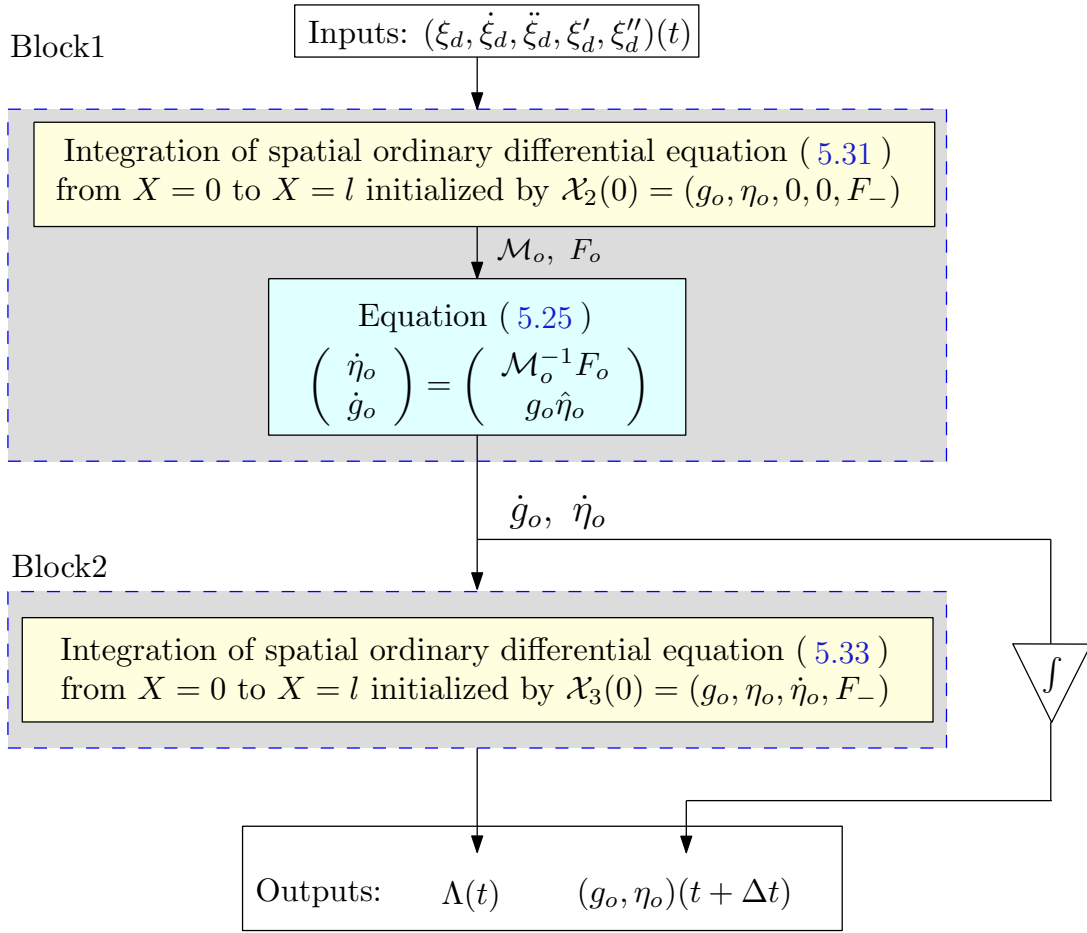


Figure 5.4 – Execution of the general algorithm of a hyper-redundant robot

2. The algorithm computes the net (reference) acceleration by solving the direct locomotion dynamics (Block1 of Fig. 5.3) which contains a model of the external forces. In general, such a model of external forces may be very complex e.g. in the case of swimming in which, at least, it requires to integrate the Navier-Stokes equations of the surrounding flow [16]. As another example of the terrestrial locomotion, the above algorithm can be used with external forces modeled as physical laws, e.g. friction laws. However, for the sake of simplicity of analysis, it can be useful to consider the contacts as ideal. In this particular case, the external contacts can be modeled as kinematic constraints instead of external forces. In the next section, we shall see that when the number of constraints is sufficient, locomotion dynamics can be replaced by kinematics and the locomotion is named as "kinematic locomotion".

5.5 Terrestrial Locomotion Model

In nature, there exists a vast variety of terrestrial locomotion modes that depends upon the body structure of the organism and the surrounding substrate (see section 2.1 of

Table 5.3 – *Contacts in terrestrial locomotion*

Type	Constraint	Locomotion	Examples
Locked anchorage	Clamped to earth	Step by step locomotion	Inchworm
Sweeping anchorage	"Rolling without slipping" type	Axial propulsion	Earthworm, big snakes
Annular contact	Non-sliding	Lateral undulation	Snakes

chapter 2). Here, we consider the limbless locomotion of elongated body animals such as snakes, earthworms, inchworms, etc. As the terrestrial locomotion is analyzed in the scenario of ideal contacts and the resulting kinematic constraints, thus the above proposed algorithm requires to be modified via the modeling of these ideal contacts which is done in the following sections.

5.5.1 Kinematic Modeling of Contacts

As pointed out in chapter 2, the nature of contact plays an important role in defining the mode of locomotion. Based upon the observations of terrestrial elongated body animals, here we will deal with two types of contacts (assumed ideal): "anchorages" and "annular contacts". Anchorages are modeled as bilateral holonomic constraints while annular contacts are modeled as bilateral nonholonomic constraints. In both cases the contacts are distributed along the body axis. In case of anchorages, two types are envisaged:

Locked anchorage: this type of anchorage is fixed on the material axis of the robot on an abscissa, noted C , constant in relation to time (see Fig. 5.5(a)).

Sweeping anchorage: in this type of anchorage, the abscissa C is either explicitly dependent on time noted as $C(t)$ or implicitly dependent on time via the system dynamics (see Fig. 5.5(b)).

On the other hand, the annular contact is always sweeping, as the robot can slide freely in the annulus formed by the annular contact.

The contacts are assumed to be attached to rigid external bodies (named obstacles) submitted to imposed relative motions in the fixed earth frame. Finally, as we will see when considering examples, these models are of great practical interest for modeling numerous locomotion modes as illustrated in table 5.3.

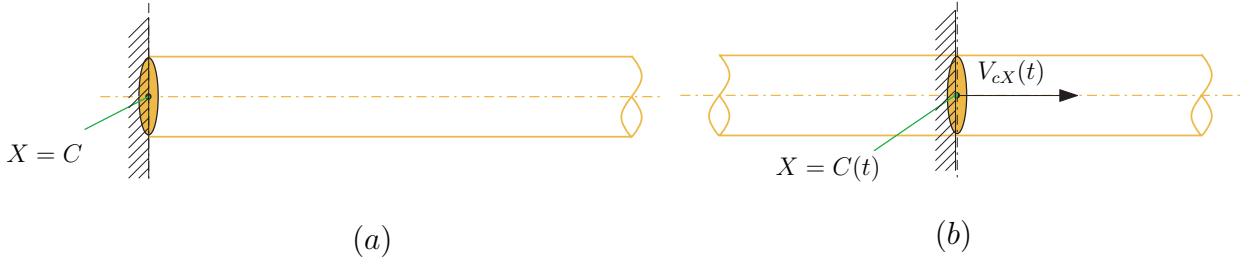


Figure 5.5 – (a) Locked anchorage; (b) sweeping anchorage

5.5.1.1 Anchorages

For a locked anchorage as shown in Fig. 5.5(a), where the robot is anchored at a fixed material point $C \in [0, l]$, the geometric model is written as follows:

$$g(C) = g_c(t), \quad (5.35)$$

where $t \mapsto g_c(t)$ denotes a function of time in G which represents the imposed motion of the anchored rigid obstacle. In particular, if g_c is independent of time, then this body is fixed, as in the case of a manipulator robot anchored in the ground or more simply a cantilevered beam (see Fig. 5.5(a)). For a sweeping anchorage as shown in Fig. 5.5(b), the geometric model of contact cannot distinguish it from a locked anchorage, both considered at the same instant t . In fact, in the case of sweeping anchorage, we still have:

$$g(C(t)) = g_c(t), \quad (5.36)$$

which coincides with (5.35) when $C = C(t)$. In contrast, the kinematic model can make the distinction since, for the sweeping anchorage, by taking total derivative with respect to time (denoted as $\frac{d}{dt}(\cdot)$) of (5.36):

$$\frac{d}{dt}g(C(t)) = \dot{g}(C(t)) + g'(C(t))\dot{C}(t) = \dot{g}_c(t), \quad (5.37)$$

which is multiplied by $g^{-1}(C(t))$ to obtain, invoking (5.36) again, the sweeping anchorage constraints in \mathfrak{g} :

$$\eta(C(t)) + \xi_d(C(t), t)\dot{C}(t) = \eta_c(t), \quad (5.38)$$

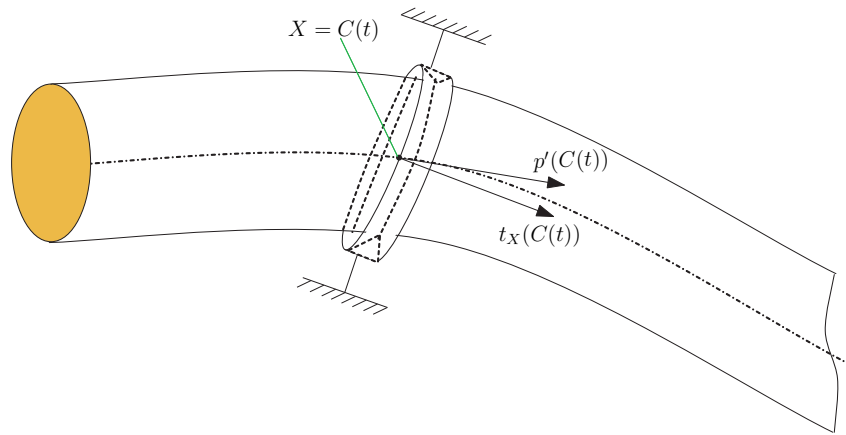


Figure 5.6 – Cross sectional follower Annular contact

where, when $G = \text{SE}(3)$:

$$\eta_c(t) = (g_c^{-1} \dot{g}_c)^\vee(t) = \begin{pmatrix} V_{cX} \\ V_{cY} \\ V_{cZ} \\ \Omega_{cX} \\ \Omega_{cY} \\ \Omega_{cZ} \end{pmatrix},$$

is the time-twist imposed on the rigid body supporting the anchorage. Furthermore, (5.38) allows one to recover the kinematic form of a locked anchorage: $\eta(C) = \eta_c(t)$ when C is time-independent. Finally, let us note that in the general case (5.38) produces a set of $\dim(\mathfrak{g})$ independent scalar constraints.

5.5.1.2 Annular Contact

Before describing the details of their modeling, let us recall that annular contacts are sweeping by nature so they can only be accounted for by kinematic constraints. Here, we consider the cross sectional follower annular contact as shown in Fig. 5.6. The cross sectional follower annular contact follows the cross section in their lateral motions while axially sweeping over it (see Fig. 5.6). It is an annular contact that prevents all relative translational velocities (of the beam with respect to the obstacle) in the plane of a given cross section of abscissa $X = C$. Thus, for a movement in the space \mathbb{R}^3 (i.e. $G = \text{SE}(3)$), such a contact exerted in any $C \in [0, l]$ is modeled by the following relations:

$$\begin{cases} (v(C(t)) - v_c(t)) \times t_X(C(t)) = 0, \\ (\omega(C(t)) - \omega_c(t))^T t_X(C(t)) = 0, \end{cases} \quad (5.39)$$

where $(v^T, \omega^T)^T(X) = (\dot{g}g^{-1})^\vee$ denotes the spatial twist of the X -cross-section while $(v_c^T, \omega_c^T)^T(t)$ is the spatial twist imposed on the rigid annular contact by the moving obstacle. After computation, (5.39) leads to the following three bilateral nonholonomic constraints:

$$\begin{cases} V_Y(C) = V_{cY}(t), \\ V_Z(C) = V_{cZ}(t), \\ \Omega_X(C) = \Omega_{cX}(t), \end{cases} \quad (5.40)$$

where $V_{cY}(t)$, $V_{cZ}(t)$ are the lateral velocities expressed in the cross section frame while $\Omega_{cX}(t)$ is the axial component of the angular velocities. All of them being imposed on the C -cross-section by the movement of the obstacle, these velocities are null if the annular contact in question is fixed in the ambient space. Furthermore, in planar motion (i.e. $G=SE(2)$), such a contact only prevents the lateral motion of the cross section in contact. Thus, the bi-lateral nonholonomic constraint is given simply as follows:

$$V_Y(C) = V_{cY}(t).$$

Finally, C can itself move along the material robot axis following a time law of the general form:

$$\dot{C} = V_{cX}(t) - V_X(C),$$

where V_{cX} is imposed by the axial motion of the support while $V_X(C)$ is, in general, ruled by the locomotion. Lastly, let us note that when the given support follows the cross section not only laterally but also axially, then $\dot{C} = V_{cX}(t) - V_X(C) = 0$.

5.5.2 Model of Contact Forces

As the contacts are ideal, the reaction (contact) forces are identified as Lagrange multipliers associated to the scalar constraints taken from (5.38) and (5.40). When $G = SE(3)$, an anchorage introduces six multipliers (i.e. the six components of a complete reaction wrench) while an annular contact transmits two lateral forces and one axial torque for a 3D movement and only one lateral force for a planar motion as shown in Fig. 5.7. When the anchorages and/or the annular contacts are imposed at the ends, the reaction forces associated with them enter into the calculation of the dynamics via a contact component of the apical external wrenches F_\pm that we note $F_{c,\pm}$ (where "c" means "contact"). As long as the contacts are defined inside the domain of the beam, i.e. if $C \in]0, l[$, then each of them adds a set of kinematic constraints in \mathfrak{g} and an associated reaction wrench (defined

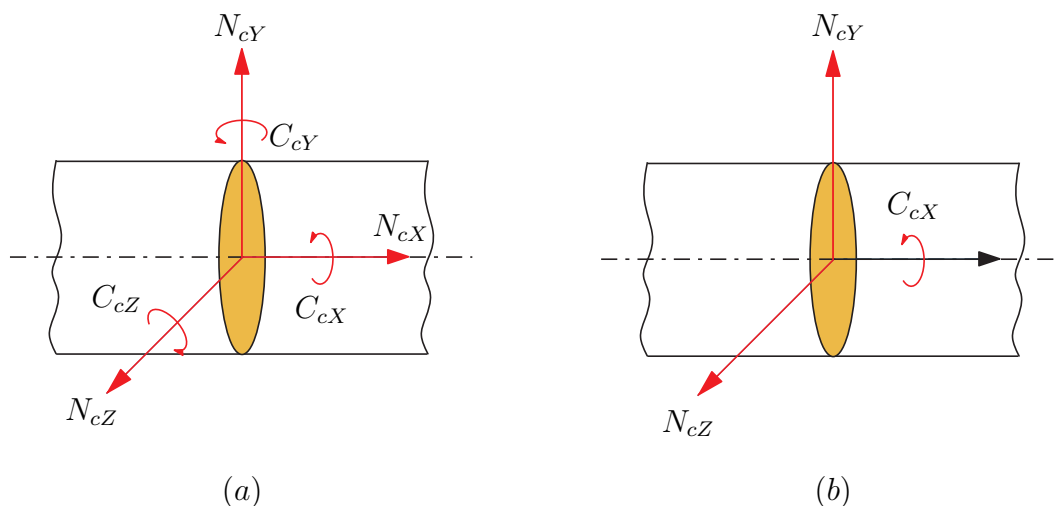


Figure 5.7 – (a) Reaction wrench on an anchored cross section; (b) Reaction wrench on a cross section in annular contact

in \mathfrak{g}^*), that enters into the model via \overline{F} which then contains a contact term of the form³: $\overline{F}_c(C)\delta(X - C)$. Finally, according to (5.27), any distribution of contacts produces a contribution to F_{ext} which is noted F_c and called the resultant of the reaction (contact) wrenches. Consequently, the external wrenches can be written as follows:

$$F_{\text{ext}} = F_c + F_{\text{other}},$$

where F_{other} , denotes the contribution to F_{ext} brought by the distribution of external forces of other origin than contact. Such a distribution (or loading) will be denoted by $(F_{\text{other},\pm}, \overline{F}_{\text{other}})$ and models external loads as gravity, pressure and viscous forces etc.

5.5.3 Algorithm in Kinematic Case

When the number of constraints (imposed by the contacts) is equal or higher than the dimension of the fiber of \mathcal{C}_2 , the system is said fully or over constrained and the net motions are entirely ruled by the kinematic model of the contacts which takes the following most general explicit form:

$$\dot{g}_o = g_o \widehat{\eta}_o = g_o \widehat{f}(g_o, \xi_d(t), \xi'_d(t), \xi''_d(t), \dots, \dot{\xi}_d(t)), \quad (5.41)$$

where f is the model of kinematic constraints and hence the model of reference accelerations can be obtained by simple time differentiation of f . In this case, the locomotion is called "kinematic locomotion" (to distinguish it from the previous dynamic locomotion case) and the locomotion dynamics (5.25) are used in their inverse form to calculate the

³Where δ is the Dirac distribution such that $\int_o^l f(X)\delta(X - C)dX = f(C)$ for any enough smooth function f .

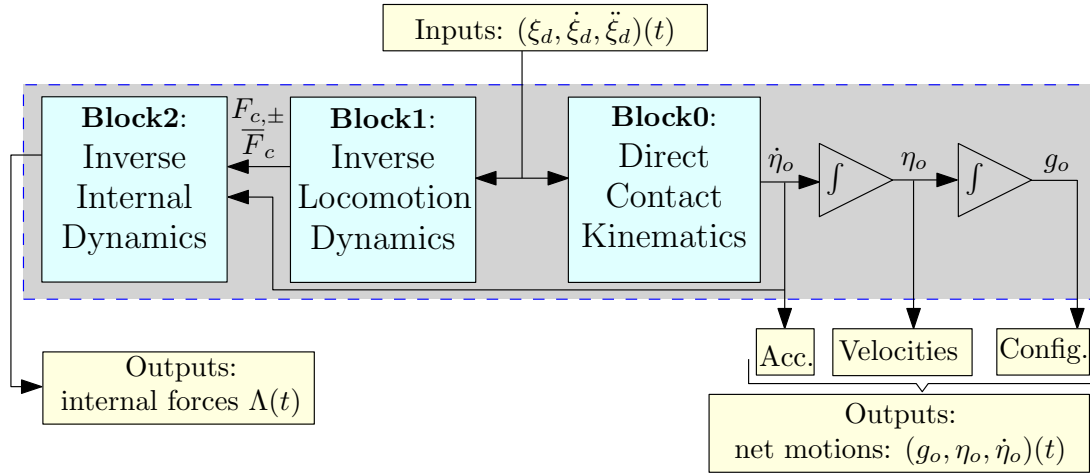


Figure 5.8 – Algorithm of a hyper-redundant robot with kinematic constraint model

contact wrench induced by the external constraints, i.e.:

$$F_c = \mathcal{M}_o \dot{\eta}_o - F_{\text{in}} - F_{\text{other}}. \quad (5.42)$$

Going further, when the number of constraints is strictly higher than the dimension of the fiber of \mathcal{C}_2 , the overall motions of the robot are over-constrained which means that: 1) the internal movements must be compatible⁴, 2) the reaction unknowns $F_{c,\pm}$ and \bar{F}_c are under-determined as they are only required to verify the locomotion dynamics (5.42). Finally, taking these considerations into account, the new constrained algorithm is shown in Fig. 5.8 and its execution is summarized in Fig. 5.9.

Remarks

1. In the rest of the thesis we do not specify the form of the locomotion kinematics beyond its expression (5.41), preferring to investigate it, case by case, for the particular examples of next chapter. Let us just say here that the function f in (5.41) must be calculated from f_1 of (5.29) and from considerations related to the way of locomotion studied (particularly based on biological observation) as well as the contact models as introduced in section 5.5.1.
2. Hyper-redundant manipulators can be considered as a subclass of fully constrained case. In fact here, the reference cross section $X = 0$ is clamped in a rigid basis enduring an imposed motion (in particular, null) defined by $\mathcal{X}_1(0) = (g_o, \eta_o, \dot{\eta}_o)(t)$. In this case, computation of Block0 and Block1 of the algorithm can be avoided.

⁴with the risk, if this is not the case of preventing mobility and, due to the hyper-statism, of producing internal stress resolved by replacing the constraints induced by the internal joints, assumed ideal, by rheological passive laws.

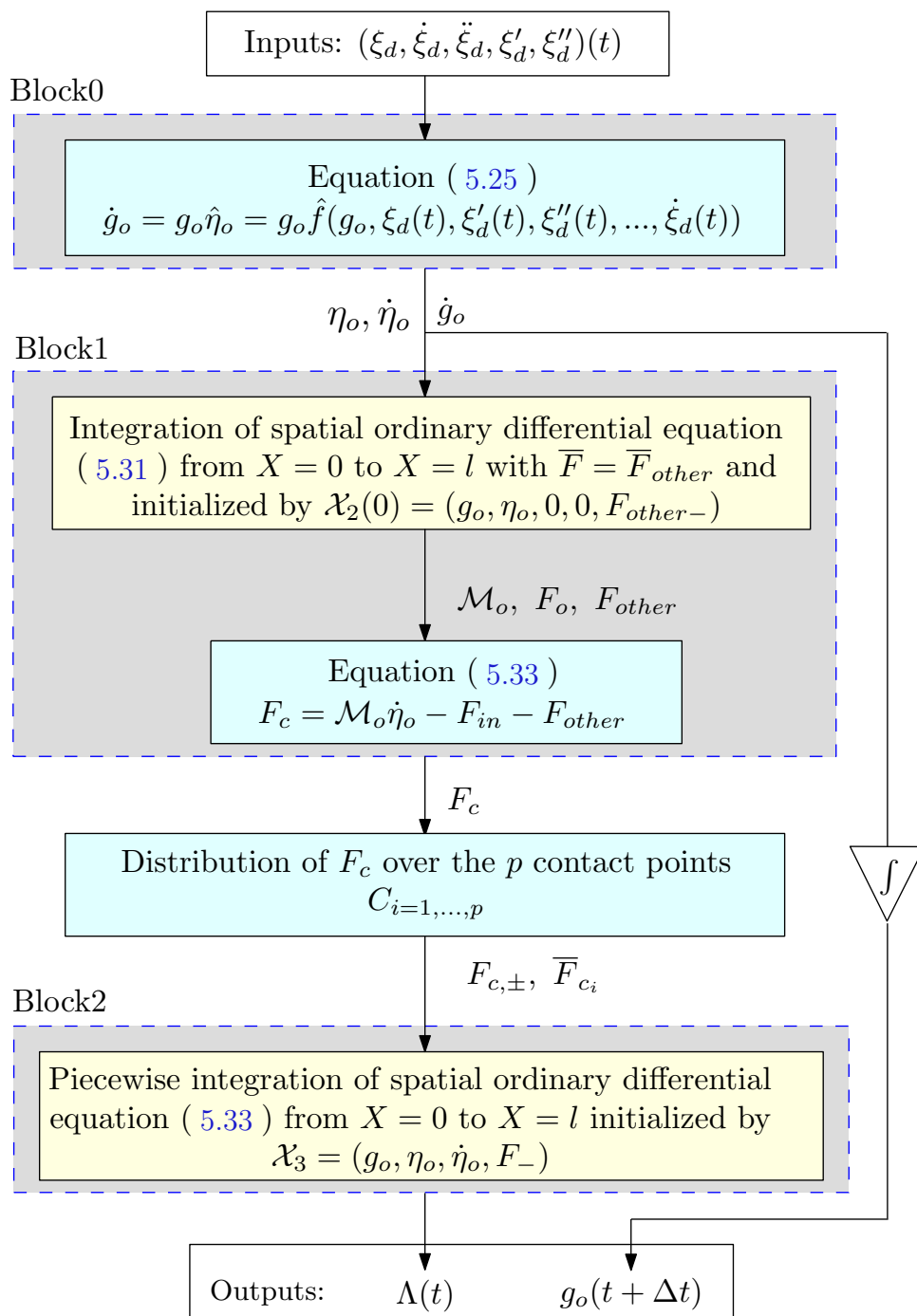


Figure 5.9 – Execution of kinematic algorithm of a hyper-redundant robot

Indeed, the reference motions require no calculations as they are known by their time laws.

- Note that if f is linear in $\dot{\xi}_d(t)$ and independent of g_o , the kinematic model under the constraints of contacts defines a principal kinematic connection on the principal fiber bundle \mathcal{C}_2 , i.e. a continuous version of the discrete connections studied in the mechanics of nonholonomic systems [8].

4. The distribution of the resultant contact wrench F_c over the p contact points is univocal if the number of constraints is equal to the dimensions of the fiber, and is multivocal if it is higher. This last case requires further assumption on the distribution of the contact forces.
5. The internal wrenches are achieved by piecewise integration of the internal dynamics on $[0, C_1] \cup [C_1, C_2] \cup \dots [C_p, l]$, using the jump conditions: $\Lambda(C_{i-}) = -\overline{F}(C_i) + \Lambda(C_{i+})$ where $\Lambda(C_{i-})$ and $\Lambda(C_{i+})$ denote the material internal wrench Λ evaluated on the left and the right sides of the cross section C_i , respectively.

5.6 Conclusions

In this chapter a continuous version of the Newton-Euler dynamics was presented. In fact, the bio-inspired systems considered here were treated as continuous 1D Cosserat beam. Once embedded in the framework of locomotion theory on the principal fiber bundle, a general unified algorithm was proposed that solves the following two problems involved in any locomotion task.

1. It enables the net motion of a reference body to be computed from the known data of internal motions (strain fields),
2. It gives the internal torques required to impose these internal (strain field) motions.

Moreover, the general macro-continuous algorithm is further modified to solve the problem of terrestrial locomotion bio-inspired from elongated body animals. This modification was done with the help of ideal contacts between the system and the substrate. In this regard, the given framework provides a continuous version of the kinematic connections proposed by geometric mechanics in [87, 60, 76]. In the next chapter, this algorithm is applied to different elongated body animals in order to solve the problem of locomotion.

6

Illustrative Examples of Hyper-Redundant Robots

6.1 Earthworm in 1D	124
6.1.1 Assumptions and Considerations	125
6.1.2 Continuous Kinematic Model	127
6.1.3 Contact Kinematic Model	127
6.1.4 Continuous Locomotion Dynamic Model	129
6.1.5 Continuous Internal Dynamic Model	131
6.1.6 Numerical Results	131
6.2 Climbing Inchworm in 2D	133
6.2.1 Assumptions and Considerations	135
6.2.2 Algorithm Execution	138
6.2.3 Numerical Results	138
6.3 2D Snake in Lateral Undulation	140
6.3.1 Assumptions and Considerations	141
6.3.2 Contact Kinematic Model	141
6.3.3 Continuous Kinematic Model	142
6.3.4 Kinematic Locomotion Model	143
6.3.5 Continuous Dynamic Models	144
6.3.6 Reissner-Snake	146
6.3.7 Numerical Results	148
6.4 3D Snake in Lateral Undulation	149
6.4.1 Continuous Dynamic Models	151
6.4.2 Numerical Results	152
6.5 Further Discussion: Application to Real Designs	153
6.6 Conclusions	155

In this chapter, the macro-continuous algorithm developed in the previous chapter is applied to several terrestrial elongated body animals. In each case, the contact between the animal and the ground is modeled through the kinematics constraints presented in section 5.5.1. Since, the terrestrial elongated body animals have normally a large (or at least equal) number of contacts than the dimensions of the fiber, thus the kinematic constraint model allows us to use the kinematic locomotion model (5.41) in order to compute the net forward motions of the animal. The internal torques and/or forces computation is done with some hypothesis over the distribution of the resultant contact forces F_c in the case of redundant contact points. Finally, the framework shows the



Figure 6.1 – A natural earthworm

generality of the algorithm toward various systems of locomotion.

6.1 Earthworm in 1D

The natural earthworm, as shown in Fig. 6.1, is a slender body invertebrate since this organism contains no backbone in its structure [97]. This soft-bodied creature has a hydrostatic skeleton¹ composed of a series of fluid-filled segments connected end to end. Each segment has a set of antagonistic muscles, i.e. the outer longitudinal and the inner circular muscles. Small and stiff hair-like bristles called setae are present on the outer body to help anchor into the soil. For detailed description of earthworms's anatomy, the reader is referred to [42, 39, 43, 86].

Principal of Locomotion

The earthworm moves by means of peristalsis [43, 38]. The net forward locomotion is produced by the propagation of a peristaltic wave in the anteroposterior direction². This wave is the result of the alternating contractions of the circular and longitudinal muscles from the anterior to the posterior end of the earthworm. When the circular muscle contracts, the longitudinal muscle relaxes and vice versa. When a segment is at maximum longitudinal contraction, its setae extend and anchor into the soil to prevent backward slipping and hence help the worm to protrude forward. Moreover, each segment is assumed to deform with constant volume constraint [23, 86].

¹There are also muscular hydrostats like tongues, trunks, tentacles etc these consist solely of muscle fibers with no fluid-filled cavity

²From the anterior to the posterior end, also called retrograde since the wave travels in opposite direction to the animal

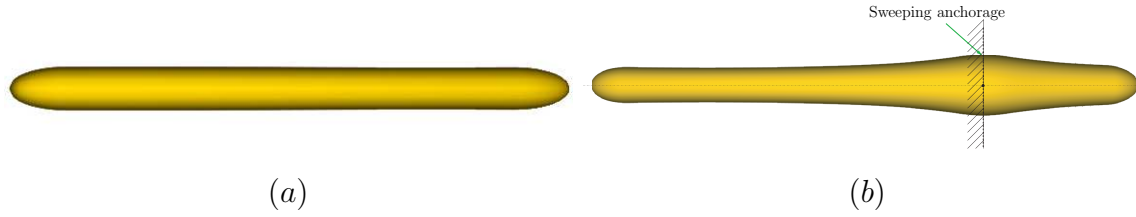


Figure 6.2 – (a) Initial reference configuration; (b) Deformed configuration with sweeping anchorage point $C(t)$

Earthworm-like Robot Mechanism

In robotics, the motivation toward modeling and analysis of earthworm's locomotion comes from its rectilinear locomotion mode which is particularly effective in constrained spaces where burrowing is required. The purpose of this section is to model the locomotion of an earthworm-like mechanism by applying a peristaltic gait as internal strain field.

6.1.1 Assumptions and Considerations

The hyper-redundant robot considered here is a burrowing robot inspired by earthworms that produces a 1D rectilinear motion. The system is modeled as a 1D extensible Kirchhoff beam axially actuated in traction-compression with its cross sections representing the segments of an earthworm. Consequently, only the axial translational degree of freedom (i.e. Γ_{dX}) is implemented as actuated strain field between any two contiguous cross sections. The remaining five degrees of freedom are constrained through design.

Consider an elongated earthworm-like system of length l initially in a relaxed configuration as shown in Fig. 6.2(a). To produce the peristalsis along the earthworm's body, a sinusoidal wave is propagated from anterior to posterior end. Such a wave generates a single degree of freedom axial traction-compression strain field of the following form:

$$\Gamma_{dX}(X, t) = 1 + \epsilon \sin\left(\frac{2\pi}{\lambda}(ct - X)\right) \quad (6.1)$$

where ϵ , λ and c are the amplitude, the wave length and the speed of propagation of the wave, respectively. From the above strain field, it can be easily concluded that:

$$\begin{cases} \Gamma_{dX}(X, t) = 1, & \text{Relaxed cross section,} \\ \Gamma_{dX}(X, t) = 1 + \epsilon, & \text{Maximum elongation,} \\ \Gamma_{dX}(C_i(t), t) = 1 - \epsilon, \text{ for } C_i(t) \in]0, l[, & \text{Maximum contraction,} \end{cases} \quad (6.2)$$

The above three states of a cross section X are interpreted in Fig. 6.3. $C_i(t)$ denotes the material abscissae of the p sweeping anchorage points at which the associated cross sections are at maximal axial contraction.

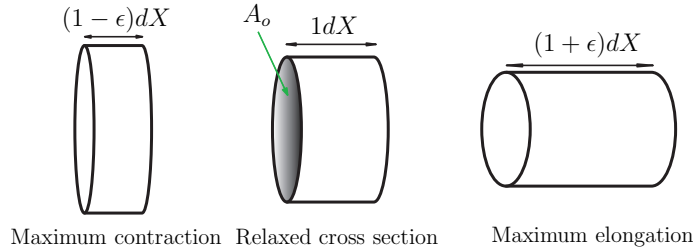


Figure 6.3 – A cylindrical cross section in three different forms. A_o is the area of relaxed cross section

The radial traction-compression of the cross sections is antagonistically controlled by relaxing the rigid cross section assumption and adding the volume preservation constraint to the Cosserat theory. The volume preservation constraint states that the volume of any cross section X at initial (i.e. at $t = 0$ s) relaxed configuration remains unchanged during the course of its deformation, i.e.:

$$\begin{aligned} \text{Volume}(X, t) &= \text{Volume}(X, 0), \\ A(X, t)dS &= A(X, 0)dX, \end{aligned}$$

where $A(X, 0) = A_o$ is the cross sectional area of initially relaxed earthworm³ and $A(X, t)$ is the area of the cross section X at an instant t , while $dS = \Gamma_{dX}dX$ is the length at current t of the part of the earthworm of initial length dX initially located at X . Then:

$$A(X, t) = \frac{A_o}{\Gamma_{dX}(X, t)}. \quad (6.3)$$

Moreover, the earthworm is assumed to have a homogenous volumetric mass ρ given by:

$$\rho = \frac{m_o}{A_o l},$$

where m_o is the total constant mass of the earthworm.

As for as the contact with soil is concerned, it is made only by the extended segments at maximal contraction (see Fig. 6.2). These contact points change its location during the course of locomotion due to the axial traction-compression strain field. Therefore, these contacts can be modeled as a sweeping anchorage detailed in section 5.5.1.1. Mathematically, the velocity of the cross sections in instant contact with the ground is zero and hence prevent the anchored cross sections from backward axial slipping. Practically, such type of contact may be achieved through bristles, spikes, passive wheels with ratchet etc. Since it is more practical to keep the same number of contact points over time thus we take the wave length $\lambda = \frac{l}{k}$ as constant over time where one should take the whole number of waves k in order to maintain the same number of contact points over the length l of the earthworm at any instant t . Furthermore, in case if the speed of propagation

³The small variations due to the curved shape at both ends are negligible

Table 6.1 – Reduction of 3D parameters to 1D

3D construction	G, g	$\eta, \dot{\eta}$	$\xi_d(t)$	$\overline{F}(C_i)$	Λ	\mathcal{M}
1D construction	\mathbb{R}, x	\dot{x}, \ddot{x}	$\Gamma_{dX}(t)$	N_{c_i}	N	m

$c(t)$ is varying over time, one can still keep the same number of contacts over time by constraining the angular frequency $\omega(t)$ as follows:

$$\omega(t) = \frac{2\pi}{\lambda}c(t).$$

Another advantage in this case is that the head velocity is independent of the number of contact points detailed later on.

For the sake of simplicity and analytical analysis, the previous general 3D dynamic model given in section 5.4 as a set of spatial ordinary differential equations can be expressed as a simple 1D continuous model. Thus, the Lie group G (as well as the lie algebra \mathfrak{g} and its dual \mathfrak{g}^*) is represented by \mathbb{R} identified with the commutative subgroup of translations along the x -axis (which also coincides with its Lie algebra and its dual). It follows that the adjoint maps disappear from the expressions and we can propose a more simple description⁴ of the system as given in table 6.1.

6.1.2 Continuous Kinematic Model

With the above assumptions and considerations, the earthworm's 3D continuous kinematic model (5.29) takes the following simple 1D form:

$$\mathcal{X}'_1 = \begin{pmatrix} x' \\ \dot{x}' \\ \ddot{x}' \end{pmatrix} = \begin{pmatrix} \Gamma_{dX}(t) \\ \dot{\Gamma}_{dX}(t) \\ \ddot{\Gamma}_{dX}(t) \end{pmatrix}, \quad (6.4)$$

whose solutions are fixed by the sweeping anchorage points $C_i \in]0, l[$.

6.1.3 Contact Kinematic Model

Any cross section anchored to the ground imposes a constraint on the movement in the fiber. It follows that the net motion of the earthworm can be derived from a contact kinematic model. Such a model can be simply obtained by imposing that the velocity of slipping is null at any sweeping anchorage point $C_i(t)$. Therefore, by invoking the contact kinematics (5.38) with $C(t) = C_i(t)$, $\eta(C(t)) = \dot{x}(C_i(t))$, $\xi_d(t) = \Gamma_{dX}(t)$, and $\eta_c(t) = 0$ (as the contact is with the fixed ground), then the 3D holonomic geometric constraint

⁴All the terms are scalar and represent only the axial component

equation (5.38) can be simply rewritten in a 1D form for an earthworm as follows:

$$\dot{x}(C_i(t)) + \Gamma_{dX}(C_i(t))\dot{C}_i(t) = 0, \quad (6.5)$$

where, due to the non-slipping condition, the anchorage is sweeping at the speed of propagation, i.e. $\dot{C}_i(t) = c(t)$. Also, we have $\Gamma_{dX}(C_i(t)) = 1 - \epsilon$ thus the above equation can be rewritten as follows:

$$\dot{x}(C_i(t)) + (1 - \epsilon)c(t) = 0. \quad (6.6)$$

Moreover, by taking the velocity of the cross section of the abscissa $C_i(t)$ from the second line of (6.4), one obtains:

$$\dot{x}(C_i(t)) = \dot{x}_o + \int_0^{C_i(t)} \dot{\Gamma}_{dX} dX, \quad (6.7)$$

which can be entered into (6.6) to give the head velocity of the earthworm as follows:

$$\dot{x}_o(t) = - \int_0^{C_i(t)} \dot{\Gamma}_{dX} dX - (1 - \epsilon)c(t). \quad (6.8)$$

Furthermore, the constrained angular frequency of the strain field Γ_{dX} shows that:

$$\int_{C_i}^{C_{i+1}(t)} \dot{\Gamma}_{dX} dX = 0, \quad (6.9)$$

therefore, the head velocity \dot{x}_o is independent of the choice of the anchorage point C_i . Consequently, taking the first anchorage point (i.e. $i = 1$), the head velocity can be simply given as follows:

$$\dot{x}_o(t) = - \int_0^{C_1(t)} \dot{\Gamma}_{dX} dX - (1 - \epsilon)c(t). \quad (6.10)$$

This is the analytical form of an earthworm's locomotion kinematic model whose general construction is given by (5.41). Equation (6.10) shows that the head velocity is a function of the amplitude ϵ and the speed $c(t)$ of the traction-compression wave. The head acceleration $\ddot{x}_o(t)$ is given by the time derivative of the above locomotion kinematic model:

$$\ddot{x}_o(t) = -\dot{\Gamma}_{dX}(C_1(t))c(t) - \Gamma_{dX}(C_1(t))\dot{c}(t) - \int_0^{C_1(t)} \ddot{\Gamma}_{dX} dX. \quad (6.11)$$

As $\Gamma_{dX}(C_1(t)) = 1 - \epsilon$, which implies that $\dot{\Gamma}_{dX}(C_1(t)) = 0$, thus the head acceleration can be more simply written as:

$$\ddot{x}_o(t) = -(1 - \epsilon)\dot{c}(t) - \int_0^{C_1(t)} \ddot{\Gamma}_{dX} dX. \quad (6.12)$$

This head acceleration will serve us later as boundary condition to solve the dynamics.

Case of Constant Speed of Propagation (c)

Before solving the dynamics of earthworm, we do an analytical analysis of the earthworm's locomotion by taking the speed of propagation c as constant over time. In this particular case the space-integration of $\dot{\Gamma}_{dX}$ between $[0, C_1(t)]$ gives:

$$\int_0^{C_1(t)} \dot{\Gamma}_{dX} dX = c\epsilon \sin(\omega t) - c\epsilon \sin\left(\omega\left(t - \frac{C_1(t)}{c}\right)\right). \quad (6.13)$$

Now putting the above equation in the locomotion kinematic model (6.10) and after simplification, the following head velocity is obtained:

$$\dot{x}_o(t) = -c(1 + \epsilon \sin(\omega t)). \quad (6.14)$$

To get the head configuration (i.e. x_o) at an instant t , we integrate the above equation as follows:

$$x_o(t) - x_o(t=0) = \int_0^t -c(1 + \epsilon \sin(\omega\tau)) d\tau. \quad (6.15)$$

Taking $\dot{x}_o(t=0) = 0$, we get:

$$x_o(t) = -\frac{c}{\omega} (\omega t + \epsilon(1 - \cos(\omega t))). \quad (6.16)$$

Finally the head acceleration is obtained by taking time derivative of (6.14) as follows:

$$\ddot{x}_o(t) = -c\epsilon\omega \cos(\omega t). \quad (6.17)$$

6.1.4 Continuous Locomotion Dynamic Model

After solving the problem of net motions of an earthworm through the locomotion kinematic model, now it is possible to use the locomotion dynamics (Block1 Fig. 5.9) for the calculation of the external axial forces applied by the environment on the earthworm via the anchorage points. This is done with the help of the locomotion dynamic model given

in equation (5.42). The simple 1D form of this model is given as follows:

$$N_c = \sum_{i=1}^{i=p} N_{c_i} = \int_0^l m(X, t) dX \ddot{x}_o - N_{\text{in}}, \quad (6.18)$$

where $\int_0^l m(X, t) dX = m_o$ is the total constant mass of the earthworm. The head acceleration \ddot{x}_o is given by equation 6.12 and N_{in} is the axial inertial force (deduced from the 3D general formula (5.28)) given by⁵:

$$N_{\text{in}} = - \int_0^l m(X, t) \left(\int_0^X \ddot{\Gamma}_{dX} d\chi \right) dX. \quad (6.19)$$

Thus equation (6.20) becomes:

$$N_c = \sum_{i=1}^{i=p} N_{c_i} = \int_0^l m(X, t) dX \ddot{x}_o + \int_0^l m(X, t) \left(\int_0^X \ddot{\Gamma}_{dX} d\chi \right) dX \quad (6.20)$$

which gives the total axial contact forces in the head frame. In case of constant speed of propagation c , we can get the N_c analytically as follows:

$$N_c = \rho A_o c^2 \log \left(\frac{\Gamma(l, t)}{\Gamma(0, t)} \right), \quad (6.21)$$

where, $A_o = A(X, 0)$ is the area of the relaxed cross section of initially relaxed earthworm at $t = 0$ s with uniform area over the length. Here it is noteworthy that due to the propagation of a whole number of waves over the length we have:

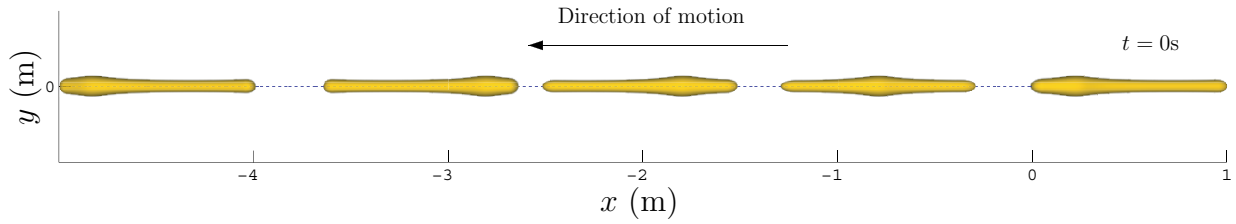
$$\Gamma(l, t) = \Gamma(0, t),$$

this implies that:

$$N_c = \rho A_o c^2 \log (1) = 0, \quad (6.22)$$

which shows that the external axial contact forces become zero in case of whole number of waves propagating with constant speed c . Therefore, in this case the axial friction force is of less importance. This scenario can be compared with that of a rolling without slipping wheel on a straight line where the wheel moving forward with constant velocity examines no external axial forces hence undergoing a pure inertial motion. It may be concluded that such locomotion mode is more efficient on low friction surfaces as it does not need high surface friction.

⁵Only contact forces are considered i.e. $F_{\text{other}} = 0$

Figure 6.4 – Earthworm locomotion along x -axis

6.1.5 Continuous Internal Dynamic Model

The internal dynamics are solved to get the internal actuation forces required to impose the desired internal strain field deformations. When the number of contacts is more than one (i.e. $p > 1$), then under-determination of the reaction forces prevents the integration of the internal dynamics. However, if an arbitrary distribution of these forces is assumed such that their resultant verifies (6.20), for example adopting an equal distribution, i.e. $N_{c_i} = \frac{N_c}{p}$, then it becomes possible to integrate (5.20) which is written here:

$$N' = m(X, t)\ddot{x} - \sum_{i=1}^{i=p} N_{c_i}\delta(X - C_i(t)), \quad (6.23)$$

with boundary conditions $N(0) = N(l) = 0$ if one assumes that the medium presents no force to the front and back of the worm⁶, and where \ddot{x} is deduced by space-integration of the continuous kinematic model (6.4) initialized by $(x_o, \dot{x}_o, \ddot{x}_o)$. Furthermore, by taking $N_c = 0$ in case of constant c , the internal control forces are simply given by the space integration of the following equation:

$$N' = m(X, t)\ddot{x}. \quad (6.24)$$

6.1.6 Numerical Results

Some of the numerical results of the simulation of the earthworm algorithm are shown here for graphical representation. First we take the constant speed of propagation c and input the strain field (6.1) with the following values:

$$\epsilon = 0.5, \quad \lambda = 1\text{m}, \quad c = 0.05\text{ms}^{-1}.$$

This will produce one contact point at a time over the whole length of the earthworm. Simulating the algorithm for 100s with the help of Matlab, we get the 1D rectilinear locomotion of the earthworm along the x -axis. The snapshots of such locomotion are depicted in Fig. 6.4. Furthermore, by using equations (6.16) and (6.14), the Fig. 6.5(a-b) shows the axial position $x_o(t)$ and the axial speed $\dot{x}_o(t)$ of the earthworm's head with

⁶Ingestion and excretion moving the earth matter from in front to behind

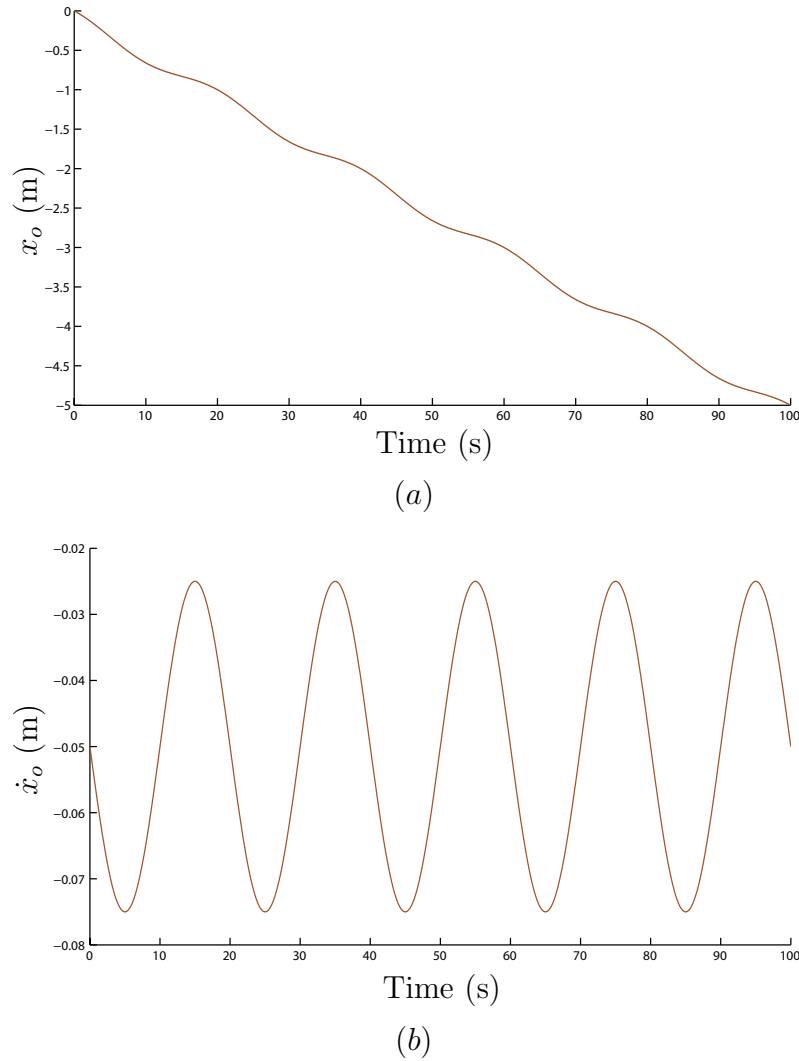


Figure 6.5 – (a) Time vs head position; (b) Time vs head velocity

respect to time, respectively. Fig. 6.5(b) shows that the average speed of the earthworm's head is equal to the speed of propagation c of the wave. Proceeding further with constant c , the inverse locomotion dynamic model is already solved analytically as given by equation (6.22). Where a whole number of waves results in no axial contact forces.

The inverse internal dynamic model (6.24) is numerically integrated to get the internal control forces $N(X, t)$. The Fig. 6.6 plots the $N(X)$ at $t = 0.5$ s where it is noteworthy that at the anchorage point $C = 0.275$ no force jump renders the internal force profile discontinuous. This is due to the fact that the external contact force N_c is zero in this particular case of constant c and constant λ .

Now let us consider the case of variable speed of propagation $c(t)$ defined as follows:

$$c(t) = at + b,$$

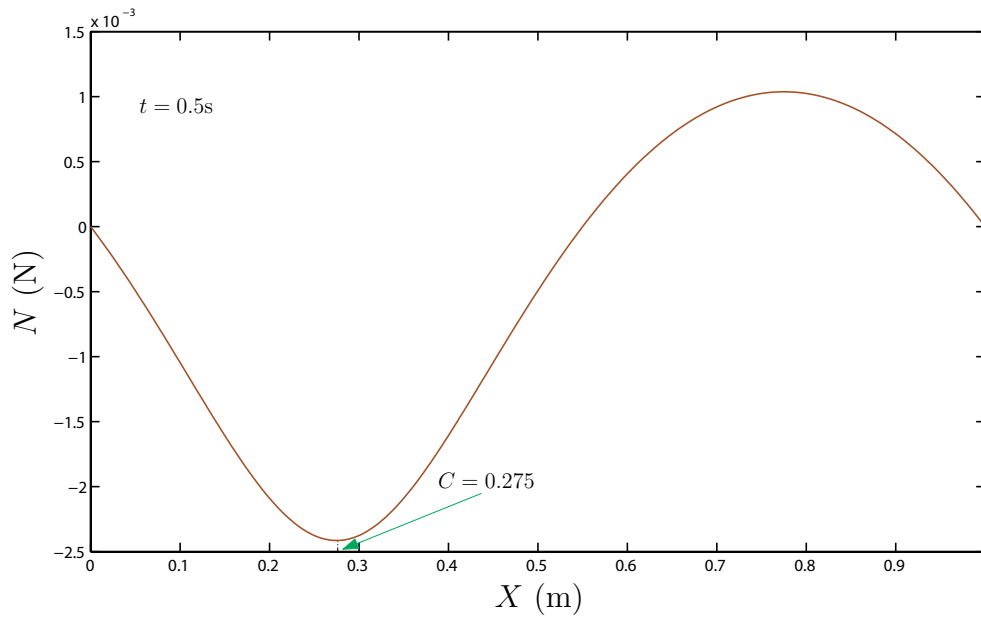


Figure 6.6 – Internal control forces $N(X)$ over the length with constant c

with $a \neq 0$. Note that in this case there is still one anchorage point at a time over the length because λ is still constant. After simulation with the above variable speed, it is noted that, due to the worm accelerations, the axial contact force (N_c) at $X = C$ is no more zero as shown in Fig. 6.7(a). Consequently, this nonzero N_c introduces a jump on the continuous profile of the internal control forces $N(X)$ at $X = C$. This discontinuity is depicted in Fig. 6.7(b) which gives the desired internal control force profile applied between cross sections over the whole length for three different instants of time.

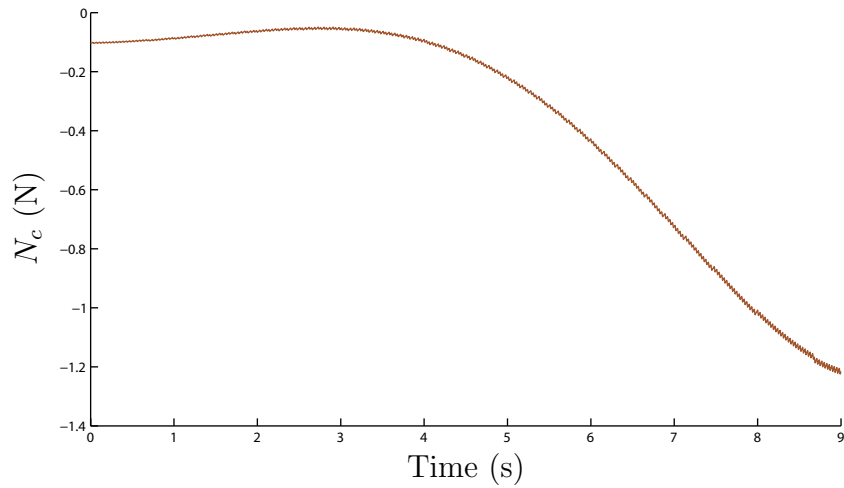
6.2 Climbing Inchworm in 2D

An inchworm (*Ascotis Selenaria*) as shown in Fig. 6.8 is a slender body invertebrate with a hydrostatic skeleton. It has a fluid-filled segmented body. It has small legs called prolegs at both ends of its body. The prolegs help the inchworm to maintain grip with environment during motion.

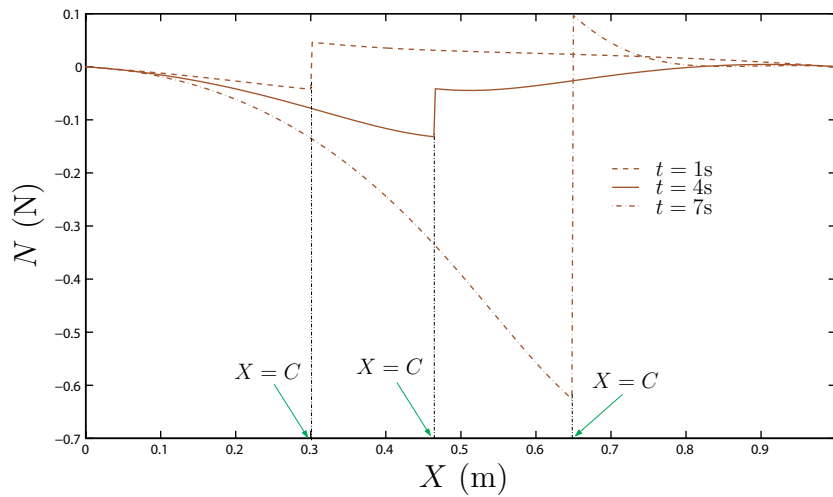
Principal of Locomotion

An inchworm is a caterpillar that can crawl and climb with a simple mode of locomotion known as Ω -shaped bending locomotion. The net forward motion is produced by alternate bending and relaxation of the body in a periodic *step* manner. The motion of an inchworm during a single *step* consists of a bending phase and relaxation phase described as follows:

Bending phase: initially the inchworm is in relaxed configuration with its anterior prolegs clamped to the surface. It starts bending the remaining parts of its body in Ω -shaped form.



(a)



(b)

Figure 6.7 – With variable $c(t)$: (a) Axial contact force N_c at $X = C$; (b) Internal control forces $N(X)$ over the length of earthworm

Relaxation phase: once reached to its maximum Ω -shaped bending, the inchworm detaches its anterior prolegs and attaches its rare prolegs to the surface and starts relaxing its body during the remaining half step.

Unlike earthworms, the inchworms do not need a sweeping anchorage. The anchorage is locked as it is not sweeping over the body but rather it is switching its location discretely from the front to the rare end. In this way, the inchworm always has at least one end of its body firmly attached to the environment during locomotion.

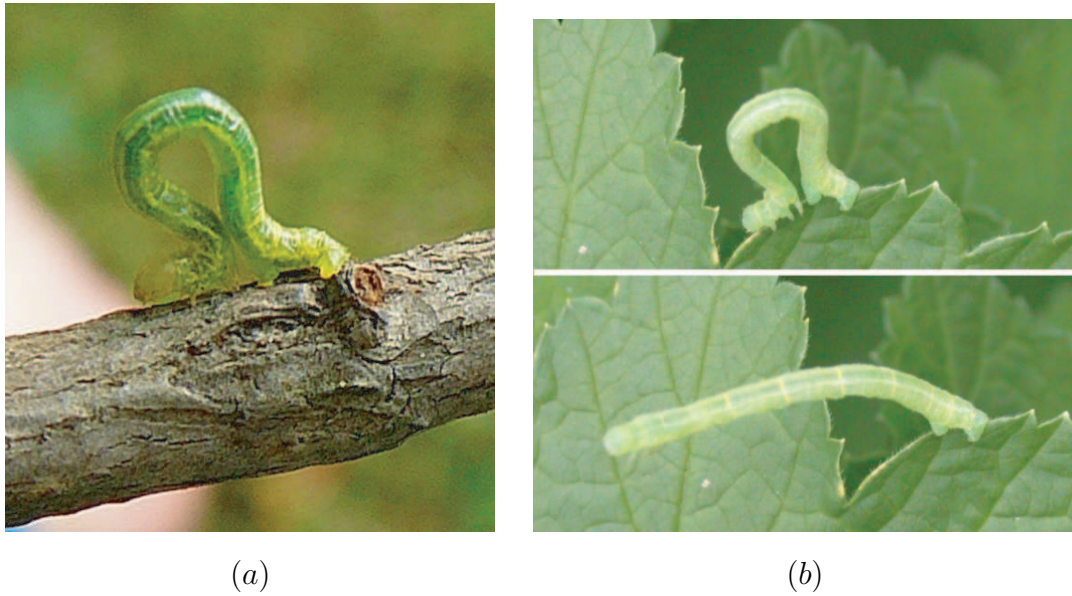


Figure 6.8 – (a) Ω -shaped bending configuration of an inchworm; (b) Inchworm in unstructured environment

Inchworm-like Robot Mechanism

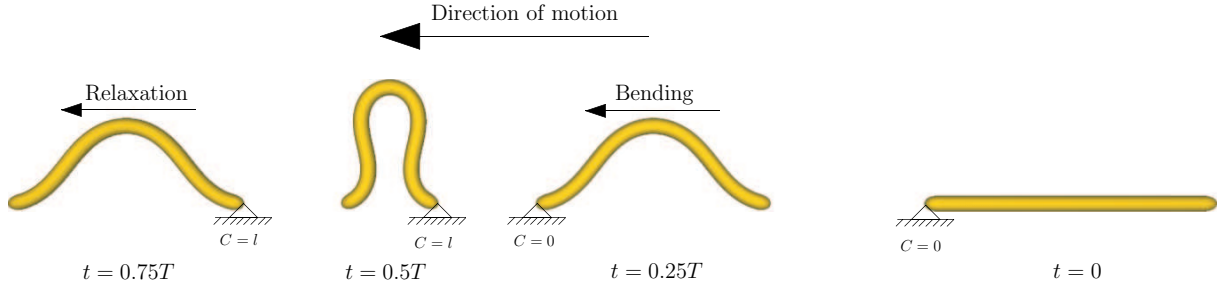
The inchworm locomotion mode is simple, stable and powerful. The inchworm-like robots are mostly inspired by such locomotion mode of natural inchworms which is particularly effective as well as efficient where climbing is required. Our purpose is to model a continuous style inchworm-like robot that produce climbing locomotion through Ω -shaped bending.

6.2.1 Assumptions and Considerations

The hyper-redundant robot considered here is a climbing inchworm robot inspired by inchworms that produce a net forward rectilinear motion by manipulating its body in a plane. The system is modeled as a Kirchhoff planar beam actuated in single bending. Consequently, only one bending degree of freedom (here $K_{dZ}(X, t)$) is implemented as strain field between any two contiguous rigid cross sections. The remaining five degrees of freedom are constrained through design. The bending curvature $K_{dZ}(X, t)$ deforms the body in xy plane.

Consider a slender inchworm-like mechanism of length l initially in a relaxed configuration. To produce the alternate bending and relaxation of the body over time, a curvature (bending) law $K_{dZ}(X, t)$ is introduced which keeps the system in planar configuration and results in rectilinear movement of the head segment. Therefore, the curvature law is an integrable variable given as:

$$K_{dZ}(X, t) = \theta'(X, t),$$

Figure 6.9 – Ω -shaped bending configuration of an inchworm

where $\theta(X, t)$ is the absolute angle of orientation of cross sections. Finally, the bending-relaxation gait is produced by introducing the angle θ as a function of time t and space X given as follows:

$$\theta(X, t) = \alpha \sin^2(\omega t) \sin\left(\frac{2\pi}{l}(X - l)\right), \quad (6.25)$$

from which the curvature law is derived as:

$$K_{dZ}(X, t) = \alpha \sin^2(\omega t) \left(\frac{2\pi}{l}\right) \cos\left(\frac{2\pi}{l}(X - l)\right), \quad (6.26)$$

where α and ω are the amplitude and frequency of the bending-relaxation gait. The space (i.e. X) dependence of the gait ensures that at any instant of time t :

$$\theta(t, X = 0) = \theta\left(t, X = \frac{l}{2}\right) = \theta(t, X = l) = 0,$$

whereas the curvature is minimal at both ends and maximal at $X = \frac{l}{2}$. Furthermore, the time dependence of the curvature law ensures the periodic bending and relaxation of the robot. Its time period T is given by:

$$T = \frac{\pi}{\omega},$$

and assures the amplification of the bending over the first half-period and its attenuation (down to 0) in the following half-period. Let us assume that the inchworm starts at $t = 0$ from a relaxed configuration, then there is anchorage at $X = 0$ at all the intervals $[kT, kT + \frac{T}{2}]$ and anchorage at $X = l$ at the intervals $[kT + \frac{T}{2}, (k + 1)T]$ as shown in Fig. 6.9. In one complete step (i.e. gait), the inchworm generates a net motion equal to one stride length l_s given as follows:

$$l_s = l - l_{\min},$$

where l_{\min} is the longitudinal span of the inchworm at maximum bending (i.e. at $0.5T$). As for as the contact is concerned, it is considered as a locked anchorage (as detailed

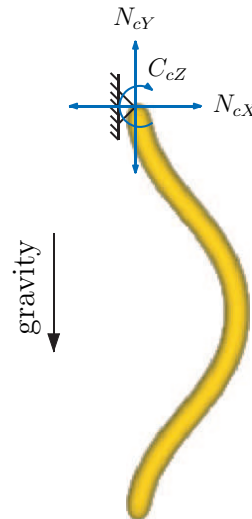


Figure 6.10 – Bilateral reaction forces at the anchorage point

in section 5.5.1.1) where the motions of the anchored cross section are imposed by the contact as follows:

$$\begin{cases} g(C) = g_c(t), \\ \eta(C) = \eta_c(t), \\ \dot{\eta}(C) = \dot{\eta}_c(t) \end{cases}$$

Usually the anchorage is fixed in the ambient space. Thus, the anchorage point provides the following geometric constraints:

$$\begin{cases} g(C) = 1, \\ \eta(C) = 0, \\ \dot{\eta}(C) = 0. \end{cases} \quad (6.27)$$

Furthermore, in this planar case, the anchorage point imposes only the planar reaction forces (n_{cX}, n_{cY}) and the reaction torque c_{cZ} as shown in Fig. 6.10.

Now as the contact is considered as a locked anchorage, then the inchworm can be modeled as a continuous manipulator whose "base" and "terminal" interchange their places at each half period of its step⁷. Where, the base represents the cross section fixed to the surface while the free end is the terminal. At the first half period the cross section $X = 0$ is the base and $X = l$ is the terminal while in the following half period, due to the interchange, the cross section $X = 0$ becomes the terminal and $X = l$ becomes the base.

⁷The base and terminal are the conventional terms used in literature for manipulators.

6.2.2 Algorithm Execution

With these considerations and the imposed strain field $\xi_d(X, t) = \begin{pmatrix} \Gamma_{dX} & \Gamma_{dY} & K_{dZ} \end{pmatrix}^T \in \text{se}(2)$ given as:

$$\xi_d(X, t) = \begin{pmatrix} 1 \\ 0 \\ K_{dZ} \end{pmatrix},$$

the general algorithm can be executed in case of inchworm as follows:

- In the first half period, the algorithm is executed with $X \in [0, l]$ and the anchorage point clamped at $X = 0$, i.e. $C = 0$.
- In the second half period, the same algorithm is executed by changing X into $l - X$ such that $C = l$

The net motions of the base are known (i.e. null here) as they are fixed by the anchorage conditions (6.27). Thus:

$$\mathcal{X}_1(C) = \begin{pmatrix} 1 \\ 0 \\ 0 \end{pmatrix}.$$

The locomotion dynamics (5.31) compute the reaction wrench F_c at the anchorage point. Finally, the internal control torques are calculated through the internal dynamics (5.33) initialized by $\mathcal{X}_3 = (1, 0, 0, 0, F_c)$.

6.2.3 Numerical Results

Some numerical results are obtained for inchworm climbing under gravity by applying the curvature law (6.26) as input to the algorithm with:

$$\alpha = 2.0, \quad \omega = \frac{\pi}{2} \text{rad/s}, \quad T = 2\text{s}.$$

Simulating the algorithm for 15s, we get the climbing motion of the inchworm in the xy plane. The snapshots of such locomotion at different instants of time are depicted in Fig. 6.11. The Fig. 6.12(a-b) plots the absolute vertical position y_o and the absolute vertical speed \dot{y}_o of the inchworms's head with respect to time, respectively. The stride length l_s depends upon the value of the α . Here, the stride length is $l_s = 0.766\text{m}$ for $\alpha = 2.0$ as pointed out in Fig. 6.12(a).

The inverse locomotion dynamics and the inverse internal dynamics of the system are solved to get the reaction wrenches at the anchorage point and the internal control torques

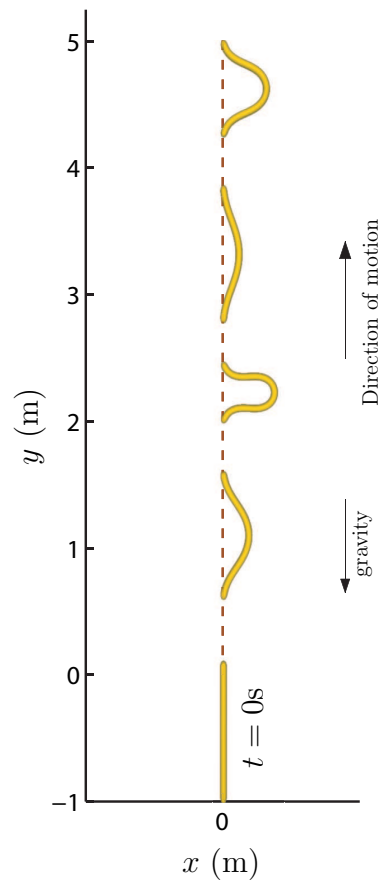
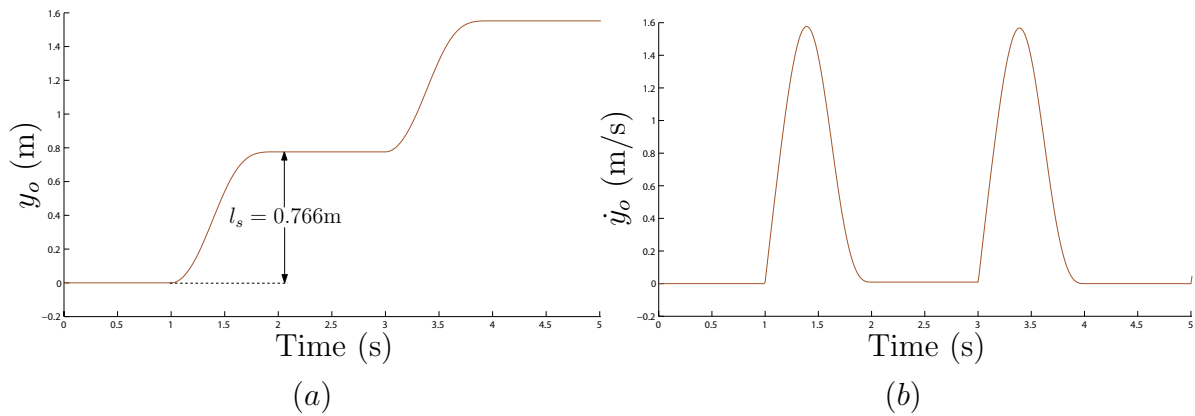
Figure 6.11 – Climbing inchworm locomotion along vertical y -axis

Figure 6.12 – (a) Time vs head position; (b) Time vs head velocity

$C_Z(X)$, respectively. The Fig. 6.13(a-b) shows the vertical reaction force $N_{cY}(X=0)$ and the reaction torque $C_{cZ}(X=0)$ at head with respect to time, respectively. The internal control torque $C_Z(X)$ along the length is presented in Fig. 6.14 at $t=0.5s$ and $t=1.5s$.

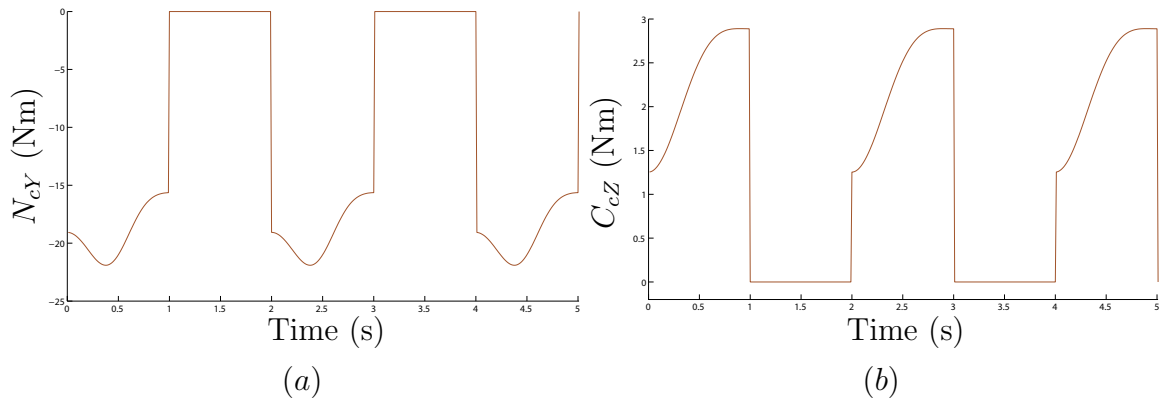


Figure 6.13 – (a) Vertical reaction force N_{cY} at head; (b) Reaction torque C_{cZ} at head

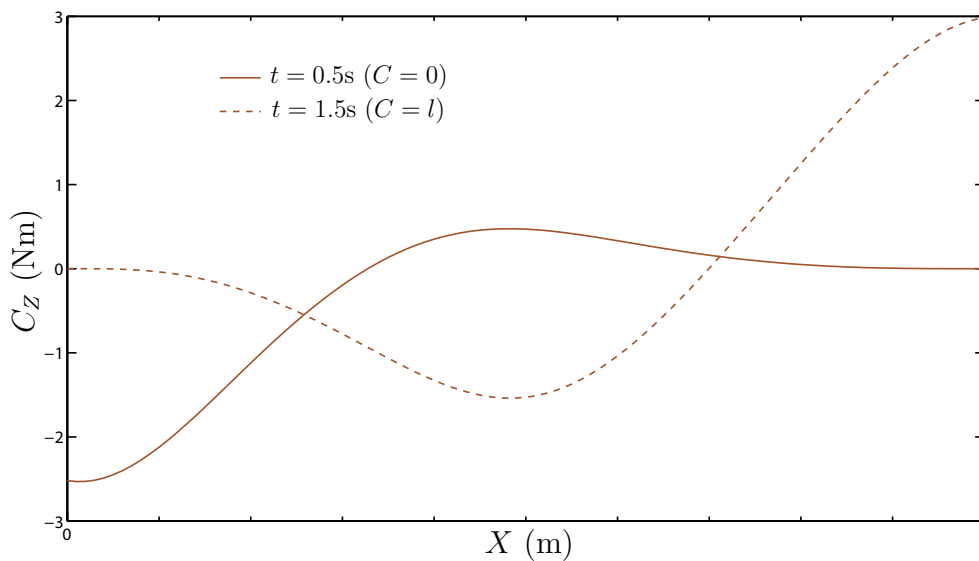


Figure 6.14 – Internal control torque over the length

6.3 2D Snake in Lateral Undulation

Snake is a slender body vertebrate since this organism contains vertebrae in its structure. It has a large number of vertebrae ranging from some 100 vertebrae to more than 300 vertebrae. This hard-bodied creature has an endoskeleton⁸ composed of a serial connection of vertebrae forming the backbone of the snake. Each vertebra has a pair of ribs on each lateral side.

Principal of Undulatory Locomotion

Undulatory locomotion is the common and efficient locomotion mode in snakes. In lateral undulation, an S-shaped wave travels along the body from head to tail. In this mode of locomotion, the snake supports itself laterally in its environment to self propel in an axial direction, i.e. by moving along the length of its backbone. As the snake progresses, each

⁸There are also exoskeleton organisms like illus, sphinx, grasshoppers etc

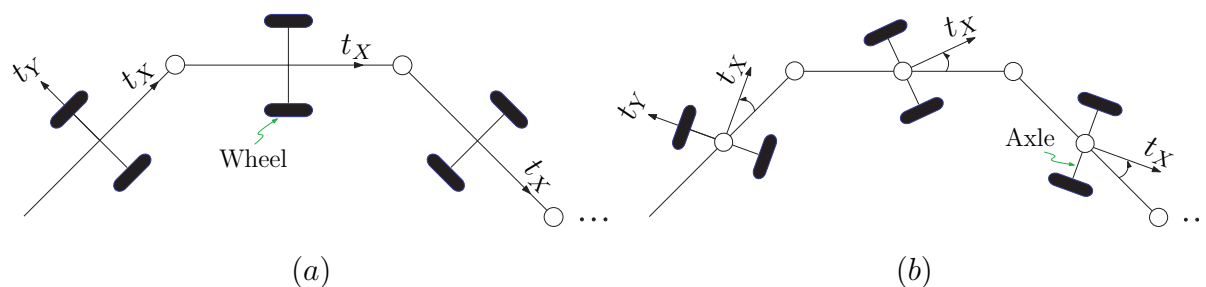


Figure 6.15 – (a) *Discrete Kirchhoff-snake*; (b) *Discrete Reissner-snake*

point along its body follows along the path established by the head.

The snake's skin has the characteristics of anisotropic sliding friction, a critical component of lateral undulation. Due to the anisotropic friction, snake generates high lateral and low axial sliding friction which can be compared to that of a wheel. During undulation, snake exhibits lateral forces by pushing onto fixed points (points d'appuis) on substrate. Lateral components cancel each other out, and the overall resultant force moves the snake in a forward direction.

6.3.1 Assumptions and Considerations

The hyper-redundant robot considered here is an undulatory snake-like robot inspired by snakes that produces a 2D undulatory motion. The system may be modeled either as a Kirchhoff beam or as a Reissner beam with its cross sections representing the vertebrae of a snake. The discrete counterparts of both systems are drawn in Fig. 6.15(a-b). Where, each mechanism is a serial combination of articulated wheeled bodies. In Fig. 6.15(a), the wheeled axles are always perpendicular to its body, i.e. there is no transverse shear in this case and hence can be interpreted as a Kirchhoff beam. While in Fig. 6.15(b), the steering of the wheeled axles can be interpreted as a beam with one lateral transverse shear, i.e. as a Reissner beam. The beam cross sections are the continuous infinitesimal counterparts of the wheeled axles of the discrete mechanisms. First we model the simple Kirchhoff-snake which corresponds to the AmphiBot [34]. In this case, only the yaw degree of freedom (here K_{dZ}) is implemented as a strain field to produce an S-shaped wave along the length of the snake.

6.3.2 Contact Kinematic Model

The undulatory locomotion is achieved by constraining the lateral sliding of the cross sections of the beam while allowing them to move in the axial direction. Practically, in case of a discrete planar mechanism such type of non sliding motion constraints are well imposed by a rolling wheel. Here, in our continuous setup we consider that such motion constraints are imposed by a cross sectional follower annular contact which pre-

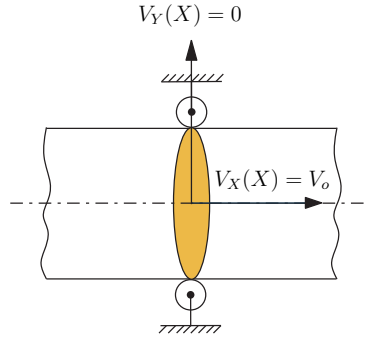


Figure 6.16 – Bilateral nonholonomic constraint imposed on cross section X by cross sectional follower annular contact

vents the cross sections from lateral sliding in case of a planar motion as shown in Fig. 6.16. Mathematically, such contacts are modeled as a nonholonomic constraint and can be simply written as:

$$V_Y(X) = V_{cY}(t), \quad \forall X \in [0, l],$$

where, by considering that the substrate is fixed in the ambient space, i.e. $V_{cY}(t) = 0$, we have:

$$V_Y(X) = 0, \quad \forall X \in [0, l]. \quad (6.28)$$

6.3.3 Continuous Kinematic Model

As mentioned above that a Kirchhoff-snake illustrated here is an undulatory planar robot. Therefore, it can be modeled as a beam with $G = \text{SE}(2)$. In this case, the desired strain field $\xi_d(X, t) = \begin{pmatrix} \Gamma_{dX} & \Gamma_{dY} & K_{dZ} \end{pmatrix}^T \in \text{se}(2)$ is given as:

$$\xi_d(X, t) = \begin{pmatrix} 1 \\ 0 \\ K_{dZ} \end{pmatrix}.$$

With this strain field, the 3D continuous kinematic model of velocities given in equation (5.12) can be simplified for a planar case with $\eta = (g^{-1}\dot{g})^\vee = \begin{pmatrix} V_X & V_Y & \Omega_Z \end{pmatrix}^T \in \text{se}(2)$, as given below:

$$\eta' = \begin{pmatrix} V'_X \\ V'_Y \\ \Omega'_Z \end{pmatrix} = \begin{pmatrix} V_Y K_{dZ} \\ \Omega_Z - V_X K_{dZ} \\ \dot{K}_{dZ} \end{pmatrix}. \quad (6.29)$$

6.3.4 Kinematic Locomotion Model

In the case where the contact with the ground is continuously distributed along the body length, then there are obviously enough of these bilateral nonholonomic constraints to completely define the net motions of the snake only as a function of internal strain field $K_{dZ}(X, t)$. In this regard, forcing the nonholonomic constraints model (6.28) into the continuous kinematic model (6.29) gives the following relations that must verify every motion compatible with the cross sectional follower annular contact:

$$\begin{pmatrix} V'_X \\ \Omega_Z \\ \Omega'_Z \end{pmatrix} = \begin{pmatrix} 0 \\ V_X K_{dZ} \\ \dot{K}_{dZ} \end{pmatrix}. \quad (6.30)$$

The first line shows that the axial speed $V_X(X, t)$ of the snake is constant with respect to X and hence is equal to that of its head, simply denoted as $V_o(t)$. From the second line, we see that $\Omega_Z = V_o K_{dZ}$, i.e. the angular velocity along the snake's backbone is only governed by the forward speed $V_o(t)$ and the body curvature $K_{dZ}(X, t)$. Thus, the above relations can be further simplified as follows:

$$\begin{pmatrix} V_X \\ \Omega_Z \\ \Omega'_Z \end{pmatrix} = \begin{pmatrix} V_o \\ V_o K_{dZ} \\ \dot{K}_{dZ} \end{pmatrix}. \quad (6.31)$$

Next, taking account of the second lines of above equation into its third line, we obtain the fundamental compatibility relation:

$$\dot{K}_{dZ} = V_o K'_{dZ}, \quad (6.32)$$

which must be verified all along the snake so that its mobility (axial propulsion) is assured. Thus, for all $X \in [0, l]$, we can write:

$$\eta(X, t) = \begin{pmatrix} V_o \\ 0 \\ \Omega_Z(X) \end{pmatrix} = \begin{pmatrix} \frac{1}{K'_{dZ}(X)} \\ 0 \\ \frac{K_{dZ}(X)}{K'_{dZ}(X)} \end{pmatrix} \dot{K}_{dZ}(X, t), \quad (6.33)$$

and, particularly, for $X = 0$:

$$\eta_o(t) = \begin{pmatrix} V_o \\ 0 \\ \Omega_o \end{pmatrix} = \begin{pmatrix} \frac{1}{K'_o} \\ 0 \\ \frac{K_o}{K'_o} \end{pmatrix} \dot{K}_o. \quad (6.34)$$

This is the general continuous form of the principal kinematic connection of the discrete case given by equation (3.45) which encodes the follower-leader kinematics of snakes in lateral undulation [30]. Therefore, the above kinematic connection can be rewritten as:

$$\eta_o(t) = -\mathcal{A}\dot{K}_o. \quad (6.35)$$

It is worth noting that, just as in the discrete case where \mathcal{A} includes the first three axes (starting from the head) to fix completely the motion of the head and that of the following links; in the continuous case, the kinematic connection (6.34) involves at most the third derivative of the position field (i.e. $K'_{dz}(0) = p'''(0)$). In the continuous setup, the principle of the follower-leader kinematics can be stated as follows: once the curvature and its derivative in $\forall X$ are specified, the speed of curvature must adapt in each X so that the cross section $X - dX$ follows the cross section X at the speed $V_o(t)$. Thus, every cross section X reoccupies at t^* such that $\int_t^{t^*} V_o d\tau = X$, the same configuration as that occupied by the head at t . This explains the impression of lateral stasis and axial movement observed in snakes, which makes their motion resemble a fluid line of a steady flow. In addition, (6.34) shows that if the axial propulsion is assured by \dot{K}_o/K'_o it is K_o that steers the snake in the plane. Thus, we can approach the 2D snake by analogy with another nonholonomic system, more familiar to the robotics engineer: the car-like platform. In this case, the angular steering of the virtual front wheel is ensured by K_o while the thrust produced by the engine is assured by the relation \dot{K}_o/K'_o .

Finally, taking account of (6.34), the locomotion kinematic model (5.41) for a 2D undulatory snake in SE(2) can be written as:

$$\dot{g}_o = g_o \hat{\eta}_o = g_o \begin{pmatrix} \frac{1}{K'_o} \\ 0 \\ \frac{K_o}{K'_o} \end{pmatrix}^\wedge \dot{K}_o, \quad (6.36)$$

and with $(\dot{g}_o)^\vee = \begin{pmatrix} \dot{x}_o & \dot{y}_o & \dot{\theta}_o \end{pmatrix}^T$, the simplified model of absolute head velocities are given as:

$$\begin{pmatrix} \dot{x}_o \\ \dot{y}_o \\ \dot{\theta}_o \end{pmatrix} = V_o \begin{pmatrix} \cos \theta_o \\ \sin \theta_o \\ K_o \end{pmatrix}. \quad (6.37)$$

6.3.5 Continuous Dynamic Models

After solving the problem of net motions of a 2D undulatory Kirchhoff-snake through the locomotion kinematic model, now it is possible to use the locomotion dynamics (Block1 of Fig. 5.9) for the calculation of the contact wrenches applied by the environment on the snake via the cross sectional follower type annular contact. This is done by integrating

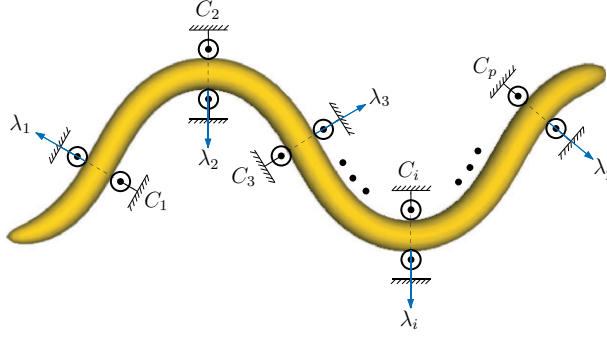


Figure 6.17 – 2D snake with cross sectional follower type annular contacts which imposes the lateral contact forces

the spatial ordinary differential equations given by (5.31). Then, knowing $\dot{\eta}_o(t)$ from the time derivative of (6.34), the algorithm computes the resultant of the contact wrenches reduced to the head, i.e. F_c via the locomotion dynamic model given in equation (5.42). In the general case where the number of constraints induced by the contacts is greater than the dimensions of the fiber (i.e. $p > 3$), the loading is hyper-static. Thus, the resolution of the internal dynamics (i.e. to compute the field of the internal forces and torques along the body length), requires to formulate an additional hypothesis related to the distribution of the resultant contact wrench F_c over the contact points. For example, assuming that the snake is permanently in contact with the ground via p cross sectional follower annular contacts whose positions are fixed in space. Thus, this distribution assumption on the distribution of the lateral contact forces $\lambda_{i=1,2,\dots,p}$, requires the pseudo-inversion of the following under-determined system:

$$F_c = \sum_{i=1}^{i=p} \text{Ad}_{k(C_i)}^* \begin{pmatrix} 0 \\ \lambda_i \\ 0 \end{pmatrix}, \quad (6.38)$$

where $k(C_i) = g^{-1}(C_i)g_o(t)$, and we consider the motion while the p points of contact $C_{1,2,\dots,p}$ are contained in $]0, l[$ (see Fig. 6.17). Once these p lateral contact forces are determined, then the algorithm integrates, in piece-wise manner (Block2 Fig. 5.9), the internal dynamics (5.33) initialized by: $(g_o(t), \eta_o(t), \dot{\eta}_o(t), 0)$ and with a distribution of the following external forces⁹:

$$\bar{F} = \sum_{i=1}^{i=p} \begin{pmatrix} 0 \\ \lambda_i \\ 0 \end{pmatrix} \delta(X - C_i).$$

⁹We only consider the contact wrenches, i.e. $\bar{F}_{\text{other}} = 0$

Curvature Law

In the case of discrete mobile multibody systems, the compatibility condition given by relation (3.44) allowed the computation of the internal shape changes of the snake-like robot in order to assure the mobility of the system. Similarly, in this continuous case the solution of the fundamental compatibility relation $\dot{K}_{dZ} = V_o K'_{dZ}$ given in (6.32) fix the curvature law for a snake given as follows:

$$K_{dZ}(X, t) = f \left(X + \int_0^t V_o(\tau) d\tau \right), \quad (6.39)$$

which corresponds to the propagation of a wave-like curvature profile along the backbone at a generally time-variable speed of propagation $V_o(t)$. It follows that such a choice of the curvature law ensures a thrust in the direction of $-t_X(0)$ at the space-constant speed $V_o(t)$. Finally, for the purpose of illustration, let us consider the case where $\dot{V}_o = 0$, then (6.32) turns to be the one-dimensional propagation equation whose general solutions are $K_{dZ}(X, t) = f(X + V_o t)$, with V_o as the constant speed of the curvature waves. Then, for environments without obstacles but where the ground plane has good properties to prevent lateral sliding, the law of curvature is a simple wave propagation from head toward tail of the snake as follows:

$$K_{dZ}(X, t) = A \cos \left(\frac{2\pi}{\lambda} (X + V_o t) \right), \quad (6.40)$$

where A is the amplitude of the propagation wave. In nature, the curvature along the body of a snake changes according to the choices made by its head, choices that depend on the obstacles that the snake avoid and on which it laterally pushes to propel itself forwards. Consequently, in Fig. 6.18, such a situation is depicted by a steady profile of curvature K_{dZ} moving at a speed $V_o(t)$ along the body, represented here by the material segment $X \in [0, l]$. In this case an additional control parameter in an exponential form is added to the above simple desired curvature law as follows:

$$K_{dZ}(X, t) = A \cos \left(\frac{2\pi}{\lambda} (X + V_o t) \right) + b \exp \left(- \frac{(t - (t_o + T_o/2) + (X/V_o))^2}{(t - (t_o + T_o/2) + (X/V_o))^2 - (T_o/2)^2} \right), \quad (6.41)$$

this ensures, up to $t = t_o$, an axial speed $-V_o t_X(0)$ of average constant direction, and from $t = t_o$ generates a turning maneuver of duration T_o .

6.3.6 Reissner-Snake

Note that the kinematics of the above mentioned Kirchhoff-snake are singular if the curvature is constant over the length, i.e. $K'_{dZ} = 0$. In this case, the conditions of mobility

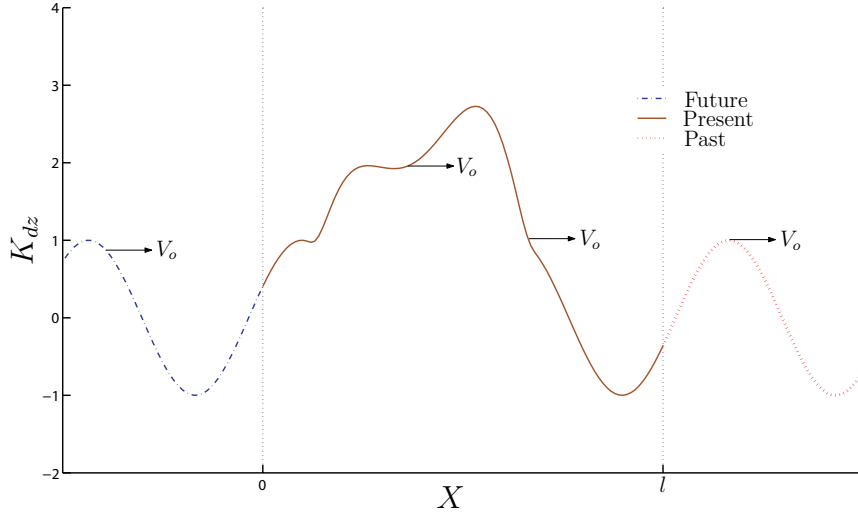


Figure 6.18 – Curvature profile along the snake's backbone

(6.32) are not verified except in the irrelevant case where the snake has a null motion. To overcome this situation, one can consider the continuous homologue of the discrete kinematics of the Fig. 6.15(b), i.e. by adding a transverse shearing (Γ_{dY}) to the present context. In this case, the kinematics become those of an actuated Reissner planar beam with the desired strain field $\xi_d(X, t) = \begin{pmatrix} \Gamma_{dX} & \Gamma_{dY} & K_{dZ} \end{pmatrix}^T \in \text{se}(2)$ as follows:

$$\xi_d(X, t) = \begin{pmatrix} 1 \\ \Gamma_{dY} \\ K_{dZ} \end{pmatrix}.$$

Now, taking into account this strain field and the nonholonomic planar constraints (6.28), the continuous kinematic model of velocities (6.29) can be rewritten as:

$$\eta' = \begin{pmatrix} V'_X \\ V'_Y \\ \Omega'_Z \end{pmatrix} = \begin{pmatrix} -V_X K_{dZ} \Gamma_{dY} \\ 0 \\ \dot{K}_{dZ} \end{pmatrix}. \quad (6.42)$$

In this case, we now have $V_X(X) = V_o e^{(-\int_0^X K_{dZ} \Gamma_{dY} dX)}$ and the mobility condition (6.32) becomes the following:

$$\dot{K}_{dZ} = (K'_{dZ} - K_{dZ}^2 \Gamma_{dY}) V_X, \quad (6.43)$$

where the presence of the control parameter Γ_{dY} as a factor of K_{dZ} ensures the mobility of the snake in all cases where $K_{dZ}(\cdot) \neq 0$. Thus, we recover that the continuous homologue of the discrete kinematics of the Fig. 6.15(b) is only singular for the straight configurations as it is only in this case that the internal movements of the odd and even joints cannot

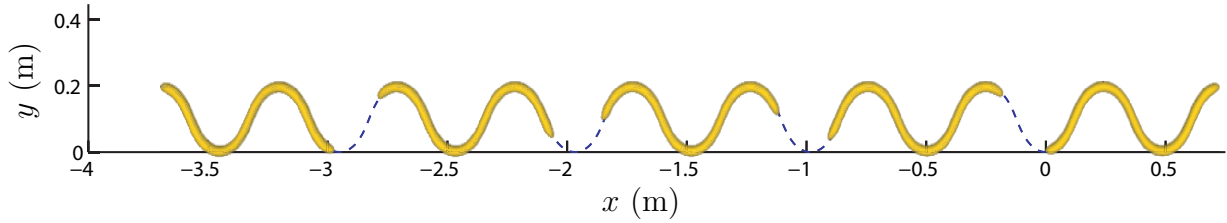


Figure 6.19 – 2D snake straight line locomotion in xy plane

produce external movement.

Finally, in case of natural snakes, the transverse shearing Γ_{dY} models the movements of the skin and the scales relative to the skeleton whose own movements are modeled by the curvature field K_{dZ} . Also, if a snake finds itself in a perfectly straight configuration, it can remove itself from this singularity by: 1) sliding laterally, 2) leaving the ground. However, if these two possibilities are forbidden (for example, if the snake is made to pass through a straight narrow tube), then only a mode of locomotion like that studied for the earthworm in traction-compression becomes possible.

6.3.7 Numerical Results

In this section we solve the kinematics and dynamics of a 2D Kirchhoff-snake by using the proposed algorithm. In case of constant speed $V_o = -0.5\text{ms}^{-1}$, we input the undulatory curvature law (6.40) with the following values:

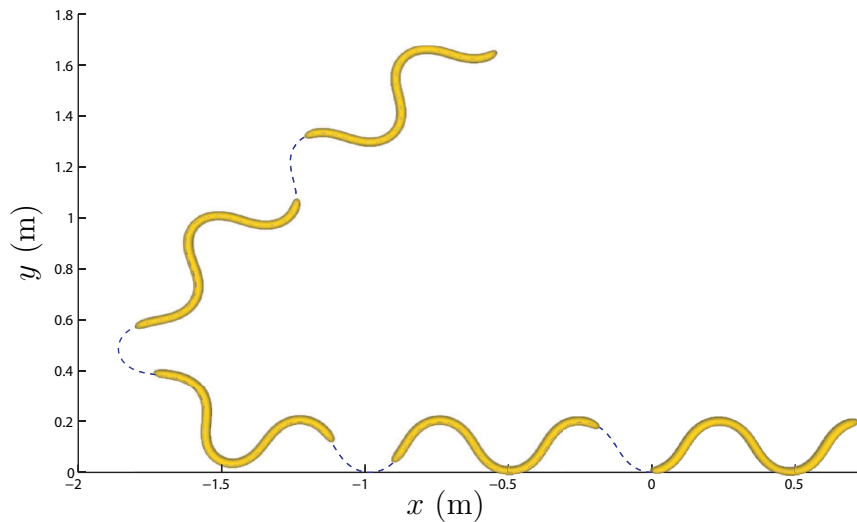
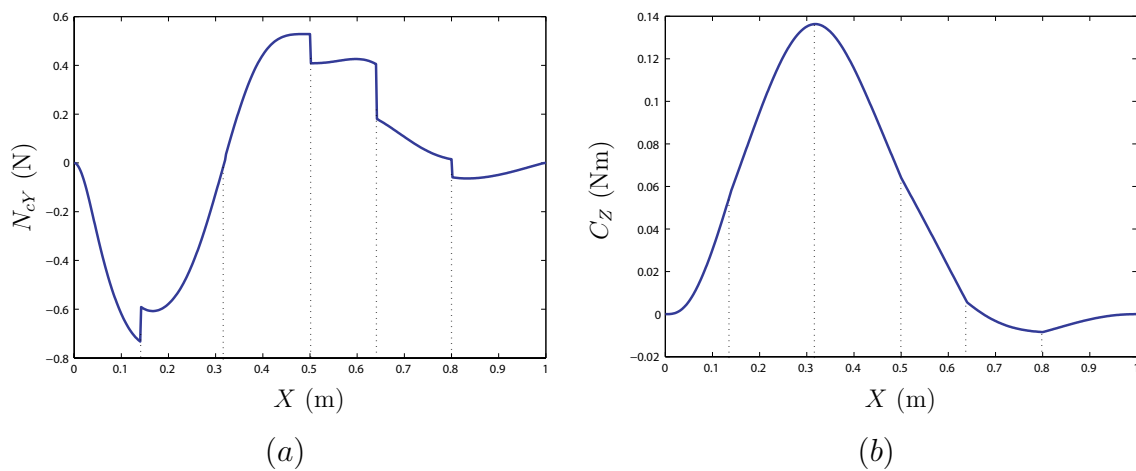
$$a = 10, \lambda = 1\text{m}.$$

Simulating the algorithm for 10s with the help of Matlab, we get the straight line locomotion of the snake in xy plane. The snapshots of such locomotion are depicted in Fig. 6.19. Where the blue line plots the snake's head position in xy plane, while the snapshots of snake's body shows that the body follows the path traced by the head. Furthermore, to examine the turning locomotion of the snake, the following additional parameters are provided to the curvature law (6.41):

$$t_o = 3.0\text{s}, T_o = 4.0\text{s}, b = 2.0$$

where b quantifies the amplitude of a turning maneuver in $\text{SE}(2)$. Again simulating for 10s, the 2D turning locomotion of the snake in the xy plane is shown in Fig. 6.20.

The locomotion dynamics and internal dynamics of the system are solved for five contact points (i.e. $p = 5$) to obtain the cross sectional reaction wrenches applied at the contact points C_1, C_2, \dots, C_5 (see Fig 6.17) and the internal control torques, respectively. For $t = 2.0\text{s}$, the Fig. 6.21(a) plots the reaction force (N_{cY}) over the length, while the Fig. 6.21(b) shows the internal control torque C_Z over the length of snake.

Figure 6.20 – 2D snake turning locomotion in xy planeFigure 6.21 – At $t = 2.0s$ (a) Contact force (N_{cY}) over the length; (b) Internal torque (C_Z) over the length

6.4 3D Snake in Lateral Undulation

Here we consider only the kinematic aspects of 3D crawling. The 3D snake is a priori modeled by Kirchhoff kinematics with torsion. In this case, we have $G = SE(3)$ and the strain field is given as:

$$\xi_d(X, t) = \begin{pmatrix} 1 \\ 0 \\ 0 \\ K_{dX} \\ K_{dY} \\ K_{dZ} \end{pmatrix},$$

so that the kinematic model (5.12) is now written as follows:

$$\begin{pmatrix} V'_X \\ V'_Y \\ V'_Z \\ \Omega'_X \\ \Omega'_Y \\ \Omega'_Z \end{pmatrix} = \begin{pmatrix} V_Y K_{dZ} - K_{dY} V_Z \\ \Omega_Z + K_{dX} V_Z - V_X K_{dZ} \\ -\Omega_Y + K_{dY} V_X - K_{dX} V_Y \\ \dot{K}_{dX} + \Omega_Y K_{dZ} - \Omega_Z K_{dY} \\ \dot{K}_{dY} + \Omega_Z K_{dX} - \Omega_X K_{dZ} \\ \dot{K}_{dZ} + \Omega_X K_{dY} - \Omega_Y K_{dX} \end{pmatrix}. \quad (6.44)$$

On the basis of this model, we shall first search the 3D homologue of the gaits previously exhibited in 2D. This requires establishing the non-sliding constraints in 3D, which is simply achieved by proposing that, for every material abscissa X , the contact is modeled by a cross sectional follower annular contact (see section 5.5.1.2) so that using the nonholonomic model (5.40) with $\Omega_{cX} = V_{cY} = V_{cZ} = 0$, one has $\forall X \in [0, l]$:

$$\begin{cases} V_Y(X) = 0, \\ V_Z(X) = 0, \\ \Omega_X(X) = 0, \end{cases} \quad (6.45)$$

which are the three nonholonomic constraints of a 3D annular contact imposed upon each of the cross sections in movement. Next, we introduce these relations into the general kinematic model (6.44). As a straightforward consequence, the first three equations of (6.44) allows one to write:

$$\begin{cases} V_X = V_o, \\ \Omega_Y = V_o K_{dY}, \\ \Omega_Z = V_o K_{dZ}, \end{cases} \quad (6.46)$$

where V_o is again the axial uniform speed along the backbone while the two last of these relations translate the fact that the internal angular velocity of the cross sections is entirely due to the axial movement along a given profile of fixed curvature. Now taking into account the above relations in the fourth equation of (6.44) in which $\Omega_X = 0$ is forced, we simply find:

$$\begin{aligned} \dot{K}_{dX} &= \Omega'_X + \Omega_Z K_{dY} - \Omega_Y K_{dZ} \\ &= 0 + V_o(K_{dY} K_{dZ} - K_{dZ} K_{dY}) = 0. \end{aligned} \quad (6.47)$$

Thus, if we assume that the robot starts (at $t = 0$) from a straight untwisted configuration, one have $K_{dX} = 0$ all along its length and at any instant of the motion. Introducing this last constraint as well as all the others into the two last relations of (6.44) allows one to

write with (6.47), the three independent relations on the strain laws:

$$\begin{pmatrix} \dot{K}_{dX} \\ \dot{K}_{dY} \\ \dot{K}_{dZ} \end{pmatrix} = \begin{pmatrix} 0 \\ V_o K'_{dY} \\ V_o K'_{dZ} \end{pmatrix}, \quad (6.48)$$

where the first of these relations can be ensured by the design (un-twistable kinematics) while the two others are imposed by the curvature control laws. Finally (6.48) defines the 3D counterpart of the planar compatibility condition (6.32), and must be verified all along the snake so that its mobility is assured. Thus, $\forall X \in [0, l]$, we can write:

$$\eta(X, t) = \begin{pmatrix} V_o \\ 0_{3 \times 1} \\ \Omega_Y(X) \\ \Omega_Z(X) \end{pmatrix} = \begin{pmatrix} 1/K'_{dY} \\ 0_{3 \times 1} \\ K_{dY}/K'_{dY} \\ K_{dZ}/K'_{dY} \end{pmatrix} (X, t) \dot{K}_{dY}(X, t), \quad (6.49)$$

and, in particular, for $X = 0$, we have:

$$\eta_o(t) = \begin{pmatrix} V_o \\ 0_{3 \times 1} \\ \Omega_{oY} \\ \Omega_{oZ} \end{pmatrix} = \begin{pmatrix} 1/K'_o \\ 0_{3 \times 1} \\ K_{oY}/K'_o \\ K_{oZ}/K'_o \end{pmatrix} \dot{K}_o, \quad (6.50)$$

with $\dot{K}_o = \frac{\partial}{\partial t} \|K_d\|(0)$ and $K'_o = \frac{\partial}{\partial X} \|K_d\|(0)$ (see section A.3 of appendix A for illustration). Finally, the locomotion kinematic model (5.41) for a 3D undulatory snake, in the form of the follower-leader connection, can be written as:

$$\dot{g}_o = g_o \begin{pmatrix} V_o \\ 0_{3 \times 1} \\ \Omega_{oY} \\ \Omega_{oZ} \end{pmatrix}^\wedge = g_o \begin{pmatrix} 1/K'_o \\ 0_{3 \times 1} \\ K_{oY}/K'_o \\ K_{oZ}/K'_o \end{pmatrix}^\wedge \dot{K}_o. \quad (6.51)$$

6.4.1 Continuous Dynamic Models

After solving the problem of net motions of a 3D undulatory Kirchhoff-snake through the locomotion kinematic model, now it is possible to use the locomotion dynamics (Block1 of Fig. 5.9) for the calculation of the contact wrenches applied by the environment on the snake via the cross sectional follower type annular contact. This is done by integrating the spatial ordinary differential equations given by (5.31). Then, knowing $\dot{\eta}_o(t)$ from the time derivative of (6.51), the algorithm computes the resultant of the contact wrenches reduced to the head, i.e. F_c via the locomotion dynamic model given in equation (5.42). In the general case where the number of constraints induced by the contacts is greater

than the dimensions of the fiber (i.e. $3p > 6$), the loading is hyper-static. Thus, the resolution of the internal dynamics (i.e. to compute the field of the internal forces and torques along the body length), requires to formulate an additional hypothesis related to the distribution of the resultant contact wrench F_c over the contact points. For example, assuming that the snake is permanently in contact with the surroundings via p cross sectional follower annular contacts fixed in space and located at each time at the body abscissa C_1, C_2, \dots, C_p , we can assume that the snake minimizes the Euclidean norm of the $(3p \times 1)$ vector of reaction forces. Thus, this distribution assumption on the distribution of the contact wrenches require the pseudo-inversion of the following under-determined system:

$$F_c = \sum_{i=1}^{i=p} \text{Ad}_{k(C_i)}^* \begin{pmatrix} 0 \\ N_{cY,i} \\ N_{cZ,i} \\ C_{cX,i} \\ 0_{2 \times 1} \end{pmatrix}, \quad (6.52)$$

where $k(C_i) = g^{-1}(C_i)g_o(t)$, and we consider the motion while the p points of contact $C_{1,2,\dots,p}$ are contained in $]0, l[$. Once these contact wrenches are determined, then the algorithm integrates, in piece-wise manner (Block2 Fig. 5.9), the internal dynamics (5.33) initialized by: $(g_o(t), \eta_o(t), \dot{\eta}_o(t), 0)$ and with a distribution of the following external forces¹⁰:

$$\bar{F} = \sum_{i=1}^{i=p} \begin{pmatrix} 0 \\ N_{cY,i} \\ N_{cZ,i} \\ C_{cX,i} \\ 0_{2 \times 1} \end{pmatrix} \delta(X - C_i).$$

6.4.2 Numerical Results

First, let us take the case of a 3D turning snake. The undulatory curvature $K_{dZ}(X, t)$ given by (6.41) along with:

$$\begin{aligned} K_{dX}(X, t) &= 0, \\ K_{dY}(X, t) &= b_y \exp\left(-\frac{(t - (t_o + T_o/2) + (X/V_o))^2}{(t - (t_o + T_o/2) + (X/V_o))^2 - (T_o/2)^2}\right), \end{aligned}$$

¹⁰We only consider the contact wrenches, i.e. $\bar{F}_{\text{other}} = 0$

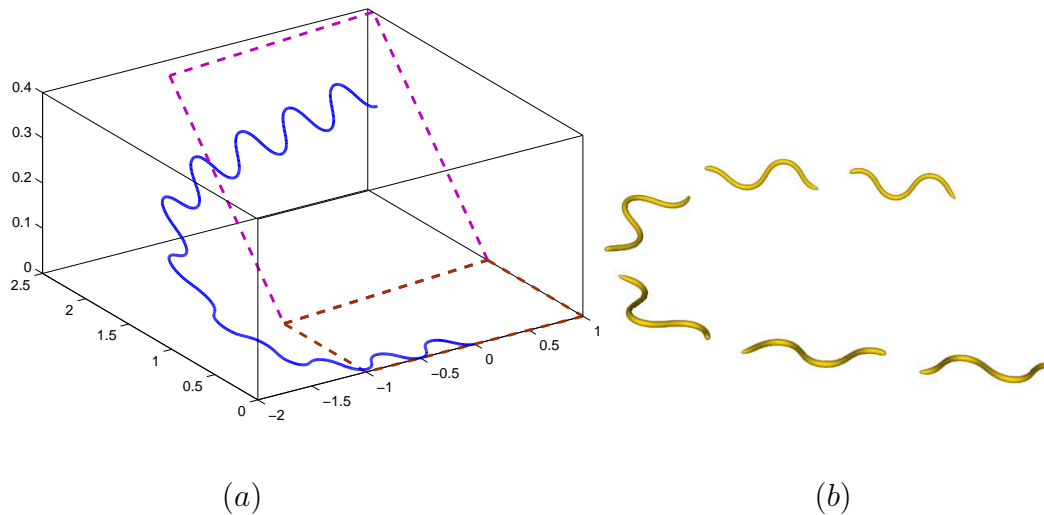


Figure 6.22 – (a) Head turning locomotion; (b) Snapshots of snake 3D turning locomotion

are the inputs to the algorithm of Fig. 5.9, with the following parameters:

$$A = 10, \quad \omega = \frac{2\pi V_o}{\lambda} \text{ rad/s}, \quad b_y = 0.5, \quad V_o = -0.5 \text{ ms}^{-1}.$$

Simulating the algorithm for 10s, the 3D turning motion of the snake in the xyz space is obtained as shown in Fig. 6.22.

In order to illustrate the dynamics of a 3D snake, let us take the case of a snake in spiral motion around a cylindrical surface. For such motions the pitch and yaw (i.e. K_{dY} and K_{dZ}) degrees of freedom are controlled through the following laws of strains field with constant roll degree of freedom:

$$\begin{aligned} K_{dX}(X, t) &= 0, \\ K_{dY}(X, t) &= -A \sin\left(\frac{2\pi}{\lambda}(X + V_o t)\right), \\ K_{dZ}(X, t) &= A \cos\left(\frac{2\pi}{\lambda}(X + V_o t)\right). \end{aligned}$$

Then the locomotion dynamics and internal dynamics of the system are solved with five contact points (i.e. $p = 5$) fixed in space, to obtain the cross sectional reaction wrenches applied at the contact points C_1, C_2, \dots, C_5 and the internal control torques, respectively. For $t = 2.0$ s, the Fig. 6.23(a) plots the reaction forces (N_{cY}, N_{cZ}) over the length, while the Fig. 6.23(b) shows the internal control torques (C_Y, C_Z) over the length of snake.

6.5 Further Discussion: Application to Real Designs

In the light of the above examples, the question of how applying these results to real designs naturally arises. About this point, the proposed approach being general, the cost

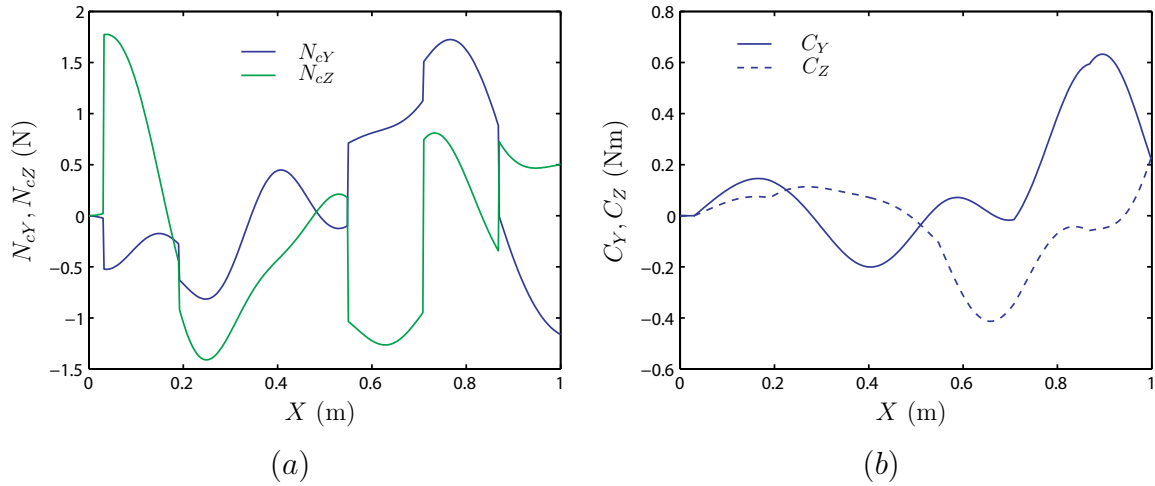


Figure 6.23 – At $t = 2.0s$ (a) Contact forces (N_{cY}, N_{cZ}) over the length; (b) Internal torques (C_Y, C_Z) over the length

to pay for this generality is a certain idealization of the model. This idealization essentially concerns two points: 1) the model of the body as an internally actuated Cosserat beam, 2) the model of the contacts between the body and its surroundings. Starting with the first point regarding Cosserat beam, we suggest to proceed case by case. For instance, for a specific technology among the numerous designs of snake-like robots today developed [69, 111, 71], one could first ask the starting questions: does the basic Cosserat beam assumption of rigid cross sections have a physical reality? And also, how this assumption can be adapted to a particular technological principle? As a first answer, let us remark that in the case of designs inspired from vertebrate animals where one can identify lateral rigid elements attached to a body line axially articulated and mimicking the backbone, the Cosserat beam model is more and more well adapted as the number of vertebrae increases (big snakes like pythons can have more than several hundred). In a design more inspired from hyper-redundant arthropods, the rigid segments can also be considered as being the cross sections of their macro-continuous model. Finally, for robots inspired from hydrostats, although the application of the approach seems less natural since these animals do not contain any rigid element in their principle, we have seen in this thesis that how we could release the Cosserat basic assumption of rigid cross sections in order to adapt the model to a simplified version of one dimensional hydrostats. Furthermore, some groups are nowadays exploring new designs in soft robotics and have chosen to mimic hydrostats as a set of rigid cross-sections interconnected through actuated cables and refer explicitly to the Cosserat model as a source of inspiration for their design [68]. Finally, as elasticity plays an important role in continuous robots, the model proposed in this thesis could be improved in this sense. About the second point regarding the model of the contacts, let us remind that in the case of snake-like robots, we have modeled the contacts through bilateral annular joints introducing a null axial friction (along the vertebral axis) as well

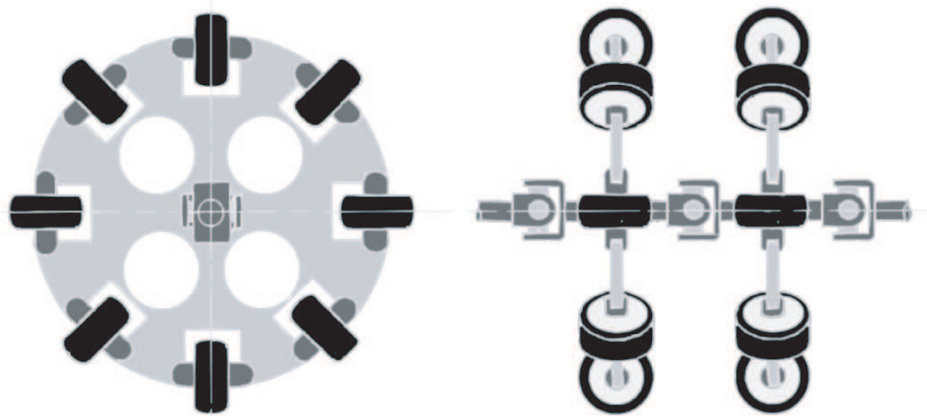


Figure 6.24 – *Proposed design of a 3D snake: (left) cross-sectional view, (right) longitudinal view*

as an infinite lateral friction force (perpendicular to the vertebral axis). In spite of its ideal character, such a model is not so far from what one can observe on real snakes. Indeed, the scales of the snakes give to their skin a strong frictional anisotropy, the axial friction being far lower than its lateral counterpart. In our case, we pushed this tendency to its ideal asymptotic limit, and also replaced the usual unilateral contacts by bilateral constraints. This second simplification, which can be released in future, requires a further discussion on the feasibility of a motion. Indeed, once the net motions are known by solving the external kinematics, one has to check whether the real contacts can generate the desired external wrench? Technically, the answer to this question depends on the solutions of a linear system of the form (6.52). In particular, if the joints are in reality unilateral contacts, as this is the case of obstacle-aided locomotion [69], the reaction forces solutions of (6.52) should have to keep a given sign all along the motion. At last, once such a loading has been found, so validating the model of contacts, one has to check whether the actuators can supply the desired motions under such a loading. To address this last problem, one can use the inverse dynamics of control torques as proposed in this thesis. Finally, if we seek a design of snake-like robot ideally adapted to our model of robot and contacts, starting from [119], this would be a multi-body system with a very high number of very small length links connected through universal joints. Each of these links would be equipped with many wheels aligned along its greater length and placed radially on the links, so bio-mimicking the scales of a 3D snake (see Fig. 6.24).

6.6 Conclusions

In this chapter, the terrestrial locomotion modeling approach presented in the previous chapter was applied to several examples inspired by natures. Through these examples, it was shown that this approach can be a useful tool for investigation when it is applied

to the analysis of mobility or gait generation of snakes. In the case of earthworm, the Cosserat assumption of beam cross sections rigidity was partially removed and replaced by the axial volume preservation constraint. This allows with small efforts to extend the approach and the algorithm to one dimensional hydrostats. Moreover, the problem of manipulation was illustrated indirectly through the example of the climbing inchworm where at each step of the "walking" the robot is a manipulator clamped into the ground.

From an algorithmic point of view, as the number of the links increases, it becomes more and more relevant to approximate the robot behavior with infinite dimensional continuous models [27, 29]. In this case, the Newton-Euler formulation allows solving the dynamics without re-parameterizing the model through a set of generalized coordinates (finite elements or assumed modes), as it is required by the Lagrangian approach of the same problem. From a pure computational aspect, when the number of degrees of freedom dramatically increases, the recursive formulations of chained systems dynamics, as that of Newton-Euler, become more and more efficient since they lead to $O(n)$ algorithms with n the number of links. Furthermore, due to their implicit character, the Newton-Euler algorithms are simple to program on a computer. In the continuous case here presented, these recursive computations are replaced by ordinary differential equations which are solved through standard adaptive step numerical integrators allowing to increase further the computational efficiency. Finally, these virtues have been exploited in this thesis to implement simulators which are faster than real time for all the reported examples.



General Discussion and Conclusions

7.1 Summary of the Thesis	157
7.2 First Conclusive Discussion: Projective vs Distributive Approach	158
7.3 Second Conclusive Discussion: Lagrangian vs Newton-Euler Modeling Approach	162
7.4 Perspectives	164

7.1 Summary of the Thesis

The motivation of this thesis was to provide to the roboticist a general methodological framework suited to the study of the locomotion of a new generation of robots bio-inspired from animals. In this context, the high complexity of the contact models as well as the increasing complexity of design require dynamicists to produce new tools able to handle a high number of internal degrees of freedom. In order to reach these constrained objectives, we have chosen to combine the abstract framework of geometric mechanics with the Newton-Euler algorithmic approach. In this perspective, the well known Luh and Walker algorithm of usual manipulators has been extended to the case of a new class of systems named "mobile multibody systems" (i.e. MMS), since contrary to the standard "multibody systems" (i.e. MS), the motion of their basis is not known but has to be computed at each step of the time integration loop through a locomotion model. More precisely, the algorithm was capable of solving the problem of locomotion by computing the following unknowns through known data of internal imposed motions:

1. The net motions of the reference body of the system.
2. The internal torques/forces of the system.

Starting with discrete systems, where the constitutive bodies are countable and in finite number, we have step by step addressed the cases of the unconstrained MMS where the eventual contacts were modeled through physical laws relating forces to motions.

Then, we have considered the specific case where the contacts are ensured through ideal wheels. In this case, the corresponding algorithm has been derived by a projection of the unconstrained algorithm onto the admissible spaces compatible with the constraints. Remarkably, all the cases and subcases that we met were conditioned by some properties such as the symmetry properties of the external forces, or the rank of a unique matrix in the kinematic model of a wheeled system.

Beyond these considerations of classification, the presented results are innovative in the sense that they propose an alternative to the Lagrangian framework much more developed till today. Moreover, when the number of degrees of freedom dramatically increases, we proposed to adopt directly a continuous approach. This approach is named macro-continuous since it is relevant at a macroscopic scale at which the robot can be considered as an internally actuated Cosserat beam. It allows to extend further the Newton-Euler algorithms to the case of a class of continuous systems composed of an infinite set of infinitesimally short links modeled by the rigid cross sections of the beam. This approach, which has been previously proposed to study the swimming of elongated body fish has been extended here to the case of terrestrial locomotion. In this context, the choice has been done to model the hard contacts with the obstacles as a set of kinematic constraints whose combined use allowed us to model several types of locomotion practiced by elongated body animals. Moreover, in this context, the macro-continuous model has shown its efficiency for the analysis of the mobility, or the gait generation, which are both difficult problems when dealing with a high number (here infinite) of internal degrees of freedom. Beyond the kinematic aspects, the macro-continuous approach also gave access to the model of the internal (control) and external (contact) forces, which is a very precious information for hyper-redundant locomotion. Finally, the macro-continuous algorithm inherits a similar structure as that of discrete case, since the partial differential equations of a Cosserat beam are merely a continuous version of the Newton-Euler model of a discrete MMS studied in chapters 3 and 4. Due to this similarity, the continuous algorithm is again recursive, the recursion on the discrete indices being replaced by spatial ordinary differential equations on the cross sections (material) label. Exploiting this recursive character allowed us to obtain efficient algorithms easy to program.

7.2 First Conclusive Discussion: Projective vs Distributive Approach

Although the discrete and continuous approaches of chapter 3 and 4 share some common points, beyond their intrinsic discrete vs continuous character, they also present deeper differences that require a further discussion. To understand these differences, let us re-

consider the principle of each of the two algorithms when they are both applied to a common system as for instance a hyper-redundant snake like robot in lateral undulation on a planar uniform ground.

In this case of snake locomotion, let us remind that the discrete algorithm computes in a first step the reference acceleration using the discrete kinematic connection. In a second step, this reference acceleration is used to initialize the recursive kinematic model which allows to compute the position-velocity-acceleration of each of the bodies of the chain. This data is then used in a third step by a reduced recursion on the interbody forces. These reduced recursions are deduced from the unconstrained case by projecting the Newton-Euler equations onto the kernel of each wheeled body. Finally, this projection cancels the reaction forces which at the end do not appear anymore in the whole algorithm.

Now let us consider the continuous case of snake locomotion. In this case, whether the first step of the algorithm is similar to the discrete case where a continuous version of the connection replaces the usual kinematic connection, the second step of computation is in fact drastically different. Indeed, the continuous algorithm does not use any projection to cancel the reaction forces. Instead of that, it first computes the resultant of external contact forces required by the external motions and then distributes this resultant onto the contacts. For a snake, the reaction forces transmitted by the contacts are in general not unique depending on the number of independent constraints forced by the contact. Obviously, in the case of a uniform contact on the ground the number of solutions is a priori infinite and it is required to do supplementary assumptions on the distribution of contacts to solve the ambiguity.

Comparing these two algorithms (discrete and continuous), it becomes obvious that their principle is radically different in the second step of computation. As a consequence, while the net motions are in both cases identical (the contrary would in fact reveal a contradiction), the computed torques are generally different. In particular, in the discrete case the joint torques are unique and requires no distribution assumption, while there are an infinite number of solutions in the continuous case. From these basic remarks, new remarks and questions arise.

First, due to the redundance of contacts, the number of sets of reaction forces ensuring the observed motion (in the following, we name such a set as loading) is in fact (in general) infinite. Thus, it is surprising that the projective approach did not require any distribution hypothesis to pursue. As a consequence of this remark, since the projective approach computes a unique vector of joint torques, what is the meaning of this particular solution?

In order to answer this question, let us go back to the Lagrangian setting which has the advantage to be more easily handled at a high level of view. Since, we discuss about the effect of reaction forces, we now state the Lagrange equations of the snake in the whole fiber bundle, i.e. before any projection. In this case, the dynamics can be written (for instance, from the principle of virtual work) in the form of the following algebraic-differential system:

Dynamic equations:

$$\begin{pmatrix} \mathcal{M} & M \\ M^T & m \end{pmatrix} \begin{pmatrix} \dot{\eta} \\ \ddot{r} \end{pmatrix} + \begin{pmatrix} F_{\text{in}} \\ Q_{\text{in}} \end{pmatrix} = \begin{pmatrix} 0 \\ \tau \end{pmatrix} + \begin{pmatrix} A^T \\ B^T \end{pmatrix} \lambda. \quad (7.1)$$

Kinematic constraints:

$$A(r)\eta + B(r)\dot{r} = 0. \quad (7.2)$$

Where λ represents a vector of Lagrange multipliers generalized reaction forces $(A^T\lambda, B^T\lambda)^T$ exerted perpendicularly to the constrained admissible subspace of $G \times \mathcal{S}$ at each time of the motion. In the physical space, λ is nothing but the vector of the reaction forces and torques transmitted by the constraints of the contacts. In particular, the first row of (7.1) can be rewritten as $F_c = A^T\lambda$, where F_c has been defined in 5 as the resultant (related to the reference frame) of the reaction contact forces. In the same manner, we will note $\tau_c = B^T\lambda$ the torques exerted by the contact force onto the actuated joint axes. Thus, using this notation, the second row of Lagrangian dynamic equation (7.1) can be rewritten as:

$$\bar{\tau}_{\text{kin}} = \tau + \tau_c,$$

where $\bar{\tau}_{\text{kin}}$ is an internal control torque given only by the information from kinematics i.e. motions. This is actually the torque of an equivalent manipulator having the same motions as that of the considered MMS, i.e.:

$$\bar{\tau}_{\text{kin}} = (m\ddot{r} + M^T\dot{\eta} + Q_{\text{in}})(r, \dot{r}, \ddot{r}),$$

where the external net motions have been deduced from the internal shape evolution via the first step of the algorithm. For this particular kinematic solution of the internal inverse problem, the inertial forces due to the motions of this virtual manipulator are integrally transmitted to the joints. This is why we denote this purely kinematic torque $\bar{\tau}_{\text{kin}}$ with an overscore to indicate that this is the maximum value of such a kinematic component. In short, in this case the number of activated contacts of (7.2) is minimum and the joints take in charge all the constraints alone so increasing their magnitude up to their maximum

values.

At the opposite, the minimum kinematic torque is also accessible. Indeed, pursuing the same ideas such a particular solution that we will note $\underline{\tau}_{\text{kin}}$, is obtained when all the contacts are activated. Hence, this torque is nothing but that particular one which is computed by the projective algorithm, where the lateral inertia forces exerted on each of the bodies by the motion, are compensated, body after body, by the reactions of the pair of wheels fixed to them.

Finally, between these two extremal cases, we find all the others corresponding to an intermediate activation of the contacts. To each of these cases, there is one corresponding kinematic torque (only explainable by the motions) defined by $\tau_{\text{kin}} = B^T \lambda_{\text{kin}}$, where λ_{kin} is a loading univocally deducible from the motion and defined by the generalized inversion of the second row of (7.1):

$$\lambda = \lambda_{\text{kin}} + \lambda_{\text{stat}} = (A^T)^\dagger F_c(r, \dot{r}, \ddot{r}) + \lambda_{\text{stat}} \quad (7.3)$$

with $F_c(r, \dot{r}, \ddot{r}) = (\mathcal{M}\dot{\eta} + M\ddot{r} + F_{\text{in}})$, whereas $\lambda_{\text{stat}} \in \ker(A^T)$ corresponds to the static loadings which do not produce any observable motion. In fact, they generate the internal stresses felt by the robot (or the snake) due to the hyper-statism of the contacts. As a corollary remark, when we increase the number of contacts, the internal torque (τ_{kin}) should tend toward the minimum torque ($\underline{\tau}_{\text{kin}}$) computed by the projective algorithm, while when the number of contact decreases, τ_{kin} tends toward $\bar{\tau}_{\text{kin}}$ given by the distributive algorithm without contact (i.e. by the usual Luh and Walker algorithm of manipulators).

Now, coming back to nature, for a snake moving in a tree for instance, the animal permanently exploits the redundancy of the first row of (7.1) (or equivalently that of equation (6.52) in the continuous case) in order to satisfy supplementary more sophisticated conditions as maximizing the adherence while minimizing the consumed energy. Among the degrees of freedom of these solutions that the snakes exploit, they can change the configuration of the activated contacts with time and, according to (7.3), can play with the internal control forces which do not produce any net motions.

At last, returning to the comparison between both algorithms (projective and distributive), each of them has its own way of modeling these intermediate possibilities. In the case of the projective algorithm, this is done by defining the bodies supporting the activated contacts as non-holonomic bodies while the other are declared as holonomic. On the other hand, in the distributive case, we just have to distribute the resultant of external

forces onto the activated contacts. However, note that whether the distributive algorithm can take into account both the changes of activated contacts and those of static loadings, the projective one seems only capable of dealing with the first source of redundancy. In this regard the distributive algorithm is more general than the projective algorithm.

7.3 Second Conclusive Discussion: Lagrangian vs Newton-Euler Modeling Approach

Beyond the differences between the algorithms they produce, the Lagrangian and Newton-Euler approaches are in fact different for other deeper reasons that we are now going to address. In order to structure our discussion, we first present, in table 7.1, the overview of the approaches discussed in this thesis. From this, new questions arise. Why we have

	Discrete systems	Continuous systems
Lagrangian approach	Chapter 2 equations (2.15, 2.23)	?
Newton-Euler approach	Chapter 3 equations (3.7-3.9, 3.11, 3.29)	Chapter 5 equations (5.29, 5.31, 5.33)

Table 7.1 – Overview of the modeling approaches discussed in the thesis

not derived a continuous model in the Lagrangian setting? And what could be such a model?

Going further, let us consider the discrete MMS for which both formulations are at our disposal. In order to compare these two formulations, we consider separately the forward external dynamics and the inverse internal dynamics.

1. Forward external dynamics: In this case, let us first remark that in both approaches (Newton-Euler and Lagrangian) the external dynamics were derived on the same definition of the configuration space, i.e. the fiber bundle $G \times \mathcal{S}$ (see equation (2.15) in chapter 2 and equation (3.29) in chapter 3). Naturally, the resulting models are the same, since in Newtonian mechanics as a whole, a dynamic model of a system is entirely determined by the definition of its configuration space. In fact, in the case of external dynamics, the two approaches differ essentially by the algorithmic way they use to derive these equations (by introducing a Lagrangian in the Poincaré equations in the case of Lagrangian approach, while using the recursions on the composite bodies in the case of Newton-Euler approach).
2. Inverse internal dynamics: in this sub-model, the definition of the configuration space differs for the two approaches. In fact, in the Lagrangian approach we used the shape space \mathcal{S} of the fiber bundle, while in the Newton-Euler approach we

stated the internal dynamics on $(G)^{p+1}$. Consequently, even if they have the same inputs and outputs, the two models are this time radically as much different as the Lagrange and Newton-Euler models of a usual manipulator are.

Finally, focusing our interest on the internal dynamics, we can say that in the Lagrangian case the shape motions are isolated from the net motions of the fiber through the natural splitting of $G \times \mathcal{S}$. On the other hand, in the Newton-Euler approach the internal dynamics formulation does not require this separation of motions, the kinematic unknown of the model being the Galilean twists of the bodies. This context can be directly related to that found in flexible multibody dynamics where it is known after J.C. Simo that there exists two approaches to measure the shape changes of a flexible link moving in a MS. In the first one, the shape is defined a priori as a field of deformations measured with respect to a moving floating frame [19]. In our case, this corresponds to the Lagrangian approach on principal fiber bundles. In the second approach, the shape is defined a posteriori by applying a nonlinear strain field to the Galilean motions of the link. In our case, this second approach which corresponds to the Newton-Euler approach has been named "Geometrically Exact" by the author. This formulation is known to be very more simple than that based on the floating frame [104, 105]. This advantage is exploited through numerical finite element methods able to solve flexible multibody dynamics without any approximation of the finite transformations [12, 106, 20].

Returning to our case of study, we recover the same arguments in favor of the Newton-Euler approach. Practically, the complexity of the internal dynamics in the form of the Newton-Euler recursion on the interbody wrenches is independent of the number of internal degrees of freedom. While on the other hand, adding more and more degrees of freedom considerably increases the complexity of the matrices of the Lagrangian model. At last, in the extreme case where this number tends toward infinity, the Lagrangian model cannot even be written (in terms of the continuous homologous of joints angles, i.e. strains) while the Newton-Euler formulation still works. This remark answers the first question previously posed. As regards the second one: what would be a Lagrangian model of a continuous MMS? Although the Lagrangian model is impossible with shape parameterized by continuous strains, the Lagrangian parametrization through a set of generalized coordinates can be achieved after the continuous formulation through standard discretization techniques such as finite elements method or assumed modes approach. For instance, in the second case, the modal coordinates become the shape variables r of the Lagrangian model.

7.4 Perspectives

The prospects of this work are numerous and we will now list down a few and comment them. First of all, as a continuation of the first of the two previous discussions, it is natural to complete the overall landscape of this work by applying the projective approach to the continuous case, and the distributive approach to the discrete case. As a result, adaptations would be required. For example, in the macro-continuous model, the matrices of the admissible space of the isolated bodies would be replaced by a function of the material abscissa $H(X)$ with X a moving point ($C(t)$) in the case of a sweeping contact. On the other hand, in case of the discrete algorithm, it would be natural to relax the assumptions of section 3.1.1 in chapter 3, and extend the algorithm to a much more wide class of multibody systems. Another extension of the results for discrete systems is to develop a single algorithm which is capable of taking into account the kinematic singularities (related to the rank of the matrix A in chapter 3) of the MMS, and hence capable of switching smoothly from a kinematic model to a dynamic model and vice versa.

More fundamentally, the direct algorithm (i.e. where torques are inputs, while internal and external motions are output) evoked in section 2.3.3 in chapter 2 is a short-term objective. Although it is not very suitable for the synthesis of gaits (to which our proposed algorithm is well suited), it is the necessary step toward the modeling of compliance or other passive deformations, inherently present in all designs of robots and basic principles of locomotion used by many animals. On this point, the passive deformations allow the animals to optimize their performance in terms of energy consumption while limiting their neuro-biological complexity. In particular, the solutions "found by the animals" to solve difficult control problems are often designed to circumvent these problems by changing (through the evolution of species) the morphology of their bodies. The subjects of applications, such as studying the "flapping tail" of a robot fish or "flapping wing" of a robot inspired by the flying insect, are in the target of these extensions. Still in the perspective of extending this work to the case of direct dynamics, although in this case a solution in the discrete unconstrained context is presented in [63], the extension to the constrained case as well as the macro-continuous are still to be addressed. All these perspectives concern the extension of the methodological framework developed here in this thesis.

Beyond these extensions of the general framework, we also plan to apply these tools to particular problems such as hyper redundant manipulation or snake-like robots. In the first case, the parallel robots with cables are nowadays a growing field in which the methodological framework presented in this thesis could naturally be applied. In this perspective, and more generally, for any design of hyper-redundant robot, the question of the model of internal forces and more particularly of their actuation is a key issue

that one must address. An idea here would be to project the macro-continuous model of the Newton-Euler/Cosserat type on a model that can take into account the technological details of the internal design of these robots. These new developments could then be sought in a general framework to adapt the macro-continuous model to a maximum of designs. Among the utilities of these generic tools, this time in the case of snake robots, the results presented above allowed us to state nice problems of optimization which would be interesting to explore in the future works. For this, the use of static terms exhibited in section 7.2, in order to optimize certain criteria related to energy or static stability, are issues that would be interesting to address. In the same field, the combination of unsteady contacts in chapter 5 and the observations of natural snakes would permit to investigate the modes of locomotion much more complex than "simple lateral undulation" such as the "concertina" or "sidewinding" discussed in Chapter 2.



Thesis Detailed Résumé in French

8.1	Introduction Générale	168
8.2	La locomotion bio-inspirée	170
8.3	Problème général abordé dans cette thèse	171
8.4	Introduction aux Systèmes Multicorps Discrets	173
8.4.1	Les hypothèses de Base	173
8.4.2	Description des systèmes multicorps mobiles	174
8.4.3	Notations	176
8.5	Dynamique inverse récursive des manipulateurs	177
8.6	Aperçu de l'algorithme	178
8.7	Les systèmes multicorps mobiles non-contraints	179
8.7.1	Dynamique de la locomotion: le calcul de $\dot{\eta}_o$	180
8.7.2	Dynamique des couples: le calcul des couples internes	181
8.7.3	Le cas non-contraint avec symétries	181
8.8	Les systèmes multicorps mobiles contraints	182
8.8.1	Cinématique d'un corps non-holonome isolé	182
8.8.2	Cinématique du corps composite S_o^+	183
8.8.3	Dynamique du système multicorps mobile contraint	185
8.9	Exemples illustratifs	189
8.9.1	Le snakeboard	189
8.9.2	Un robot serpent	191
8.10	Introduction aux Robots Hyper-Redondants	193
8.11	Notations et définitions	194
8.12	Cinématique de la poutre et des robots hyper-redondants	195
8.13	Modèle continu des robots hyper-redondants	196
8.13.1	Modèle continu géométrique	196
8.13.2	Modèle continu des vitesses	196
8.13.3	Modèle des accélérations	196
8.13.4	Dynamique sur \mathcal{C}_1 : modèle de Newton-Euler continu	197
8.13.5	Dynamique sur \mathcal{C}_2 : dynamique du corps de référence	198
8.14	Algorithme dynamique des robots continus	199
8.15	Modélisation cinématique des contacts	200
8.15.1	Cas des ancrages	201
8.15.2	Cas des contacts annulaires	202
8.15.3	Modèles des efforts de contact	203
8.16	Algorithme dans le cas cinématique	203

8.17 Exemples illustratifs	205
8.17.1 Ver fouisseur en 1D	205
8.17.2 Chenille arpenreuse en 2D	207
8.17.3 Serpent 2D en ondulation latérale	209
8.18 Conclusions	214

8.1 Introduction Générale

Plus ou moins délibérément, depuis son commencement, la robotique s'inspire de la nature pour concevoir ses robots. Ainsi, aux origines, des robots ressemblant à des bras humains ont été conçus en utilisant des mécanismes discrets dévolus aux tâches de manipulation des chaînes d'assemblage industrielles. Ces mécanismes discrets consistent en des chaînes sériels de corps rigides connectés par des articulations et sont aujourd'hui inclus dans la classe plus vaste des systèmes multicorps. Après les manipulateurs, les roboticiens commencèrent à construire des robots mobiles conçus comme des plateformes à roues. Si ces systèmes ont donné des résultats dans des environnements structurés, lorsque les environnements deviennent moins structurés, les pattes sont plus adaptées que les roues et la robotique mobile orienta ses études sur les robots à pattes inspirés des animaux marcheurs, ouvrant consciemment la voie de la bio-inspiration. Avec le temps, en puisant leur inspiration dans la grande diversité du règne animal, les chercheurs ont dans ce domaine commencé à développer des mécanismes comprenant de plus en plus de degrés de liberté internes, introduisant ainsi une nouvelle génération de robots appelés "hyper-redondants", puisqu'ils peuvent être considérés comme ayant un degré de redondance infini relativement aux 6 ddls de la tâche consistant à mouvoir un corps rigide dans l'espace. Poussant plus loin cette tendance, de nos jours, la robotique est entrée dans l'ère de la robotique "soft" où les robots n'ont plus de corps rigides dans leur structure. Dans ce cas, la source de bio-inspiration est fournie par les animaux mous appelés hydrostats, tels les vers de terre, les chenilles et autres pieuvres. Du point de vue du mécanicien, ces systèmes peuvent être considérés comme des systèmes continus ayant un nombre infini de degrés de liberté. Cette complexité croissante de la morphologie est en particulier due à la diversification des modes de locomotion impliquant des milieux d'appuis de plus en plus variés tels les sols non-uniformes, l'air, l'eau, etc. Aujourd'hui, des recherches en bionique nous permettent de découvrir progressivement les mécanismes subtils que les animaux ont découvert au fil de l'évolution des espèces pour améliorer leur performances dynamiques en terme de consommation énergétique ou de manoeuvrabilité. Aussi les systèmes de locomotion deviennent de plus en plus complexes, comme leur modèles mathématiques. En conséquence, nous avons besoin aujourd'hui d'outils efficaces qui peuvent aider les roboticiens à modéliser, concevoir, commander une nouvelle génération de robots. A cet effet les modèles dynamiques et leurs algorithmes associés sont d'un grand intérêt

pour les chercheurs du fait de leur rôle effectif dans la simulation, la conception et le contrôle. Gardant en tête cet intérêt grandissant, nous proposons dans cette thèse un cadre méthodologique unifié capable de traiter la locomotion bio-inspirée en toute généralité. Plus précisément, dans cette thèse nous poursuivons deux objectifs. D'abord contribuer à la classification des robots locomoteurs. Puis proposer de nouveaux outils efficaces pour la modélisation et la simulation rapide de ces robots locomoteurs. Concernant le premier objectif, nous utiliserons des outils mathématiques introduits par l'école américaine de géométrie mécanique après Marsden. Concrètement, ces outils nous permettront d'exhiber la structure géométrique commune à la différents modes de locomotion en apparence différents comme les serpents rampants ou la nage à haut Reynolds. Concernant le second objectif, partant des manipulateurs, rappelons qu'il existe deux approches algorithmiques majeures pour résoudre les problèmes de dynamique des robots. La première est fondée sur la mécanique Lagrangienne et mène à des formulations explicites paramétrées par un jeu minimal de coordonnées généralisées indépendantes [92]. La seconde approche est fondée sur la formulation de Newton-Euler appliquée à chacun des corps [4]. Qu'elle soit appliquée à la dynamique inverse à travers l'algorithme de Luh et Walker [115] ou à la dynamique directe à travers l'algorithme de Featherstone [40], la formulation de Newton Euler mène à des algorithmes d'une complexité en $O(n)$ (où n est le nombre de corps). Inversement, la formulation Lagrangienne mène à des algorithmes en $O(n)$ ou $O(n^4)$ selon qu'ils soient récursifs (comme les algorithmes fondés sur la méthode de Newton-Euler) [54] ou non [114, 58]. Quoiqu'il en soit l'approche de Newton Euler, une fois associée à un code symbolique adapté, conduit aux algorithmes les plus efficaces [64]. Cet avantage est crucial lorsque l'on étudie des systèmes présentant un grand nombre de liaisons et degrés de liberté comme les manipulateurs hyper-redondants [52, 100, 25, 72]. Qui plus est, les algorithmes de Newton Euler sont particulièrement intéressants lorsque l'on considère des robots modulaires ou reconfigurables [24], puisque dans ce cas, changer la topologie du système revient à changer l'indexation des corps sans compromettre la structure des algorithmes.

Malgré ces avantages, jusqu'à aujourd'hui un corpus général fondé sur l'approche de Newton Euler n'existe que pour les manipulateurs, c'est à dire pour des systèmes multi-corps ayant une base fixe [40], alors que la théorie la plus unifiée de la dynamique des systèmes locomoteurs est fondée sur l'approche Lagrangienne sur les fibrés principaux [87, 60, 76, 101]. Finalement, comme cas limite, nous verrons que la dynamique des robots hyper redondants peut être modélisée par une version continue de la formulation de Newton-Euler, et que dans ce cas cette formulation n'a aucune contrepartie Lagrangienne [14, 16]. Concernant ces systèmes, les approches existantes utilisées pour modéliser les robots hyper redondants peuvent être classées en deux principaux groupes selon que le robot est considéré comme un système multi-corps discret avec un grand nombre de degrés de liberté [63, 78] ou directement comme un milieu continu déformable. Dans le premier cas, la

modélisation est facilitée par le fait que les outils mathématiques issus de la robotique classique discrète sont déjà disponibles. Néanmoins, adopter un modèle continu dès le départ peut grandement faciliter la formulation, l'analyse et la résolution des problèmes de robotique liés à la manipulation [26, 83] et à la locomotion [52, 18, 50]. Cette thèse traite à la fois de la modélisation et du développement d'une classification unifiée et de méthodes algorithmiques pour des systèmes multicorps discrets ainsi que des systèmes continus.

8.2 La locomotion bio-inspirée

La locomotion animale est l'étude de la façon dont les animaux se déplacent dans le monde. La locomotion est la capacité de passer de place en place. Pour un système, que ce soit naturel ou artificielle, la locomotion peut être définie plus précisément comme suit. "Le processus de production de déplacement (mouvement) globale d'un système à travers les changements de forme interne (déformations) et l'interaction avec le monde extérieur." Dans la nature, les changements de forme interne varie d'un organisme à organisme, selon leurs caractéristiques structurelles et un moyen d'interaction. Lorsque ces changements de forme internes se trouvent être manoeuvres cyclique, ils sont connus comme des allures "gait" de locomotion. Les animaux aussi effectuent certaines manoeuvres transitoires telles que le virage, sauter, etc. Une vaste variété de locomotion est observée chez les animaux. Par exemple, un vol d'un oiseau, marche d'un chat, la course d'un cheval, undulation d'un serpent, nage d'un poisson, l'enfouissement d'un ver, etc. Dans tous ces cas, la locomotion est possible grâce au contact avec l'entourant moyennes, par exemple l'air, l'eau, la terre, etc. Dans son essence, la locomotion est basé sur le principe suivant. Tout animal lors de déplacements dans l'espace change tout d'abord sa forme en vue d'exercer certaines forces sur son environnement. Puis, en vertu du principal de action-réaction, l'environnement exerce une certaine force de réaction sur le corps de l'animal dont la résultante le propulse dans l'espace. Les forces de réaction exercée par le monde sur le corps de l'animal dépend de la taille du corps de l'animal, et les propriétés physiques du milieu d'appuis sur lequel l'animal se penche pour se déplacer. Par exemple, la natation et le vol à nombres élevés de Reynolds implique des forces inertielle (pression) (produit par l'accélération du fluide environnant l'animal), à nombres bas de Reynolds, de petits animaux tels que les protistes flagelles, cilliae utilisent des forces visqueux (frottement) pour se déplacer. En cas de marche, les forces de contact durs discontinus sont impliqués, tandis que les serpents adaptent leur surface corporelle en contact avec le sol afin de maximiser les forces de réaction propulsive. Parmi les modes de locomotion le plus mystérieux, nous trouvons les lézard de sable qui est capable de nager dans le sable.

Du point de vue des roboticien, la morphologie des animaux peuvent être grossièrement classés en trois catégories selon qu'ils ont un endosquelette, un exosquelette ou pas de

squelette à tous. Une autre grande catégorie d'morphologies pertinentes à la robotique sera topologie du corps, le corps de chaque animal étant éventuellement symbolisée par une chaîne topologique ceux que traités par la mécanique des systèmes multicorps. Dans ce cas, des systèmes simples à chaîne ouverte comme les animaux allongé, sont en fait très intéressant pour les roboticiens, depuis une même morphologie simple, ils montrent un large éventail de possibilités allant de la natation, comme les anguilles, aux fouisseurs comme les vers, rampant comme des serpents et ainsi de suite. Une des raisons du succès de cette morphologie dans le règne animal, est probablement dû au fait que ces animaux ont un nombre élevé de degrés de liberté internes (certains gros serpents ont plus de 500 vertèbres) et les roboticien les appellent "les systèmes hyper-redondants".

Au-delà de ces considérations bio-physique, les roboticiens également s'inspirer de l'étendue des capacités de locomotion animale pour s'adapter à différents environnements. Par exemple, une même espèce de serpent a la capacité de se glisser à travers l'ondulation, side-winding, mouvement rectiligne ou en accordéon. Tout cela est possible avec la même morphologie tout en décalant d'un ensemble de déformations internes à un autre qui répond bien aux changements environnementaux.

Pour toutes les raisons mentionnées ci-dessus, un très grand intérêt a été montré au cours des dernières années vers la conception des robots inspirés par la locomotion des animaux. Au début, les robots de locomotion ont été conçus sur la base d'une connaissance préalable des manipulateurs industriels conventionnels, i.e. systèmes multicorps discrets. En outre, avec le passage du temps, les aspects conception des systèmes de locomotion artificielle devenaient de plus en plus l'inspiration de la nature. À cet égard, les conceptions de robot ont été déplacé de la mécanismes conventionnels discrète envers les structures hyper-redondants continues avec une augmentation **spectaculaire** de degrés de liberté internes ainsi que le nombre de corps. Ces systèmes hyper-redondants trouvent l'inspiration à partir d'animaux allongé tels que des serpents, des anguilles, etc.

8.3 Problème général abordé dans cette thèse

Le problème général de la locomotion peut être envisagé de plusieurs manières. Dans cette thèse, nous allons résoudre le problème suivant. Connaître les évolution dans le temps sur les articulations internes, nous cherchons à calculer:

1. Les mouvements externes, ce qui correspond à résoudre la dynamique directe externe appelé "dynamique directe de la locomotion".
2. Les couples internes, ce qui correspond à résoudre la dynamique inverse interne ou plus simplement la «dynamique inverse des couples».

Ce calcul sera effectué par un algorithme détaillé dans les chapitres suivants. La première dynamique est nommés "dynamique de la locomotion" puisque mettant en relation les

degrés de liberté internes avec les degrés de liberté externes, ils implique un modèle de la résultante des forces de contact à l'origine de la locomotion. D'autre part, la seconde dynamique est celle habituellement rencontrés sur le système multicorps conventionnel comme dans le cas des manipulateurs où il trouve ses applications dans les algorithmes de calcul des couple. Une question se pose naturelle de cette déclaration: Pourquoi avons-nous opter pour le choix des mouvements internes comme entrées, pourquoi ne pas prendre les couples comme entrée? Il y a deux raisons principales. Premièrement, il est facile de préciser les mouvements externes d'un robot locomoteur en fonction de ses mouvements internes, tandis que d'autre part, il n'est pas facile du tout de deviner les mouvements d'un robot mobile à partir des couples exercée par ses actionneurs sur ses articulations internes. Deuxièmement, en relation avec le premier argument, ce problème (et sa solution) peut être couplée à des expériences biologiques basés sur des films de locomotion des animaux. En fait, une fois les mouvements internes sont extraites du film, ils peuvent être imposées comme des entrées de l'algorithme qui renvoie les mouvements externes. Ensuite, ces mouvements externes peuvent être comparés à ceux extraits de films, et l'appariement des mouvements externe mesurés et calculés est un outil précieux pour l'étude du modèle du contact. En parallèle, la dynamique de couple inverse permet de qualifier la faisabilité des mouvements internes imposées à l'égard des ressources d'actionneurs.

Afin de résoudre la dynamique directe de la locomotion, nous avons besoin de développer une relation entre ces deux types de mouvements (i.e. externes et internes) sur le fibré principal. En général pour développer une telle relation, un modèle dynamique est nécessaire, i.e. la dynamique entre le système et le milieu environnant est d'être résolu. Cependant, il y a certains cas particuliers élégants où la locomotion est entièrement défini par la cinématique. C'est quand le modèle du contact est codée dans ce que nous nommons une "connexion" sur le fibré principal de configurations. Par conséquent, nous pouvons rapidement conclure qu'il existe deux types de modèles de la locomotion.

Modèle dynamique de la locomotion: où les mouvements externes du système multicorps mobile sont liés à des mouvements internes via un modèle dynamique.

Modèle cinématique de la locomotion: où les mouvements externes du système multicorps mobile sont liés à des mouvements internes via un modèle cinématique.

Maintenant, nous allons développer ces modèles et leurs algorithmes associés afin de résoudre le problème de la locomotion. Pour atteindre cet objectif, le reste du chapitre est divisé en deux parties. La première partie traite des systèmes multicorps discrets tandis que la seconde partie est consacrée aux systèmes continus.

Partie-I: Les Systèmes Discrets

8.4 Introduction aux Systèmes Multicorps Discrets

Partant du modèle des systèmes multicorps rigides, certains travaux de recherche récents ont initié l'application de la formulation de Newton-Euler à certains systèmes de locomotion bio-inspirés. Dans [72], la formulation de Newton-Euler a été utilisée avec un modèle de contact de type frottement de Coulomb afin d'aborder le problème inverse de la dynamique d'un serpent rampant. Dans [110], la formulation de Newton-Euler a été utilisée pour résoudre la dynamique directe d'un serpent plan soumis à des forces de contact non régulières. Néanmoins, bien que ces travaux utilisent la formulation de Newton-Euler pour modéliser la dynamique des systèmes multicorps, les algorithmes qui en découlent n'exploitent pas les vertus de la récursivité de cette formulation. Aussi, aucun de ces travaux sur les robots serpent n'a à notre connaissance généralisé (à la locomotion), soit l'algorithme inverse de Luh et Walker soit l'algorithme direct du à Featherstone. Au plus proche de nos objectifs, dans [62] l'algorithme inverse de Luh et Walker et l'algorithme direct de Featherstone ont été proposés pour étudier la locomotion d'un robot anguille, tandis que dans [82] un algorithme de Luh et Walker pour le calcul des couples a été proposé pour résoudre la dynamique inverse d'un manipulateur mobile. En dépit de ces récents travaux, à notre connaissance, aucun cadre général de la formulation de Newton-Euler pour la dynamique inverse récursive des systèmes multicorps avec des liaisons pivots et des roues n'a été proposé à ce jour. Bien que la formulation de Newton-Euler ait été discutée par différents auteurs, sa mise en oeuvre dans un cadre unifié pour la dynamique de la locomotion dans le contexte de la mécanique géométrique reste à faire. Pour pallier ce manque, ce travail de recherche présente une méthode de calcul de la dynamique inverse basée sur la formulation de Newton-Euler pour les systèmes multicorps mobile de type arborescentes [10]. De plus, en utilisant certains des concepts géométriques de la mécanique, l'approche propose aussi un classement général d'une large gamme de systèmes, allant des systèmes complètement contraintes (par exemple un robot serpent), aux systèmes flottants (bras de navettes, les satellites, etc.), en passant par les manipulateurs à base fixe ou mobile, ainsi que les systèmes sous-actionnés non-holonomes tels le snakeboard, le Trikke, etc.

8.4.1 Les hypothèses de Base

En fait, les seules limitations de l'algorithme proposé sont fixées par les hypothèses de base suivantes.

1. Le sol est considéré comme une surface horizontale plane. Cette hypothèse impose trois contraintes de planéité holonomes sur les mouvements généraux 3D des corps à

- roues. L'une de ces contraintes va empêcher le corps de se translater verticalement, les deux autres vont l'empêcher de faire des mouvements de roulis et de tangage.
2. Toutes les roues actionnées quand il y en a, sont disposées sur un corps unique.
 3. Les inerties des roues sont négligeables comparés à celles des corps. Par conséquent, les roues n'interviennent dans la modélisation que via la cinématique.
 4. Les éventuelles roues folles ont pour unique rôle de maintenir l'équilibre statique horizontal par rapport au sol. Par conséquent, elles n'apparaissent pas dans la modélisation.
 5. Tous les corps du système sont connectés les uns aux autres par des liaisons (holonomes), supposées idéales (pas de frottement) et actionnées.
 6. Toutes les roues sont supposées être idéales. Ainsi, elles peuvent être modélisées par les contraintes non-holonomes qui vérifient les conditions de non-dérapiage et de roulement sans glissement.
 7. Nous supposons que les conditions de compatibilité nécessaires pour assurer la mobilité du mécanisme sous les contraintes induites par les roues vérifiées grâce à la conception et la planification du mouvement.

Notons que les deux dernières hypothèses ne concernent que le cas des roues idéales.

8.4.2 Description des systèmes multicorps mobiles

Dans la suite, nous considérons un système multicorps mobile avec une topologie arborescente composée de $p+1$ corps rigides, notés $S_o, S_1, S_2, \dots, S_p$. Chaque paire de corps successifs est connectée par une seule articulation rotoïde¹. En outre, tous les corps peuvent être en contact avec le sol par des roues (voir Fig. 8.1(b)) qui sont principalement classées en deux types: omni et uni-directionnel. Les roues uni-directionnelles sont subdivisées elles-mêmes en roues «orientables», «castor» ou «fixes» selon que leurs axes normaux au sol sont actionnés, libres ou ancrés au corps. Les corps sont classés en "corps à roues" (dont l'ensemble des indices est noté \mathbb{N}_w) et "corps sans roues" (avec des indices dans \mathbb{N}_{uw}). Lorsque le système possède des roues actionnées, le seul corps muni de roues actionné sera étiqueté comme S_o (voir hypothèse n°2 de la section 8.4.1). Dans les autres cas, le choix de S_o est libre. Nous suivons les conventions de Newton-Euler pour les structures arborescentes présentées dans [64]. Les indices des corps augmentent de S_o vers les corps terminaux comme illustré dans la Fig. 8.1. Dans tous les calculs détaillés ci-après, l'indice

¹Ces restrictions ne sont pas comptées comme des hypothèses de base puisque tout ce qui suit peut être facilement étendu à des systèmes multicorps mobiles comprenant d'autres types d'articulations et aux structures avec des chaînes fermées.

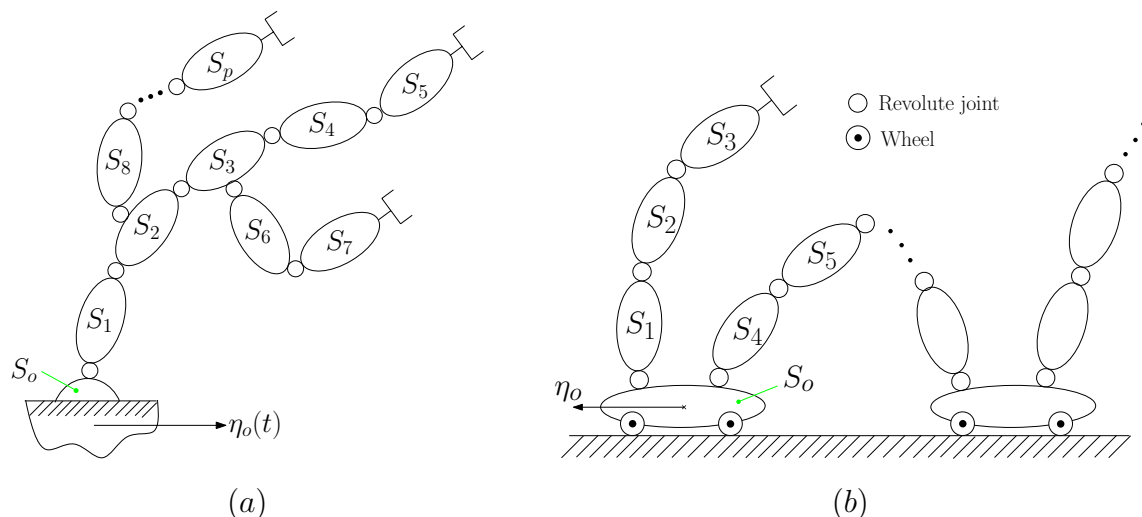


Figure 8.1 – Structures arborescentes d'un système multicorps mobile: (a) un manipulateur; (b) un système à roues

i est réservé pour désigner l'antécédent de l'indice courant j . Enfin, dans la suite, nous aurons aussi besoin d'utiliser le concept de "corps composite" [117]. Un corps composite S_j^+ est un corps rigide composé de S_j et de tous les successeurs figés dans la forme courante et animés par le mouvement de S_j . En particulier, le corps composite S_o^+ (Fig. 8.1) est composé de toute la structure figée dans la forme courante et animés par le mouvement de S_o . Enfin, dans la suite, S_o^+ signifie que S_o est connecté au reste de la structure, tandis que S_o signifie que le corps S_o est un simple corps isolé.

Lorsque nous traiterons de la dynamique récursive des couples, l'espace de configuration du système multicorps mobile sera défini comme suit:

$$\mathcal{C}_1 = \underbrace{G \times G \times \dots G}_{p+1 \text{ copies}} = G^{p+1}, \quad (8.1)$$

où chaque copie de G représente le groupe de Lie des configurations de chacun des $p+1$ corps considérés comme isolés des autres. Aussi, dans cette première définition S_o ne se distingue pas des autres corps. D'autre part, lorsqu'il s'agit du modèle de locomotion, S_o devient le corps de référence, c'est à dire un corps dont les mouvements fixent les mouvements rigides de l'ensemble de la structure par rapport auxquels les variations de la forme interne sont mesurées. En tant que tel, le mouvement de S_o peut être imposé par les lois horaires connues (comme dans le cas particulier d'un manipulateur où S_o est la base) ou, plus généralement, il sera calculé par l'intégration (par rapport au temps) d'un modèle dynamique de la locomotion dont l'espace de configuration est définie comme le fibré principal:

$$\mathcal{C}_2 = G \times (S^1)^p. \quad (8.2)$$

Dans cette seconde définition de l'espace de configuration d'un système multicorps mobile, $(S^1)^p$ correspond à la configuration de forme interne \mathcal{S} des p articulations paramétrées par le vecteur $r = (r_1, r_2, \dots, r_p)^T$, tandis que G est le groupe de Lie des configurations de S_o , à présent considéré comme connecté à l'ensemble de la structure, i.e. celui de S_o^+ . Enfin, puisque de toute façon $G \subseteq SE(3)$, nous considérons généralement que $G = SE(3)$ et relâcherons cette hypothèse en abordant les exemples illustratifs.

Enfin, la modélisation requiert également deux autres ensembles de paramètres cinématiques qui, en raison de la négligence des inerties des roues, ne sont pas considérés comme des paramètres de configuration. La première série est celle des angles des roues orientables, rassemblés dans le vecteur β . La deuxième série est celle des angles de roulement: $\{\theta_j = (\theta_{j,1}, \theta_{j,2}, \dots, \theta_{j,N_j})^T$, avec N_j le nombre total de roues (roues castor exclus) de chaque corps $S_j, j \in \mathbb{N}_w\}$. Dans le cas de S_o et N_a de ses roues étant actionnées autour de leurs axes de roulement (parallèles au sol), θ_o sera divisé en blocs des vecteurs des roues actionnées et libres (passive) comme suit: $\theta_o = (\theta_{oa}^T, \theta_{of}^T)^T$, avec $\dim(\theta_o) = N_a$.

8.4.3 Notations

Avant de commencer la modélisation mathématique des systèmes multicorps mobiles, nous présentons d'abord quelques termes et expressions mathématiques de base. Chaque corps S_j est muni d'un repère orthonormé $\mathcal{F}_j = (O_j, s_j, n_j, a_j)$ de centre O_j , où a_j est l'axe de rotation du seul degré de liberté. L'espace ambiant est muni d'un repère spatial fixe noté $\mathcal{F}_e = (O_e, s_e, n_e, a_e)$. La transformation du corps rigide (élément de $SE(3)$), qui transforme un repère orthonormé \mathcal{F}_l en n'importe quel autre repère orthonormé \mathcal{F}_k est représentée par une matrice homogène de dimension (4×4) notée ${}^l g_k \in SE(3)$, par exemple, la transformation de matrice ${}^i g_j$ qui applique le repère \mathcal{F}_i du corps S_i sur le repère \mathcal{F}_j du corps S_j , est donnée comme suit:

$${}^i g_j = \begin{pmatrix} {}^i R_j & {}^i P_j \\ 0 & 1 \end{pmatrix},$$

où, ${}^i P_j = {}^i(O_i O_j)$ et ${}^i R_j$ est une matrice (3×3) qui décrit l'orientation de repère \mathcal{F}_j par rapport à \mathcal{F}_i . Par ailleurs, \mathcal{M}_j désigne la matrice (6×6) d'inertie, contenant les composantes d'inertie du corps S_j sur $SE(3)$, exprimé dans \mathcal{F}_j , avec:

$$\mathcal{M}_j = \begin{pmatrix} m_j 1_3 & -m_j \hat{s}_j \\ m_j \hat{s}_j & I_j \end{pmatrix}, \quad (8.3)$$

où, m_j est la masse du corps S_j , alors que $m_j s_j$ et I_j sont le vecteur des premiers moments d'inertie et la matrice des seconds moments, respectivement, tous exprimés dans \mathcal{F}_j . Notons que si un tenseur est exprimé dans un repère autre que celui du corps auquel il est

relatif, alors un exposant en position avant haute précise l'indice du repère en question, e.g. ${}^o\mathcal{M}_j$ désigne le tenseur d'inertie du corps S_j exprimée dans \mathcal{F}_o , alors que \mathcal{M}_j désigne le tenseur d'inertie du corps de S_j exprimée dans \mathcal{F}_j . Par ailleurs, en adoptant l'espace des twists \mathbb{R}^6 comme définition de $\mathfrak{so}(3)$, le "twist" de S_j est défini par un vecteur (6×1) notée η_j qui contient les composantes de la vitesse du corps S_j exprimée dans \mathcal{F}_j , tandis que sa dérivée par rapport au temps $\dot{\eta}_j$ désigne le vecteur (6×1) des accélérations du corps S_j , où:

$$\eta_j = \begin{pmatrix} V_j \\ \Omega_j \end{pmatrix}, \quad \dot{\eta}_j = \begin{pmatrix} \dot{V}_j \\ \dot{\Omega}_j \end{pmatrix}.$$

Passant à l'espace "dual" F_j désigne la résultante des forces (6×1) appliquées sur le corps S_j par le corps antécédent S_i , exprimées dans son propre repère \mathcal{F}_j , où:

$$F_j = \begin{pmatrix} N_j \\ C_j \end{pmatrix}.$$

En outre, un twist peut être poussé vers l'avant de \mathcal{F}_i à \mathcal{F}_j par la relation: ${}^j\eta_i = \text{Ad}_{jg_i}\eta_i$, où Ad_{jg_i} est appelé "opérateur adjoint" et se détaille comme suit:

$$\text{Ad}_{jg_i} = \begin{pmatrix} {}^jR_i & {}^jR_i {}^i\hat{P}_j^T \\ 0 & {}^jR_i \end{pmatrix}. \quad (8.4)$$

Du côté "dual", une force peut être tirée vers l'arrière de \mathcal{F}_j à \mathcal{F}_i par: ${}^iF_j = \text{Ad}_{jg_i}^T F_j$. Enfin, $F_{\text{gyr},j}$ et $F_{\text{ext},j}$ dénotent les forces gyroscopiques et externes appliquées sur S_j , respectivement.

8.5 Dynamique inverse récursive des manipulateurs

Nous rappelons ici l'algorithme de calcul des couples de Luh et Walker [115] pour un manipulateur de type arborescent avec des liaisons rotoïdes où le mouvement de S_o est prédéfini comme indiqué dans la Fig. 8.1(a). Le but de l'algorithme consiste à calculer, à chaque pas t d'une boucle de temps globale, le vecteur des couples articulaires (sorties) $\tau(t)$, en connaissant les valeurs actuelles des entrées: $({}^e g_o, \eta_o, \dot{\eta}_o, r, \dot{r}, \ddot{r})(t)$. Ce calcul est réalisé en exécutant d'abord les récurrences cinématiques avant: pour $j = 1, 2, \dots, p$ et avec conditions aux bords: $({}^e g_o, \eta_o, \dot{\eta}_o) = ({}^e g_o, \eta_o, \dot{\eta}_o)(t)$:

Calcul des transformations du corps:

$${}^e g_j = {}^e g_i {}^i g_j(r_j). \quad (8.5)$$

Calcul de la vitesse du corps:

$$\eta_j = \text{Ad}_{jg_i} \eta_i + \dot{r}_j A_j. \quad (8.6)$$

Calcul des accélérations du corps:

$$\dot{\eta}_j = \text{Ad}_{jg_i} \dot{\eta}_i + \zeta_j(\dot{r}_j, \ddot{r}_j). \quad (8.7)$$

Où, A_j est un vecteur (6×1):

$$A_j = \begin{pmatrix} 0 \\ a_j \end{pmatrix}, \text{ avec } a_j = \begin{pmatrix} 0 \\ 0 \\ 1 \end{pmatrix}.$$

Nous noterons aussi par $\zeta_j(\dot{r}_j, \ddot{r}_j)$, un vecteur (6×1) défini comme suit:

$$\zeta_j = \begin{pmatrix} {}^j R_i(\Omega_i \times (\Omega_i \times {}^i P_j)) \\ {}^j \Omega_i \times \dot{r}_j a_j \end{pmatrix} + \ddot{r}_j A_j. \quad (8.8)$$

Une fois la cinématique résolue, l'algorithme connaissant les états actuels de tous les corps individuels, il peut exécuter la récurrence arrière sur les torseurs de contact interne: pour $j = p + 1, p, \dots, 1$, avec $F_j = 0$ si S_i est un corps terminal:

$$\begin{cases} \text{if } i = j - 1 : & F_i = \mathcal{M}_i \dot{\eta}_i - F_{\text{ext},i} - F_{\text{gyr},i} + \text{Ad}_{jg_i}^T F_j; \\ \text{else:} & F_{\text{gyr},i} = F_{\text{gyr},i} - \text{Ad}_{jg_i}^T F_j. \end{cases} \quad (8.9)$$

Où, $F_{\text{gyr},i}$ est le vecteur (6×1) des efforts gyroscopiques:

$$F_{\text{gyr},i} = - \begin{pmatrix} \Omega_i \times (\Omega_i \times m_i s_i) + \Omega_i \times m_i V_i \\ \Omega_i \times (I_i \Omega_i) + m_i s_i \times (\Omega_i \times V_i) \end{pmatrix}. \quad (8.10)$$

Enfin, les forces internes sont projetées sur les axes des articulations pour obtenir les couples comme suit:

$$\text{for } j = 1, 2, \dots, p : \quad \tau_j = A_j^T F_j. \quad (8.11)$$

8.6 Aperçu de l'algorithme

L'algorithme de Luh et Walker est limité aux cas où les mouvements du corps de référence S_o sont imposés a priori. Maintenant, pour discuter de la généralisation de cet algorithme au cas des systèmes multicorps mobiles nous considérons un système mobile plan avec des roues, comme indiqué dans la Fig. 8.2, où les corps à roues sont connectés par des liaisons rotoïdes simples et actionnées. En imposant des mouvements sur les articulations

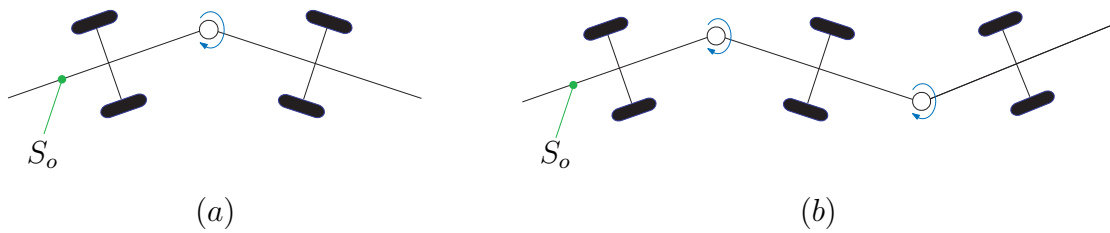


Figure 8.2 – *Systèmes multicorps à roues: (a) Système multicorps avec deux essieux; (b) Système multicorps avec three essieux*

actionnées, les corps de ce système sont soumis non seulement à des mouvements internes, comme ceux rencontrés sur un manipulateur, mais aussi à des mouvements rigides externes de l'ensemble de la structure définis comme étant ceux d'un corps de référence arbitraire S_o par rapport à un repère fixé à l'espace. En conséquence, la généralisation attendue de l'algorithme de Luh et Walker nécessite une connaissance des mouvements externes de S_o qui ne sont généralement plus imposés mais doivent être calculés à partir d'un nouveau modèle, appelé ici "modèle de la locomotion". Ce modèle est un modèle direct, car il relie les mouvements des articulations à ceux du corps de référence S_o . Comme évoqué précédemment, cette relation peut être modélisée soit par un modèle cinématique simple (i.e. n'impliquant pas les forces), soit par un modèle dynamique.

Avant d'entrer dans la discussion détaillée de tels modèles de la locomotion, notons qu'à l'exception de celles transmises pas les roues, les forces externes de toute nature telles celles imprimées par le contact avec un fluide, sont supposées connues comme des fonctions de l'état via des lois physiques (de comportement). Au contraire, dans le cas des roues, supposées idéales, le contact est modélisé par des contraintes non-holonomes (voir hypothèse n°6 de la section 8.4.1). Dans ces conditions, les systèmes multicorps mobiles peuvent être classés en deux grandes catégories:

Systèmes multicorps mobiles non-contraints: les systèmes multicorps mobiles (à roues ou sans roues) dont les contacts externes sont modélisés par le modèle des forces extérieures en appliquant certaines lois physiques, par exemple, l'utilisation d'un modèle de frottement pour un contact avec le sol via des roues non-idéales.

Systèmes multicorps mobiles contraints: les systèmes multicorps mobiles en contact avec le sol via les roues où le contact est modélisé via les contraintes non-holonômes (de non-dérapage et/ou de roulement sans glissement).

8.7 Les systèmes multicorps mobiles non-contraints

Dans cette section, nous étendons l'algorithme standard de Luh et Walker de la section 8.5 au cas d'un système multicorps mobile non-contraint. L'objet de la section 8.7.1 est de calculer l'accélération actuelle $\dot{\eta}_o$ de S_o^+ à partir des entrées actuelles et l'état de référence

actuel. Ensuite, cette accélération de référence est utilisée comme condition aux bord pour les calculs récursifs des couples internes et l'intégration par rapport au temps, dans la section 8.7.2. Enfin, dans la section 8.7.3 nous introduirons un cas où la dynamique de la locomotion dégénère en cinématique.

8.7.1 Dynamique de la locomotion: le calcul de $\dot{\eta}_o$

Ce calcul est basé sur la dynamique du corps de référence contrôlé par les mouvements internes imposés du reste de la structure. Cette dynamique nommée «dynamique de la locomotion» est simplement celle de S_o^+ et peut être définie comme suit:

$$\begin{pmatrix} \dot{\eta}_o \\ {}^e\dot{g}_o \end{pmatrix} = \begin{pmatrix} (\mathcal{M}_o^+)^{-1} F_o^+ \\ {}^e g_o \hat{\eta}_o \end{pmatrix}, \quad (8.12)$$

où la deuxième ligne est l'équation de reconstruction cinématique de η_o à ${}^e g_o$, tandis que dans la première ligne $\mathcal{M}_o^+(r(t)) = \sum_{l=0}^{l=p} \text{Ad}_{l_{g_o}}^T \mathcal{M}_l \text{Ad}_{l_{g_o}}$ dénote la matrice d'inertie du corps composite S_o^+ , et $F_o^+(r(t), \dot{r}(t), \ddot{r}(t), {}^e g_o, \eta_o)$ est le torseur des forces (d'inertie et externes) exercées sur S_o^+ :

$$F_o^+ = F_{\text{gyr},o} + F_{\text{ext},o} + \sum_{j=1}^{j=p} \text{Ad}_{j_{g_o}}^T \left(F_{\text{gyr},j} + F_{\text{ext},j} - \mathcal{M}_j \left(\sum_{l=1}^{l=j} \text{Ad}_{j_{g_l}} \zeta_l \right) \right). \quad (8.13)$$

Notons que \mathcal{M}_o^+ et F_o^+ peuvent être calculés numériquement par les calculs suivants avec les récurrences arrières initialisées par les conditions aux bords: $\mathcal{M}_j^+ = 0$, $F_j^+ = 0$ si S_i est un corps terminal: pour $j = p + 1, p, \dots, 1$:

- Calcul de \mathcal{M}_o^+ :

$$\begin{cases} \text{si } i = j - 1 : & \mathcal{M}_i^+ = \mathcal{M}_i + \text{Ad}_{j_{g_i}}^T \mathcal{M}_j^+ \text{Ad}_{j_{g_i}}; \\ \text{sinon:} & \mathcal{M}_i = \mathcal{M}_i + \text{Ad}_{j_{g_i}}^T \mathcal{M}_j^+ \text{Ad}_{j_{g_i}}. \end{cases} \quad (8.14)$$

- Calcul de F_o^+ :

$$\begin{cases} \text{si } i = j - 1 : & F_i^+ = F_{\text{gyr},i} + F_{\text{ext},i} - \text{Ad}_{j_{g_i}}^T \mathcal{M}_j^+ \zeta_j - \text{Ad}_{j_{g_i}}^T F_j^+; \\ \text{sinon:} & F_{\text{gyr},i} = F_{\text{gyr},i} - \text{Ad}_{j_{g_i}}^T F_j^+ - \text{Ad}_{j_{g_i}}^T \mathcal{M}_j^+ \zeta_j. \end{cases} \quad (8.15)$$

Techniquement, (8.12) peut être déduite du principe des travaux virtuels appliqué à l'ensemble de tous les corps soumis à tout champ virtuel compatible avec la rigidité du corps et la cinématique articulaire.

8.7.2 Dynamique des couples: le calcul des couples internes

Une fois que $(\dot{\eta}_o, \eta_o)$ et ${}^e g_o$ sont connus, ils initialisent les deux récurrences de l'algorithme standard de Luh et Walker (voir la section 8.5) qui donne finalement le vecteur des couples moteurs τ .

En bref, l'extension de l'algorithme de Luh et Walker au cas d'un système multicorps mobile non-contraint ne nécessite que la dynamique de locomotion (3.29) et (3.27,3.28) en plus de la dynamique des couples (3.7-3.12). Enfin, afin de mettre à jour l'état de référence pour la prochaine étape de la boucle du temps, (3.29) est numériquement intégrée, par exemple, avec un intégrateur géométriques sur les groupes de Lie [91] ou plus simplement avec un intégrateur basé sur les quaternions. Ces deux intégrateurs ont l'avantage d'être libre de singularités et de non-linéarités artificielles comme celles introduites par toute paramétrisation impliquant trois angles d'orientations de S_o .

8.7.3 Le cas non-contraint avec symétries

Lorsqu'un robot est soit: 1) immergé dans un fluide idéal initialement au repos ou 2) flottant dans l'espace, tel que par exemple, un bras de navette spatiale ou un satellite équipé d'un système de réorientation, alors les forces externes $F_{ext,i}$ sont ${}^e g_o$ -indépendantes et lagrangienne [7]. Mathématiquement, cela signifie qu'il existe une fonction de Lagrange $l_{ext} = l_{ext}(\eta_o, r, \dot{r})$ (égale à l'énergie cinétique ajoutée par le fluide dans le premier cas [67], et tout simplement égale à zéro dans le second), tels que:

$$F_{ext,o}^+ = \frac{d}{dt} \left(\frac{\partial l_{ext}}{\partial(\dot{\eta}_o)} \right) - ad_{(\eta_o)}^* \left(\frac{\partial l_{ext}}{\partial(\eta_o)} \right), \quad (8.16)$$

où $ad_{(\cdot)}^*(\cdot) : se(3) \times se(3)^* \rightarrow se(3)^*$ est l'opérateur co-adjoint de SE(3). Une analyse plus approfondie de ces cas montre que, avec $l_{ext} + l = \frac{1}{2}\eta_o^T(\widetilde{\mathcal{M}}_o^+ \eta_o + {}^o \widetilde{M}_r \dot{r})$, l étant le lagrangien du système libre de forces externes, la partie accélération de (8.12) peut être explicitement intégrée par rapport au temps pour se ramener au jeu de contraintes non-holonômes suivant:

$$\widetilde{\mathcal{M}}_o^+ \eta_o + {}^o \widetilde{M}_r \dot{r} = 0, \quad (8.17)$$

qui assurent la conservation de la quantité de mouvement cinétique pour un système initialement au repos. Par ailleurs, dans (8.17), ${}^o \widetilde{M}_r$ est une matrice $6 \times p$ couplant les accélérations externes aux internes. Enfin, la relation (8.17) permet de remplacer le modèle dynamique de la locomotion (8.12) par le modèle cinématique de la locomotion comme suit:

$$\dot{\eta}_o = {}^e g_o^{-1e} \dot{g}_o = (-\mathcal{A}_m \dot{r})^\wedge, \quad \dot{\eta}_o = -\mathcal{A}_m \ddot{r} - \dot{\mathcal{A}}_m \dot{r}, \quad (8.18)$$

où $\mathcal{A}_m = (\widetilde{\mathcal{M}}_o^+)^{-1} \circ \widetilde{\mathcal{M}}_r$ est la forme locale de la connexion sur le fibré principal \mathcal{C}_2 appelé "connexion mécanique" [76, 89, 59]. Dans ce cas, la dynamique de la locomotion dégénère en un modèle cinématique en raison des propriétés de symétrie de la dynamique du système [76].

8.8 Les systèmes multicorps mobiles contraints

A présent, nous allons étendre l'algorithme des systèmes multicorps mobiles non-contraints au cas des systèmes multicorps mobiles contraints. Comme mentionné plus tôt, par système contraint on entend une structure multicorps en contact permanent avec le sol via des roues idéales. Ainsi, cette extension est essentiellement un processus de réduction basée sur les contraintes non-holonômes des roues. Avant d'effectuer ce processus de réduction, nous rappelons d'abord la cinématique non-holonome d'un système multicorps mobile contraint. Notons que, dans ce cas, chaque corps à roues est également désigné comme un corps non-holonome puisque limité par des contraintes cinématiques de même nature. En conséquence, chaque corps sans roues est appelé corps holonome.

8.8.1 Cinématique d'un corps non-holonome isolé

Ici nous allons traiter le modèle cinématique de chaque corps non-holonômes S_j , $j \in \mathbb{N}_w$ considéré comme isolé du reste de la structure. Mathématiquement, c'est équivalent à considérer les contraintes non-holonomes sur la définition (8.1) de l'espace de configuration, c'est à dire sur chaque copie de SE(3). Dans le cas des roues idéales, chaque roue uni-directionnelle impose deux contraintes, l'une due à la condition de roulement sans glissement, l'autre à la condition de non-dérapiage latéral. Alors que chaque roue omnidirectionnelle n'impose qu'une seule contrainte de roulement sans glissement. Chaque "twist" de S_j compatible avec les m_j contraintes indépendantes de non-dérapiage imposées par ses roues peut être exprimé comme suit:

$$\forall j \in \mathbb{N}_w : \eta_j = H_j(t)\eta_{rj}, \quad (8.19)$$

où l'espace engendré par les colonnes de H_j (notée $\mathcal{V}_j = \text{span}(H_j)$ dans la suite) est nommé «l'espace admissible» forcé par les m_j contraintes de non-dérapiage du corps S_j , plus les 3 contraintes de sol plan. La relation (8.19) définit la cinématique réduite de S_j seul, où η_{rj} définit le vecteur $(n_j \times 1)$ des composantes de η_j dans la base de \mathcal{V}_j , avec $n_j = 6 - (m_j + 3)$. Ce vecteur est nommé le "twist réduit" de S_j . H_j est nommé $(6 \times n_j)$ "matrice de réduction" du corps S_j isolé. En outre, tout complément orthogonal à H_j , notée H_j^\perp est défini par:

$$H_j^T H_j^\perp = 0_{n_j \times (m_j + 3)}. \quad (8.20)$$

Enfin, afin d'identifier l'espace admissible \mathcal{V}_j à son espace dual \mathcal{V}_j^* nous imposons que les colonnes de H_j sont orthonormées pour la métrique euclidienne de \mathbb{R}^6 , i.e.:

$$\forall j \in \mathbb{N}_{nh} : H_j^T H_j = 1_{n_j}, \quad (8.21)$$

où 1_{n_j} est une matrice identité ($n_j \times n_j$).

En ce qui concerne les contraintes de roulement sans glissement, nous pouvons récupérer l'évolution de chacune des roues de S_j en transportant le twist (8.19) de la plate-forme au centre de chacune des roues. A partir de cela, nous obtenons pour chaque corps S_j , une relation de la forme suivante:

$$\dot{\theta}_j = B_j(t)\eta_{r_j}, \quad (8.22)$$

où B_j est une matrice ($N_j \times n_j$) dépendant de la géométrie fixe de plate-forme et des roues, ainsi que du temps courant via β .

8.8.2 Cinématique du corps composite S_o^+

Nous allons maintenant examiner les conséquences des contraintes de non-dérapiage sur tout le système, i.e. sur les mouvements de S_o^+ , c'est à dire sur l'espace de configuration \mathcal{C}_2 . Notons qu'en raison de l'existence éventuelle d'autres corps non-holonomes dans la structure, l'espace admissible \mathcal{V} de S_o^+ est généralement plus contraint que celui de S_o isolé. Allant plus loin, nous pouvons toujours présenter un ensemble maximal des $m(\geq m_o)$ "1-forms" de contrainte indépendantes sur $T(\text{SE}(3) \times \mathcal{S})$ qui sont dépendantes du temps, à cause des roues orientables et des articulations holonômes. Par ailleurs, en raison des conditions de non-dérapiage, ces contraintes sont G -invariantes par rapport à l'action à gauche de $\text{SE}(3)$ sur le fibré principal des configurations. Par conséquent, une fois réunies avec les trois contraintes imposées par le sol plan, les $m+3$ contraintes peuvent être écrites sous la forme matricielle suivante:

$$A(t, r(t))\eta_o + B(t, r(t))\dot{r}(t) = 0, \quad (8.23)$$

où A est une matrice $(m+3) \times 6$ et B est une matrice de $(m+3) \times p$. Le rang de la matrice A joue un rôle important dans l'analyse de la mobilité de ces systèmes non-holonômes. En fait, dans l'expression (8.23), nous identifions deux cas en fonction de la valeur relative de $\dim(\text{SE}(3))=6$ et $\text{rang}(A)$,: (a) $\text{rank}(A) = 6$ et (b) $\text{rang}(A) < 6$. Dans le cas (a), (8.23) peut être divisé en deux blocs:

$$\begin{pmatrix} \bar{A} \\ \tilde{A} \end{pmatrix} \eta_o + \begin{pmatrix} \bar{B} \\ \tilde{B} \end{pmatrix} \dot{r} = \begin{pmatrix} 0 \\ 0 \end{pmatrix}, \quad (8.24)$$

avec \bar{A} une matrice inversible et carrée de 6×6 . Dans ce cas, la matrice \bar{A} étant inversible, η_o est complètement défini par l'évolution temporelle de r et β , et le mouvement du mécanisme est complètement calculable à partir de la cinématique. Géométriquement, si l'on concatène le vecteur β avec le vecteur r , cela permet de définir $\mathcal{A}_k \triangleq \bar{A}^{-1}\bar{B}$ comme la forme locale d'une connexion sur le fibré principal des configurations [66]. Par ailleurs, si $m + 3 = 6$, alors le système multicorps mobile peut se déplacer dans tous les cas sous l'hypothèse n°7 de la section 8.4.1, tandis que si $m + 3 > 6$, alors les $m + 3 - 6 = m - 3$ équations résiduelles de (8.24) peuvent être utilisés pour trouver les vitesses \dot{r} qui préservent la mobilité de l'ensemble du système (c'est à dire vérifiant: $\dot{r} \neq 0$ et telles que: $(\tilde{B} - \tilde{A}\mathcal{A}_k)(r)\dot{r} = 0$). Enfin, dans le cas (a), il y a suffisamment de contraintes indépendantes de non-dérapiage pour remplacer entièrement la dynamique de la locomotion (8.12) de la section 8.7 par le modèle cinématique suivant:

$$\eta_o = -\mathcal{A}_k(r)\dot{r}(t), \quad (8.25)$$

auquel s'ajoutent ses conséquences différentielles et intégrales:

$$\dot{\eta}_o = -\dot{\mathcal{A}}_k(r)\dot{r}(t) - \mathcal{A}_k(r)\ddot{r}(t), \quad {}^e\dot{g}_o = {}^e g_o(-\mathcal{A}_k\dot{r})^\wedge. \quad (8.26)$$

En ce qui concerne le cas (b), il n'y a pas assez de contraintes de non-dérapiage pour définir le mouvement du mécanisme uniquement par la cinématique et donc, une analyse additionnelle est nécessaire. L'application de l'inversion généralisée à (8.23) permet d'affirmer que tout twist de S_o^+ doit vérifier:

$$\eta_o = H(t)\eta_r + J(t)\dot{r}(t), \quad (8.27)$$

où, si A^\dagger désigne la pseudo-inverse de la matrice A , alors $J = -A^\dagger B$ et H est une matrice de $(6 \times (6 - rang))$ dont les colonnes engendrent le noyau de A . Ainsi, η_r représente un vecteur indéterminé de $(6 - rang(A)) \times 1$ au niveau cinématique. Géométriquement, ce vecteur prend naturellement le sens du twist réduit de S_o inséré dans la structure entière, c'est à dire de S_o^+ . Ainsi, dans le cas (b) le "twist réduit" η_r ne peut pas être déterminé uniquement à partir des contraintes de non-dérapiage, mais nécessite des contraintes de roulement sans glissement ou/et de la dynamique. Par ailleurs, S_o peut être équipé de roues actionnées ainsi que de roues non-actionnées (autour de leur axe de rotation). Pour les distinguer, nous introduisons une partition de η_r et réécrivons (8.27) sous une forme plus détaillée:

$$\eta_o = (H_a(t), H_f(t)) \begin{pmatrix} \eta_{ra}(t) \\ \eta_{rf} \end{pmatrix} + J(t)\dot{r}(t), \quad (8.28)$$

où, avec $n \triangleq 6 - \text{rang}(A) = n_a + n_f$, $t \in \mathbb{R}^+ \mapsto \eta_{ra}(t)$ est un vecteur $(n_a \times 1)$ de twist (actionné) imposé (connu par la planification de mouvement et les lois de commande), tandis que η_{rf} est la composante non-actionnée de dimension $(n_f \times 1)$. Cette composante est inconnue et sera calculée par l'algorithme dynamique dans la suite. Il est à noter que, si $n = n_a$, (8.28) se réécrit comme suit:

$$\eta_o = -\mathcal{A}_k(\bar{r})\dot{\bar{r}}, \quad (8.29)$$

ici avec $\mathcal{A}_k = -(J, H_a(\bar{B}_{aa})^{-1})$; $\bar{r} = (r, \bar{\theta}_{oa})$, tandis que $\bar{\theta}_{oa}$ et \bar{B}_{aa} sont respectivement le vecteur des roues indépendantes actionnées de S_o et une matrice carrée définie par les contraintes de roulement sans glissement. Dans la littérature sur la dynamique lagrangienne, \mathcal{A}_k est souvent mentionné comme la forme locale de la connexion cinématique principale [87, 60]. Finalement, (8.28) définit la forme la plus générale de la cinématique réduite de S_o^+ .

En ce qui concerne les contraintes de roulement sans glissement, une relation similaire à (8.22) peut être dérivée, mais cette fois pour S_o^+ . En outre, S_o peut être équipé de roues actionnées et libres, et il est alors utile de diviser ses angles roulants en angles libres et actionnés, et d'écrire dans le cas général:

$$\begin{pmatrix} \dot{\theta}_{oa}(t) \\ \dot{\theta}_{of} \end{pmatrix} = \begin{pmatrix} B_{aa} & 0 \\ B_{fa} & B_{ff} \end{pmatrix} \begin{pmatrix} \eta_{ra}(t) \\ \eta_{rf} \end{pmatrix}. \quad (8.30)$$

Par ailleurs, nous avons $n_a \leq N_a$ (N_a est le nombre de degrés de liberté actionnés de S_o^+ tandis que N_a est son nombre de roues actionnées). Par conséquent, il est toujours possible d'extraire de B_{aa} une matrice carrée $n_a \times n_a$ de rang n_a noté \bar{B}_{aa} et de déclarer un système linéaire inversible:

$$\dot{\bar{\theta}}_{oa} = \bar{B}_{aa}{}^{ra} \eta_{ra}, \quad (8.31)$$

avec $B_{aa} = (\bar{B}_{aa}^T, \tilde{B}_{aa}^T)^T$ et $\theta_{oa} = (\bar{\theta}_{oa}^T, \tilde{\theta}_{oa}^T)^T$. Notons que (8.31) implique la relation subsidiaire:

$$\dot{\tilde{\theta}}_{oa} = \tilde{B}_{aaa}(\bar{B}_{aaa})^{-1}\dot{\bar{\theta}}_{oa}, \quad (8.32)$$

qui peut être interprétée comme un ensemble de relations de compatibilité pour les contraintes de roulement sans glissement des roues actionnées (i.e. si (8.32) est violée alors certaines des roues actionnées glissent sur le sol).

8.8.3 Dynamique du système multicorps mobile contraint

Dans cette section, nous reconsidérons le modèle dynamique de la locomotion (8.12) ainsi que la dynamique récursive des couples internes (qui est simplement la dynamique stan-

dard de Luh et Walker) d'un système multicorps mobile contraint où, dans le cas d'un système à roues, les roues ont été modélisées par des forces de réaction du sol (section 8.7). Ensuite, puisque les roues sont idéales dans le cas d'un système multicorps mobile contraint, nous appliquerons successivement deux processus de réduction sur la locomotion dynamique de l'algorithme du système multicorps mobiles non-contraint afin d'obtenir la dynamique réduite de locomotion pour un système multicorps mobiles contraint.

1. Projeter le modèle dynamique de la locomotion (8.12) sur l'espace admissible \mathcal{V} du corps de référence composite S_o^+ . Cela nous donnera un modèle dynamique réduit de la locomotion.
2. Projeter la dynamique des couples sur l'espace admissible \mathcal{V}_j de chacun des corps (isolés) S_j 's. Cela donnera la dynamique réduite des couples.

Notons que le but de ces projections sur les espaces admissibles est simplement d'éliminer toutes les forces latérales de contact (externe) qui sont toujours perpendiculaires à l'espace admissible et sont imposées par le sol en raison des contraintes de non-dérapiage. D'autre part, il y a un autre type de forces de contact externe, notée $F_{\text{ext},ra}$ qui agissent dans l'espace admissible \mathcal{V} et sont imposées par le sol en raison des contraintes de roulement sans glissement des roues actionnées. L'algorithme doit calculer ces forces $F_{\text{ext},ra}$ pour résoudre la dynamique. A la fin, le modèle résultant donne une forme généralisée de celle de la section 8.7 qui peut être appliquée à tout type de système de la Fig. 8.1(b).

8.8.3.1 Modèle dynamique réduit de la locomotion

Cette première étape du processus de réduction concerne la projection du modèle dynamique de la locomotion (8.12) de S_o^+ sur son espace admissible \mathcal{V} . En outre, puisque $\mathcal{V} = \mathcal{V}_a \oplus \mathcal{V}_f$, l'algorithme doit calculer les deux inconnues suivantes à chaque pas de temps.

1. L'accélération réduite $\dot{\eta}_{rf}$ du corps de référence composite S_o^+ dans son sous-espace admissible libre (non-actionné) \mathcal{V}_f .
2. Les efforts externes réduits $F_{\text{ext},ra}^+$ du corps de référence composite S_o^+ transmis par le sol via les contraintes de roulement sans glissement des roues actionnées.

Ces calculs sont détaillés dans les sections suivantes.

Calcul de $\dot{\eta}_{rf}(t)$

Comme les forces de réaction latérales induites par le sol sont orthogonales à \mathcal{V}_f , on trouve après la projection de (8.12) sur \mathcal{V}_f :

$$\begin{pmatrix} \dot{\eta}_{rf} \\ {}^e\dot{g}_o \end{pmatrix} = \begin{pmatrix} (\mathcal{M}_{rf}^+)^{-1}(F_{rf}^+) \\ {}^e g_o(H_f \eta_{rf} + (H_a \eta_{ra} + J\dot{r})(t))^\wedge \end{pmatrix}, \quad (8.33)$$

où l'on introduit les matrices réduites:

$$\begin{cases} \mathcal{M}_{rf}^+ = H_f^T \mathcal{M}_o^+ H_f, \\ F_{rf}^+ = H_f^T (F_{in,o}^+ - \mathcal{M}_o^+ (H_a \dot{\eta}_{ra} + \dot{H} \eta_r + \dot{J} \dot{r} + J \ddot{r})). \end{cases} \quad (8.34)$$

Enfin, à chaque étape de la boucle du temps globale, le calcul de (8.33) donne le $\dot{\eta}_{rf}(t)$ actuel, alors que l'intégration par rapport au temps de la deuxième ligne de (8.33) permet de mettre à jour l'état de référence.

Calcul de $F_{ext,ra}^+(t)$

Maintenant, si nous projetons (8.12) sur $\mathcal{V} = \mathcal{V}_a \oplus \mathcal{V}_f$ (au lieu de \mathcal{V}_f comme dans la section précédente), nous obtenons le modèle dynamique de la locomotion comme suit:

$$\begin{pmatrix} \mathcal{M}_{ra}^+ & {}^{ra}\mathcal{M}_{rf}^+ \\ {}^{rf}\mathcal{M}_{ra}^+ & \mathcal{M}_{rf}^+ \end{pmatrix} \begin{pmatrix} \dot{\eta}_{ra}(t) \\ \dot{\eta}_{rf} \end{pmatrix} = \begin{pmatrix} F_{in,ra}^+ + F_{ext,ra}^+ \\ {}^{rf}F_f^+ \end{pmatrix}. \quad (8.35)$$

De la première ligne, nous pouvons déduire les efforts externes réduits $F_{ext,ra}^+$ de S_o^+ comme suit:

$$F_{ext,ra}^+ = {}^{ra}\mathcal{M}_{rf}^+ \dot{\eta}_{rf} + \mathcal{M}_{ra}^+ \dot{\eta}_{ra}(t) - F_{in,ra}^+, \quad (8.36)$$

où les termes sur le côté droit de l'expression sont donnés par:

$$\begin{cases} {}^{ra}\mathcal{M}_{rf}^+ = H_a^T \mathcal{M}_o^+ H_f, \\ \mathcal{M}_{ra}^+ = H_a^T \mathcal{M}_o^+ H_a, \\ F_{in,ra}^+ = H_a^T F_{in,o}^+. \end{cases} \quad (8.37)$$

Les accélérations $\dot{\eta}_{rf}$ et $\dot{\eta}_{ra}(t)$ sont données par (8.33) et la dérivée temporelle de (8.31), respectivement.

8.8.3.2 Dynamique réduite des couples

Il s'agit de la deuxième étape du processus de réduction, consistant à réduire la dynamique de Luh et Walker par projection de ses deux modèles récursifs sur les espaces admissibles pour calculer les couples internes.

Cinématique recursive réduite

Comme il s'agit d'une projection corps par corps, nous allons insérer en premier lieu (8.19) et sa dérivée par rapport au temps dans (8.6) et (8.7), puis nous appliquons à gauche l'opérateur de projection H_j^T (sur \mathcal{V}_j), et enfin, nous invoquons la propriété d'orthonormalité (8.21), ce qui donne une cinématique réduite recursive: for $j = 1, 2, \dots, p$:

Calcul des vitesses réduites:

$$\eta_{rj} = \text{Ad}_{rj_{g_{ri}}} \eta_{ri} + \dot{r}_j A_{rj}. \quad (8.38)$$

Calcul des accélérations réduites:

$$\dot{\eta}_{rj} = \text{Ad}_{rj_{g_{ri}}} \dot{\eta}_{ri} + \zeta_{rj}(\dot{r}_j, \ddot{r}_j), \quad (8.39)$$

où, les notations suivantes sont introduites:

$$\begin{cases} \text{Ad}_{rj_{g_{ri}}} = H_j^T \text{Ad}_{j_{g_i}} H_i, \\ A_{rj} = H_j^T A_j, \\ \zeta_{rj} = H_j^T (\text{Ad}_{j_{g_i}} \dot{H}_i \eta_{ri} - \dot{H}_j \eta_{rj} + \zeta_j). \end{cases} \quad (8.40)$$

Récurrence réduite sur les forces internes

En projetant la dynamique de Newton-Euler (8.9) de chaque corps S_j sur son espace admissible \mathcal{V}_j , nous trouvons la récurrence sur les forces internes réduites ${}^{rj}F_{rj} = H_j^{Tj} F_j$; pour $j = p+1, \dots, 1$:

$$\begin{cases} \text{if } i = j-1 : & F_{ri} = \mathcal{M}_{ri} \dot{\eta}_{ri} - F_{\text{gyr},ri} + \text{Ad}_{rj_{g_{ri}}}^T F_{rj}; \\ \text{else:} & F_{\text{gyr},ri} = F_{\text{gyr},ri} - \text{Ad}_{rj_{g_{ri}}}^T F_{rj}, \end{cases} \quad (8.41)$$

avec les notations suivantes:

$$\begin{cases} \mathcal{M}_{ri} = H_i^T \mathcal{M}_i H_i, \\ F_{\text{gyr},ri} = -H_i^T (\mathcal{M}_i \dot{H}_i \eta_{ri} - F_{\text{gyr},i}). \end{cases} \quad (8.42)$$

Ensuite, les couples sont déduits de la projection réduite suivante:

$$j = 1, 2, \dots, p : \tau_j = F_{rj}^T A_{rj}. \quad (8.43)$$

Quant aux couples des roues actionnées Γ , nous pouvons définir la partition bloc de $\Gamma = (\bar{\Gamma}^T, \tilde{\Gamma}^T)^T$, duale de $\dot{\theta}_{oa} = (\dot{\theta}_{oa}^T, \tilde{\theta}_{oa}^T)^T$. $F_{\text{ext},ra}^+$ appartient à l'espace dual de η_{ra} 's et modélise les forces exercées par le sol sur S_o^+ à travers les roues actionnés. Ensuite, puisque les roues sont idéales, nous avons en vertu du principe d'action-réaction:

$$\bar{B}_{aa}^T \bar{\Gamma} + \tilde{B}_{aa}^T \tilde{\Gamma} = -F_{\text{ext},ra}^+, \quad (8.44)$$

où, en raison de l'éventuel caractère sur-actionné de l'espace admissible actionné ($N_a > n_a$), dans le cas général une infinité de couples aux roues Γ sont capables de fournir le $F_{\text{ext},ra}^+$ désiré.

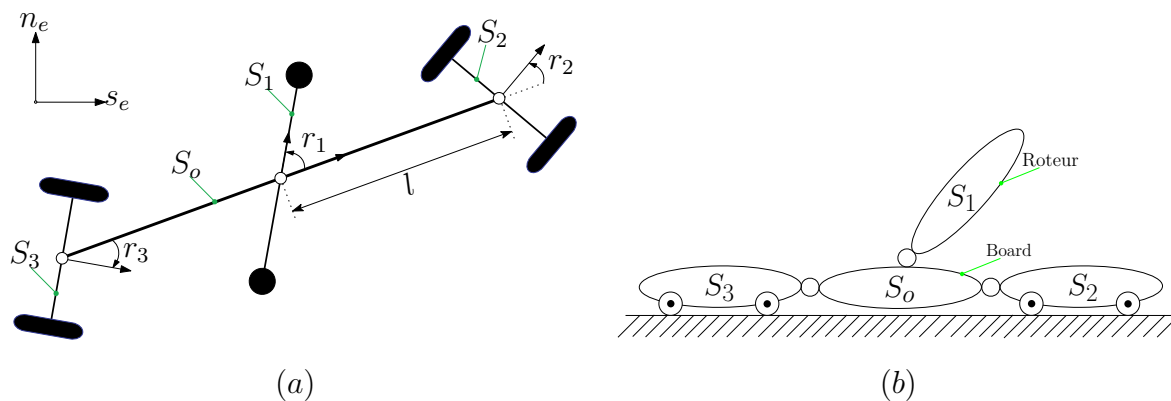


Figure 8.3 – Le Snakeboard

8.9 Exemples illustratifs

8.9.1 Le snakeboard

Dans cette section, nous prenons l'exemple du "snakeboard" (voir Fig. 8.3) qui est un système plan avec la topologie arborescente. Comme ce robot n'a que des roues non-actionnées, le choix du corps de référence S_o est libre. Suivant la description et les notations de [87], $-\phi$, ϕ et ψ sont les angles des articulations de S_2 par rapport à S_o , S_3 par rapport au S_o et S_1 par rapport à S_o , respectivement. En raison des symétries du design, les centres de masse des S_o , S_2 et S_3 sont alignés le long du grand axe de la plateforme. En faisant une hypothèse supplémentaire basée sur [87], nous écrivons: $m = m_o + m_r + 2m_w$ et $I = I_o + I_r + 2I_w = ml^2$, où les indices r et w présentent le rotor et le corps à roues, respectivement, alors que l est la longueur entre le centre de masse et la base des roues (voir Fig. 8.3(a)). Comme le mouvement du corps de référence S_o est contraint à l'espace admissible uni-dimensionnel, nous noterons $\eta_{rf} = \xi$. Nous commençons notre calcul en définissant les matrices réduites:

$$H_f = (-2lc2\phi, 0, s2\phi)^T, H_2 = H_3 = \begin{pmatrix} 1 & 0 & 0 \\ 0 & 0 & 1 \end{pmatrix}^T$$

et $H_o = H_1 = 1_3$.

Afin de calculer la dynamique réduite de la locomotion, nous calculons d'abord l'inertie réduite composite du snakeboard par (8.34) avec (8.14) comme suit:

$$\mathcal{M}_{rf}^+ = H_f^T \left(\sum_{j=0}^3 \text{Ad}_{j_{g_o}}^T \mathcal{M}_j \text{Ad}_{j_{g_o}} \right) H_f = 4ml^2 c2\phi. \quad (8.45)$$

Ensuite, nous calculons les forces composites en utilisant l'équation (8.34):

$$F_{rf}^+ = H_f^T F_o^+ - H_f^T (\mathcal{M}_o^+ \dot{H}_f \xi) = -I_r s2\phi \ddot{\psi} + 2ml^2 s2\phi \dot{\phi} \xi. \quad (8.46)$$

Enfin, ceci nous permet de calculer l'accélération réduite du snakeboard en utilisant la relation (8.33):

$$\dot{\xi} = tg\phi \left(-\frac{I_r}{2ml2} \ddot{\psi} + \dot{\phi}\xi \right). \quad (8.47)$$

qui doit être complétée par:

$$\eta_o = H_f \xi = (-2lc2\phi, 0, s2\phi)^T \xi. \quad (8.48)$$

L'ensemble des équations (8.47-8.48) réalise la forme simplifiée de (8.33) pour le snakeboard.

Le calcul des couples se fait en calculant d'abord l'accélération $\dot{\eta}_{rj}$ de chaque corps S_j par l'équation récursive (8.39) initialisée par:

$$\begin{aligned} \dot{\eta}_o &= H_f \dot{\xi} + \dot{H}_f \xi \\ &= \frac{I_r}{2ml2} \begin{pmatrix} ls2\phi \\ 0 \\ -2s2\phi \end{pmatrix} \ddot{\psi} + \begin{pmatrix} ls2\phi \\ 0 \\ 2c2\phi \end{pmatrix} \dot{\phi}\xi. \end{aligned} \quad (8.49)$$

Ensuite, l'algorithme utilise la relation sur les couples (8.43) pour projeter in fine les forces sur les axes articulaires:

$$\begin{aligned} \tau_1 &= A_1^T (\mathcal{M}_1 \dot{\eta}_1 - F_{gyr,1}), \\ \tau_j &= A_{rj}^T (\mathcal{M}_{rj} \dot{\eta}_{rj} - F_{gyr,rj}), \quad j = 2, 3, \end{aligned}$$

où pour le snakeboard $A_1^T = (0, 0, 1)$ et $A_{rj}^T = (0, 1)$. Le mouvement plan du snakeboard et aussi la projection des forces sur l'axe de rotation vérifient l'implication seulement de la troisième composante de l'équation (8.49) dans le calcul des couples, i.e.:

$$\begin{aligned} \tau_1 &= (I_r - (I_r/2/ml2)s2\phi) \ddot{\psi} + 2c2\phi I_r \dot{\phi}\xi, \\ \tau_2 &= -(I_w I_r / ml2) s2\phi \ddot{\psi} + 2c2\phi I_w \dot{\phi}\xi - I_w \ddot{\phi}, \\ \tau_3 &= -(I_w I_r / ml2) s2\phi \ddot{\psi} + 2c2\phi I_w \dot{\phi}\xi + I_w \ddot{\phi} \end{aligned}$$

Alternativement, en terme de forces généralisées appliquées aux deux coordonnées internes indépendants, nous obtenons:

$$\begin{aligned} \tau_\psi &= I_r ((1 - (I_r/ml2)s2\phi) \ddot{\psi} + 2c2\phi \dot{\phi}\xi), \\ \tau_\phi &= \tau_3 - \tau_2 = 2I_w \ddot{\phi}. \end{aligned} \quad (8.50)$$

Les couples ci-dessus sont le résultat souhaité de l'algorithme. En particulier, les équations (8.47) et (8.50) sont en accord avec la dynamique telle que calculée par [87] dans le cadre

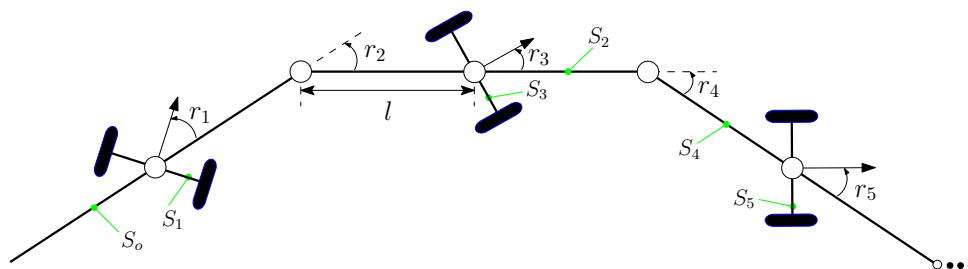


Figure 8.4 – Les trois premiers modules du robot serpent

Lagrangien.

8.9.2 Un robot serpent

Le robot serpent présenté ici est l'Active Cord Mecanism plan de Hirose [53]. C'est un système multicorps arborescent avec des roues non-actionnées. Il se compose de $p+1$ corps rigides connectés par des articulations rotoïdes simples. Un repère $\mathcal{F}_j = (O_j, s_j, n_j, a_j)$ est attachée au centre d'articulation de chaque corps S_j . Ici, nous considérons que chaque corps sans roues est connectée au corps voisin qui en possède (appelé collectivement un "module") via leurs centres de masse. La numérotation des corps est la suivante: $\mathbb{N}_{uw} = \{0, 2, 4, \dots, p-1\}$ et $\mathbb{N}_w = \{1, 3, 5, \dots, p\}$ définissent les ensembles d'indices des corps sans roues et des corps à roues, respectivement.

Ce robot possède suffisamment de contraintes non-holonomes pour que les mouvements externes puissent être modélisés par la cinématique réduite du corps de référence sans que la dynamique ne soit requise [88]. En fait, une fois réunies, les conditions de non-dérapiage imposées par les trois premiers modules prennent la forme de (8.24) où \bar{A} est une matrice (3×3) inversible de rang plein \bar{B} est une matrice (3×2) définies par:

$$\bar{A} = \begin{pmatrix} -sr_1 & cr_1 & 0 \\ -s\bar{r}_3 & c\bar{r}_3 & a_{23} \\ -s\bar{r}_5 & c\bar{r}_5 & a_{33} \end{pmatrix}, \quad \bar{B} = \begin{pmatrix} 0 & 0 \\ lcr_3 & 0 \\ b_{31} & lcr_5 \end{pmatrix},$$

avec $\bar{r}_3 = r_2 + r_3$, $\bar{r}_5 = r_2 + r_4 + r_5$, $a_{23} = l(cr_3 + c\bar{r}_3)$, $b_{31} = l(cr_5 + 2c(r_4 + r_5))$ et $a_{33} = b_{31} + lc\bar{r}_5$. Ainsi, la matrice \bar{A} étant inversible, on peut calculer la vitesse de la tête sous la forme (8.25), où $\mathcal{A}_k(r) = \bar{A}^{-1}\bar{B}$ correspond à la forme locale de la connexion cinématique principale du robot serpent. Enfin, dans ce cas dégénéré, les équations (8.25) et (8.26) seront utilisées pour initialiser la cinématique directe récursive, tandis que le reste du problème est résolu numériquement.

Pour les résultats numériques de l'algorithme, l'allure *serpentine* est imposée à un robot serpent de 20 corps (i.e. $p = 19$) avec les mouvements sinusoïdaux des articulations don-

nées par:

$$r_j = a_j \sin(w_j t + \phi_j),$$

où a_j , w_j et ϕ_j sont l'amplitude, la fréquence et la phase de l'articulation j respectivement. En plus, pour $j = 1, \dots, 5$: $a_j = (0.2, 0.6, -0.2, 0.6, 0.2)$, $w_j = 1$, and $\phi_j = (\frac{\pi}{16}, \frac{9\pi}{16}, 0, \frac{7\pi}{16}, -\frac{\pi}{16})$. Après simulation pendant 20sec, nous obtenons le mouvement externe du corps de référence S_o dans le plan xy comme indiqué dans la Fig. 8.5(a). La Fig. 8.5(b) montre l'évolution temporelle du couple appliqué entre les corps S_8 et S_{10} au cours des 20sec de la simulation.

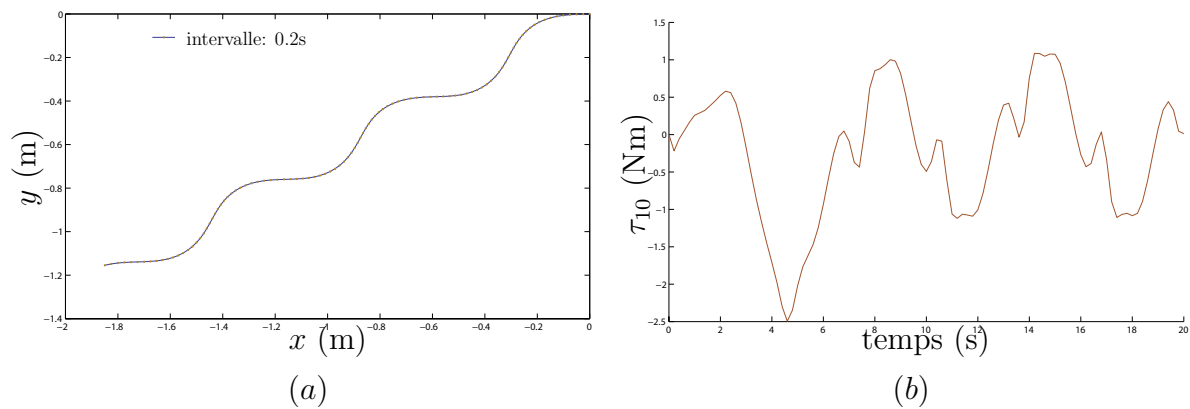


Figure 8.5 – (a) le mouvement de S_o dans le plan xy ; (b) couple articulaire τ_{10}

Partie-II: Les Systèmes Continues

8.10 Introduction aux Robots Hyper-Redondants

Dans le contexte de la locomotion, les systèmes hyper-redondants sont généralement inspirés des animaux allongés vertébrés comme les serpents [52] et les poissons anguilliforme [13], où les vertèbres correspondent aux corps rigides du système multicorps associé. Ces animaux possédant un nombre élevé de vertèbres, et leur corps étant recouvert d'une enveloppe de tissus déformables, il est légitime de les considérer comme véritablement continus. Aujourd'hui, grâce aux recherches en bio-robotique, de nouveaux concepts de robots continus, aux corps mous, étendent ces idées encore plus loin. En effet, contrairement aux robots traditionnels, ces robots inspirés par les organismes invertébrés, connu sous le nom d'hydrostats, ne contiennent pas d'organes rigides. En outre, leurs changements de forme sont continus sur toute la longueur de leur corps, semblable à ceux d'une trompe d'éléphant [48], des chenilles [9], des lombrics [65], des bras d'une pieuvre [68], etc. Finalement, tous ces systèmes forment aujourd'hui la classe générale des robots continus. L'extension des modèles basiques des robots (modèles géométriques, cinématiques et dynamiques) à ces nouveaux systèmes est une étape cruciale vers leur succès futur. Sur ce point, plusieurs chercheurs ont accompli un travail considérable sur le sujet des robots continus afin d'investiguer les problèmes habituels de la robotique tels que la planification de mouvement, la génération des allures, la modélisation cinématique et dynamique, la conception et la commande, etc. Nous renvoyons le lecteur à [113] pour un état de l'art sur la robotique continue. De nombreuses contributions à la modélisation cinématique ont été proposés [28, 18, 85, 57, 48]. Concernant la dynamique des robots continus, quelques travaux sur ce thème ont été proposées [29, 41, 83, 108].

En fait, adopter un modèle continu dès le début de la modélisation peut grandement faciliter la formulation, l'analyse et la résolution des problèmes robotique liés à la manipulation [26, 83], et à la locomotion [52, 18, 50]. Toutefois, l'application de ce type d'approche nécessite de donner une réalité matérielle à la cinématique continue. Par exemple, dans l'approche par "backbone-curves" telle que développée dans [28, 18], la "courbe vertébrale" se doit d'être enrichie d'une extension matérielle latérale permettant de modéliser l'inertie du robot. Cette tentative a été faite dans [26, 83] pour les robots plans. Alternativement, la théorie des poutres géométriquement exactes de J. C. Simo [105, 104] a été utilisé pour la modélisation des aiguilles passives orientables dans le contexte de la robotique médicale [116, 95], tandis que dans [113] et [112], elle a été appliquée à un robot mou nommé OctArm [46]. Dans [13, 16, 15], cette approche a été appliquée à la locomotion des poissons anguilliformes et à leur artéfacts robotiques.

8.11 Notations et définitions

Dans la suite, l'espace est muni d'un repère orthonormé $\mathcal{F}_s = (O, e_x, e_y, e_z)$. En accord avec [13], un robot hyper-redondant peut être modélisé par une poutre Cosserat en grandes transformations, petite contraintes si l'on assimile la ligne vertébrale du robot avec la ligne des centroids de la poutre. Dans cette approche, chaque section de la poutre, supposée rigide, est labellée par la position qu'occupe son centroid dans la configuration initiale de la poutre que l'on suppose droite et telle que sa ligne centroidale soit alignée sur (O, e_x) . A chaque section rigide, est attaché un repère orthonormé mobile $\mathcal{F}_m(X, t) = (P, t_X, t_Y, t_Z)(X, t)$ dont l'origine P et le premier vecteur t_X coïncident respectivement avec le centre de la section et sa normale unitaire. Avec ce choix la configuration de chaque repère mobile est définie par l'action d'un élément de $g \in \text{SE}(3)$ appliquée au repère fixe. Aussi devient-il possible d'introduire une première définition de son espace des configurations comme un espace fonctionnel de courbes paramétrées dans un groupe de Lie G :

$$\mathcal{C}_1 = \{g : \forall X \in [0, l] \mapsto g(X) \in G\} \quad (8.51)$$

Ulterieurement, nous introduirons une seconde définition de l'espace des configurations comme une fibré principal dont l'espace des formes est défini par un espace fonctionnel de courbes dans l'algèbre de Lie \mathfrak{g} du groupe. Dans la suite, on pointe (respect. prime) une dérivée par rapport au temps (respect. par rapport à l'espace). Sur la poutre, on définit deux champs de vecteur dans \mathfrak{g} , le premier est le champ de time-twist:

$$\hat{\eta} : X \in [0, l] \mapsto \hat{\eta}(X, t) = g^{-1}\dot{g} \in \mathfrak{g}, \quad (8.52)$$

où $\eta(X, t)$ définit la transformation infinitésimale subit par la section X entre deux instants infiniment proches t et $t + dt$. Le second champ est celui des space-twist tel que:

$$\hat{\xi} : X \in [0, l] \mapsto \hat{\xi}(X, t) = g^{-1}g' \in \mathfrak{g}, \quad (8.53)$$

où $\xi(X, t)$ définit la transformation infinitésimale subit par la section X à t fixé lorsque l'on glisse le long de l'axe matériel de X en $X + dX$. Dans la suite, comme certains des degrés de libertés de la poutre sont commandés tandis que d'autres son forcés à des valeurs constantes par la conception des liaisons internes que l'on suppose parfaites et infiniment rigides, on identifiera le champ $\hat{\xi}$ à un champ désiré (commandé) explicitement dépendant du temps noté $\hat{\xi}_d(t)$.

8.12 Cinématique de la poutre et des robots hyper-redondants

Rappelons que jusqu'à nouvel ordre on identifie G à $SE(3)$. On va recenser les différentes cinématiques de poutres et les robots associés. A chaque cinématique infinitésimale, on associe une liaison mécanique finie et lorsque possible, une structure passive déformable. Pour cela, partons de la définition (8.53) que l'on détaille selon:

$$g^{-1}g' = \begin{pmatrix} R^T R' & R^T p' \\ 0 & 0 \end{pmatrix} = \begin{pmatrix} \widehat{K}_d(t) & \Gamma_d(t) \\ 0 & 0 \end{pmatrix} = \widehat{\xi}_d(t) \quad (8.54)$$

Où $K_d = (K_{dX}, K_{dY}, K_{dZ})$ et $\Gamma_d = (\Gamma_{dX}, \Gamma_{dY}, \Gamma_{dZ})$. Dont les composantes prennent le sens suivant. K_{dX} est le taux de torsion de la poutre, tandis que K_{dY} et K_{dZ} représente respectivement les courbures de sa ligne centroidale dans les plans (P, t_X, t_Z) et (P, t_X, t_Y) . De même, $\Gamma_{dX} - 1$ est le taux d'extension de la ligne des centroides tandis que Γ_{dY} et Γ_{dZ} sont respectivement les rotations locales de cisaillement transverse autour des axes (P, t_Z) et (P, t_Y) . A présent, selon que ces champs scalaires soient actionnés ou non, on a les différents cas possibles en partant du cas où la cinématique interne est la plus actionnée au cas où elle l'est le moins (pour les 5 premiers cas, chacun est inclus dans le suivant), et en ne considérant que les cas les plus pertinents pour le roboticien:

1. Si tous les degrés de libertés internes sont actionnés, alors on a six degrés de liberté entre chaque section. La cinématique de poutre est celle de Reissner-Timoshenko.
2. Si l'on force $\Gamma_{dY} = \Gamma_{dZ} = 0$, alors on force les sections à rester perpendiculaires à l'axe vertébrale tandis que la traction compression est autorisée. La cinématique de poutre est celle des poutres de Kirchhoff extensibles.
3. Si en plus on impose $\Gamma_{dX} = 1$ alors la poutre devient inextensible et la cinématique interne est celle des poutres inextensibles de Kirchhoff. Elle réalise la version infinitésimale d'une liaison rotule.
4. La cinématique suivante est particulièrement pertinente pour le roboticien puisqu'elle permet de réaliser un robot se déplaçant en 3D avec le minimum de degrés de liberté interne. Elle se déduit de la précédente en imposant la contrainte supplémentaire $K_{dX} = 0$, i.e. en forçant la torsion à zéro. Aucune structure passive ne lui correspond puisque on ne peut générer de la flexion 3D sans produire de la torsion.
5. Si ensuite, on supprime l'une des deux flexions en forçant par exemple $K_{dY} = 0$, on obtient la cinématique minimale permettant de manipuler un objet dans les trois dimensions du plan (i.e. dans $SE(2)$). La théorie de poutres qui lui correspond est celle des poutres de Kirchhoff planes inextensibles.

6. Le cas suivant est utile pour l'ondulation latérale des serpents, il se déduit du cas générale en posant $K_{dX} = K_{dY} = 0$, ainsi que $\Gamma_{dX} = 1, \Gamma_{dZ} = 0$. La théorie de poutre correspondante est celle des poutres de Timoshenko-Reissner planes.
7. Enfin le dernier cas, représente le plus dégénéré puisque tous les degrés de liberté y sont forcés à zéro excepté Γ_X qui est contrôlé. La poutre est une simple barre en traction compression.

Finalement, chacune de ces cinématiques trouve dans la nature ses applications à des animaux allongés et à leur modes de locomotion associés. En particulier, si l'on considère le cas de la locomotion serpentiforme, sur les deux courbures K_Y et K_Z l'une figure le lacet dans le plan de la propulsion, tandis que l'autre actionne le tangage pour des manoeuvres 3D complexes impliquant le corps tandis que la torsion K_X permet d'agir directement sur le roulis dont le contrôle est crucial pour stabiliser l'orientation de la tête des robots bioinspirés des serpents, anguille. Pour ce qui est des degrés de liberté linéaires, Γ_X actionne la traction-compression telle qu'utilisée par les gros serpents, tandis que Γ_Y et Γ_Z peuvent être utilisés par le mécanicien pour modéliser des mouvements relatifs de la peau et des écailles.

8.13 Modèle continu des robots hyper-redondants

8.13.1 Modèle continu géométrique

Il se déduit immédiatement de la définition (8.54) des degrés de liberté internes:

$$g' = g \cdot \widehat{\xi}_d(t), \quad (8.55)$$

avec comme conditions aux bords (boundary conditions]: $g(X=0) = g_o$.

8.13.2 Modèle continu des vitesses

En dérivant (8.52) par rapport à X , et en invoquant (8.54), il vient:

$$\eta' = -ad_{\xi_d(t)}(\eta) + \dot{\xi}_d(t), \quad (8.56)$$

avec comme conditions aux bords: $\eta(X=0) = \eta_o = (g_o^{-1} \cdot \dot{g}_o)^\vee$.

8.13.3 Modèle des accélérations

Il se déduit de la dérivation par rapport au temps du modèle précédent:

$$\dot{\eta}' = -ad_{\xi_d(t)}(\dot{\eta}) - ad_{\dot{\xi}_d(t)}(\eta) + \ddot{\xi}_d(t), \quad (8.57)$$

avec comme conditions aux bords: $\dot{\eta}(X=0) = \dot{\eta}_o = (g_o^{-1}\ddot{g}_o - g_o^{-1}\dot{g}_o g_o^{-1}\dot{g}_o)^\vee$.

En reconsidérant le modèle cinématique continu (8.55), il devient évident qu'il est toujours possible de reconstruire la configuration de la poutre à partir de la connaissance de g_o et du champ de déformation ξ_d . Aussi, peut on donner une seconde définition de l'espace des configuration du robot comme le fibré principal:

$$\mathcal{C}_2 = G \times \mathcal{S}, \quad (8.58)$$

où G représente la configuration du repère attaché à la tête, tandis que \mathcal{S} est l'espace de la forme interne ici défini comme l'espace fonctionnel des courbes dans l'algèbre de Lie:

$$\mathcal{S} = \{\xi : \forall X \in [0, l] \mapsto \xi(X) \in \mathfrak{g}\}. \quad (8.59)$$

8.13.4 Dynamique sur \mathcal{C}_1 : modèle de Newton-Euler continu

En appliquant sur \mathcal{C}_1 le principe d'Hamilton au robot continu soumis à une densité de torseur imposé \overline{F} sur $]0, l[$ et deux torseurs ponctuels F_+ et F_- respectivement imposés en $X=0$ et $X=l$, on trouve ses equations aux dérivées partielles:

$$\frac{\partial}{\partial t} \left(\frac{\partial \mathfrak{L}}{\partial \eta} \right) - ad_\eta^* \left(\frac{\partial \mathfrak{L}}{\partial \eta} \right) + \frac{\partial}{\partial X} \left(\frac{\partial \mathfrak{L}}{\partial \xi} \right) - ad_\xi^* \left(\frac{\partial \mathfrak{L}}{\partial \xi} \right) = \overline{F}, \quad (8.60)$$

dont les solutions à chaque instant sont fixées par les conditions aux limites:

$$\frac{\partial \mathfrak{L}}{\partial \xi}(0) = -F_-, \text{ and: } \frac{\partial \mathfrak{L}}{\partial \xi}(l) = F_+, \quad (8.61)$$

Où l'on a introduit la densité de Lagrangien du robot continu $\mathfrak{L} = \mathfrak{T} - \mathfrak{U} = (1/2)(\eta^T(\mathcal{M}\eta) - \Lambda^T(\xi - \xi_d(t)))$, avec: $\mathcal{M} \in \mathfrak{g}^* \otimes \mathfrak{g}$, la densité de tenseur d'inertie, et $\Lambda \in \mathfrak{g}^*$, la densité de torseur des efforts internes assurant le forçage des contraintes internes: $\xi = \xi_d(t)$. Remarquons à ce sujet, que Λ prend le sens d'un champ de multiplicateurs de Lagrange, et que pour les degrés de liberté internes actionnés, les multiplicateurs associés sont des commandes (en effort ou en couple) tandis que pour les degrés de liberté non-actionnés, les multiplicateurs sont des forces ou couple de réaction internes. De plus, si l'on convient de noter $\mathcal{M}\eta = \partial \mathfrak{T} / \partial \eta$ la densité de torseur cinétique le long du robot, on trouve:

$$\mathcal{M}\dot{\eta} - ad_\eta^*(\mathcal{M}\eta) - \Lambda' + ad_{\xi_d(t)}^*(\Lambda) = \overline{F}, \quad (8.62)$$

avec les conditions aux limites:

$$\text{en } X=0: \Lambda(0) = -F_-, \text{ en } X=l: \Lambda(l) = F_+. \quad (8.63)$$

Enfin, (8.62) et (8.63) sont considérés dans la suite comme la dynamique des efforts interne ou plus simplement comme la «dynamique interne».

8.13.5 Dynamique sur \mathcal{C}_2 : dynamique du corps de référence

La dynamique sur \mathcal{C}_2 se déduit de celle sur \mathcal{C}_1 en repartant du principe d'Hamilton (qui nous a conduit précédemment à (8.62)-(8.63)) et en y forçant les champs de vitesse (virtuels et réels) à vérifier la contrainte:

$$\eta = Ad_k(\eta_o), \quad (8.64)$$

où comme $k = g^{-1}g_o$, le champ (8.64) n'est autre que le champ de time-twist sur la poutre induit par le mouvement de la tête seul, alors que le corps est figé dans sa configuration courante. Il vient dans ces conditions, les efforts internes ne travaillant pas dans un tel champs:

$$\int_0^l Ad_k^*(\mathcal{M}\dot{\eta} - ad_\eta^*(\mathcal{M}\eta) - \overline{F})dX = Ad_{k_+}^*F_+ - F_-, \quad (8.65)$$

où l'on remplace $\dot{\eta}$ par le champ d'accélération compatible avec (8.64):

$$\dot{\eta} = Ad_k(\dot{\eta}_o) + ad_\eta(Ad_k(\eta_o)) + Ad_k(\eta_o^2) - (Ad_k(\eta_o))^2 = Ad_k(\dot{\eta}_o) + \zeta, \quad (8.66)$$

où $\zeta(X)$ représente l'accélération matérielle de la section X induite par la déformation du corps et le mouvement de la tête exceptée son acceleration pure (i.e. due à $\dot{\eta}_o$). Finalement, tout calcul fait et en tenant compte de l'équation de reconstruction cinématique de la section $X = 0$, les équations de la dynamique du robot sur \mathcal{C}_2 s'écrivent:

$$\begin{pmatrix} \dot{\eta}_o \\ \dot{g}_o \end{pmatrix} = \begin{pmatrix} \mathcal{M}_o(\xi_d)^{-1}F_o(\xi_d, \dot{\xi}_d, \ddot{\xi}_d, g_o, \eta_o) \\ g_o\widehat{\eta}_o \end{pmatrix} \quad (8.67)$$

avec: $F_o = F_{in} + F_{ext}$, et où l'on a introduit le tenseur d'inertie de l'ensemble du robot ramené à la section de référence i.e. en $X = 0$:

$$\mathcal{M}_o = \int_0^l Ad_k^*\mathcal{M}Ad_kdX, \quad (8.68)$$

le torseur des efforts extérieurs, ramenés à la section de référence:

$$F_{ext} = -F_- + Ad_{k_+}^*F_+ + \int_0^l Ad_k^*(\overline{F})dX, \quad (8.69)$$

le torseur des efforts d'inertie ramenés à la section de référence:

$$F_{in} = - \int_0^l Ad_k^*(\mathcal{M}\zeta - ad_\eta^*(\mathcal{M}\eta))dX. \quad (8.70)$$

Dans la suite, (8.67) sera considérée comme la dynamique des mouvements du corps de référence contrôlés par les variations des mouvement interne, appelé la «dynamique de la locomotion».

8.14 Algorithme dynamique des robots continus

Finalement, en posant le vecteur d'état cinématique $\mathcal{X}_1 = (g, \eta, \dot{\eta})$, les modèles cinématiques (8.55,8.56,8.57) peuvent être regroupés dans l'unique équation aux dérivées ordinaires en espace:

$$\mathcal{X}'_1 = f_1(\mathcal{X}_1, \xi_d(t), \dot{\xi}_d(t), \ddot{\xi}_d(t)). \quad (8.71)$$

De même, la dynamique interne (8.62) peut se remettre sous la forme de l'équation aux dérivées ordinaires suivante en espace, de vecteur d'état $\mathcal{X}_2 = (\mathcal{X}_1, \Lambda)$:

$$\mathcal{X}'_2 = f_2(\mathcal{X}_2, \xi_d(t), \dot{\xi}_d(t), \ddot{\xi}_d(t)), \quad (8.72)$$

avec:

$$f_2 = \begin{pmatrix} f_1 \\ ad_{\xi_d(t)}^*(\Lambda) + \mathcal{M}\dot{\eta} - ad_{\eta}^*(\mathcal{M}\eta) - \bar{F} \end{pmatrix}. \quad (8.73)$$

Finalement, les termes apparaissant dans la dynamique externe (8.67) peuvent être également calculés par intégration spatiale d'une unique ODE de vecteur d'état $\mathcal{X}_3 = (\mathcal{X}_1, \mathcal{M}_o, F_o)$:

$$\mathcal{X}'_3 = f_3(\mathcal{X}_3, \xi_d(t), \dot{\xi}_d(t), \ddot{\xi}_d(t)), \quad (8.74)$$

avec:

$$f_3 = \begin{pmatrix} f_1 \\ Ad_k^* \mathcal{M} Ad_k \\ Ad_k^*(-\mathcal{M}\dot{\eta} + ad_{\eta}^*(\mathcal{M}\eta) + \bar{F}) \end{pmatrix}.$$

Où le ζ de (8.68) peut être remplacé par $\dot{\eta}$ dans (8.75) si les conditions initiales en espace de (8.74) vérifient $\dot{\eta}(X=0) = \dot{\eta}_o = 0$. En effet dans ce cas $\zeta = \dot{\eta}$ tout le long de la poutre. Finalement, comme nous allons le voir à présent, dans tous les cas l'algorithme intègre (8.74) dans ces conditions, de sorte que (8.75) fait sense. Toutes les equations aux dérivées ordinaires ci-dessus construisent un algorithme generale pour résoudre la dynamique d'un robot hyper-redundant. L'exécution de cet algorithme est expliqué comme suit:

1. Intégrer l'équation (8.74) de $X = 0$ à $X = l$ initialisée par $\mathcal{X}_3(0) = (g_o, \eta_o, 0, 0, F_-)$ donne \mathcal{M}_o et F_o .
2. Intégrer (8.67) entre t et $t + \Delta t$ afin d'en déduire le nouvel état de référence (pour

le pas de temps suivant): $(g_o, \eta_o)(t + \Delta t)$.

3. Intégrer l'équation (8.72) de $X = 0$ à $X = l$ initialisée par $\mathcal{X}_2(0) = (g_o, \eta_o, \dot{\eta}_o, F_-)$ donne Λ .

L'algorithme résout la dynamique directe en calculant l'accélération d'un modèle des efforts extérieures. En général, un tel modèle peut être très complexe comme dans le cas de la nage dans lequel, à la rigueur, elle nécessite d'intégrer les équations de Navier-Stokes [16]. Dans le cas de la locomotion terrestre, l'algorithme ci-dessus peut être utilisé avec des efforts extérieures modélisés comme des lois physiques, par exemple, la loi du frottement. Cependant, pour des raisons de simplicité de l'analyse, il peut être utile d'examiner les contacts comme idéal. Dans ce cas, ils peuvent être modélisés comme des contraintes au lieu d'efforts tel que discuté dans la section suivante. Dans la prochaine étape, nous allons voir que lorsque le nombre de contraintes est suffisante, la dynamique de la locomotion peut être remplacée par une cinématique et dans ce cas la locomotion est nommé comme «la locomotion cinématique».

8.15 Modélisation cinématique des contacts

La nature du contact joue un rôle important dans la définition du mode de locomotion. Basé sur le contact terrestre des animaux allongée, ici nous traitons avec deux types de contacts (supposé comme idéal): ancrages et des contacts annulaires. Ancrages sont modélisés comme des contraintes bilatérales holonomes tandis que les contacts annulaires sont modélisés comme des contraintes bilatérales non-holonômes. Dans les deux cas, les contacts sont répartis le long de l'axe du corps. En cas d'ancrages, deux types sont envisagées:

Ancrage verrouillé: ce type d'ancrage est fixé sur l'axe matériel du robot sur une abscisse, noté C , constante par rapport au temps (voir Fig. 8.6(a)).

Ancrage glissant: dans ce type d'ancrage, l'abscisse C est soit explicitement dépendant du temps noté $C(t)$ ou implicitement dépendant du temps via la dynamique du système (voir Fig. 8.6(b)).

D'autre part, le contact annulaire est toujours glissant, puisque le robot peut coulisser librement dans l'anneau formé par le contact annulaire.

Finalement, toutes ces contacts sont supposées attachées à des obstacles (ou supports) en mouvement relatifs imposés par rapport au référentiel terrestre. Enfin, comme nous le verrons lors des exemples, ces modèles sont d'un grand intérêt pratique pour la modélisation des nombreux modes de locomotion.

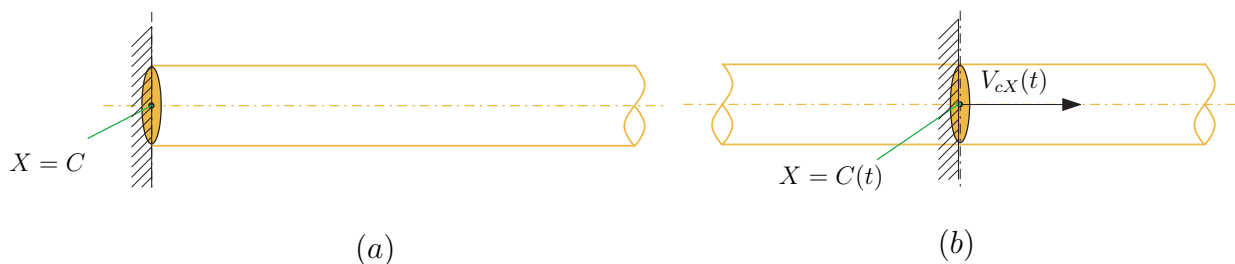


Figure 8.6 – (a) Ancre verrouillé; (b) Ancre glissant

8.15.1 Cas des ancrages

Dans le cas d'un ancrage verrouillé, on écrira, si le robot est ancré en un point matériel, noté C (cf. Fig. 8.6(a)):

$$g(C) = g_c(t), \quad (8.75)$$

où la fonction $g_c(t)$ dénote une fonction du temps imposée dans G . En particulier, si g_c est indépendante du temps, alors il s'agit d'un ancrage fixe, tels ceux requis par les robots manipulateurs ancrés dans le sol. Dans le cas des ancrages glissants, le modèle géométrique du contact ne peut faire la différence d'avec un ancrage verrouillé tout deux considérés au même instant t . En effet dans le second cas, on a encore:

$$g(C(t)) = g_c(t). \quad (8.76)$$

En revanche, le modèle cinématique de la liaison fait la différence puisqu'alors, on a dans le cas glissant en dérivant (8.76), et $d(\cdot)/dt$ dénotant la dérivée totale par rapport au temps:

$$\frac{dg(C(t))}{dt} = \dot{g}(C(t)) + g'(C(t))\dot{C}(t) = \dot{g}_c(t), \quad (8.77)$$

que l'on multiplie par $g^{-1}(C(t))$ pour obtenir, en invoquant de nouveau (8.76), les contraintes d'ancrage glissant dans \mathfrak{g} :

$$\eta(C(t)) + \xi_d(C(t))\dot{C}(t) = \eta_c(t), \quad (8.78)$$

où $\hat{\eta}_c(t) = (g_c^{-1}\dot{g}_c)(t)$ est le time-twist imposé à l'ancrage et où (8.78) donne la forme cinématique d'un ancrage fixe: $\eta(C) = \eta_c(t)$ lorsque C est indépendant du temps. Finalement, notons que (8.78) réalise un jeu de $\dim(\mathfrak{g})$ contraintes scalaires indépendantes.

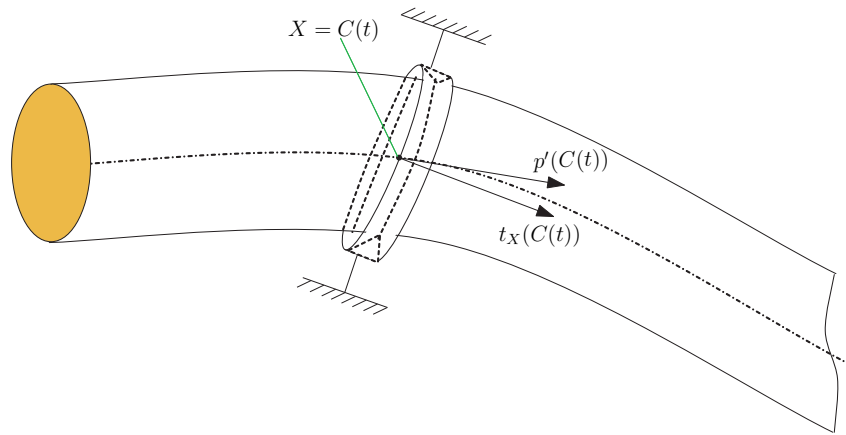


Figure 8.7 – Contact annulaire

8.15.2 Cas des contacts annulaires

Avant de décrire les détails de leur modélisation, rappelons-nous que les contacts annulaires sont, par nature, glissant ainsi ils ne peuvent être mises en contraintes cinématiques. Ici, nous considérons le contact annulaire qui suit les sections dans leurs mouvements latéraux, comme indiqué dans la Fig. 8.7. Il s'agit d'un contact annulaire qui empêche toutes les vitesses relatives translationnelle (de la section en contact par rapport au contact annulaire) dans le plan d'une section d'abscisse $X = C$. Ainsi, pour un mouvement dans l'espace \mathbb{R}^3 ($G = SE(3)$), un tel contact exercée dans tous les $C \in [0, l]$ est modélisé par la relation suivante:

$$\begin{cases} (v(C(t)) - v_c(t)) \times t_X(C(t)) = 0, \\ (\omega(C(t)) - \omega_c(t))^T t_X(C(t)) = 0, \end{cases} \quad (8.79)$$

ici $\omega(X) = (\dot{R}R^T)^\vee(X)$ désigne la vitesse angulaire spatiale de la section X , alors que $(v_c^T, \omega_c^T)^T(t)$ est la torsion spatiale imposée sur le contact annulaire rigide. Après calcul, (8.79) conduit à la suite de trois contraintes bilatérales non-holonômes:

$$\begin{cases} V_Y(C) = V_{cY}(t), \\ V_Z(C) = V_{cZ}(t), \\ \Omega_X(C) = \Omega_{cX}(t), \end{cases} \quad (8.80)$$

où $V_{cY}(t), V_{cZ}(t)$ sont les vitesses latéraux exprimé dans le repère de la section, alors que $\Omega_{cX}(t)$ est la composante axiale de la vitesse angulaire, toutes les composantes étant imposées à la section C par le mouvement de l'obstacle. Ces vitesses sont nulles si le contact annulaire en question est fixe dans l'espace ambiant. En outre, dans le mouvement planaire ($G=SE(2)$), un tel contact empêche le mouvement latéral de la section en contact.

Ainsi, la contrainte bi-latérale non-holonôme est donnée simplement comme suit:

$$V_Y(C) = V_{cY}(t).$$

8.15.3 Modèles des efforts de contact

Les contacts définis étant parfaits, les efforts de contact s'identifient aux multiplicateurs de Lagrange associées aux contraintes scalaires tirées de (8.78), (8.80). En cas de $G=SE(3)$, un ancrage en introduit six (i.e. les six composantes d'un torseur de réaction complet). Quant au contact annulaire, il transmet deux forces latérales et un couple axial pour un mouvement tridimensionnel tandis que une seule force latérale dans le cas d'un mouvement plan. Lorsque les ancrages et/ou contacts annulaires sont imposés aux extrémités, les efforts de réaction qui leur sont associés entrent dans la formulation de la dynamique via les torseurs externes apicaux F_{\pm} . Tandis que si les contacts sont définis à l'intérieur du domaine de la poutre, i.e. si $C \in]0, l[$, alors chacun d'entre eux ajoute un jeu de contraintes cinématiques dans \mathfrak{g} et un torseur de réaction associé (défini dans \mathfrak{g}^*), entrant dans le modèle des efforts distribués \overline{F} via une distribution de Dirac: $\overline{F}_c(C)\delta(X - C)$. Finalement, notons que dans F_{ext} on trouve une contribution F_c appelée résultante des torseurs de réaction produits par les liaisons et ramenés à la section de référence.

8.16 Algorithme dans le cas cinématique

Lorsque le nombre de contraintes (imposées par les contacts) est égal ou supérieur à la dimension de la fibre de \mathcal{C}_2 , le système est dit complètement ou sur contraints et les mouvements externe sont entièrement régi par le modèle cinématique des contacts de la forme explicite la plus générale:

$$\dot{g}_o = g_o \hat{\eta}_o = g_o \hat{f}(g_o, \xi_d(t), \xi'_d(t), \xi''_d(t), \dots, \dot{\xi}_d(t)), \quad (8.81)$$

dont on déduit par simple dérivation de f , la première ligne le modèle des accélérations. Dans ce cas, la locomotion est dite "locomotion cinématique" et la dynamique externe (8.67) sert à calculer le torseur de réaction induit par les contraintes externes, i.e.:

$$F_c = \mathcal{M}_o \dot{\eta}_o - F_{in} - F_{autre}, \quad (8.82)$$

où $F_{autre} = F_{\text{ext}} - F_c$, dénote la contribution induite par les autres origines de forces extérieures: gravité, effort de pression et de viscosité.

De plus, lorsque le nombre de contraintes est strictement supérieur à la dimension de la fibre de \mathcal{C}_2 , les mouvements externe du robot est sur-contraint qui signifie que: 1)

les mouvements internes doivent être compatibles², 2) les inconnues de réaction sont sous-déterminées puisqu'elles ne sont assujéties qu'à vérifier la dynamique externe qui s'écrit encore sous la forme (8.82). Finalement, ces considérations permettent d'élaborer l'algorithme résolvant le problème de la locomotion cinématique.

1. Intégrer l'équation (8.74) de $X = 0$ à $X = l$ initialisée par $\mathcal{X}_3(0) = (g_o, \eta_o, 0, 0, 0)$ et avec $\bar{F} = 0$, donne \mathcal{M}_o et F_{in} .
2. Calculer $(\eta_o, \dot{\eta}_o)$ à partir de (8.81) et intégrer η_o entre t et $t + \Delta t$ afin d'en déduire la nouvelle configuration de la section de référence (pour le pas de temps suivant): $g_o(t + \Delta t)$.
3. Calculer grâce à (8.82), la résultante des torseurs de réaction induits par les contacts.
4. Après répartition arbitraire de la résultante des forces de réaction aux points d'ancrage F_c , intégrer l'équation (8.72) de $X = 0$ à $X = l$ soumises aux torseurs de réaction F_{c_i} appliqués aux points de contact, et initialisée par $\mathcal{X}_2(0) = (g_o, \eta_o, \dot{\eta}_o, F_-)$.

Remarque1: dans le cas contraint, nous ne précisons pas la forme de la cinématique externe au-delà de son expression (8.81) et préférons la mettre à jour au cas par cas sur des exemples particuliers. Disons simplement ici, que la fonction f dans (8.81) doit être calculé à partir de f_1 de (8.71) et de considérations relatives au mode de locomotion étudié (en particulier issues de l'observation biologique) ainsi que du modèle des contacts.

Remarque2: comme sous-cas particulier des systèmes complètement contraint, on trouve les manipulateurs hyper-redondants. En effet dans ce cas, la section de référence est encadrée sur un support de mouvement imposé (en particulier nul) défini par $\mathcal{X}_1(0) = (g_o, \eta_o, \dot{\eta}_o)(t)$. Dans ce cas, les étapes 1, 2 et 3 de l'algorithme peuvent être évitées. En effet, les mouvements externes ne requièrent aucun calcul puisqu'il sont connus par leur lois horaires, tandis que le torseur de réaction au niveau de l'ancrage en $X = 0$ se déduit par simple intégration de la dynamique interne (8.72) de $X = l$ à $X = 0$.

Remarque3: notons que si f dans (8.81) est linéaire en $\dot{\xi}_d$ et indépendant de g_o , le modèle cinématique sous les contraintes des contacts réalise une connexion cinématique principale sur le fibré principal \mathcal{C}_2 , i.e. une version continue des connexions discrètes étudiées en mécanique des systèmes non-holonomes [8].

²sous peine d'interdire la mobilité et par hyperstatisme de produire des tensions internes résolues en remplaçant les contraintes induites par les liaisons internes supposées parfaites, par des lois de comportement passives.

8.17 Exemples illustratifs

8.17.1 Ver fousseur en 1D

C'est un robot fousseur inspiré des lombrics. Le lombric est supposé de masse volumique homogène ρ . Partant des connaissances biologiques, c'est la dilatation radiale des sections provoquée par la compression axiale qui assure l'ancrage sur le milieu: un tunnel creusé par digestion préalable de la terre en amont de la tête. Localement, l'ancrage radiale est réalisé par des soies rigides qui s'encastrent radialement dans la terre lorsque la dilatation de la section est maximale (cf. figure). Le modèle de poutre est celui d'une barre en traction-compression. L'allure d'avance est réalisée par une onde rétrograde de traction-compression de la forme:

$$\Gamma_{dX}(X, t) = 1 + \epsilon \sin\left(\frac{2\pi}{\lambda}(ct - X)\right), \quad (8.83)$$

la dilatation (striction) des sections est contrôlée par la traction en ajoutant à la théorie Cosserat précédemment exposée la contrainte de préservation du volume qui s'écrit:

$$A(X, t) = A(X, 0)/\Gamma_{dX}(X, t), \quad (8.84)$$

que l'on déduit simplement de: $A(X, t)dS = A(X, 0)dX$ où $A(X, t)$ est l'aire de la section X à l'instant t , tandis que $dS = \Gamma_{dX}dX$ est la longueur à t courant du tronçon de ver de longueur initiale dX situé en X .

Dans ce cas de figure, la construction générale s'applique en remplaçant G (ainsi que \mathfrak{g} et \mathfrak{g}^*) par \mathbb{R} identifié au sous groupe des translations le long de l'axe des x (ainsi que its Lie algebra and its dual). Il s'en suit que les applications adjointes disparaissent des expressions tandis que l'on pose plus simplement $g = x$, $g_o = x_o$, $\eta = \dot{x}$, $\xi_d = \Gamma_{dX}$, $\bar{F} = \sum_{i=1}^{i=p} N_{c_i} \delta(X - C_i(t))$, $\Lambda = N$ où les C_i dénotent les abscisses matérielles des p points d'ancrage définies à chaque instant par la condition de contraction locale maximale:

$$C_i(t) \in [0, l], \text{ tel que: } \Gamma_{dX}(C_i(t), t) = 1 - \epsilon. \quad (8.85)$$

Avec ces considérations, le modèle cinématique continu prends la forme (8.71) avec:

$$\mathcal{X}'_1 = (x', \dot{x}', \ddot{x}')^T = (\Gamma_{dX}(t), \dot{\Gamma}_{dX}(t), \ddot{\Gamma}_{dX}(t))^T, \quad (8.86)$$

dont les intégrale en espace vont être fixées (cf. à suivre) par les points d'ancrage. En particulier, remarquons que chaque section ancrée (anchored section] au sol par ses soies, impose une contrainte au mouvement dans la fibre ici identifiée à \mathbb{R} . Il s'en suit que les mouvements externes se déduisent d'un modèle cinématique. Un tel modèle se déduit simplement en imposant qu'en n'importe quel point d'ancrage $C_i(t)$, la vitesse de glisse-

ment est nulle, i.e. $C_i(t)$ réalise un point d'ancrage glissant. Aussi, en invoquant (8.78) avec $C(t) = C_i(t)$, $\eta(C(t)) = \dot{x}(C_i(t))$, $\xi_d(t) = \Gamma_{dX}(t)$ et $\eta_c(t) = 0$, les obstacles étant fixes, il vient:

$$\dot{x}(C_i(t)) + (1 - \epsilon)c(t) = 0. \quad (8.87)$$

De sorte qu'en tirant de la seconde des lignes de (8.86) la vitesse de la section d'abscisse $C_i(t)$, on trouve:

$$\dot{x}(C_i(t)) = \dot{x}_o + \int_0^{C_i(t)} \dot{\Gamma}_{dX} dX, \quad (8.88)$$

que l'on injecte dans (8.87) pour trouver le modèle cinématique du ver:

$$\dot{x}_o(t) = - \int_0^{C_1(t)} \dot{\Gamma}_{dX} dX - (1 - \epsilon)c(t). \quad (8.89)$$

Qui plus est, on montre aisément que pour la loi de propagation (8.83), (8.89) est indépendante du point d'ancrage considéré. En particulier, \dot{C}_i n'est autre que la célérité c de l'onde de contraction de sorte que la cinématique externe se réécrit plus simplement après dérivation par rapport au temps:

$$\ddot{x}_o = -\Gamma_{dX}(C_1(t))\dot{c} - \dot{\Gamma}_{dX}(C_1(t))c - \int_0^{C_1(t)} \ddot{\Gamma}_{dX} dX, \quad (8.90)$$

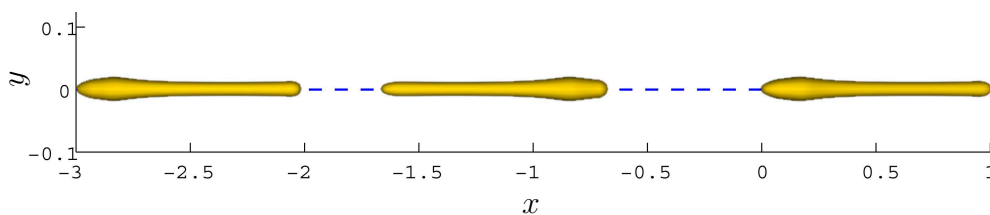
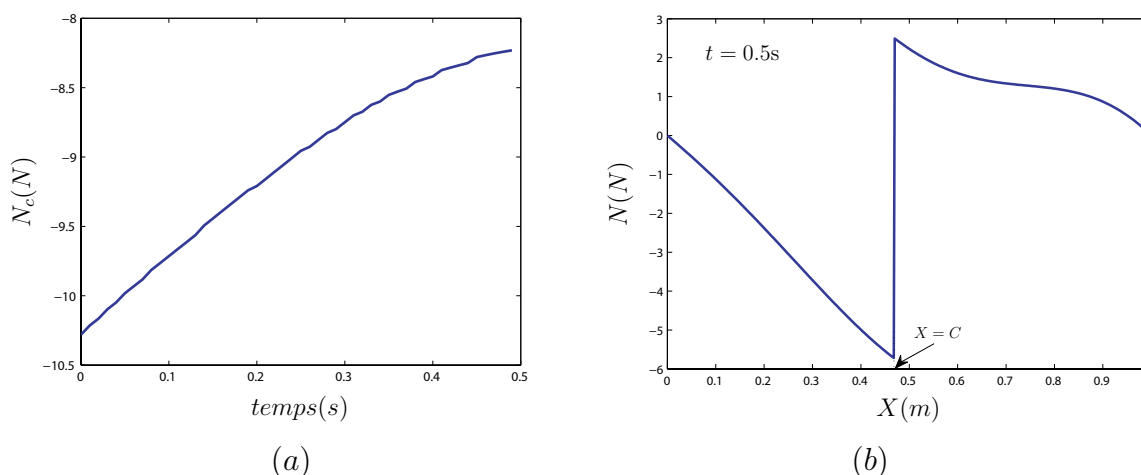
équation qui permet de calculer \ddot{x}_o . Ceci fait, il devient possible grâce à la dynamique externe (8.82) de calculer la résultante des forces de réaction transmises par l'environnement au ver via les points d'ancrage:

$$N_c = \sum_{i=1}^{i=p} N_{c_i} = \int_0^l m(X, t) dX \ddot{x}_o - \int_0^l m(X, t) \int_0^X \ddot{\Gamma}_{dX} d\chi dX \quad (8.91)$$

où le ζ de la construction générale a été calculé par intégration du modèle continu des accélérations initialisé en espace par $\ddot{x} = 0$. Finalement, la sous-détermination des efforts de réaction ne permet pas d'intégrer la dynamique interne. En revanche si l'on se fixe une répartition arbitraire de ces efforts de sorte que leur résultante vérifie (8.91), par exemple une équi-répartition, i.e. $N_{c_i} = N_c/p$, alors il devient possible d'intégrer (8.62) qui s'écrit ici, en remplaçant $\mathcal{M}(X)$ par $m(X, t)$, masse linéique de la poutre-ver:

$$N' = m(X, t)\ddot{x} - \sum_{i=1}^{i=p} N_{c_i} \delta(X - C_i(t)) \quad (8.92)$$

avec les conditions aux limites: $N(0) = N(l) = 0$ si l'on suppose que le milieu n'oppose aucune force au front du ver (l'ingestion et l'excretion déplaçant la matière du sol d'avant

Figure 8.8 – La locomotion du ver dans le plan xy Figure 8.9 – Avec c variable: (a) les forces externes de reaction N_c ; (b) les forces internes N

en arriere), et où \ddot{x} est déduit par intégration du modèle cinématique (8.86) initialisé en espace par: $(x_o, \dot{x}_o, \ddot{x}_o)$.

Application numérique: pour l'illustration numérique de la locomotion dynamique du ver, une allure du type (8.83) avec $\epsilon = 0,004$ et $\lambda = 1$, est introduit dans l'algorithme général appliqué au ver. Simuler pour 10s, on obtient le mouvement 1D du ver dans le plan xy comme indiqué dans la Fig. 8.8. Par ailleurs, en introduisant la vitesse de propagation $c(t) = at + b$ (avec $a \neq 0$), il est noté que, en raison de l'accélération du ver, les efforts de réaction axiale (N_c) à $X = C$ ne sont pas nul, comme indiqué dans la Fig. 8.9(a), et donc introduit un saut sur les efforts interne de commande à $X = C$. Ceci apparaît sur la Fig. 8.9(b) qui donne le profil des efforts interne de commande appliquées entre des sections sur toute la longueur.

8.17.2 Chenille arpenteuse en 2D

Une poutre actionnée en flexion avec un encastrement ponctuel alternant d'une extrémité à l'autre à "chaque pas". C'est un robot grimpeur. Un tel robot continu peut être modélisé par une poutre plane de Kirchhoff actionnée en coubure, i.e. en invoquant la construction générale précédente avec $SE(2)$ à la place de G et ξ_d remplacé par $(1, 0, K_{dZ})$ qui dans ce cas est une variable intégrable puisque $K_{dZ} = \theta'$ où θ est l'angle qui paramètre l'orientation

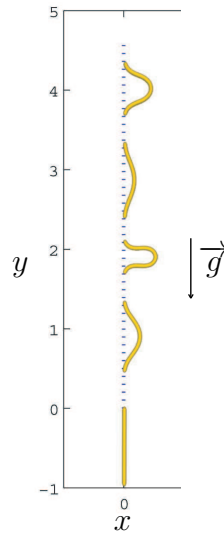


Figure 8.10 – La locomotion de la chenille dans le plan xy plane

des sections dans le plan. Ceci dit, la locomotion de la chenille peut être modélisée en la considérant comme un manipulateur dont la base et l'extrémité s'échangent à chaque demi période de l'allure. Dans ces conditions, l'algorithme précédent (avec point d'ancrage fixe en $X = 0$) peut être reconduit en changeant X en $l - X$ dans les o.d.e. en espace, et ce à chaque demi-période telle que $C = l$. L'allure peut être simplement définie par l'angle θ comme:

$$\theta(X, t) = \alpha \sin^2(\omega t) \sin\left(\frac{2\pi}{l}(X - l)\right), \quad (8.93)$$

dont on déduit, la loi de courbure:

$$K_{dZ}(X, t) = \alpha \sin^2(\omega t) \left(\frac{2\pi}{l}\right) \cos\left(\frac{2\pi}{l}(X - l)\right). \quad (8.94)$$

Cette loi assure qu'à tout instant, on a: $\theta(t, X = 0) = \theta(t, X = l) = \theta(t, X = l/2) = 0$ alors que la courbure est minimale en les deux extrémités et maximale en $X = l/2$. Finalement, la fonction du temps en facteur de cette fonction de forme assure la détente et la flexion périodique du robot. Sa période est π/ω et elle garantit l'amplification de la déflexion sur une demi-période et son atténuation (jusqu'à 0), la demi période suivante. Ainsi, en supposant que la chenille part à $t = 0$ en position étendue, on aura ancrage en $X = 0$ sur tous les intervalles $[kT, kT + T/2]$ et ancrage en $X = l$ sur les intervalles $[kT + T/2, (k + 1)T]$. Dans les deux cas, les mouvements externes sont nuls puisque fixés par les conditions d'ancrage: $\mathcal{X}_1(C) = (1, 0, 0)$, tandis que la dynamique externe permet de calculer le torseur de réaction au point d'ancrage et que la dynamique interne s'intègre sans difficulté (on a $\zeta = \dot{\eta}$ dans ce cas) pour donner les torseurs internes.

Application numérique: Quelques résultats numériques sont obtenus pour la chenille

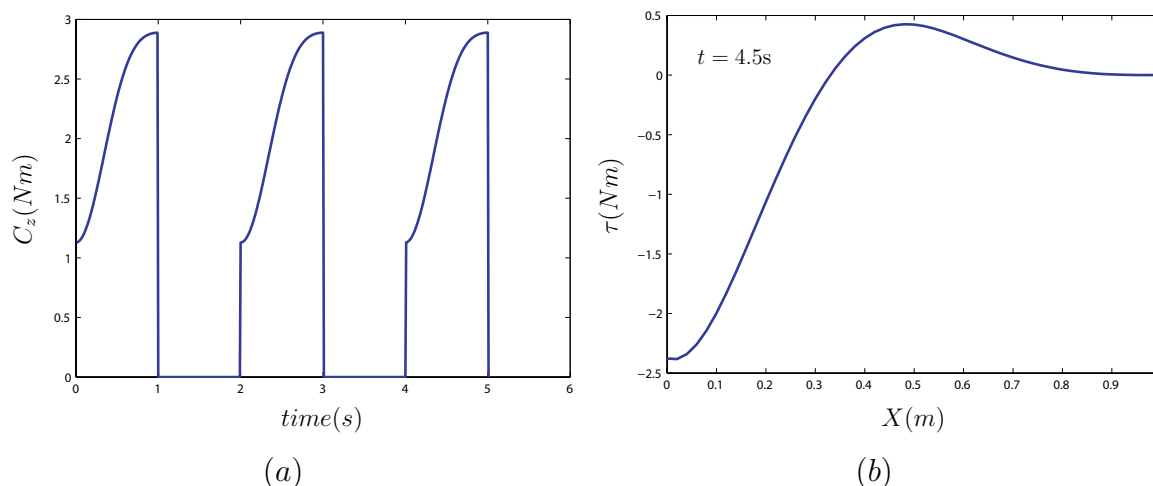


Figure 8.11 – (a) Couple de reaction externe à la tête; (b) les couples internes

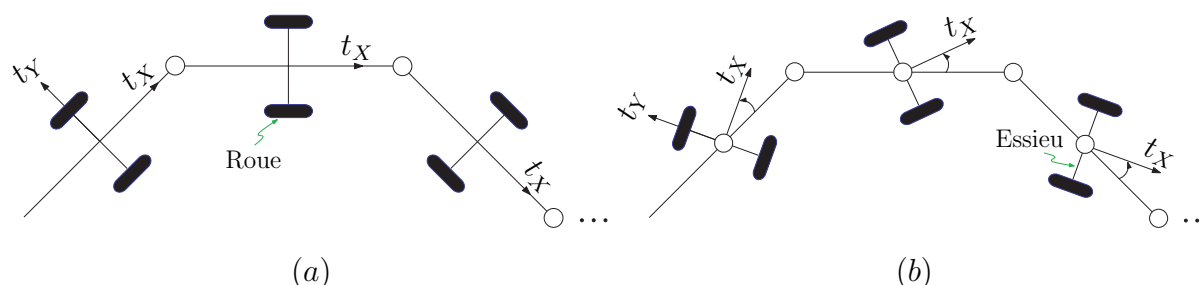


Figure 8.12 – (a) Serpent-Kirchhoff discret; (b) Serpent-Reissner discret

d'escalade dans la gravité en appliquant la courbure (8.94) comme entrée, avec $\alpha = 1.8$ et $\omega = 2\pi 0.25$. Simuler pour 14sec, on obtient le mouvement de la chenille dans le plan xy , comme indiqué dans la Fig. 8.10. La dynamique inverse de la locomotion et la dynamique inverse internes du système sont résolus pour obtenir les efforts de réaction au niveau des points d'ancrage et les couples de contrôle interne, respectivement. La Fig. 8.11(a) montre la réaction du couple $C_Z(X = 0)$, tandis que la répartition du couple sur toute la longueur est présenté dans la Fig. 8.11(b) à $t = 4.5$ s.

8.17.3 Serpent 2D en ondulation latérale

On considère un serpent en ondulation latérale. Le serpent est modélisé par une cinématique de poutre de type Kirchhoff ou alternativement Reissner en 2D dont les pendents discrets sont dessinées dans la Fig. 8.12. Ici, nous opterons pour le premier choix puisque c'est le plus simple et qu'il correspond aux robots de S. Hirose tandis que le second, tels que proposé par J. Ostrowsky, bien que plus complexe, a des avantages que nous évoquerons ultérieurement. Dans le cas de l'ondulation latérale, le serpent s'appuie latéralement sur son environnement pour se propulser dans le sens axial, i.e. en se déplaçant le long de

son axe vertébrale. Mathématiquement, ces appuis sont modélisés par des contraintes non-holonomes interdisant aux sections du serpent de dérapier latéralement. Ces contraintes sont en nombre suffisant pour que les déplacements externes soient entièrement fixés par la cinématique interne du serpent. Afin d'établir ce modèle cinématique, commençons par écrire le modèle cinématique des vitesses (8.56) dans le cas de $G = SE(2)$ et $\xi_d(t) = (1, 0, K_{dZ})$. Il vient avec $\eta = (g^{-1}\dot{g})^\vee = (V_X, V_Y, \Omega_Z)^T$:

$$\begin{pmatrix} V'_X \\ V'_Y \\ \Omega'_Z \end{pmatrix} = \begin{pmatrix} V_Y K_{dZ} \\ \Omega_Z - V_X K_{dZ} \\ \dot{K}_{dZ} \end{pmatrix}. \quad (8.95)$$

En modélisant le contact en chaque point X par un contact annulaire planaire, les contraintes s'écrivent simplement $V_Y(X) = 0$, pour $\forall X \in [0, l]$ (les obstacles étant fixes). A présent, en forçant ces contraintes (de non dérapage) dans (8.95), on trouve les relations que doit vérifier n'importe quelle allure compatible avec les contacts:

$$\begin{pmatrix} V'_X \\ \Omega_Z \\ \Omega'_Z \end{pmatrix} = \begin{pmatrix} 0 \\ V_X K_{dZ} \\ \dot{K}_{dZ} \end{pmatrix}. \quad (8.96)$$

De la première ligne de (8.96), on tire que la vitesse axiale du serpent est constante par rapport à X et égale donc à celle de sa tête que l'on notera plus simplement V_o . De la seconde, on tire que $\Omega_Z = V_o K_{dZ}$, i.e. que la vitesse angulaire le long de la colonne vertébrale du serpent est réglée par la vitesse d'avance et la courbure du corps. Enfin, tenant compte des lignes 1 et 2 dans la troisième, on obtient la relation fondamentale:

$$\dot{K}_{dZ} = V_o K'_{dZ}, \quad (8.97)$$

qui doit être vérifiée le long de tout le serpent pour que sa mobilité (propulsion axiale) soit garantie. Finalement, la solution de l'équation (8.97) prend une forme générale suivante:

$$K_{dZ}(X, t) = f\left(X + \int_0^t V_o(\tau) d\tau\right), \quad (8.98)$$

ce qui correspond à la propagation d'un profil de courbure donnée le long du colonne vertébrale généralement à vitesse variable par rapport aux temps $V_o(t)$. Il s'en suit qu'un tel choix de la loi de courbure garantie l'avance du serpent dans le sens de $-t_X(0)$ à la vitesse constante V_o . Qui plus est, on a dans ces conditions d'allures, et pour tout

$X \in [0, l]$:

$$\eta(X, t) = \begin{pmatrix} V_o \\ 0 \\ \Omega_Z(X) \end{pmatrix} = \begin{pmatrix} 1/K'_{dZ} \\ 0 \\ K_{dZ}/K'_{dZ} \end{pmatrix} (X)\dot{K}_{dZ}(X, t), \quad (8.99)$$

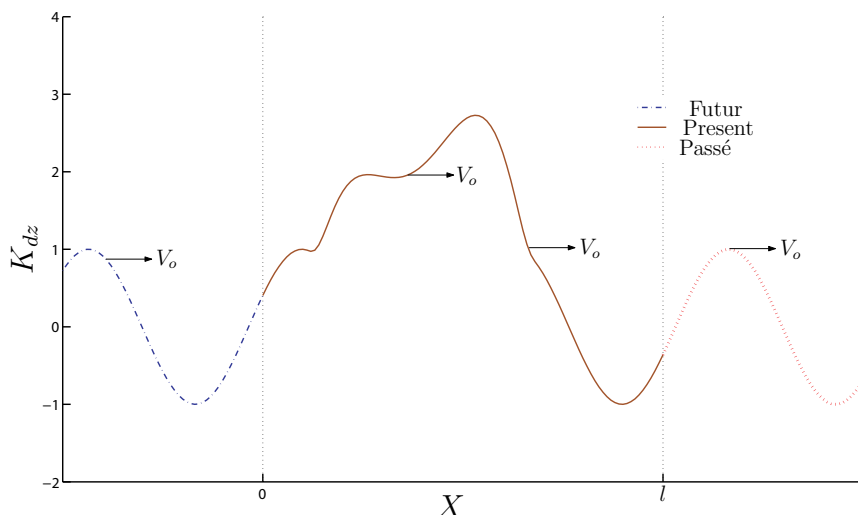
et, en particulier, pour $X = 0$ (et en indiquant d'un zéro toute fonction évaluée en $X = 0$):

$$\eta_o(t) = \begin{pmatrix} V_o \\ 0 \\ \Omega_o \end{pmatrix} = \begin{pmatrix} 1/K'_o \\ 0 \\ K_o/K'_o \end{pmatrix} \dot{K}_o. \quad (8.100)$$

Où l'on retrouve la connexion du cas discret qui encode l'allure follower-leader des serpents en ondulation latérale. En particulier, notons que de même que dans le cas discret les trois premiers essieux (partant de la tête) fixent complètement les mouvements de la tête et ceux des segments qui les suivent, dans le cas continu, la connexion (8.100) fait intervenir au maximum la dérivée troisième du champ de position (i.e. $K_{dZ}(0)' = p'''(0)$). Qui plus est, une fois spécifiée la courbure et sa dérivée en $\forall X$, la vitesse de courbure doit s'adapter en chaque X pour que la section $X - dX$ suive la section X à la vitesse V_o . Ainsi, toute section X réoccupera à t^* tel que $\int_t^{t^*} V_o d\tau = X$, la même configuration que celle occupée par la tête à t . Ceci explique cette impression de statisme latérale et de mouvement axial observé chez les serpents qui apparente leur mouvement à celui d'une ligne fluide en écoulement stationnaire. Qui plus est, (8.100) montre que si la propulsion axiale est assurée par \dot{K}_o/K'_o , c'est K_o qui guide le serpent en virage. Ainsi, si l'on rapproche par analogie le serpent 2D avec un autre système non-holonyme, plus familier du roboticien: la voiture. Dans ce cas, le guidage angulaire des roues avants est assuré par K_o tandis que la propulsion produite par leur motorisation est assurée par le rapport \dot{K}_o/K'_o . Revenant à la biologie, dans la nature la courbure le long du corps d'un serpent évolue au grès des choix réalisés par sa tête, choix qui dépendent des obstacles que le serpent contourne et sur lesquels il s'appuie pour se propulser en avant. Comme montré dans la Fig. 8.13, ce contexte peut être figuré par la donnée d'un profil de courbure stationnaire défilant à la vitesse $V_o(t)$ devant le corps du serpent ici représenté par le segment matériel $[0, l]$. Finalement, pour les environnements sans obstacles mais où le sol plan présente des bonnes propriétés pour interdire le dérapage latéral, la loi de courbure:

$$K_{dZ}(X, t) = A \cos\left(\frac{2\pi}{\lambda}(X + V_o t)\right) + b \exp\left(-\frac{(t - (t_o + T_o/2) + (X/V_o))^2}{(t - (t_o + T_o/2) + (X/V_o))^2 - (T_o/2)^2}\right), \quad (8.101)$$

garantie jusqu'à $t = t_o$ une propulsion axiale de vitesse V_o de direction moyenne constante, puis génère un virage à partir de $t = t_o$ d'une durée T_o . Enfin, notons que cette cinématique

Figure 8.13 – *Profile de courbure du serpent*

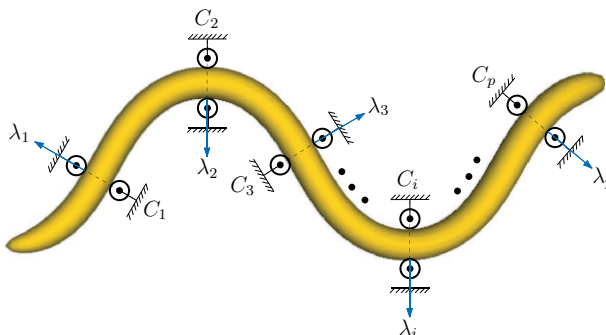
est singulière lorsque $K'_{dz} = 0$ puisque dans ce cas, la conditions de mobilité (8.97) n'est pas vérifiée. Pour dépasser cette situation, on peut considérer l'homologue continu de la cinématique discrete de la Fig. 8.12(b), i.e. ajouter un cisaillement transverse au contexte présent. Dans ce cas, la cinématique est celle d'une poutre de Reissner plane et le modèle continu des vitesses se réécrit comme (8.95) en y remplaçant la première ligne par la suivante:

$$V'_X = -K_{dz} V_X \Gamma_{dY}, \quad (8.102)$$

de sorte que l'on a à présent $V_X(X) = V_o e^{(-\int_0^X K_{dz} \Gamma_{dY} dX)}$ et que la condition de mobilité (8.97) se change en la suivante:

$$\dot{K}_{dz} = (K'_{dz} - K_{dz}^2 \Gamma_{dY}) V_X, \quad (8.103)$$

où la présence de la commande Γ_{dY} en facteur de K_{dz} garantie la mobilité du serpent dans tous les cas où $K_{dz}(\cdot) \neq 0$. Ainsi, on retrouve que la cinématique discrète de la Fig. 8.12(b) n'est singulière que pour les configurations droites puisque ce n'est que dans ce cas que les mouvements internes des articulations pairs et impaires ne peuvent produire de mouvement externe. Finalement, dans le cas des serpents, le cisaillement transverse modélise les mouvements relatifs de la peau et des écailles par rapport au squelette dont le mouvement propre est modélisé par le champ de courbure. Et si d'aventure, un serpent se retrouvait en configuration parfaitement droite alors le serpent peut, pour sortir de cette singularité: 1) glisser latéralement, 2) décoller du sol, tandis que, si ces deux possibilités sont proscrites (le serpent est par exemple contraint de passer dans un tuyau droit), alors seul un mode de locomotion du type de celui étudié pour le ver en traction-compression devient possible. Finalement, du côté des mouvements l'algorithme se réduit

Figure 8.14 – Serpent 2D avec p contacts annulaires

à l'intégration de (8.81) qui s'écrit ici, tenant compte de (8.100), comme le système dans SE(2):

$$\dot{g}_o = g_o \hat{\eta}_o = g_o \cdot \begin{pmatrix} 1/K'_o \\ 0 \\ K_o/K'_o \end{pmatrix}^\wedge \dot{K}_o. \quad (8.104)$$

Du côté des efforts, l'algorithme intègre à chaque pas de temps t , le système (8.74) de $X = 0$ à $X = l$ initialisé en espace par $(g_o(t), \eta_o(t), 0, 0, 0)$. Puis, connaissant $\dot{\eta}_o(t)$ par l'expression de la dérivée temporelle de (8.100) calculée en t , l'algorithme calcule via (8.82) la résultante des torseurs de contact ramenés à la tête: F_c . Connaissant cette résultante, il nous faut faire alors une hypothèse sur la répartition des efforts de contact pour connaître la distribution des forces internes. Par exemple, si l'on suppose que le serpent est en permanence en contact avec le sol au travers de p contacts annulaires dont la position est fixé dans l'espace ambiant (Fig. 8.14), le chargement est généralement hyper-statique (si $p > 3$) et la distribution des efforts de réaction $\lambda_{i=1,2,\dots,p}$ est donnée par inversion généralisé d'un système suivant:

$$F_c = \sum_{i=1}^{i=p} Ad_{k(C_i)}^* \begin{pmatrix} 0 \\ \lambda_i \\ 0 \end{pmatrix} \quad (8.105)$$

où rappelons le $k(C_i) = g^{-1}(C_i) \cdot g_o(t)$, et où l'on a supposé que les trois points de contacts $C_{1,2,3}$ sont contenus dans $]0, l[$ (Fig. 8.14). Une fois ces trois efforts connus, l'algorithme peut intégrer la dynamique interne (8.72) avec comme conditions initiales en espace $(g_o(t), \eta_o(t), \dot{\eta}_o(t), 0)$ et comme distribution d'efforts externes: $\bar{F} = \sum_{i=1}^p (0, \lambda_i, 0)^T \delta(X - C_i)$.

Application numérique: dans le cas du serpent 2D, une courbure ondulatoire de la forme (8.101) est imposée en entrée de l'algorithme. L'ondulation est fourni avec $b \neq 0$ pour certaine période de temps T_o qui quantifie l'amplitude d'une manoeuvre de virage

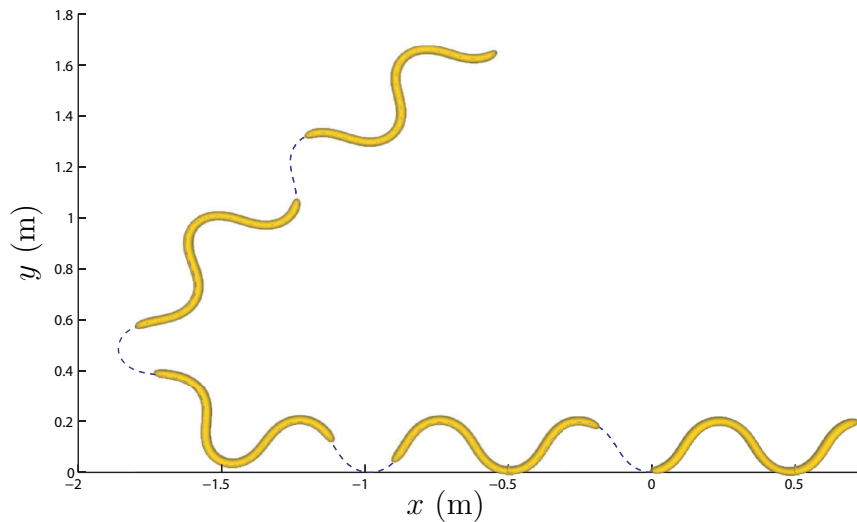


Figure 8.15 – Le mouvement du serpent 2D avec le virage dans un plan xy

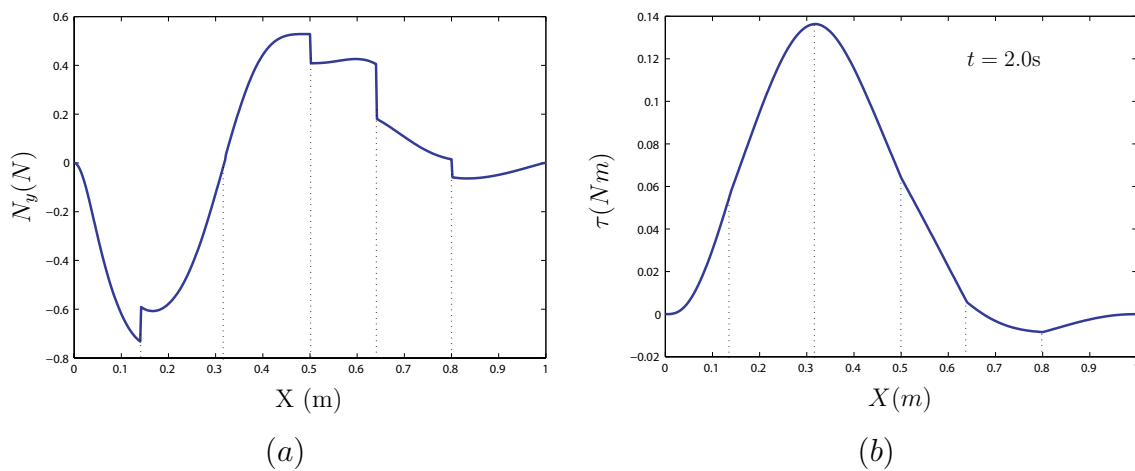


Figure 8.16 – (a) Forces de contact (N_y); (b) les couples internes

en $SE(2)$, où $A = 10$, $\lambda = 1.5$ et $V_o = -0.5m/s$. Simuler pour $10s$, le mouvement 2D du serpent dans le plan xy est indiqué dans la Fig. 8.15.

Par ailleurs, la dynamique interne et de la locomotion du système sont résolues pour $p = 5$ pour obtenir les efforts de réaction appliqués aux points de contact C_1, C_2, \dots, C_5 et les couples de contrôle interne, respectivement. La Fig. 8.16(a) trace les efforts de réaction (N_y), tandis que la Fig. 8.16(b) montre la répartition du couple sur toute la longueur du serpent à $t = 2.0s$.

8.18 Conclusions

Cette thèse contribue au domaine en plein expansion des robots locomoteurs. Dans cette thèse, en utilisant des techniques de la mécanique géométrique appliquée à la locomotion, nous avons développé un cadre unifié adapté aux problèmes posés par la locomotion. Les

algorithmes ont été développés à la fois pour les systèmes multicorps discrets et continus. Dans les deux cas, nous avons proposé un algorithme capable de calculer les inconnues suivantes grâce à des données connues des mouvements internes imposées:

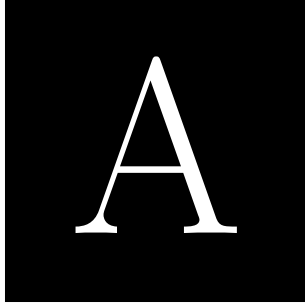
1. les mouvements externes du corps de référence du système,
2. les couples/forces internes du système.

Par ailleurs, l'approche de modélisation utilise la formulation de Newton-Euler. La nature récursive de la formulation de Newton-Euler nous a permis d'étendre nos investigations aux systèmes continus.

Dans la première partie de cette thèse, l'algorithme de Luh et Walker pour les manipulateurs a été étendu à une plus large classe de systèmes de la locomotion où le problème supplémentaire de calcul des mouvements externes du système est résolu. Ce nouveau cadre unifié a ensuite été utilisé pour une analyse approfondie de certains systèmes existants constitués de corps munis de roues, tels que le snakeboard, les robots serpents à roues passives, etc, où l'algorithme a montré sa généralité pour résoudre un large éventail de systèmes multicorps. En fait, ce cadre basé sur la formulation de Newton-Euler couvre un large éventail de problèmes de modélisation de la locomotion jusqu'alors résolus par l'approche lagrangienne. À cet égard, nous dirions que le cadre proposé a fourni un homologue du modèle dynamique lagrangien proposée par les mécaniciens géométriques [87, 60, 76]. Par ailleurs, une analyse en profondeur des modèles mathématiques nous a permis de répertorier les modèles de locomotion en apparence différents dans des même classes. Ces aspects sont utiles à une meilleure compréhension et analyse des cas particuliers de la locomotion. D'un point de vue algorithmique, il est remarquable que, malgré son application à une large gamme de systèmes, l'algorithme proposé conserve la même structure. Par ailleurs, l'algorithme final est très facile à mettre en oeuvre et la complexité du mécanisme initial n'a aucun effet sur sa mise en oeuvre puisque, grâce à son caractère récursif, l'ajout de plus en plus de corps augmente simplement les indices des récurrences sans changer la structure des programmes.

Dans la seconde partie de cette thèse, nous avons proposé un cadre général pour la modélisation d'une classe de robots continus à l'échelle macroscopique. La solution se révèle être une contrepartie continue de la dynamique de Newton-Euler des systèmes multicorps discrets tel que proposée dans la première partie de cette thèse. Dans cette approche de la modélisation continue, le robot a été considéré comme une poutre Cosserat actionné via des mouvements internes imposés. Une fois intégrés dans le cadre de la théorie de la locomotion sur les fibrés principaux, l'approche est exploitée pour dériver un algorithme capable de calculer les couples ainsi que les mouvements externes impliqués dans les tâches de locomotion. L'approche dans son ensemble a ensuite été appliquée au cas de la locomotion au sol où le modèle des forces externes est remplacé par les contraintes cinématique

holonome et/ou non-holonomes d'un ensemble de modèles de contact jouant un rôle pratique dans la locomotion terrestre. Enfin, pour montrer son application, l'algorithme a été ensuite appliqué à plusieurs exemples inspirés par la nature. A travers ces exemples, l'algorithme montre qu'il peut être un outil utile d'investigation quand il est appliqué à des problèmes tels que l'analyse de la mobilité ou la générations d'allure. Dans le cas du ver de terre, l'hypothèse Cosserat des sections rigides a été supprimée au profit d'une contrainte de conservation du volume axiale. Ceci permet à moindre frais pour le modélisateur d'étendre l'approche et l'algorithme au hydrostats uni-dimensionnels. Le problème de la manipulation est illustré indirectement par l'exemple de la chenille arpenreuse où à chaque étape de la "marche", le robot est un manipulateur continue ancré dans le sol.



Appendix A

A.1	Extension of the Luh and Walker Algorithm to Closed Loop Kinematics	217
A.2	Covariants	218
A.3	3D Snake: Compatibility Condition	219

A.1 Extension of the Luh and Walker Algorithm to Closed Loop Kinematics

The goal of this section is to briefly recall how it is possible to extend the proposed algorithm to the case of a mobile multibody system with closed loop kinematics. For this purpose, we first have to (virtually) cut all the eventual loops at the level of a passive joint in order to obtain a tree-like structure of the type studied till now. Then, the vector of the joint angles, denoted as r , of this tree-like structure is block-partitioned into active and passive joints as $r = \begin{pmatrix} r_a^T & r_p^T \end{pmatrix}^T$ (where a stands for "active" and p stands for "passive"). On the dual side, $\tau = \begin{pmatrix} \tau_a^T & \tau_p^T \end{pmatrix}^T$ corresponds to the block-partition of the joint torques vector of the tree-like structure. With these conventions, the constraints forced by the connection at the cut levels can be easily put in the following form:

$$\begin{pmatrix} W_a & W_p \end{pmatrix} \begin{pmatrix} \dot{r}_a \\ \dot{r}_p \end{pmatrix} = 0 \tag{A.1}$$

where $\begin{pmatrix} W_a & W_p \end{pmatrix}$ is the Jacobian matrix of the geometric constraints imposed by the loop closures at the cut levels. Now, invoking temporarily the Lagrange equations of the structure, we have:

$$\begin{pmatrix} \tau_a \\ \tau_p \end{pmatrix} = \frac{d}{dt} \begin{pmatrix} \frac{\partial L}{\partial \dot{r}} \end{pmatrix} - \frac{\partial L}{\partial r} + \begin{pmatrix} W_a^T \\ W_p^T \end{pmatrix} \lambda, \tag{A.2}$$

where from left to right, we find the torque vector of the closed loop structure, the torque vector (given by the Lagrange operator term) of the tree-like structure moving with the same motion, and finally the constraint joint torque vector forced by the closure constraints of the loops. Now, let us remark that since $\tau_p = 0$, the vector of Lagrange multipliers λ can be detailed as:

$$\lambda = -W_p^{-T} \tau_{p,\text{tree}} \quad (\text{A.3})$$

where we decide to denote $\frac{d}{dt} \left(\frac{\partial L}{\partial \dot{r}} \right) - \frac{\partial L}{\partial r} = (\tau_{a,\text{tree}}^T, \tau_{p,\text{tree}}^T)^T$ the torque vector of the tree-like structure animated by the same motions as the closed one. Then, inserting (A.3) into (A.2) gives the torque vector of a structure with closed loops:

$$\tau_a = \tau_{a,\text{tree}} - (W_a^T W_p^{-T}) \tau_{p,\text{tree}} \quad (\text{A.4})$$

where W_p^T is necessarily an invertible square matrix in order to preserve the mobility of the loops kinematics. Finally, we now have at our disposal all the material required by the extension of the Luh algorithm from tree-like to closed kinematics. In fact, from (A.1) one can compute the time evolution of the passive joints from that of the active ones which is specified as an input of the algorithm and thus obtain the complete time evolution of r, \dot{r} and \ddot{r} . These motions are used as inputs of the standard algorithm of tree-like structures in order to compute $(\tau_{a,\text{tree}}^T, \tau_{p,\text{tree}}^T)^T$. Finally, invoking (A.4) allows the motor torques of any structures containing kinematic loops to be calculated.

A.2 Covariants

If the reduced base of \mathcal{V}_j is orthonormed for the Euclidean metric of \mathbb{R}^6 , then the covariant reduced components of F_j and their associative contravariant reduced components of η_j transform identically. To prove this, let us consider a vector \vec{u} in a two dimensional oblique rectilinear coordinate system. Using Einstein notation, the contravariant and covariant components of the vector \vec{u} are given as follows:

$$\begin{aligned} \vec{u} &= u^1 \vec{g}_1 + u^2 \vec{g}_2, \\ u_1 &= \vec{u} \cdot \vec{g}_1, \quad u_2 = \vec{u} \cdot \vec{g}_2. \end{aligned} \quad (\text{A.5})$$

Where the u^1 and u^2 are called contravariant components while u_1 and u_2 are called covariant components. Furthermore, vectors are called contravariant vectors because both transforms in the same way with the changes in basis, and covectors are called covariant vectors for the same reason. It is worth noting that both contravariant vectors and covariant vectors transform differently with the changes in basis (from (\vec{g}_1, \vec{g}_2) to (\vec{g}'_1, \vec{g}'_2))

as expressed below:

$$\begin{aligned} \begin{pmatrix} u^1 \\ u^2 \end{pmatrix} &= (H) \begin{pmatrix} u'^1 \\ u'^2 \end{pmatrix}, \\ \begin{pmatrix} u_1 \\ u_2 \end{pmatrix} &= (H^{-1})^T \begin{pmatrix} u'_1 \\ u'_2 \end{pmatrix}. \end{aligned} \quad (\text{A.6})$$

Thus we conclude that covariant and contravariant vectors transform identically if and only if the basis are orthonormal. Consequently, we say that $H = (H^{-1})^T$, or in other words we say that H is an orthogonal matrix i.e. $HH^T = 1$. Since, in this article, the reduced base of \mathcal{V}_j is orthonormal, thus if the velocity vector (contravariant vector) transforms in the following way:

$$\eta_j = H_j \eta_{rj}, \quad (\text{A.7})$$

then the force vector (covariant vector) transforms identically as follows:

$$F_j = H_j F_{rj}, \quad (\text{A.8})$$

hence proved.

A.3 3D Snake: Compatibility Condition

As from equation (6.48), for $X = 0$ we have:

$$V_o = \frac{\dot{K}_{oY}}{K'_{oY}} = \frac{\dot{K}_{oZ}}{K'_{oZ}}. \quad (\text{A.9})$$

The modulus of the strain field is given by:

$$\| K_o \| = \sqrt{(K_{oY})^2 + (K_{oZ})^2}.$$

First, taking the derivative of above relation with respect to X and t , respectively, gives the following two relations:

$$\frac{\partial}{\partial X} \| K_o \| = \frac{K'_{oY} K_{oY} + K'_{oZ} K_{oZ}}{\| K_o \|},$$

$$\frac{\partial}{\partial t} \| K_o \| = \frac{\dot{K}_{oY} K_{oY} + \dot{K}_{oZ} K_{oZ}}{\| K_o \|}.$$

Finally, their ratio is given by:

$$\frac{\frac{\partial}{\partial t} \| K_o \|}{\frac{\partial}{\partial X} \| K_o \|} = \frac{\dot{K}_{oY} K_{oY} + \dot{K}_{oZ} K_{oZ}}{K'_{oY} K_{oY} + K'_{oZ} K_{oZ}}.$$

Now taking into account equation (A.9), we have:

$$\frac{\frac{\partial}{\partial t} \| K_o \|}{\frac{\partial}{\partial X} \| K_o \|} = \frac{V_o K'_{oY} K_{oY} + V_o K'_{oZ} K_{oZ}}{K'_{oY} K_{oY} + K'_{oZ} K_{oZ}},$$

which implies that:

$$\frac{\frac{\partial}{\partial t} \| K_o \|}{\frac{\partial}{\partial X} \| K_o \|} = V_o \left(\frac{K'_{oY} K_{oY} + K'_{oZ} K_{oZ}}{K'_{oY} K_{oY} + K'_{oZ} K_{oZ}} \right).$$

Finally, we have:

$$\frac{\frac{\partial}{\partial t} \| K_o \|}{\frac{\partial}{\partial X} \| K_o \|} = V_o,$$

which verifies the compatibility condition for 3D snake.



Fundamentals of Lie Group Theory

B.1 Lie Group	221
B.1.1 Lie Algebra	222
B.2 Adjoint Operators	223
B.2.1 Action Mapping of a Lie Group	223
B.2.2 Action Mapping of a Lie Algebra	224
B.3 Lie Group in 2D Space (G=SE(2))	224

B.1 Lie Group

The Lie group G is a set of elements or objects, called transformations denoted by g , which satisfies the properties of both a group and a smooth manifold. Due to the geometric structure of manifold, any g can be localized in a set of smooth charts (atlas) on G . The Lie group G is called a group because it satisfies the following algebraic properties:

1. Closure/composition property: if $g_1, g_2 \in G$, then $g_1g_2 \in G$
2. Identity: there exists an identity element, e , such that $ge = eg = g$ for every $g \in G$
3. Inverse: for any element $g \in G$, there exists an inverse, $g^{-1} \in G$, such that $gg^{-1} = g^{-1}g = e$
4. Associativity: if $g_1, g_2, g_3 \in G$, then $(g_1g_2)g_3 = g_1(g_2g_3)$

In mechanics, and more generally in physics, Lie groups are group of continuous transformations. In this case, they can be represented by matrices (as in the case of rotation matrices) and the group internal composition law as the matrix product. Then the commutator of two such matrices is defined by $[g_1, g_2] = g_1g_2 - g_2g_1$. When the commutator of any two matrices is zero, the group is said "commutative" or "Abelian". Vector spaces are examples of Abelian group for vector addition.

B.1.1 Lie Algebra

A key concept related to each Lie group is the *Lie algebra*. Intuitively, whether G is the set of finite transformations, its Lie algebra corresponds to the associated set of infinitesimal transformations. Since G is a manifold, any parameterized curve $t \in [t_1, t_2] \mapsto g(t) \in G$ admits a velocity in $g(0)$ with $0 \in [t_1, t_2]$ defined by $\dot{g}(0)$. This velocity belongs to the tangent linear space to G in $g(0)$ noted $T_{g(0)}G$. We said that it's a tangent vector to the group in $g(0)$. Conversely, $T_{g(0)}G$ is defined by the set of all the tangent vectors to G in $g(0)$. Now considering the tangent space taken at the identity element of G . When $g(0) = 1$, each element of this space is a linear perturbation of the identity transformation, and as such, does define an infinitesimal transformation. Then the commutator of two infinitesimal transformations defining a third infinitesimal transformation, it is natural to endow T_1G with the commutator of matrices. As such, T_1G is called the *Lie algebra*, denoted as \mathfrak{g} , of the Lie group and the commutator of its elements is then the Lie bracket. The Lie algebra associated with the Lie group $\text{SO}(3)$, denoted by $\text{so}(3)$, is determined by evaluating the tangent vector to a smooth curve $R(t)$ on $\text{SO}(3)$ where $R(0) = 1$, which is given by the skew symmetric matrix:

$$\widehat{\Omega} = \begin{pmatrix} 0 & -\Omega_z & \Omega_y \\ \Omega_z & 0 & -\Omega_x \\ -\Omega_y & \Omega_x & 0 \end{pmatrix} \in \text{so}(3). \quad (\text{B.1})$$

In mechanics, R generally defines the configuration of a rigid body with a fixed point (the rigid top) and Ω represents a possible angular velocity of such a system. In the same manner, the Lie algebra of $\text{SE}(3)$ denoted by $\text{se}(3)$ is the set of vectors given by:

$$\widehat{\eta} = \begin{pmatrix} \widehat{\Omega} & V \\ 0 & 0 \end{pmatrix}. \quad (\text{B.2})$$

We can translate any velocity on a group \dot{g}_1 , on its left or on its right by any transformation g_2 of the group. In matrix notation, this will be simply denoted as $g_2\dot{g}_1$ and \dot{g}_1g_2 . As a particular case, left translation by g^{-1} of any tangent vector $\dot{g} \in T_gG$, with $G = \text{SE}(3)$ defines a twist:

$$\begin{pmatrix} R^T \dot{R} & R^T \dot{p} \\ 0 & 0 \end{pmatrix} = \begin{pmatrix} \widehat{\Omega} & V \\ 0 & 0 \end{pmatrix} = \widehat{\eta}. \quad (\text{B.3})$$

From the point of view of rigid body mechanics, this twist is named body (or material) twist since we recognize in $(\Omega \in \mathbb{R}^3)$ and $(V \in \mathbb{R}^3)$ the angular and linear velocity of a body frame with position of its origin p , once they are expressed in the mobile basis. Twists are usually defined as vector $\eta = (V, \Omega)$ of \mathbb{R}^6 endowed with the induced Lie bracket

on this space defined by:

$$[\eta_1, \eta_2] = (\widehat{\eta}_1 \widehat{\eta}_2 - \widehat{\eta}_2 \widehat{\eta}_1)^\vee, \quad (\text{B.4})$$

for any two $\eta_1, \eta_2 \in \text{se}(3)$, where \wedge and \vee define the morphism associating a twist defined as a 4×4 matrix to its definition as a 6×1 vector, while \vee does the reverse.

While discussing further, there comes the forces, denoted $F = (N, C) \in \mathbb{R}^6$. These forces, acting on a rigid body, can be described by the elements of the dual space to $\mathfrak{g} \in \text{se}(3)$, denoted as $\mathfrak{g}^* \in \text{se}(3)^*$. This distinction is due to the fact that the forces (which behaves as co-vectors) transform in a reciprocal (transposal) manner under a change of coordinates than twists (which behave as tangent vectors). This force represented in screw form is often called a *wrench*.

B.2 Adjoint Operators

B.2.1 Action Mapping of a Lie Group

Given an element h of a Lie group G , one defines the action map¹ Ad_g of G on \mathfrak{g} by differentiating the group automorphism ghg^{-1} with respect to h at the identity (i.e. $h = 1$). Thus, in other words, the adjoint operation (or action mapping) is the transformation on $\text{se}(3)$ which change vectors (i.e. twists) from one reference frame to another by the use of Lie group elements. For example, if $\widehat{\eta} \in \text{se}(3)$ is a twist with $\eta \in \mathbb{R}^6$, then for any Lie group element g , $g\widehat{\eta}g^{-1}$ is a twist $\text{Ad}_g(\eta) : \text{se}(3) \mapsto \text{se}(3)$, where:

$$\text{Ad}_g = \begin{pmatrix} R & -R \widehat{p} \\ 0 & R \end{pmatrix}. \quad (\text{B.5})$$

Thus, Ad_g is a (6×6) matrix that once applied to a vector (or twist) changes it from one frame to another frame separated by Lie group (finite) transformation element g .

Furthermore, the co-action map (or co-adjoint operator) Ad_g^* of a Lie group G is the dual of the action map. Thus, Ad_g^* is the action of Lie group G on \mathfrak{g}^* , the dual space to \mathfrak{g} . More geometrically, G acts by conjugation on its cotangent space at the identity ($g = 1$), and this linear representation is Ad_g^* . Thus the dual adjoint operation is the coordinate transformation on $\text{se}(3)^*$ which transforms forces from one reference frame to another by the use of Lie group elements. For example, if $F \in \text{se}(3)^*$ is a force with force coordinates $F \in \mathbb{R}^6$, then for any Lie group element g , $g^{-1}\widehat{F}g$ is a force with force

¹In literature, it is also named as adjoint action or adjoint operator

coordinates $\text{Ad}_g^*(F) : \text{se}(3)^* \mapsto \text{se}(3)^*$ is given by:

$$\text{Ad}_g^* = \begin{pmatrix} R^T & 0 \\ R^T \hat{p}^T & R^T \end{pmatrix}. \quad (\text{B.6})$$

Here we can observe that the matrix used for dual operator Ad_g^* is actually the transpose of the one used for the operator Ad_g i.e. $\text{Ad}_g^* = \text{Ad}_g^T$.

B.2.2 Action Mapping of a Lie Algebra

Now, differentiating the Ad_g with respect to g at $g = 1$ defines the adjoint map of \mathfrak{g} on \mathfrak{g} . Given an element η_1 of a Lie algebra \mathfrak{g} , one defines the adjoint action of η_1 on \mathfrak{g} as the endomorphism $\text{ad}_{\eta_1} : \mathfrak{g} \rightarrow \mathfrak{g}$ with:

$$\text{ad}_{\eta_1}(\eta_2) = [\eta_1, \eta_2], \quad (\text{B.7})$$

for all η_2 in \mathfrak{g} . ad_{η_1} is an action that is linear.

For a given $\eta = (V, \Omega) \in \mathbb{R}^6$, ad_η is a (6×6) matrix that once applied to a vector (or twist), changes it from one frame to another frame separated by the infinitesimal transformation $(1 + \hat{\eta})$:

$$\text{ad}_\eta = \begin{pmatrix} \hat{\Omega} & \hat{V} \\ 0 & \hat{\Omega} \end{pmatrix}. \quad (\text{B.8})$$

Passing to dual, ad_η^* is the co-adjoint operator of Lie group G , and defines the (6×6) matrix that change any dual vector (or forces) from one frame to another frame separated by $(1 + \hat{\eta})^T$, respectively. Where, $\text{ad}_\eta^* = \text{ad}_\eta^T$.

B.3 Lie Group in 2D Space ($G = \text{SE}(2)$)

Consider motion of a rigid body in xy plane. In this case the Lie group $G = \text{SE}(2)$ becomes a subgroup of $G = \text{SE}(3)$, which is actually a Lie group of rotations and translations in the xy plane. Here a brief description of this subgroup is given while keeping the same notations as that of $G = \text{SE}(3)$. Thus, an element $g = (x, y, \theta) \in \text{SE}(2)$ can be given by the following homogenous coordinates:

$$g = \begin{pmatrix} R & p \\ 0 & 1 \end{pmatrix} \quad (\text{B.9})$$

but this time with $R \in \text{SO}(2)$ and $p \in \mathbb{R}$. Where, R is a (2×2) rotation matrix that represents a counter-clockwise rotation about the axis vertical to the xy plane and is

given as follows:

$$R = \begin{pmatrix} \cos \theta & -\sin \theta \\ \sin \theta & \cos \theta \end{pmatrix}, \quad (\text{B.10})$$

while $p = (x, y)^T \in \mathbb{R}$ is a (2×1) vector of position. Finally, the element g is given by:

$$g = \begin{pmatrix} \cos \theta & -\sin \theta & x \\ \sin \theta & \cos \theta & y \\ 0 & 0 & 1 \end{pmatrix}, \quad (\text{B.11})$$

References

- [1] <http://people.biology.ufl.edu/sahilber/VertZooLab2007/Lab6.htm>. 2.1
- [2] <http://www.youtube.com/watch?v=HfHRHoCBZCc>. 2.2
- [3] <http://www.octopusproject.eu/results.html>. 2.2.1
- [4] ARMSTRONG, W. W. Recursive solution to the equation of motion of an n-links manipulator. *Proc. 5th World Congress on Theory of Machines and Mechanisms, Montreal* (1979), 1343–1346. 1.1, 8.1
- [5] ARNOLD, V. I. Sur la geometrie differentielle des groupes de lie de dimension infinie et ses applications a l'hydrodynamique des fluides parfaits. *Ann. Inst. J. Fourier* 16, 1 (1966), 319–361. 2.3.5
- [6] BEAL, D. N., HOVER, F. S., TRIANTAFYLLOU, M. S., LIAO, J. C., AND LAUDER, G. V. Passive propulsion in vortex wakes. *Journal of Fluid Mechanics* 549 (2006), 385–402. 2.1
- [7] BIRKHOFF, G. *Hydrodynamics: A Study in Logic, Fact and Similitude*. Greenwood Press, 1978. 2.3.5, 3.4.3, 8.7.3
- [8] BLOCH, A., CROUCH, P., BAILLIEUL, J., AND MARSDEN, J. *Nonholonomic Mechanics and Control*. Springer-Verlag, New York, 2007. 2.3.4, 2.3.4, 5.1, 3, 8.16
- [9] BOSE, K., AND DORFMANN, A. Computational aspects of a pseudo-elastic constitutive model for muscle properties in a soft-bodied arthropod. *International Journal of Non-Linear Mechanics* 44, 1 (2009), 42–50. 5, 8.10
- [10] BOYER, F., AND ALI, S. Recursive inverse dynamics of mobile multibody systems with joints and wheels. *IEEE Trans. Robot.* 27, 2 (April 2011), 215 – 228. 2.3.5, 3, 5.1, 8.4

- [11] BOYER, F., ALI, S., AND POREZ, M. Macro-continuous dynamics for hyper-redundant robots: application to kinematic locomotion bio-inspired by elongated body animals. *to be appeared in IEEE Transaction on Robotics*. 2.3.5, 5
- [12] BOYER, F., NAYER, G. D., LEROYER, A., AND VISONNEAU, M. Geometrically exact kirchhoff beam theory: Application to cable dynamics. *Journal of Computational and Nonlinear Dynamics* 6, 4 (2011). 7.3
- [13] BOYER, F., POREZ, M., AND KHALIL, W. Macro-continuous computed torque algorithm for a three-dimensional eel-like robot. *IEEE Trans. Robot.* 22, 4 (Aug. 2006), 763–775. 1.1, 5, 5.1, 5.1, 8.10, 8.11
- [14] BOYER, F., POREZ, M., AND KHALIL, W. Macro-continuous computed torque algorithm for a three-dimensional eel-like robot. *Robotics, IEEE Transactions on* 22, 4 (Aug. 2006), 763–775. 8.1
- [15] BOYER, F., POREZ, M., AND LEROYER, A. Poincaré-Cosserat equations for the lighthill three-dimensional large amplitude elongated body theory: Application to robotics. *Journal of Nonlinear Science* 20 (2010), 47–79. 5.3.4, 8.10
- [16] BOYER, F., POREZ, M., LEROYER, A., AND VISONNEAU, M. Fast dynamics of an eel-like robot-comparisons with navier-stokes simulations. *Robotics, IEEE Transactions on* 24, 6 (Dec. 2008), 1274–1288. 1.1, 2, 8.1, 8.10, 8.14
- [17] BOYER, F., AND PRIMAULT, D. The Poincaré-Chetayev equations and flexible multibody systems. *Journal of Applied Mathematics and Mechanics* 69, 6 (2005), 925 – 942. 2.3.5, 2.3.5
- [18] BURDICK, J. W., RADFORD, J., AND CHIRIKJIAN, G. S. A ‘sidewinding’ locomotion gait for hyper-redundant robots. In *Proc. IEEE Int. Conf. Robot. Autom.* (May. 1993), pp. 101–106. 1.1, 5, 8.1, 8.10
- [19] CANAVIN, J., AND LIKINS, P. Floating reference frames for flexible spacecraft. *Journal of Spacecraft and Rockets* 14, 12 (1977), 924–732. 7.3
- [20] CARDONA, A., GERADIN, M., AND DOAN, D. Rigid and flexible joint modelling in multibody dynamics using finite elements. *Computer Methods in Applied Mechanics and Engineering* 89, 1-3 (1991), 395 – 418. 7.3
- [21] CARTAN, E. *Leçons sur la géométrie des espaces de Riemann*, 2nd ed. Gauthier-Villars, Paris, 1946. 2.3.4
- [22] CETAJEV, N. G. Sur les équations de Poincaré. *Comptes rendus de l’Académie des Sciences de Paris* (1927). 2.3.5

-
- [23] CHAPMAN, G. Of the movement of worms. *Journal of Experimental Biology* 27, 1 (1950), 29–39. [6.1](#)
- [24] CHEN, I.-M., AND YANG, G. Automatic model generation for modular reconfigurable robot dynamics. *J. of Dyn. Syst., Measurement and Control* 120, 3 (1998), 346–352. [1.1](#), [8.1](#)
- [25] CHIRIKJIAN, G., AND BURDICK, J. The kinematics of hyper-redundant robot locomotion. *Robotics and Automation, IEEE Transactions on* 11, 6 (Dec 1995), 781–793. [1.1](#), [8.1](#)
- [26] CHIRIKJIAN, G. S. A continuum approach to hyper-redundant manipulator dynamics. In *Proc. IEEE/RSJ Int. Conf. Intell. Robots Syst.* (Jul. 1993), vol. 2, pp. 1059–1066 vol.2. [1.1](#), [5](#), [5.1](#), [8.1](#), [8.10](#)
- [27] CHIRIKJIAN, G. S. Hyper-redundant manipulator dynamics: A continuum approach. *Advanced Robotics* 9, 3 (1994), 217–243. [6.6](#)
- [28] CHIRIKJIAN, G. S., AND BURDICK, J. W. A hyper-redundant manipulator. *IEEE Robot. Automat. Mag.* (Dec. 1994), 22–29. [5](#), [8.10](#)
- [29] CHIRIKJIAN, G. S., AND BURDICK, J. W. The kinematics of hyper-redundant robot locomotion. *IEEE Trans. Robot. Autom.* 11, 6 (Dec. 1995), 781–793. [6.6](#), [8.10](#)
- [30] CHOSET, H., AND HENNING, W. A follow-the-leader approach to serpentine robot motion planning. *ASCE Journal of Aerospace Engineering* 12 (1999). [6.3.4](#)
- [31] CIANCHETTI, M., ARIENTI, A., FOLLADOR, M., MAZZOLAI, B., DARIO, P., AND LASCHI, C. Design concept and validation of a robotic arm inspired by the octopus. *Materials Science and Engineering: C* 31, 6 (2011), 1230 – 1239. [2.2.1](#)
- [32] COQUEREAUX, R. *Espaces Fibrés et Connexions*, 3rd ed. Centre de Physique Théorique de Luminy, Marseille, 2002. ([document](#)), [2.20](#)
- [33] COSSERAT, E., AND COSSERAT, F. *Théorie des corps déformables*. Hermann, Paris, 1909. [5.1](#), [5.1.1](#)
- [34] CRESPI, A., BADERTSCHER, A., GUIGNARD, A., AND IJSPEERT, A. J. Amphibot I: an amphibious snake-like robot. *Robotics and Autonomous Systems* 50, 4 (2005), 163–175. [6.3.1](#)
- [35] CRESPI, A., AND IJSPEERT, A. Amphibot ii: An amphibious snake robot that crawls and swims using a central pattern generator. In *Proceedings of the 9th International Conference on Climbing and Walking Robots* (2006). [2.2](#)

- [36] DICKINSON, M. H., LEHMANN, F.-O., AND SANE, S. P. Wing rotation and the aerodynamic basis of insect flight. *Science* 284, 5422 (1999), 1954–1960. [2.1](#)
- [37] EHRESMANN, C. Les connexions infinitésimales dans un espace fibré différentiable. *Colloque de Topologie, Bruxelles* (1950), 29–55. [2.3.4](#)
- [38] ELDER, H., AND TRUEMAN, E. *Aspects of animal movement*. Seminar series. Cambridge University Press, 1980. [6.1](#)
- [39] ELDER, H. Y. Direct peristaltic progression and the functional significance of the dermal connective tissues during burrowing in the polychaete *polyphysia crassa* (oersted). *Journal of Experimental Biology* 58, 3 (1973), 637–655. [6.1](#)
- [40] FEATHERSTONE, R. *Robot dynamics algorithms*. Kluwer Academic Publishers, 1987. [1.1](#), [3](#), [8.1](#)
- [41] GRAVAGNE, I. A., RAHN, C. D., AND WALKER, I. D. Good vibrations: a vibration damping setpoint controller for continuum robots. In *Proc. IEEE Int. Conf. Robot. Autom.* (2001), vol. 4, pp. 3877–3884. [5](#), [8.10](#)
- [42] GRAY, J. *Animal locomotion*. Weidenfeld and Nicolson, London, 1968. [6.1](#)
- [43] GRAY, J., AND LISSMANN, H. W. Studies in animal locomotion. *Journal of Experimental Biology* 15, 4 (1938), 506–517. [6.1](#), [6.1](#)
- [44] GRAY, J., AND LISSMANN, H. W. The kinetics of locomotion of the grass-snake. *Journal of Experimental Biology* 26, 4 (1950), 354–367. [2.2.1](#)
- [45] GRILLNER, S., DELIAGINA, T., EL-MANIRA, A., HILL, R., ORLOVSKY, G., WALLEN, P., EKEBERG, O., AND LANSNER, A. Neural networks that co-ordinate locomotion and body orientation in lamprey. *Trends in Neurosciences* 18, 6 (1995), 270–279. [2.2.1](#)
- [46] GRISSOM, M. D., CHITRAKARAN, V., DIENNO, D., CSENCITS, M., PRITTS, M., JONES, B., MCMAHAN, W., DAWSON, D., RAHN, C., AND WALKER, I. Design and experimental testing of the OctArm soft robot manipulator. In *Society of Photo-Optical Instrumentation Engineers (SPIE) Conference Series* (2006), vol. 6230. [5](#), [8.10](#)
- [47] HANNAN, M. W., AND WALKER, I. D. Analysis and experiments with an elephant’s trunk robot. *Advanced Robotics* (2001), 847–858. [2.2.1](#)
- [48] HANNAN, M. W., AND WALKER, I. D. Kinematics and the implementation of an elephant’s trunk manipulator and other continuum style robots. *J. Robot. syst.* 20, 2 (2003), 45–63. [5](#), [8.10](#)

-
- [49] HATTON, R. L., BURTON, L. J., HOSOI, A. E., AND CHOSET, H. Geometric maneuverability with applications to low reynolds number swimming. In *International Conference on Intelligent Robots and Systems* (sept. 2011), pp. 3893–3898. [1.1](#), [2.3.5](#)
- [50] HATTON, R. L., AND CHOSET, H. Generating gaits for snake robots by annealed chain fitting and keyframe wave extraction. In *Proc. IEEE/RSJ Int. Conf. Intell. Robots syst.* (2009), IROS'09, pp. 840–845. [1.1](#), [2.2.1](#), [5.1](#), [8.1](#), [8.10](#)
- [51] HATTON, R. L., AND CHOSET, H. Geometric motion planning: The local connection, stokes' theorem, and the importance of coordinate choice. *The International Journal of Robotics Research* 30, 8 (2011), 988–1014. [2.3.4](#)
- [52] HIROSE, S. *Biologically inspired robots: Snake-like locomotors and manipulators*. Oxford Univ. Press, Oxford, 1993. [1.1](#), [2.2.1](#), [5](#), [8.1](#), [8.10](#)
- [53] HIROSE, S., AND MORISHIMA, A. Design and control of a mobile robot with an articulated body. *I. J. Robotic Res.* 9, 2 (1990), 99–114. [4.3](#), [8.9.2](#)
- [54] HOLLERBACH, J. M. A recursive lagrangian formulation of manipulator dynamics and a comparative study of dynamics formulation complexity. *Systems, Man and Cybernetics, IEEE Transactions on* 10, 11 (Nov. 1980), 730–736. [1.1](#), [8.1](#)
- [55] HU, D. L., NIRODY, J., SCOTT, T., AND SHELLEY, M. J. The mechanics of slithering locomotion. *Proceedings of the National Academy of Sciences* (2009). [2.2.1](#)
- [56] IJSPEERT, A. J., CRESPI, A., RYCZKO, D., AND CABELGUEN, J.-M. From swimming to walking with a salamander robot driven by a spinal cord model. *Science* 315, 5817 (2007), 1416–20. [2.2.1](#)
- [57] JONES, B. A., AND WALKER, I. D. Kinematics for multisection continuum robots. *IEEE Trans. Robot.* 22, 1 (2006), 43–55. [5](#), [8.10](#)
- [58] KAHN, M. E. *The near-minimum-time control of open-loop articulated kinematic chains*. PhD thesis, Stanford Artificial Intelligence Project Memo. AIM-106, Dec. 1969. [1.1](#), [8.1](#)
- [59] KANSO, E., MARSDEN, J., ROWLEY, C., AND MELLI-HUBER, J. Locomotion of articulated bodies in a perfect planar fluid. *Journal of Nonlinear Science* 15, 4 (2005), 255–289. [1.1](#), [2.3.5](#), [3.4.3](#), [8.7.3](#)
- [60] KELLY, S. D., AND MURRAY, R. M. Geometric phases and robotic locomotion. *J. Robotic Systems* 12, 6 (1995), 417–431. [1.1](#), [2.3.4](#), [3.6.2.1](#), [3.9](#), [5.6](#), [8.1](#), [8.8.2](#), [8.18](#)

- [61] KELLY, S. D., AND MURRAY, R. M. The geometry and control of dissipative systems. *Proceedings of the 35th IEEE conference on Decision and Control 1* (1996), 981–986. [2.3.5](#)
- [62] KHALIL, W., GALLOT, G., AND BOYER, F. Dynamic modeling and simulation of a 3-d serial eel like robot. *IEEE Trans on Sys, Man, and Cybernetics, Part C: Applications and Reviews* 37, 6 (2007), 1259–1268. [3](#), [8.4](#)
- [63] KHALIL, W., GALLOT, G., IBRAHIM, O., AND BOYER, F. Dynamic modeling of a 3-D serial eel-like robot. In *Proc. IEEE Int. Conf. Robot. Autom.* (Apr. 2005), pp. 1270–1275. [1.1](#), [1](#), [7.4](#), [8.1](#)
- [64] KHALIL, W., AND KLEINFINGER, J.-F. Minimum operations and minimum parameters of the dynamic models of tree structure robots. *Robotics and Automation, IEEE Journal of* 3, 6 (December 1987), 517–526. [1.1](#), [3.1](#), [8.1](#), [8.4.2](#)
- [65] KIM, B., LEE, M. G., LEE, Y. P., KIM, Y., AND LEE, G. An earthworm-like micro robot using shape memory alloy actuator. *Sensors and Actuators A: Physical* 125, 2 (2006), 429–437. [5](#), [8.10](#)
- [66] KOBAYASHI, S., AND NOMIZU, K. *Foundation of differential geometry*. John Wiley and Sons, 1963. [3.6.2.1](#), [8.8.2](#)
- [67] LAMB, H. *Hydrodynamics*. Cambridge University Press, 1932. [2.3.5](#), [3.4.3](#), [8.7.3](#)
- [68] LASCHI, C., MAZZOLAI, B., MATTOLI, V., CIANCHETTI, M., AND DARIO, P. Design of a biomimetic robotic octopus arm. *Bioinspiration & Biomimetics* 4, 1 (2009), 015006 (8pp). [5](#), [6.5](#), [8.10](#)
- [69] LILJEBACK, P., PETTERSEN, K. Y., STAVDAHL, O., AND GRAVDAHL, J. T. Experimental investigation of obstacle-aided locomotion with a snake robot. *Robotics, IEEE Transactions on* 27, 4 (aug. 2011), 792–800. [6.5](#)
- [70] LILJEBACK, P., PETTERSEN, K. Y., STAVDAHL, O., AND GRAVDAHL, J. T. Snake robot locomotion in environments with obstacles. *Mechatronics, IEEE/ASME Transactions on PP*, 99 (2011), 1–12. [2.2.1](#)
- [71] LIM, G., MINAMI, K., YAMAMOTO, K., SUGIHARA, M., UCHIYAMA, M., AND ESASHI, M. Multi-link active catheter snake-like motion. *Robotica* 14, 05 (1996), 499–506. [6.5](#)
- [72] MA, S., OHMAMEUDA, Y., AND INOUE, K. Dynamic analysis of 3-dimensional snake robots. In *Proceedings International Conference on Intelligent Robots and Systems* (2004), vol. 1, pp. 767–772 vol.1. [1.1](#), [3](#), [8.1](#), [8.4](#)

-
- [73] MALADEN, R. D., DING, Y., LI, C., AND GOLDMAN, D. I. Undulatory swimming in sand: Subsurface locomotion of the sandfish lizard. *Science* 325, 5938 (2009), 314–318. [2.1](#)
- [74] MALADEN, R. D., DING, Y., UMBANHOWAR, P. B., AND GOLDMAN, D. I. Undulatory swimming in sand: experimental and simulation studies of a robotic sandfish. *The International Journal of Robotics Research* 30, 7 (2011), 793–805. [2.2.1](#)
- [75] MARSDEN, J. E. Lectures on mechanics. *London Math. Society, Lecture Notes Ser. 174*, Cambridge University Press, Cambridge, UK (1990). [2.3.5](#)
- [76] MARSDEN, J. E., MONTGOMERY, R., AND RATIU, T. S. Reduction, symmetry, and phases in mechanics. *Memoire AMS* 436 (1990). [1.1](#), [3.4.3](#), [3.9](#), [5.1](#), [5.1](#), [5.6](#), [8.1](#), [8.7.3](#), [8.18](#)
- [77] MARSDEN, J. E., AND RATIU, T. S. *Introduction to Mechanics and Symmetry*, 2nd ed. Springer-Verlag, 1999. [2.3.5](#)
- [78] MATSUNO, F., AND SATO, H. Trajectory tracking control of snake robots based on dynamic model. In *Proc. IEEE Int. Conf. Robot. Autom.* (Apr. 2005), pp. 3029–3034. [1.1](#), [8.1](#)
- [79] MCMAHAN, W., JONES, B. A., AND WALKER, I. D. Design and implementation of a multi-section continuum robot: Air-octor. In *Proc. IEEE/RSJ Int. Conf. Intell. Robots Syst.* (Aug. 2005), pp. 2578–2585. [5](#)
- [80] MEIROVITCH, L. *Methods of Analytical Dynamics*. McGraw-Hill, New York, 1970. [5.3.4](#)
- [81] MELLI, J. B., ROWLEY, C. W., AND RUFAT, D. S. Motion planning for an articulated body in a perfect planar fluid. *SIAM J. Appl. Dyn. Syst.* [2.3.5](#)
- [82] MINAMI, M., ASAKURA, T., FUJIWARA, N., AND KANBARA, K. Inverse dynamics compensation method for pws mobile manipulators. *JSME International Journal. Series C, dynamics, control, robotics, design and manufacturing* 40, 2 (1997), 291–298. [3](#), [8.4](#)
- [83] MOCHIYAMA, H., AND SUZUKI, T. Kinematics and dynamics of a cable-like hyper-flexible manipulator. In *Proc. IEEE Int. Conf. Robot. Autom.* (2003), vol. 3, pp. 3672–3677. [1.1](#), [5](#), [8.1](#), [8.10](#)
- [84] MONTGOMERY, R. Gauge theory of the falling cat in dynamics and control of mechanical systems. *American Mathematical Society* 1 (1993). [2.3.4](#)

- [85] NEPPALLI, S., CSENSITS, M. A., JONES, B. A., AND WALKER, I. D. A geometrical approach to inverse kinematics for continuum manipulators. In *Proc. IEEE/RSJ Int. Conf. Intell. Robots Syst.* (Sept. 2008), pp. 3565–3570. [5](#), [8.10](#)
- [86] NEWELL, G. E. The role of the coelomic fluid in the movements of earthworms. *Journal of Experimental Biology* 27, 1 (1950), 110–122. [6.1](#), [6.1](#)
- [87] OSTROWSKI, J. Computing reduced equations for robotic systems with constraints and symmetries. *Robotics and Automation, IEEE Transactions on* 15, 1 (Feb 1999), 111–123. [1.1](#), [2.3.6](#), [3.6.2.1](#), [3.6.2.1](#), [3.9](#), [4.1.1](#), [4.2](#), [4.2.1](#), [4.2.2](#), [5.6](#), [8.1](#), [8.8.2](#), [8.9.1](#), [8.9.1](#), [8.18](#)
- [88] OSTROWSKI, J., AND BURDICK, J. Gait kinematics for a serpentine robot. In *Proc. IEEE Int. Conf. on Rob. and Autom.* (1996), pp. 1294–1299. [4.3.1](#), [8.9.2](#)
- [89] OSTROWSKI, J. P., AND BURDICK, J. W. The geometric mechanics of undulatory robotics locomotion. *The International Journal of Robotics Research* 17, 7 (1998), 683–701. [2.3.4](#), [3.4.3](#), [8.7.3](#)
- [90] OTA, T., DEGANI, A., SCHWARTZMAN, D., ZUBIATE, B., MCGARVEY, J., CHOSET, H., AND ZENATI, M. A highly articulated robotic surgical system for minimally invasive surgery. *The Annals of Thoracic Surgery* 87 (April 2009), 1253–1256. [2.2.1](#)
- [91] PARK, J., AND CHUNG, W.-K. Geometric integration on euclidean group with application to articulated multibody systems. *Robotics, IEEE Transactions on* 21, 5 (Oct. 2005), 850–863. [3.4.1](#), [8.7.2](#)
- [92] PAUL, R. P. C. *Modelling, trajectory calculation and servoing of a computer controlled arm*. PhD thesis, Stanford, CA, USA, 1972. [1.1](#), [8.1](#)
- [93] POINCARÉ, H. Sur une forme nouvelle des équations de la mécanique. *Compte rendu de l'académie des sciences de Paris* 132 (1901), 369–371. [2.3.5](#), [2.3.5](#)
- [94] PURCELL, E. M. Life at low reynolds number. *American Journal of Physics* 45, 1 (1977). [2.3.5](#)
- [95] RUCKER, D. C., JONES, B. A., AND WEBSTER, R. J. A geometrically exact model for externally loaded concentric-tube continuum robots. *IEEE Trans. Robot.* 26, 5 (Oct. 2010), 769–780. [5](#), [8.10](#)
- [96] RUMYANTSEV, V. V. On the Poincaré and Chetayev equations. *Journal of Applied Mathematics and Mechanics* 62, 4 (1998), 495–502. [2.3.5](#)

-
- [97] RUPPERT, E., AND BARNES, R. *Invertebrate Zoology*. Saunders College Publishers, Fort Worth, TX, 1994. [6.1](#)
- [98] SANE, S. P. The aerodynamics of insect flight. *Journal of Experimental Biology* *206*, 23 (2003), 4191–4208. [2.1](#)
- [99] SHAMMAS, E., CHOSET, H., AND RIZZI, A. Natural gait generation techniques for principally kinematic mechanical systems. In *Proceedings of Robotics: Science and Systems* (Cambridge, USA, June 2005). [2.3.4](#)
- [100] SHAMMAS, E., WOLF, A., H. BEN BROWN, J., AND CHOSET, H. New joint design for three-dimensional hyper redundant robots. In *In IEEE/RSJ International Conference on Intelligent Robots and Systems* (2003), pp. 3594–3599. [1.1](#), [8.1](#)
- [101] SHAMMAS, E. A., CHOSET, H., AND RIZZI, A. A. Towards a unified approach to motion planning for dynamic underactuated mechanical systems with non-holonomic constraints. *Int. J. Rob. Res.* *26*, 10 (2007), 1075–1124. [1.1](#), [3.3.1.1](#), [8.1](#)
- [102] SHAPER, A., AND WILCZEK, F. Efficiencies of self-propulsion at low reynolds number. *Journal of Fluid Mechanics* *198* (1989), 587–599. [2.3.5](#)
- [103] SHAPER, A., AND WILCZEK, F. Geometry of self-propulsion at low reynolds number. *Journal of Fluid Mechanics* *198* (1989), 557–585. [2.3.5](#)
- [104] SIMO, J. C. A finite strain beam formulation. The three-dimensional dynamic problem. Part I: Formulation and optimal parametrization. *Comp. Meth. Appl. Mech. Eng.* *72* (1989), 267–304. [5](#), [7.3](#), [8.10](#)
- [105] SIMO, J. C., AND VU-QUOC, L. A three-dimensional finite-strain rod model. Part II: Computational aspects. *Comp. Meth. Appl. Mech. Eng.* *58* (1986), 79–116. [5](#), [7.3](#), [8.10](#)
- [106] SIMO, J. C., AND VU-QUOC, L. On the dynamics in space of rods undergoing large motions – a geometrically exact approach. *Computer Methods in Applied Mechanics and Engineering* *66*, 2 (1988), 125 – 161. [5.1.1](#), [7.3](#)
- [107] TAKANOBU, H., TANDAI, T., AND MIURA, H. Multi-dof flexible robot base on tongue. In *Proc. IEEE Int. Conf. Robot. Autom.* (2004), vol. 3, pp. 2673–2678. [5](#)
- [108] TATLICIOGLU, E., WALKER, I. D., AND DAWSON, D. M. Dynamic modelling for planar extensible continuum robot manipulators. In *Proc. IEEE Int. Conf. Robot. Autom.* (Apr. 2007), pp. 1357–1362. [5](#), [8.10](#)

- [109] TESCH, M., LIPKIN, K., BROWN, I., HATTON, R., PECK, A., REMBISZ, J., AND CHOSET, H. Parameterized and scripted gaits for modular snake robots. *Advanced Robotics* 23, 9 (2009), 1131–1158. [2.2.1](#)
- [110] TRANSETH, A., LEINE, R., GLOCKER, C., PETTERSEN, K., AND LILJEBACK, P. Snake robot obstacle-aided locomotion: Modeling, simulations, and experiments. *Robotics, IEEE Transactions on* 24, 1 (Feb. 2008), 88–104. [3](#), [8.4](#)
- [111] TRANSETH, A. A., PETTERSEN, K. Y., AND LILJEBACK, P. A survey on snake robot modeling and locomotion. *Robotica* 27, 07 (2009), 999–1015. [6.5](#)
- [112] TRIVEDI, D., LOTFI, A., AND RAHN, C. D. Geometrically exact models for soft robotic manipulators. *IEEE Trans. Robot.* 24, 4 (Aug. 2008), 773–780. [5](#), [8.10](#)
- [113] TRIVEDI, D., RAHN, C. D., KIER, W. M., AND WALKER, I. D. Soft robotics: Biological inspiration, state of the art, and future research. *Applied Bionics and Biomechanics* 5, 3 (2008), 99–117. [5](#), [8.10](#)
- [114] UICKER, J. J. *On the dynamic analysis of spatial linkages using 4×4 matrices*. PhD thesis, Northwestern Univ., Aug. 1965. [1.1](#), [8.1](#)
- [115] WALKER, M. W., LUH, J. Y. S., AND PAUL, R. C. P. On-line computational scheme for mechanical manipulator. *Transaction ASME, J. of Dyn. Syst., Measurement and Control* 102, 2 (1980), 69–76. [1.1](#), [3](#), [3.2](#), [8.1](#), [8.5](#)
- [116] WEBSTER, R. J., KIM, J. S., COWAN, N. J., CHIRIKJIAN, G. S., AND OKAMURA, A. M. Nonholonomic modeling of needle steering. *Int. J. Rob. Res.* 25, 5-6 (2006), 509–525. [5](#), [8.10](#)
- [117] WITTENBERG, J. *Dynamics of systems of rigid bodies*. Stuttgart: Tubner, 1977. [3.1](#), [8.4.2](#)
- [118] WRIGHT, C., JOHNSON, A., PECK, A., MCCORD, Z., NAAKTGEBOREN, A., GIANFORTONI, P., GONZALEZ-RIVERO, M., HATTON, R., AND CHOSET, H. Design of a modular snake robot. In *IEEE/RSJ International Conference on Intelligent Robots and Systems* (2007), pp. 2609–2614. [2.2.1](#)
- [119] YAMADA, H., CHIGISAKI, S., MORI, M., TAKITA, K., OGAMI, K., AND HIROSE, S. Development of amphibious snake-like robot ACM-R5. In *Proc. 36th Int. Symposium on Robotics* (2005). [2.2](#), [2.2.1](#), [6.5](#)

Shaukat ALI

Newton-Euler approach for bio-robotics locomotion dynamics: from discret to continuous systems

Résumé

Cette thèse propose un cadre méthodologique général et unifié adapté à l'étude de la locomotion d'une large gamme de robots, en particulier bio-inspirés. L'objectif de cette thèse est double. Tout d'abord, elle contribue à la classification des robots locomoteurs en adoptant les outils mathématiques mis en place par l'école américaine de mécanique géométrique. Deuxièmement, en profitant de la nature récursive de la formulation de Newton-Euler, elle propose de nouveaux outils efficaces sous la forme d'algorithmes aptes à résoudre les dynamiques externe directe et interne inverse de tout robot locomoteur approximable par un système multi-corps mobile. Ces outils génériques peuvent aider l'ingénieur ou le chercheur dans la conception, la commande, la planification de mouvement des robots locomoteurs ou manipulateurs comprenant un grand nombre de degrés de liberté internes. Des algorithmes effectifs sont proposés pour les robots discrets ainsi que continus. Ces outils méthodologiques sont appliqués à de nombreux exemples illustratifs empruntés à la robotique bio-inspirée tels les robots serpents, chenilles et autres snake-board...

Mots-clés: locomotion bio-inspirée, dynamique des robots, formulation de Newton-Euler, mécanique géométrique, robots serpents, robots continus

Abstract

This thesis proposes a general and unified methodological framework suitable for studying the locomotion of a wide range of robots, especially bio-inspired. The objective of this thesis is twofold. First, it contributes to the classification of locomotion robots by adopting the mathematical tools developed by the American school of geometric mechanics. Secondly, by taking advantage of the recursive nature of the Newton-Euler formulation, it proposes numerous efficient tools in the form of computational algorithms capable of solving the external direct dynamics and the internal inverse dynamics of any locomotion robot considered as a mobile multi-body system. These generic tools can help the engineers or researchers in the design, control and motion planning of manipulators as well as locomotion robots with a large number of internal degrees of freedom. The efficient algorithms are proposed for discrete and continuous robots. These methodological tools are applied to numerous illustrative examples taken from the bio-inspired robotics such as snake-like robots, caterpillars, and others like snake-board, etc.

Keywords: bio-inspired locomotion, robot dynamics, Newton-Euler formulation, geometric mechanics, snake-like robots, continuum robots